

Design and adjustment of weighing cells for vacuum mass comparators

Maximilian Darnieder

Darnieder, Maximilian

Design and adjustment of weighing cells for vacuum mass comparators

Berichte aus dem INSTITUT FÜR MASCHINEN- UND GERÄTEKONSTRUKTION (IMGK)

Herausgegeben von

Univ.-Prof. Dr.-Ing. Stephan Husung (Produkt- und Systementwicklung),

Univ.-Prof. Dr.-Ing. Ulf Kletzin (Maschinenelemente) und

Univ.-Prof. Dr.-Ing. René Theska (Feinwerktechnik)

aus dem Institut für Maschinen- und Gerätekonstruktion (IMGK) an der TU
Ilmenau.

Band 41

Diese Reihe setzt die „Berichte aus dem Institut für Maschinenelemente
und Konstruktion“ fort.

Design and adjustment of weighing cells for vacuum mass comparators

Darnieder, Maximilian



Universitätsverlag Ilmenau
2024

Impressum

Bibliografische Information der Deutschen Nationalbibliothek

Die Deutsche Nationalbibliothek verzeichnet diese Publikation in der Deutschen Nationalbibliografie; detaillierte bibliografische Angaben sind im Internet über <http://dnb.d-nb.de> abrufbar.

Diese Arbeit hat der Fakultät für Maschinenbau der Technischen Universität Ilmenau als Dissertation vorgelegen.

Tag der Einreichung: 27. Februar 2023

1. Gutachter: Univ.-Prof. Dr.-Ing. René Theska
(Technische Universität Ilmenau)

2. Gutachter: Univ.-Prof. Dr.-Ing. Thomas Fröhlich
(Technische Universität Ilmenau)

3. Gutachter: Dr. Matthias Geisler
(Sartorius Lab Instruments GmbH & Co.KG)

Tag der Verteidigung: 11. Januar 2024

Technische Universität Ilmenau/Universitätsbibliothek

Universitätsverlag Ilmenau

Postfach 10 05 65

98684 Ilmenau

<https://www.tu-ilmenau.de/universitaetsverlag>

ISSN 2191-8082

DOI 10.22032/dbt.59666

URN urn:nbn:de:gbv:ilm1-2024000040



Dieses Werk - mit Ausnahme der anders gekennzeichneten Teile und des Umschlags - ist lizenziert unter einer [Creative Commons Namensnennung - Weitergabe unter gleichen Bedingungen 4.0 International Lizenz](https://creativecommons.org/licenses/by-sa/4.0/) (CC BY-SA 4.0):
<https://creativecommons.org/licenses/by-sa/4.0/>

Geleitwort der Herausgeber

Die Konstruktion von Maschinen und Geräten sowie die zugehörigen Methoden und Werkzeuge sind seit den frühen 1950er Jahren ein profilbildender Schwerpunkt an der Technischen Universität Ilmenau und ihren Vorgängerinstitutionen. Es war daher ein nahe liegender Schritt, dass die drei konstruktiv orientierten Fachgebiete der Fakultät für Maschinenbau – Maschinenelemente, Feinwerktechnik/Precision Engineering, Konstruktionstechnik – im Mai 2008 das Institut für Maschinen- und Gerätekonstruktion (IMGK) neu gegründet haben. Das IMGK steht in der Tradition einer Kette ähnlicher Vorgängerinstitute, deren wechselnde Zusammensetzung hauptsächlich durch sich über der Zeit ändernde Universitätsstrukturen bedingt war. Zweck des Institutes ist es, die Kompetenzen und Ressourcen der beteiligten Fachgebiete zu bündeln, um Forschung und Lehre zu verbessern und erzielte wissenschaftliche Ergebnisse gemeinsam in die Fachöffentlichkeit zu tragen. Ein wesentliches Instrument hierzu ist die Schriftenreihe des Instituts für Maschinen- und Gerätekonstruktion. Sie führt eine erfolgreiche Schriftenreihe des im Jahr 1991 gegründeten unmittelbaren Vorgängerinstitutes IMK (Institut für Maschinenelemente und Konstruktion) fort. In der Schriftenreihe erscheinen in erster Linie die am Institut entstandenen Dissertationen, daneben werden aber auch andere Forschungsberichte, die in den thematischen Rahmen passen und von allgemeinem Interesse sind, in die Schriftenreihe aufgenommen.

Der vorliegende Band 41 ist als Dissertation am Fachgebiet Feinwerktechnik unter der wissenschaftlichen Betreuung von Univ.-Prof. Dr.-Ing. René Theska entstanden. Die Herausgeber wünschen sich reges Interesse an der Schriftenreihe und würden sich freuen, wenn sie zum fruchtbaren Dialog in Wissenschaft und Praxis beitragen würde.

Ilmenau, im Februar 2024

Univ.-Prof. Dr.-Ing. Stephan Husung (Produkt- und Systementwicklung)

Univ.-Prof. Dr.-Ing. Ulf Kletzin (Maschinenelemente)

Univ.-Prof. Dr.-Ing. René Theska (Feinwerktechnik)

Abstract

Weighing cells based on compliant mechanisms are the backbone of mass metrology. The mechanical properties of the instruments and their adjustment define the metrological performance. The current work focuses on the design and adjustment of weighing cell mechanisms for a 1 kg vacuum mass comparator application. Three mechanical parameters of the compliant mechanisms define the metrological performance: stiffness, tilt sensitivity and off-center load sensitivity. An entire chapter is devoted to the ultra-thin flexure hinges used in the weighing cell mechanism. It covers their modeling, their manufacturing, and measurement. Starting from the concept level, two weighing cell prototypes were developed, assembled, and tested. Mechanical modeling, ranging from analytical models to finite element models, was used throughout the development. A quasi-independent adjustment of stiffness and tilt sensitivity based on the combination of trim masses was modeled and experimentally verified. A metrological model was used to define the requirements for the robust design of the final weighing cell. It allows the compensation of manufacturing deviations. The implemented adjustment methods were designed to eliminate the mechanical first-order error components of the weighing cell and thus enable a further reduction of measurement uncertainties in the mass comparison process.

Kurzzusammenfassung

Wägezellen, die auf nachgiebigen Mechanismen basieren, sind von entscheidender Bedeutung in der Massenmetrologie. Die mechanischen Eigenschaften und ihre Justierung bestimmen die messtechnische Leistungsfähigkeit der Instrumente. Die vorliegende Dissertation behandelt die Konstruktion und Justierung von nachgiebigen Mechanismen für Wägezellen in Vakuum - Massekomparatoren. Wichtigster Bestandteil dieser speziellen Mechanismen sind ultradünne Festkörpergelenke. Ein Kapitel ist deren Modellierung, Fertigung und Messung gewidmet. Darauffolgend wird die mechanische Modellbildung des gesamten Mechanismus diskutiert und ein analytisches Starrkörpermodell hergeleitet. Dieses wird durch den Vergleich mit numerischen Modellen verifiziert. Ein besonderer Fokus liegt hierbei auf den mechanischen Eigenschaften Steifigkeit, Neigungsempfindlichkeit und Ecklastempfindlichkeit. Ziel ist es deren Unsicherheitsbeiträge erster Ordnung durch Justierung umfassend zu eliminieren. Ausgehend von der Konzeptebene wurden zwei Wägezellen-Prototypen entwickelt, montiert und experimentell untersucht. Eine quasi-unabhängige Justierung der Steifigkeit und Neigungsempfindlichkeit durch die Kombination von Trimmassen im nachgiebigen Mechanismus wurde modelliert und experimentell verifiziert. Die starke Empfindlichkeit der Festkörpergelenke gegenüber Fertigungsabweichungen erforderte die Entwicklung einer neuartigen einstellbaren Justierung. Dieses Konzept wurde in einem weiteren Wägezellenprototyp umgesetzt. Die implementierten Justiereinrichtungen sind darauf ausgelegt, die mechanischen Fehlerkomponenten erster Ordnung der Wägezelle zu eliminieren und ermöglichen so eine weitere Verringerung der Messunsicherheit für Massekomparatoren.

*If I have seen further than others,
it is by standing upon the shoulders of giants.*

ISAAC NEWTON

Contents

Acronyms	xvii
Symbols	xix
Greek Symbols	xxiii
1 Introduction	1
2 State of the art	5
2.1 Mass comparator system	7
2.2 Weighing process and evaluation	11
2.3 Error sources for the weighing process	12
2.4 Mechanical behavior	13
2.4.1 Mechanical models of weighing devices	14
2.4.2 Astatization	16
2.4.3 Ground motion and tilt sensitivity	20
2.4.4 Off-centre loading	23
2.4.5 Deformations within the weighing system	25
2.5 Chapter summary	26
3 Scope and objectives of the present work	27
4 Flexure hinges	31
4.1 Review of bearings for precision instruments	31
4.2 Classification of monolithic flexure hinges	33
4.3 Mechanical modeling of monolithic flexure hinges	35
4.3.1 Analytical models	36
4.3.2 Finite element analysis	37
4.3.3 Transversal contraction	42
4.4 Imperfections of thin flexures	42
4.5 Approaches for the determination of the rotational stiffness	45
4.5.1 Quasi-static stiffness measurement	46

4.5.2	Stiffness determination based on natural frequency	52
4.5.3	Dimensional measurement	56
4.5.4	Comparison of qualification methods	57
4.6	Chapter summary	59
5	Mechanical modeling and adjustment strategies	61
5.1	Overview mechanical models	62
5.1.1	Rigid body models	63
5.1.2	Finite element models	63
5.2	Analytical rigid body model	65
5.2.1	Coordinate system and definition of parameters	65
5.2.2	Trim mass	66
5.2.3	Weighing cell mechanism	68
5.3	Mechanical effects within the monolithic weighing mechanism	71
5.3.1	Manipulation of the centers of mass	71
5.3.2	Astatization	73
5.3.3	Combination of adjustment measures	76
5.3.4	Off-center load sensitivity adjustment	76
5.4	Electro-magnetic force compensation	79
5.4.1	Zero-indicator	79
5.4.2	Actuator	80
5.4.3	Modeling of electromechanical components	81
5.5	Chapter summary	82
6	Weighing cell prototypes	85
6.1	Prototype weighing cells	85
6.1.1	Standard kinematic mechanism: PROT-S	86
6.1.2	Equal-arm weighing cell: PROT-EA	87
6.2	Measurement methods and results	88
6.2.1	Stiffness measurement	88
6.2.2	Tilt sensitivity measurements	93
6.3	Experimental verification of the adjustment concept	95
6.4	Chapter summary	97
7	Metrological model	101
7.1	Uncertainty consideration for weighing cell	102
7.2	Metrological model for a mass comparator application	103
7.3	Chapter summary	107

8	Prototype mass comparator weighing cell	109
8.1	Concept development	110
8.1.1	Proof of concept for stiffness adjustment	111
8.1.2	Detailed solution concept	113
8.2	Monolithic weighing cell design	115
8.2.1	Arrangement of subsystems and mitigation of cross-sensitivities	115
8.2.2	Stiffness adjustment and compensation of manufacturing de- viations	118
8.2.3	Experimental verification	121
8.2.4	In-vacuo adjustment capability	124
8.3	Chapter summary	124
9	Conclusion and outlook	127
9.1	Summary	127
9.2	Conclusion	130
9.3	Outlook	131
A	Publications	133
B	Definitions and Modeling	135
B.1	Performance measures for mass comparators	135
B.2	Further disturbances	138
B.2.1	Gravitational acceleration	138
B.2.2	Buoyancy	138
B.2.3	Sorption, contaminations, and cleaning	139
B.2.4	Electrostatic and electromagnetic fields	140
B.2.5	Temperature fluctuations	141
B.2.6	Noise	142
B.3	Material properties	143
B.4	Semi-circular flexure hinge	143
B.5	Nonlinear coupling within the weighing cell mechanism	144
B.6	Finite element models	149
C	Measurements and Experiments	151
C.1	Quasi-static flexure hinge stiffness measurement	151
C.2	Dynamic stiffness measurement	152
C.3	Tactile measurements on flexure hinges and related computational methods	153
C.3.1	Stiffness evaluation from dimensional data	155

C.3.2 Tactile probing simulation 158

C.3.3 Uncertainty estimation for tactile probing 160

C.4 Weighing cell operation 161

C.5 Influence of deformations on the off-center load sensitivity 161

C.6 Preliminary test of stiffness adjustment concept 163

Acronyms

Acronym	Description
2D	two-dimensional
3D	three-dimensional
ANSYS®	finite element software by ANSYS, Inc., USA (release: 21.2)
APDL	ANSYS Parametric Design Language
ARB	analytical rigid body
BIPM	Bureau International des Poids et Mesures
CLVA	closed-loop-vertical-assembled
CMM	coordinate measuring machine
CoG	center of gravity
CoR	center of rotation
DMM	digital multimeter
DOF	degree of freedom
EMFC	electromagnetic force compensation
FE	finite element
FFT	fast FOURIER transform
GUM	Guide to the Expression of Uncertainty in Measurement
IPK	International Prototype Kilogram
LED	light emitting diode
MATLAB	numeric computing software by The MathWorks, Inc., USA (release: R2020a)
MPC	multi point constraint
NF	natural frequency measurement
NMI	National Metrological Institute
NRB	numerical rigid body
OLHD	open-loop-horizontal-disassembled
PC	personal computer
PDF	probability density function
PROT-ASC	advanced stiffness compensation prototype
PROT-EA	equal-arm prototype
PROT-S	standard kinematic prototype
SR	significant region
VFH	V-shaped flexure hinges
WEDM	wire electrical discharge machining
XRCD	x-ray crystal density

Symbols

Symbol	Unit	Description
a	m s^{-2}	acceleration
M_B	N m	moment balance
\mathbf{C}		stiffness matrix
\mathbf{F}		load vector
Bl	T m	actuator constant
\mathbf{u}		displacement vector
C	N m^{-1}	stiffness at load carrier
C_A	N m rad^{-1}	rotational stiffness joint A
C_B	N m rad^{-1}	rotational stiffness joint B
C_C	N m rad^{-1}	rotational stiffness joint C
C_D	N m rad^{-1}	rotational stiffness joint D
C_E	N m rad^{-1}	rotational stiffness joint E
C_{el}	N m^{-1}	elastic stiffness
C_{EMFC}	N m^{-1}	overall system stiffness
C_F	N m rad^{-1}	rotational stiffness joint F
C_f	N m rad^{-1}	rotational stiffness of the flexure
C_f^*	N m rad^{-1}	nominal rotational stiffness of the flexure hinge
C_G	N m rad^{-1}	rotational stiffness joint G
C_{grav}	N m^{-1}	gravitational stiffness
C_H	N m rad^{-1}	rotational stiffness joint H
C_{HG}	N m rad^{-1}	rotational stiffness introduced by h_{HG}
$C_{rot,grav}$	N m rad^{-1}	gravitational component of rotational stiffness
C_{T2}	N m rad^{-1}	rotational stiffness of the trim mass T2
D	N rad^{-1}	tilt sensitivity at load carrier
d_{CMM}	m	diameter probe sphere
D_P	m	pulley diameter
D_Φ	N rad^{-1}	tilt sensitivity for tilt about x-axis
D_Θ	N rad^{-1}	tilt sensitivity for tilt about y-axis
$D_{\Theta,T2}$	N rad^{-1}	tilt sensitivity of trim mass T2
E	N mm^{-2}	YOUNG's modulus
E_L	$\text{N kg}^{-1} \text{mm}^{-1}$	off-center load sensitivity
E_{Lx}	$\text{N kg}^{-1} \text{mm}^{-1}$	off-center load sensitivity x axis
E_{Ly}	$\text{N kg}^{-1} \text{mm}^{-1}$	off-center load sensitivity y axis
\vec{e}_x		unit vector x axis

Symbols

Symbol	Unit	Description
\vec{e}_y		unit vector y axis
\vec{e}_z		unit vector z axis
F	N	force
f	Hz	frequency
f_0	Hz	undamped eigenfrequency
F_{EMFC}	N	actuator force
F_{F}	N	force at flexure F
F_{K}	N	force at the actuator
F_{L}	N	weight force at the counter mass
F_{par}	N	parasitic force on the weighing system
F_{S}	N	weight force of the sample mass
f_{s}	Hz	sampling rate
F_{S6}	N	weight force of m_{S6}
g	m s^{-2}	gravitational acceleration
h	m	minimum notch height
h_{AB}	m	$e_z : \overline{AB}$
h_{B}	m	vertical offset of the beam's center of gravity
h_{DC}	m	$e_z : \overline{DC}$
h_{FG}	m	$e_z : \overline{FG}$
h_{F1G1}	m	$e_z : \overline{F1G1}$
h_{F2G2}	m	$e_z : \overline{F2G2}$
h_{HG}	m	$e_z : \overline{HG}$
h_{H0G0}	m	$e_z : \overline{H0G0}$
h_{H1G1}	m	$e_z : \overline{H1G1}$
h_{H2G2}	m	$e_z : \overline{H2G2}$
h_{HL}	m	$e_z : \overline{HL}$
h_{N2}	m	$e_z : \overline{AN2}$
h_{N3}	m	$e_z : \overline{AN3}$
h_{N7}	m	$e_z : \overline{FN7}$
h_{N8}	m	$e_z : \overline{HN8}$
h_{nom}	m	nominal minimum notch height
h_{S5E}	m	$e_z : \overline{S5E}$
h_{S}	m	substitute minimum notch height
h_{T}	m	cross-section height of tape
h_{T2}	m	$e_z : \overline{AT2}$
h_{T23}	m	$e_z : \overline{AT2} = \overline{BT3}$
h_{T23}^*	m	adjustment parameter for $C = D_{\Theta} = 0$, $e_z : \overline{AT2} = \overline{BT3}$
h_{T3}	m	$e_z : \overline{BT3}$
h_{T8}	m	$e_z : \overline{HT8}$
h_{T8}^*	m	adjustment parameter for $C = D_{\Theta} = 0$, $e_z : \overline{HT8}$
h_{TB}	m	height of the tape coupling point
I_{C}	A	coil current
I_z	m^3	second moment of inertia about z

Symbol	Unit	Description
J	kg m^2	moment of inertia
$K_{\Phi K_Y}$	m rad^{-1}	lateral deflection constant for tilt at location K
$K_{\Phi M_Y}$	m rad^{-1}	lateral deflection constant for tilt at location M
K_{eD}	m rad^{-1}	tilt sensitivity contribution to off-center load
K_{eK_Y}	m rad^{-1}	lateral deflection constant for off-center load at location K
K_{eM_Y}	m rad^{-1}	lateral deflection constant for off-center load at location M
K_{hwp}		torque reduction factor hanging weighing pan
K_{ml}		correction factor for measurement length
K_x		correction factor for transversal contraction
K_{xz}		combined correction factor
K_z		correction factor for geometry in x direction
L	N m	LAGRANGE function
l_{AD}	m	$e_x : \overline{AD}$
L_B	m	length between attachment points
l_{BC}	m	$e_x : \overline{BC}$
d_{SR}	m	effective length of the flexure
l_{HG}	m	$e_x : \overline{HG}$
l_{HK}	m	$e_x : \overline{HK}$
l_{HL}	m	$e_x : \overline{HL}$
l_{H1L1}	m	$e_x : \overline{H1 L1}$
l_{H2L2}	m	$e_x : \overline{H2 L2}$
l_{N2}	m	$e_x : \overline{A N2}$
l_{N3}	m	$e_x : \overline{A N3}$
L_T	m	length of tape suspended on one side of the lever
l_{T2}	m	horizontal position trim mass
l_{T3}	m	horizontal position trim mass
M	N m	moment
m	kg	mass
m_B	kg	mass of the beam
m_C	kg	counter mass
m_{C1}	kg	counter mass on lever 1
m_{C2}	kg	counter mass on lever 2
m_{cal}	kg	calibration mass
m_f		mobility of a mechanism
m_G	kg	mass suspended at G
m_{N2}	kg	net mass lower lever
m_{N3}	kg	net mass upper lever
m_{N4}	kg	net mass load carrier
m_{N5}	kg	net mass lower weighing pan
m_{N6}	kg	net mass upper weighing pan
m_{N7}	kg	net mass coupling element
m_{N8}	kg	net mass transmission lever

Symbols

Symbol	Unit	Description
m_S	kg	sample mass
m_{S5}	kg	sample mass/upper weighing pan
m_{S6}	kg	sample mass/lower weighing pan
m_{T2}	kg	trim mass on lower lever
m_{T3}	kg	trim mass on upper lever
m_{T8}	kg	trim mass on transmission lever
m_{T8F}	kg	trim mass on transmission lever (fine)
p	Pa	atmospheric air pressure
q_2	rad	deflection angle of lower lever (2)
q_4	rad	deflection angle of load carrier (4)
q_7	rad	deflection angle of the coupling element (7)
q_8	rad	deflection angle of the transmission lever (8)
R	m	radius of semi-circular flexure
$R_{p0.2}$	N mm^{-2}	yield strength
r_{S5}	m	position vector to center of gravity of sample mass/upper weighing pan m_{S5}
r_{S6}	m	position vector to center of gravity of sample mass/lower weighing pan m_{S6}
T	K	temperature
t	s	time
t_{cycle}	s	weighing cycle duration
T_{kin}	N m	kinetic energy
t_{pg}	s	periode of the tides
t_{ps}	s	time phase shift relative to noon
t_{pT}	s	periode of the temperature fluctuation
t_{ran}	s	random time offset
u		measurement uncertainty
U_{el}	N m	potential energy in elastic deformation
U_{grav}	N m	potential energy in the earth's gravitational field
U	N m	potential energy
u_x	m	displacement along x axis
u_y	m	displacement along y axis
u_z	m	displacement along z axis
w	m	width of flexure
w_T	m	cross-section width of tape
x	m	x coordinate
y	m	y coordinate
y_K	m	y position of the coils within the actuator
z	m	z coordinate
z_K	m	z position of the coils within the actuator
z_M	m	z position of the lever at the position sensor

Greek Symbols

Symbol	Unit	Description
α	rad	angular misalignment of position sensor housing about x axis
β_B	rad	beam deflection angle
β_B^*	rad	nonlinearity of beam deflection angle
ϑ		damping ratio
δ	s^{-1}	decay constant
δ_F	m	infinitesimal vertical displacement of F
δ_G	m	infinitesimal vertical displacement of G
ϵ_{S_x}	m	sample mass eccentricity in x
ϵ_{S_y}	m	sample mass eccentricity in y
ϵ_{S_z}	m	sample mass eccentricity in z
Γ	m	effective h_{HG} of a two-lever concept
ι		nonlinear transmission ratio between subsystems at $q_8 = 0$
ν		POISSON ratio
ω	Hz	angular frequency
φ_P	rad	pulley rotation angle
φ_x	rad	rotation angle about x axis
φ_y	rad	rotation angle about y axis
φ_z	rad	rotation angle about z axis
ρ	$kg\ m^{-3}$	density
ρ_0	$kg\ m^{-3}$	density air
ρ_B	$kg\ m^{-3}$	density of the beam
ρ_T	$kg\ m^{-3}$	density of tape material
σ		standard deviation
τ	m	factor nonlinear transmission ratio
Φ	rad	tilt angle about x -axis
Θ	rad	tilt angle about y -axis
ξ		transmission ratio between subsystems at $q_8 = 0$

Chapter 1

Introduction

To date, the absence of a viable solution for the direct measurement of mass has challenged generations of scientists. Mass is the strictly positive proportionality constant between force \vec{F} and acceleration \vec{a} :

$$\vec{F} = m \vec{a} \quad (1.1)$$

If \vec{a} is replaced by \vec{g} and \vec{g} is parallel to \vec{e}_z , (1.1) simplifies to:

$$\vec{e}_z : F_z = -m g \quad (1.2)$$

Here, F_z is defined as the object's weight with the mass m . Consequently, the mass of a body can be determined by measuring its weight, which is the measurement of a force. The trouble with the terms mass and weight has been very well put by JAEGER et al.: „It is only because most people live exclusively on the surface of the earth that weight and mass are often confused.“, [JDS84].

Mass measurement requires the measurement of a force - and vice versa. Thus, highly demanding force measurements in numerous fields of science and industry require a reliable system of reference masses. The relevance of a reliable definition of the mass unit has been one driving force behind the recent redefinition of the unit kilogram (kg). After decades of preparation, the scientific community took a big step forward in 2019 by a new kilogram definition based on the PLANCK constant - a fundamental constant. Two distinct and independent experiments had been qualified to realize the new kilogram definition: the KIBBLE balance (KB) and the Avogadro project (XRCD). The execution of the experiments is laborious and costly, which makes the accurate comparison of mass standards with mass comparators a persistently important element in the dissemination chain of the unit kilogram.

A mass comparator is a weighing device specially designed to compare weight forces with the best possible metrological characteristics. The key measure in achieving this goal is the comparison of masses with smallest mass differences compared to their nominal mass. It enables the design of a weighing instrument with an extremely restricted weighing range around the nominal mass. With a weighing range of $<2\text{ g}$ for 1 kg reference masses, mass changes smaller than $1\times 10^{-10}\text{ kg}$ can be resolved with commercially available systems [Sar14; Met18].

Mechanical beam balances have been under operation long before the International Prototype Kilogram (IPK) has been established by the General Conference on Weights and Measures (CGPM) in 1889. The kinematic system with one mechanical lever suspended centrally using one rotational pivot and weighing pans with gimballed mounts is convenient for mass comparisons. Reference has been made that such devices were used in Egyptian society around 3000 BC [GB09; Gup12]. Even earlier systems are listed with relative resolutions between 1 part in 10^2 and 1 part in 10^3 [KG00]. Progress in the general technological potential of humankind provided an increase in the performance of weighing systems. Relevant progress began in the 18th century and continues up to date. A comprehensive tabular overview in [Koc89] shows the development of precision weighing devices and their subsystems.

For high-precision mass comparators, the principle of electromagnetic force compensation (EMFC) has become established since it allows very high resolutions of up to 50×10^6 divisions of the output scale (scale intervals) [Bor+12]. The operating principle of this type of weighing cell is based on the compensation method [Kra04a; SGR12]. The EMFC system restores the initial position of the mechanical system after the application of an external load. The EMFC system consists of a position sensor, an electromagnetic actuator and an analog or a digital controller. If a mass is placed on the weighing pan, the weight force increases, and the weighing pan tends to move downwards, resulting in a deflection of the weighing cell mechanism. The position sensor detects the deflection and the controller adjusts the actuator force to keep the system in balance and close to zero deflection. The actuator force, a LORENTZ force, is generated by an electrical current driven through the coil, which sits in the annular air gap of a permanent magnet system. By calibration, the change in coil current is a measure for the mass difference on the weighing pan.

The compliant mechanism of modern EMFC weighing systems is largely manufactured from one piece [LM99; Eme01]. The monolithic design provides tight tolerances and strongly reduces the number of mechanical interfaces with uncertain

properties. The compliant mechanism of the weighing system broadly defines the metrological performance of the system. It is thus placed in the focus of the present work both in terms of its design and its adjustment. Chapter 2 provides an overview of the literature on relevant aspects of precision weighing devices. Emphasis is placed on the common knowledge about error sources on the weighing process, ultimately limiting the achievable minimal uncertainty for mass comparisons. The subsequent Chapter 3 defines the scope and the objectives for the present work. Chapter 4 is dedicated to a crucial element of the weighing cell mechanism - its flexure hinges. The results from modeling to the experimental determination of the rotational stiffness are outlined. Expanding on the findings, Chapter 5 describes the mechanical model of the weighing cell mechanism, including adjustment measures. The experimental investigation of self-developed prototype weighing cells is used to verify the developed mechanical models in Chapter 6. The development of a new weighing cell concept is started by setting the requirement based on a metrological model in Chapter 7. Chapter 8 describes the development of the new prototype mass comparator weighing cell.

Chapter 2

State of the art

The capability of making traceable force measurements in the micro-, nano-, or even piconewton range becomes more and more important [KAH16]. Traceable force measurements have a various applications in science and technology. Based on the traceability to a kilogram artifact, masses and corresponding weight forces close to 1 kg can be calibrated with minor uncertainties. However, in the low mass/force range, the traceability to the 1 kg reference mass constitutes a considerable challenge. Here, a combination of mass standards has to be calibrated against a kilogram reference standard. Since every mass and reference standard has a particular uncertainty, the uncertainties increase for masses deviating from 1 kg. An extrapolation of the uncertainties for current mass standards exhibits an uncertainty equal to the nominal mass value for 1 ng [Sha18].

According to [OIML R 111-1:2004], the weights in legal mass metrology are limited to a mass range from 5000 kg down to 1 mg, but even smaller mass standards are required. Exemplary application fields are the chemical and pharmaceutical industries, handling and manipulating biological tissue, micro-indentation instruments, and scientific experiments in general [GB09]. Other applications are tactile dimensional metrology [DIN 32567-3:2014-10; KAH16] and sensitivity error measurements for mass comparators [Wan+15].

Now and for many years to come, mass comparators represent the backbone of the dissemination chain of the unit kilogram. Presently, the relative measurement uncertainty for mass comparisons is in the range of 1×10^{-9} [RFD16]. This uncertainty is one magnitude below the uncertainties reported for the experiments realizing the new kilogram definition which are in the range of 2×10^{-8} [HKL20]. However, it can be expected that these uncertainties will be reduced in the future.

Figure 2.1 highlights some top-level applications of the most accurate mass comparators (prototype balances) given the new quantum-based kilogram definition.

The equal arm beam balances depict the application of a mass comparator. In the top left corner, the Si^{28} -spheres used for the x-ray crystal density (XRCD) method (Avogadro project) are compared to the IPK or its copies respectively to link the value of the PLANCK constant to the old kilogram definition. Following the definition of the PLANCK constant as a natural constant - which has been put into power in 2019 [Bip19] - the process can be reversed to *produce* new mass standards. These top-level mass standards have to be linked to lower class mass standards (dissemination) - a task for mass comparators. On the right-hand side of Fig. 2.1, the corresponding mass comparator deployment for the KIBBLE balance experiment is presented. Concluding, mass comparators have posed a prerequisite for the new kilogram definition and a persistingly relevant element in the dissemination chain of the unit kilogram.

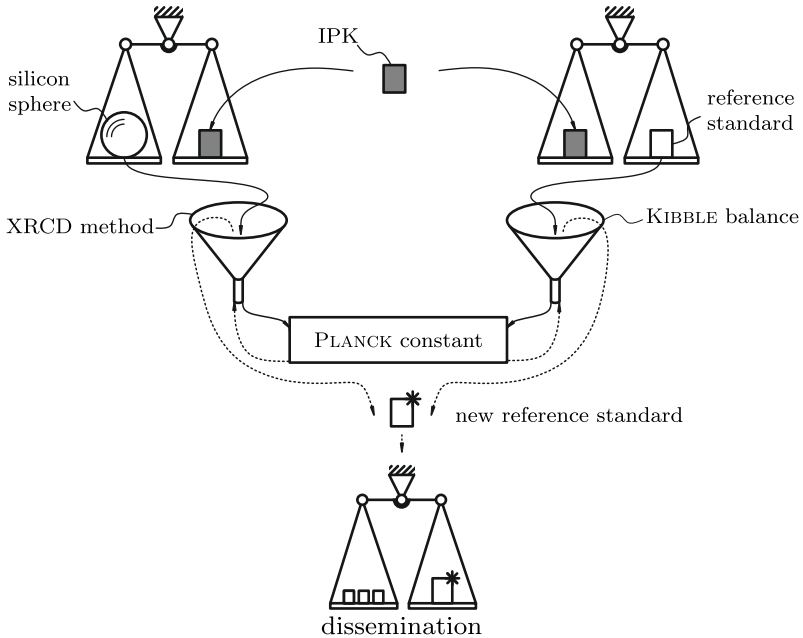


Figure 2.1 – Top-level applications for the most accurate mass comparators (depicted as equal arm beam balances) in conjunction with the redefinition of the unit kg.

Alternative instrument concepts are presently under development. They make use of the new option to directly qualify mass standards with a nominal mass other than 1 kg using the quantum-based kilogram definition [Kno+19]. Based on the KIBBLE balance principle, these table-top devices, denominated as PLANCK balances, may replace mass comparators in the future since they are traceable based on electrical quantities rather than calibrated mass standards [Rot+18]. Being largely similar in their mechanical structure, developments on mass comparators are highly relevant for future PLANCK balances [HRF17].

Another important aspect is the vacuum environment for mass comparators. While the former definition of the mass standards was defined under atmospheric conditions, the new definition can and will be realized under vacuum conditions [BS16]. Thus, further enhanced vacuum mass comparators represent a valuable investment for future mass metrology devices.

2.1 Mass comparator system

Mass comparators are analytical balances with highly limited weighing ranges [GB09]. Apart from that, there is no fundamental difference to analytical balances concerning the mechanical design. Concepts used in analytical balances, see [Sch12], are applied to mass comparators, emphasizing high resolution and low measurement uncertainty rather than cost and robustness. However, mass comparator and analytical balance differ in their use and the evaluation of measurements [Val17]. Mass comparators are operated using a differential weighing method, meaning that only mass differences as fractions of the nominal mass are determined. Compared to proportional weighing with continuous weighing ranges, smaller relative uncertainties can be achieved [Bor+12]. National Metrological Institutes (NMIs) and the Bureau International des Poids et Mesures (BIPM) uses this fundamental comparator principle to realize and maintain traceability of the unit kilogram. Mass comparators used in this context are referred to as prototype balances. These are exclusively designed for a nominal mass of 1 kg [Bor+12].

Two main concepts of 1 kg prototype balances have been put into practice by the BIPM and the NMIs and find application up to now: equal arm beam balances and, more recently, weighing cells with built-in counter masses. Equal arm beam balances with two weighing pans offer the possibility to be operated in two modes. During the so-called transposition or GAUSS method, the sample masses on each weighing pan are interchanged simultaneously. On the contrary, the substitution or BORDA

method requires only one weighing pan and can be used with balances, including a fixed counter-mass. This concept requires to place two masses subsequently onto a single weighing pan [Bor+12]. Even though equal arm beam balances like BIPM FB-2 still provide the most accurate weighing results, they are more and more replaced by compact weighing cells with integrated counter-masses [GB09]. The latter rely on the substitution weighing method.

The demand on measurement precision complicates the rather simple function of comparing the weight forces of two objects. Every subsystem of the mass comparator needs to be highly optimized to fulfill its highly-demanding function. The main functional elements are structured in Fig. 2.2, revealing the interdependence of its functional units.

All functional units of the mass comparator are located within a pressure-tight enclosure. It shields the sensitive components from external disturbances lead to a highly constant temperature. Moreover, it can be evacuated if required.

As a first step in the mass comparison process, the sample masses and mass standards need to be transferred into the vacuum chamber, undergoing a transition from atmospheric- to high-vacuum conditions. Opening the vacuum chamber together with a subsequent evacuation is one option. A more convenient method is the use of an optional vacuum transfer unit, which enables the quick replacement of sample masses without disturbing the vacuum conditions inside the vacuum chamber [Feh+13]. The sample masses are then stored in a magazine within the vacuum chamber, having multiple storage positions. The magazine enables the comparison of several sample masses. Usually, the magazine is part of the mass-exchange mechanism, requiring a lifting mechanism to transfer the sample mass from the magazine to the hanging weighing pan.

The automatized mass-exchange process is inevitable for mass comparators since it minimizes positioning errors, prevents operator heat input, and enables a strict and repeatable time scheme [Hil+10]. The realization of a mass-exchange mechanism for substitution weighing is comparably simple since only one weighing pan is loaded at once.

The engineering materials used to design the compliant mechanisms for weighing cells exhibit anelastic relaxation under strain which can be measured under controlled environmental conditions [Küh13]. For comparator weighing cells, loaded and unloaded multiple times during a measurement cycle, this *actual* behavior of the material represents a source of systematic measurement deviation. It contributes to the uncertainty of the measurement result. The most convenient solution is the

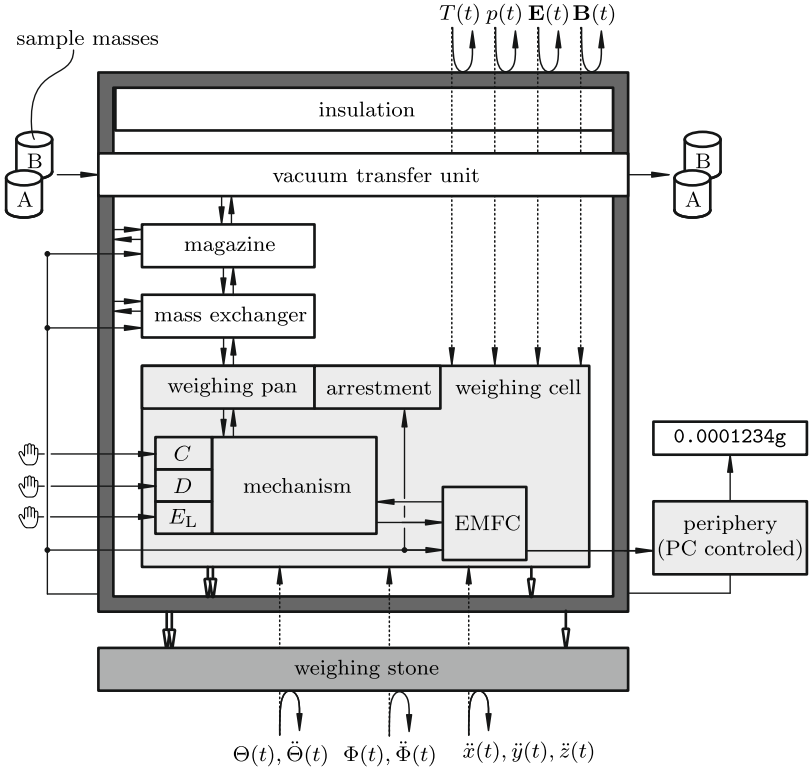


Figure 2.2 – Simplified function structure of a prototype mass comparator following the system definition in [Kra00; VDI 2221-1:2018-03]. The weighing cell's sub-functions are adjustment units for C - stiffness, D - tilt sensitivity, and off-center load sensitivity E_L which are manually operated. External influence quantities are: $T(t)$ - temperature fluctuations, $p(t)$ - air pressure variations, $\mathbf{E}(t)$ - electric field, $\mathbf{B}(t)$ - magnetic vector potential, $\Theta(t)$ - ground tilt (nick), $\Phi(t)$ - ground tilt (roll), $x(t)$, $y(t)$, $z(t)$ - ground displacement, t - time.

suppression of any mechanism deflection during the weight exchange process. A constant load device [FFH05] or load receptor arrester [GB09] is used to precisely arrest the mechanism during the mass exchange. Then, the force flow through the mechanism and its deformation state remain virtually constant.

The heart piece of the mass comparator is its EMFC weighing cell based on a highly specialized compliant mechanism. It ensures an undisturbed and accurate transmission of the weight forces to the counter-balance side. Depending on the setup, a counter mass or a second weighing pan is used to counter-balance the most significant portion of the mass on the weighing pan. Residual imbalances - the mass difference, including spurious disturbance - are compensated using a variable driving force according to the *compensation principle*, see Def. 2.1.

Definition 2.1 (compensation principle). A sensor element changes its state due to the measurand's physical effect. Rather than measuring the state change directly (deflection method), the physical effect is compensated, and the sensor element is returned to its original state. The amount of compensation is evaluated to obtain the measurand.

An important part of the weighing cell is its transducer which converts the weight force on the weighing pan into a measurable electrical signal [Gup12]. Numerous physical principles are applied. In literature, transducers like strain gauges, vibrating string, tuning fork, gyroscope, optical interference, magneto-elastic, capacitive, hydraulic, photoelectric, piezoelectric, semiconductor, surface wave, inductive worm, LVDT, and nucleonic are listed [KM87; Gup12; Erd82]. The work [Šte11] provides overview of commonly used transducers in force measurements, which is originally published in [Sch83].

The use of a feedback loop is common in instrument science [Jon79]. Position control of mechanism in combination with the method of substitution weighing has been realized by KIBBLE, who reported a twentyfold increase in accuracy [Kib75]. The compensation control for weighing cells is realized by an EMFC system. It provides a large number of scale intervals and short measurement times. The electromagnetic force is commonly generated using a voice coil actuator. An alternative actuation principle is a capacitive actuator with a small force range. Most capacitive actuators are used in microbalances and beyond.

The EMFC can be viewed as a position control always maintaining a predefined zero position of the mechanism. To this end, a high-resolution position sensor is required. The most commonly used sensor is an optical slit aperture sensor, including a LED and a dual photodiode. The displacement / signal behavior is approximately linear in a limited motion range and a resolution in the nanometre range can be achieved [Die+10]. Performance measures relative to the spot diameter are given in [BG70]. In [Die+14], a position repeatability of <0.17 nm was achieved at the weighing pan of a commercial weighing cell. Considering the transmission ratio from the weighing

pan to the position sensor, this results in ≈ 1 nm sensor resolution. In [KFF18], a resolution limit of ≈ 50 pm is stated as the maximum achievable resolution limited by signal noise. Other sensor principles use the angular deflection of a mirror [BM59] and capacitive measurement principles [Puf+13].

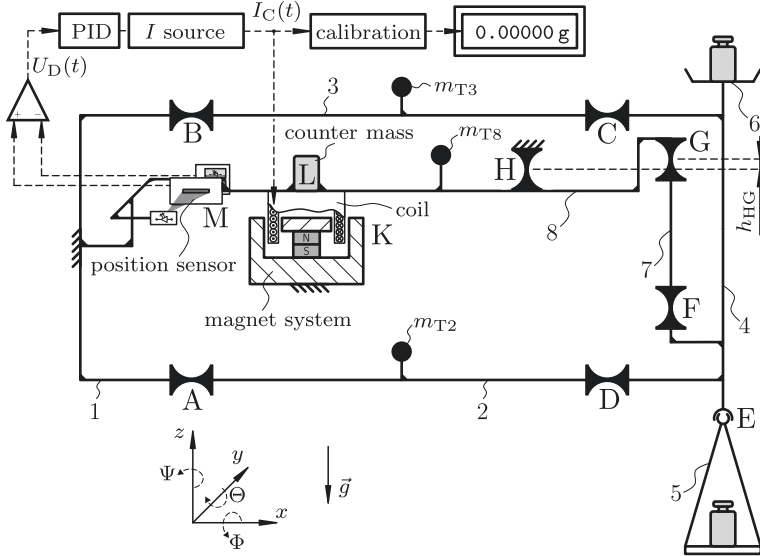


Figure 2.3 – Schematic drawing of an electromagnetic force compensated weighing cell after [Dar+18c] including an introduction of the notation and the definition of the coordinate system. Depicted adjustment measures are the trim masses m_{T_x} and the vertical distance between pivot H and G (h_{HG}).

2.2 Weighing process and evaluation

By nature, each measurement is subject to errors, which requires a quantification of the trustworthiness of the measurement result [Trä14]. The quality of a measurement result is typically characterized by its measurement uncertainty, providing a measure for the reliability of the numerical value. A recent book on measurement uncertainties is [Gra14]. More specific calibration and key comparisons are described in [CH06]. Following the Guide to the Expression of Uncertainty in Measurement

(GUM), measurement uncertainty is distinguished according to the method of evaluation to type A and type B [JCGM 100:2008]. The experimental uncertainty (type A) for a comparative measurement depends on the measurement sequence used. For mass comparisons, two common sequences are available, the ABA and the ABBA sequence, where the latter is more efficient compared to the first [DPB04]. A so-called ABBA weighing sequence can eliminate a linear drift of the balance. However, this sequence is sensitive to higher-order drift effects. In [SC94], circular comparison sequences of the type $(AB\dots)_n$ are investigated in terms of the order of drift correction used and the required repetitions n to cancel out drifts effects up to the third order. Matrix-based calculation methods are applied to calibrate multiple weights against a mass standard [BCH94; SBS07]. The description of the methodology and the mathematical background is complex. Further detail about this extensive field is omitted since the present work's objective is to improve measurement uncertainty for a given standard weighing sequence $ABBA_n$. As an extension of the statistical evaluation of measurement results, Type B uncertainties enable the consideration of non-statistical influence parameters [Trä14]. Based on a mathematical model of the measurement, the uncertainty can be either calculated based on the propagation of uncertainty for linear models described in the GUM [JCGM 100:2008] or using the general approach based on the MONTE CARLO method [Esw+07; MWR08; HC14]. The latter is described in Supplement 1 of the GUM [JCG08].

2.3 Error sources for the weighing process

The following section provides an overview of the collective knowledge concerning the disturbance of the weighing process. A large number of external and internal influences need to be considered. It is necessary to estimate the disturbing physical effects in combination with the sensitivity coefficients of the measurement system to determine their influence on the weighing result. In literature, many influences on the weighing process are listed, which have been arranged in an ISHIKAWA diagram, see Fig. 2.4. The mechanical behavior is described in more detail in the following. For sources of disturbance, not in the focus of this work, refer to B.2.

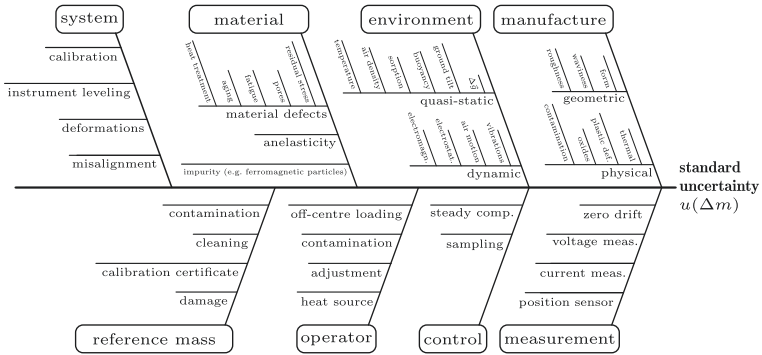


Figure 2.4 – ISHIKAWA diagram of external and internal influences on the weighing process.

2.4 Mechanical behavior

The compliant mechanism of a precision weighing cell represents a compromise between mass sensitivity in measurement direction and rigidity for all other directions. The lateral force components have different causes: Tilt angles between the vector of the gravitational acceleration \vec{g} and the z axis of the weighing cell result in lateral force components. Eccentric mass positioning on the weighing pan (off-center load) is another source of lateral forces since additional torque is applied relative to the reference position of the weighing pan. Mechanical models of weighing cells are highly relevant for the analysis, synthesis, and the adjustment of precision weighing cells.

Definition 2.2 (Off-center load). Off-center loading refers to a lateral misalignment of the center of gravity (CoG) of a sample mass on a weighing pan with respect to a reference position (typically the centerline of the coupling element (parallel to \vec{e}_z)). Eccentricities are considered in \vec{e}_x and \vec{e}_y direction.

Some basic definitions from the literature are recalled using a typical example, the mathematical pendulum supplemented by a torsion spring. A graph is given in Fig. 2.5 with exemplary torque-displacement curves for quasi-static deflections. Stiffness is typically associated with the elastic deformation of a structural element.

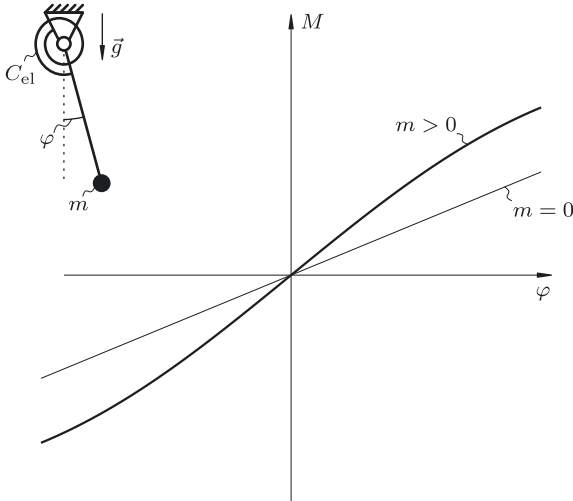


Figure 2.5 – Stiffness of a simple pendulum having two sub-types: *elastic stiffness* and *geometric stiffness*. ($m = 0$) - *elastic stiffness*; ($m \geq 0$) - *elastic stiffness + geometric stiffness*.

Here, a torsional spring represents a linear-elastic stiffness in the 1-degree of freedom (DOF) pendulum model. In literature, this type of stiffness is referred to as elastic stiffness, see, e.g., [Lac13]. The torque is a linear function over the deflection angle, if the pendulum’s mass is zero. For a mass $m > 0$, the linear stiffness characteristic is superimposed by a nonlinear component which is a gravitational restoring torque. This stiffness is referred to as geometric stiffness [Lac13], and in more specific literature the term gravitational stiffness is used [Pfe96]. The combination of elastic stiffness and gravitational stiffness is highly relevant for the adjustment of weighing cells. The following subsection reviews the modeling approaches applied to precision weighing devices in the revised literature.

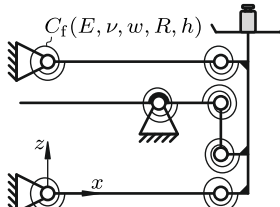
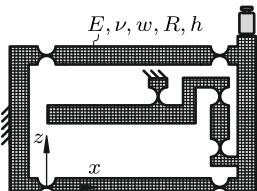
2.4.1 Mechanical models of weighing devices

The first known mechanical models for weighing devices have been developed for equal arm balances with knife-edge bearings. These models are based on rigid body model assumptions. However, details like the finite radii of the knife-edge bearings, their measurement, and the corresponding change in arm length of the beam balance

have been included [Con22; HC52; Wal55]. The authors in [Pin+07] derive a rigid body model for a flexure hinge-based equal-arm beam balance. The finite element (FE) method was applied in [Bau15] to optimize a dynamically operated EMFC weighing cell and its control design. The authors in [Mar+17] derive an analytical model for EMFC weighing cells with linearized equations for the stiffness and tilt sensitivity of the mechanism verified based on multi-body simulations. This work includes adjustment measures and considers the influence of a change in the geometry of the mechanism.

Dynamic models of EMFC weighing cells have been investigated in [Bee83]. The author distinguishes between systems with and without lever transmission. A third-order system would be adequate for the latter, while the first would require 15 orders to be sufficiently accurate. The mechanical modeling is based on a rigid body model with spring and damper elements between bodies and attached point masses. A comprehensive model for the dynamic behavior of EMFC weighing cells has been developed by FRANZ [Fra93]. This model is based on an elastic multi-body system where elastic deformations of relevant structural parts within the mechanism are considered using the RITZ approach. The RITZ trial functions for complex geometries are derived from the Eigenmode which is determined by preceding FE computations.

Table 2.1 – Modeling approaches for the compliant mechanisms of weighing cell.

rigid body model	finite element analysis
	
rigid links pivots (1-DOF) const. rotational stiffness (according to [Tor18]) no deformation quasi-static/dynamic planar analysis - only first Eigenmode linearized analytical solution, multi-body simulation (numeric) low computational effort e.g.: [Zen14],[HMO13]	deformable links flexure hinges (6-DOF) stiffness matrix (nonlinear) deformation of links and structure quasi-static/dynamic three-dimensional analysis evaluation of stress state higher-order Eigenmodes numeric high computational effort [Bau15]

The common trade-off is between a simple model and the consideration of all significant influences affecting the properties of the weighing instrument. A modeling approach for a precision weighing device was selected according to the objective of the respective analysis. For example, to estimate the stiffness of the mechanism or to design a controller, it was sufficient to use simple models based on the rigid body model in Tab. 2.1. For other calculations, like determining the tilt reaction in two axes or the influence of off-center load on the weighing pan, a three-dimensional model was required to cover the corresponding mechanical effects within the structure.

2.4.2 Astatization

The stiffness C of the weighing cell's monolithic mechanism is highly relevant. The stiffness is given as the difference quotient between force and linear displacement at the weighing pan unless otherwise stated. Hence, the stiffness indicates the amount of force required to introduce a certain deflection of the mechanism.

In analogy to the distinction of the parameters *sensitivity* and *sensibility* (see Sec. B.1), the stiffness can either be purely mechanical or under further consideration of actuator and position sensor. The pure mechanical stiffness is given the variable C , whereas the weighing system stiffness is assigned C_{EMFC} . Given a resolution of the position sensor, C_{EMFC} can be used to derive the mass resolution Δm at the weighing pan with a given resolution of the position sensor.

The sensitivity of the weighing cell defines the minimum resolvable mass changes if particular readability of the angular deflection is presupposed. A very high sensitivity thus limits the permissible load imbalance in the system due to the resulting large deflections. However, this restriction is not valid for an EMFC balance with closed-loop control. Therefore, it is favorable to attain a mechanical stiffness of zero, which corresponds to an infinite sensitivity.

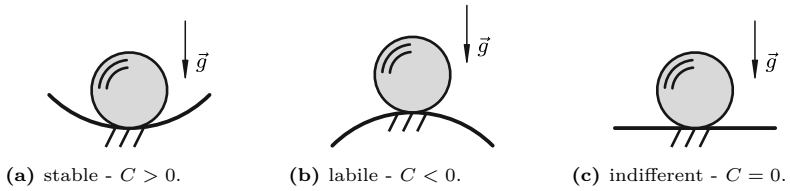


Figure 2.6 – Equilibrium types of mechanical systems after [GF11].

Astatisation, see Def. 2.3 is a measure to enhance the sensitivity of a measurement device to reach a state preferably close to an indifferent equilibrium (cf. Fig. 2.6c).

Definition 2.3 (astatization). Measure to transform a physical system into an indifferent state, in which the created astatic system shows no response to at least one external parameter. A mechanical system takes the indifferent state for $C = 0$ and an external displacement results in no reaction force and no change in potential energy. In force measurement applications, approaching the astatic state equals an increase in sensitivity.

A weighing cell in an ideal astatic state additionally makes the force measurement invariant to the deflection state of the mechanism. Invariance means that the output parameter shows no correlation with an input parameter. Thus, the error component of the position sensor can be eliminated for an ideal weighing cell and mitigated for a real system.

An illustrative example for the indifferent state is the sphere on a perfectly flat plane perpendicular to \vec{g} , see 2.6c. The sphere is stable, independent of its position on the plane. In other words, there is no restoring force acting on the sphere.

The astatic state is highly favorable for mechanisms used in EMFC weighing cells since restoring forces limit the sensitivity of the weighing device and contribute to the measurement uncertainty through imperfections of the position sensor. Astatization enables the design of compact measurement devices with properties of systems that would have to be designed impractically large without astatic adjustment.

The term astatization is frequently used in measurement devices used in geophysical instruments like seismometers or gravimeters. Fig. 2.7 shows different solution principles for astatic systems. Each system involves a component with a positive

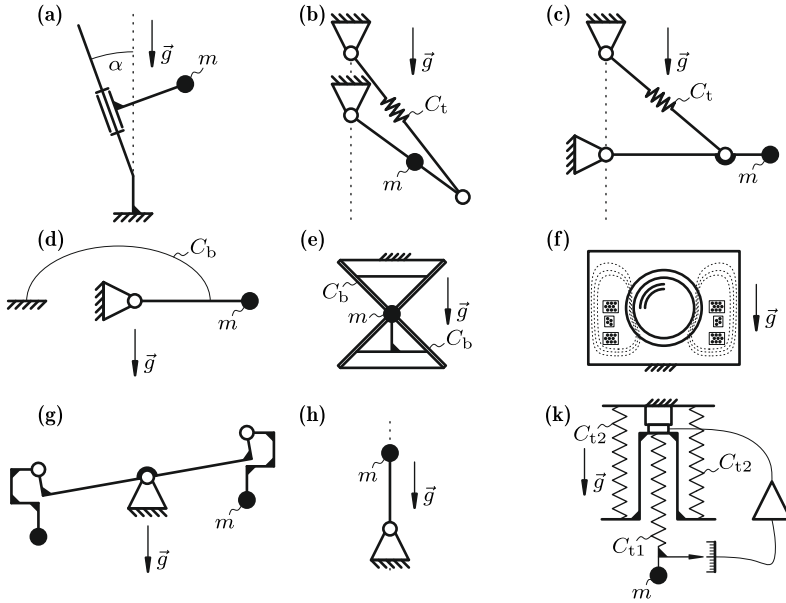


Figure 2.7 – Concepts for astatic systems: (a) garden gate suspension [Wie10], (b) pendulum with pre-tensioned tension spring, (c) LA COSTE suspension [LaC34], (d) leaf spring suspension [Wie75], (e) cross-flexure pivot under tensile load [Wit48], (f) magnetic constant force levitation [Goo99], (g) nonlinear transmission ratio [Wal55], (h) trim masses (inverted pendulum), (k) FALLER-RINKER super spring [FR80].

mechanical stiffness and an adjustable negative stiffness component. If both absolute values are equal, the system is in an indifferent state. This way, astaticization measures enable measurement devices with a high sensitivity to the measurand. A torsion pendulum stiffness adjustment with tilt corresponding to Fig. 2.7 a) is described in [Pet90]. A zero stiffness flexure hinge according to the principle in Fig. 2.7 b) is presented in [Eas35] and [MH10]. Figure 2.7 c) and d) are different concepts that have been applied in seismometer and gravimeter designs. Principles f) and k) deviate from the pure mechanical principles. The principle in f) is a magnetic levitation system used in superconducting gravimeters. The magnetic field is shaped such that the force-displacement curve has a gradient close to zero around the operating point. Principle k) is a super spring that is artificially elongated using a closed-loop control. This way, systems with ultra-long periods can be designed. A cross flexure pivot with leaf springs Fig. 2.7 e) under tensile load with its application

point in the initial center of rotation (CoR) approaches negative stiffness values for increasing load [Wit48].

A well-established method in weighing technology is the use of vertically adjustable trim masses to adjust the sensitivity, which corresponds to Fig. 2.7 h). Formerly, these trim masses have been referred to as poise weights [Eas35]. The stiffness- or sensitivity effect of the adjustable trim mass as well as a load dependent change of the stiffness resulting from a vertical offset of pivots, as shown in Fig. 2.7 g), has been discussed in early publications on equal arm beam balances. The sensitivity

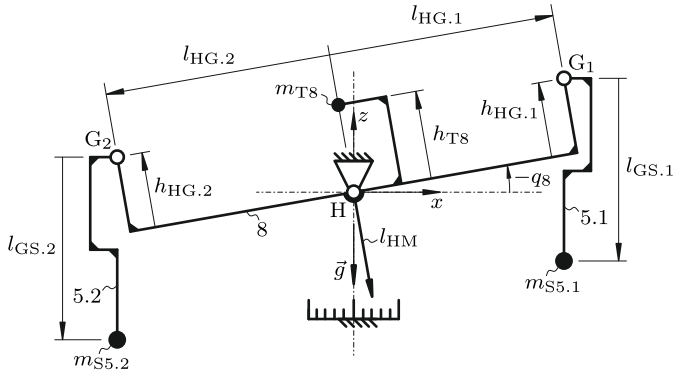


Figure 2.8 – Mechanical model of an idealized equal arm beam balance in the notation used throughout this work: trim masses and corresponding lengths are assigned with T and the number of the body they are attached to; the lengths are denominated l for horizontal- and h for vertical dimensions. The index notation includes the starting point and the end point to avoid ambiguity concerning the sign.

of knife-edge and flexure strip beam balances has been modeled by many authors [Wal55; CD82; Spe87; Qui92]. The resulting equations have good readability as they are derived based on rigid body model assumptions. According to the small-angle approximation, linearization around the zero position is another common simplification. CAGE et al. derive an isostability diagram based on the MATHIEU equation with an indication of the optimal solution for a precision balance [CD82], which combines the attributes of low damping and high sensitivity.

WALDERSEE has used his experimentally verified model to identify the geometrical parameter defining the load dependency of the balance sensitivity [Wal55]. In the rigid body model in Fig. 2.8, the parameter h_{HG} represents this parameter. For the knife-edge balance, this is the vertical distance between the central knife (H) and

the terminal knife edges (G1, G2). The effect depends on the radii of the knife edges used [Wal55]. This effect has been confirmed in [Spe87], where the consideration is extended to flexure strips. After noting different definitions in the mechanical model, the authors in [CD82] come to the same conclusions. The stiffness effect C_{HG} resulting from the parameter h_{HG} is consistently modeled as:

$$C_{HG} = -m_G g h_{HG} \quad [C_{HG}] = \text{N m rad}^{-1}$$

An increase in sensitivity - or a destabilization of the mechanical system - can be obtained by shifting the CoG of the balance beam in the opposite direction of \vec{g} [GB09]. This negative stiffness contribution is exactly the stiffness effect of the trim mass C_T described earlier:

$$C_T = -m_T g h_T \quad [C_T] = \text{N m rad}^{-1}$$

However, the decrease in stiffness is gained at the cost of an increase in the disadvantageous tilt sensitivity. For this reason, a limit in stiffness for an equal arm balance of 4 N m^{-1} is mentioned in [Pin+07].

2.4.3 Ground motion and tilt sensitivity

A common issue in precision engineering and instrumentation is that the earth's surface, against our daily perception, is always in motion. There are many sources of disturbances that affect the base frame of the precision instrument. [LS18]:

- machines, airplanes, vehicles
- wind load on buildings, floodings
- acoustic noise
- distant seismic activities
- deformations due to tides and the position of the moon
- thermal effects

It is generally recommended to locate precision balances in the basement of a building [CW80]. To further reduce the introduction of dynamic ground effects, the weighing device is placed upon a heavy weighing stone in combination with elastic support with a preferably low stiffness acting as a mechanical low pass [CW80]. Vibration criteria for metrology laboratories are defined in [Bes+99].

Evidence for tidal effects of $20\ \mu\text{g}$ amplitude on a precision beam balance with a period of a month are reported in [Dat+03]. Smaller diurnal effects are mentioned as well. Table 2.2 provides a literature survey for measured ground tilts in different locations to estimate common amplitudes of ground tilts. The natural sources (RAYLEIGH waves) lead to relatively small ground tilts of $\approx 200\ \text{nrad}$ [GJJ07]. Laboratory measurements reveal larger values due to additional, mostly artificial, influences in the near surrounding [Küh+14a]. These so-called cultural noises have periods between 0.05 to 0.2s, whereas earth tides and oceans cause variation with periods of 2 to 10 s [Han95].

Table 2.2 – Measured quasi-static ground tilt - a literature survey.

description	tilt amplitude / (nrad)	reference
WNW tilt with a 12.5 h period [Ilmenau, Germany]	<100	[Küh+14b]
max. amplitude in 33 h [Ilmenau, Germany]	125	[KFF18]
Mt. Etna [Italy]	150	[Fer+11]
borehole tiltmeter 24 m deep [California, USA]	100	[KL93]
sea bottom analysis [Tokyo, Japan]	500	[Tak+11]
person (70 kg) passing by a weighing stone in the laboratory [Ilmenau, Germany]	500	[Küh+14b]
person changing the position relative to tilt sensor (mounted on 660 kg steel slab on concrete foundation) [Australia]	1000	[Che+02]
own measurement in laboratory [Ilmenau, Germany]	4000	-

Quasi-static rotations of the earth’s upper crust are in the 100 nrad range. However, these measurements are recorded by borehole tiltmeters located several meters below the surface. Other effects are superimposed on the surface, where laboratory building are typically located. These stem from human activities, distant earthquakes, local winds, atmospheric pressure changes, and heavy rainfall. Evidence has been made that these effects can produce local tiltings in the single microradian-range.

Exposed to ground tilts, a tilt-sensitive weighing cell shows erroneous changes in indication. It can be distinguished between two directions of tilt: a *pitch* motion (Θ) about the rotation axis of the transmission lever (y axis) and a *roll* motion (Φ) about the axis of the transmission lever (x axis). The tilt sensitivities D_Θ and D_Φ are given in N rad^{-1} . Their sign depends on the tilt angle and the resulting force at the weighing pan. The force is always projected to a force at the weighing pan and is considered a positive sign if it corresponds to a rising mass indication. In Fig. 2.9 the negative tilt angle combined with a positive vertical distance of the trim mass imposes an additional torque on the lever, resulting in an apparent

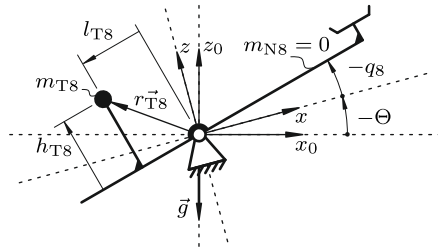


Figure 2.9 – Definitions concerning the tilt sensitivity of a simplified weighing system. For $\Theta = 0$, the system is in the static equilibrium.

negative mass change on the weighing pan $-\Delta m$. By definition, the tilt sensitivity has a positive sign. A negative adjustment parameter $-h_{T8}$ yields a negative tilt sensitivity.

In 1922, CONRADY discovered the possibility to adjust equal arm beam balances with three knife-edges to a state with high sensitivity and low disturbance [Con22]. CONRADY coined the term autostatic state and explained the reduced disturbance of his balance by insensitivity to ground tilt. Essentially, the center of mass of the balance beam is adjusted vertically until it coincides with the center of rotation or the vertical position of the fixed centrod of the balance beam. The discovered phenomenon of the autostatic adjustment was considered in [Spe87] to develop a 1 kg-mass comparator. The autostatic state was mechanically described in theory for knife-edge bearings and flexure hinges. By adjusting the CoG of the balance beam in the CoR, the stiffness and the rotational inertia are manipulated. Naturally, this results in a change in the natural frequency of the mechanical system. Thus, some authors refer to the autostatic period when talking about an autostatically adjusted balance [Sho+97]. PICARD has described the autostatic adjustment as a tedious but necessary adjustment for the proper operation of a mass comparator. For the BIPM FB-2 balance, a tilt sensitivity as low as $2 \times 10^{-5} \text{ N rad}^{-1}$ at the weighing pan has been achieved [Pic04]. The tilt sensitivity can be measured by introducing quasi-static tilts of the foundation, e.g., by displacing heavy weights [Nes+09].

Additionally, a dynamic description of the system can be found in [Spe87]. An essential and favorable conclusion drawn in [Spe87] is that a beam balance in the autostatic state is insensitive to quasi-static ground tilt and insensitive to horizontal ground vibrations. The bespoken horizontal ground vibrations also trigger the

pendulum-type hanging weighing pan oscillation. The pan swing leads to additional dynamic forces at the coupling point to the balance beam, horizontal and vertical. The vertical component is the centripetal force that constrains the rotary motion of the pendulum in the radial direction. The horizontal or tangential component reaches its peak value at the turning points of the pan oscillation. In [CD82], it is concluded that the effect of the tangential component is larger than the centripetal component if the deflection of the beam is more significant than the amplitude of the oscillation of the hanging weighing pan. Vertical ground vibrations can generally be ignored for the equal arm beam balance in equilibrium as long as no swing of the hanging weighing pans is triggered. This excitation would occur if the vibration frequency is twice the natural frequency of the pan swing [Qui92]. Damping of pan swing has been realized by eddy-current dampers [Qui92] and controlled external impulses [Wen92].

Assuming ground vibrations cause the coil to move within the actuator's magnet system, the slightly nonlinear characteristic curve of the actuator constant $Bl(z)$ would result in a measurement error, see [Fra93] and [MPS16].

2.4.4 Off-centre loading

The sensitivity of a weighing cell structure to eccentric masses on the weighing pan is deeply related to geometric imperfections concerning the parallelogram linkage guiding the weighing pan. Ideally, all lateral force components relative to the measurement direction are directly guided to the base without influencing the force balance in measurement direction. If the parallelism of the parallelogram guide levers is not given, as shown in Fig. 2.10, the additional torque of an eccentric mass on the weighing pan increases or decreases the indicated mass of the mass comparator. The off-center load sensitivity indicates the magnitude of the erroneous behavior of the weighing cell. If the levers were perfectly parallel, the off-center load sensitivity would be zero, and off-center loads would not impact the indicated mass. Finite accuracy for centering sample masses on the weighing pans of a balance is especially problematic for manually operated balances. Assuming a sample mass of 1 kg is placed on a weighing pan with an offset of 1 mm. Then, the balance is loaded by the exact same mass, but the additional torque of about 10 N mm is exerted on the load carrier of the weighing cell. If the indication of the balance differs as a result of the additional torque, the balance is sensitive to off-center loading. Equal arm beam balances have been equipped with hanging weighing pans to mitigate the problem of off-center loading by the self-centering behavior of the

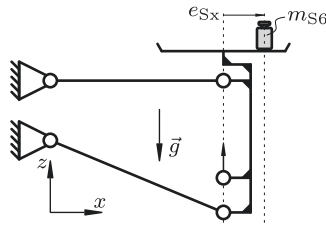




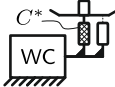
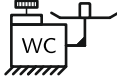
Figure 2.10 – Definition of the off-center load sensitivity with a pronounced angular deviation of the lower lever. The off-center load sensitivity is positive, since the mass indication increases with growing positive eccentricity (sample mass eccentricity in x e_{Sx}).

gimbal-mounted pendulum-type hanging weighing pans. Top-loaded balances are preferred to achieve a more user-friendly weighing process with reduced weighing times and better accessibility of the weighing pans, The ROBERVAL mechanism enabled this type of table-top balance by directing the additional torque from a non-centered weight directly to the base. In other words, the balance is guided almost linearly by a parallelogram linkage [Koc89; Nat+08; RJK14].

Present analytical balances are equipped with a quasi-linear guide in the form of a parallelogram linkage. Imperfections in the geometry of the parallelogram linkage result in an off-center load sensitivity. However, this means that the indication varies depending on the sample mass position on the weighing cell [Met96; Cho+04]. METZING derives equations for the estimation of the off-center loading error in two axes and proposes a sensor-based electronic compensation concept to circumvent tedious and costly mechanical adjustments [Met96]. The principle of D’ALEMBERT has been applied to derive the effect on the indication of the weighing cell. The equations indicate that the parallelism of the parallelogram levers can be restored by adjusting the positions of the rotational joints. In modern EMFC weighing cells, patented solutions exist to realize the bespoke adjustment, mainly by a set screw and an additional compliant mechanism [Cho+04]. Plastic deformation of the compliant adjustment mechanism would be beneficial for the long-term stability of the adjustment [EP 2615433 B1]. Other concepts realize the tiny adjustment motions by thermal expansion of structural parts [EP 1409971 B1]. Many patents provide sensor solutions to indirectly measure the off-center load and electronically correct the error in indication, see Tab. 2.3. Additional automatic and reproducible sample mass centering mechanisms have been introduced for top-loaded balances, see Tab. 2.3. In mass comparators, the hanging weighing pan is gimbal-mounted, which

reduces the magnitude of the introduced torque and thus reduces the adjustment demands on the parallelism adjustment, see Tab. 2.3.

Table 2.3 – Solution principles for counter-measures against off-center loads on the weighing pan.

gimbal mount ^a	centering ^b	correction ^c	int. measures
			
[BM60] [Qui92]	[DE 4103619 C1] [PD98]	[DE 102008062742 B4] [WO 2010054743 A1] [EP 2041531 B1] [DE 102009015029 B4] [DE 19502694 C1] [Met96]	[DE 9404206 U1] [EP 0393323 A1] [DE 9010327 U1] [WO 2008145427 A1] [CH 698191 B1] [EP 1409971 B1] [DE 19741584 C1] [EP 2615433 B1] [Cho+04]

^a mass comparators

^b top loaded analytical balances (*Centermatic* (Sartorius), *Levelmatic* (Mettler Toledo))

^c different concepts

2.4.5 Deformations within the weighing system

Forces deviating from the measurement direction introduce parasitic deformations within the mechanism of the weighing system. These deformations displace attached components of the EMFC system. The nonlinear response resulting from a varied position of the coil within the magnet system has been determined experimentally [Pfe96], [Die17] and numerically [Die17], [Mar+18].

The optical position sensor ideally detects deflections of the transmission lever in z direction only. In fact, the design is largely unaffected by lateral displacements of the aperture slit, which is mounted to the transmission lever of the weighing system. These effects have been discussed in [Mar19]:

- the sensitivity linearly increases if the aperture slit is moved laterally from the light emitting diode (LED) towards the dual photodiode

- a relative positioning of the aperture slit in measurement direction away from zero position leads to a quadratic decrease of the sensitivity

An analytical model for the characteristic curve of the position sensor under manipulation in all 6 degrees of freedom is developed in [Pfe96]. PFEIFFER considers the elliptical light intensity distribution of the LED to increase the accordance between measurement and model.

2.5 Chapter summary

The state of the art starts with a general description of the mass comparator system, followed by a brief description of the historical development. The focus then shifts to the performance of the system and its quantification, followed by a selection of error sources for the weighing process. The content is narrowed down to the mechanical behavior of analytical balances and mass comparators. Finally, this section outlines the literature review on mechanical modeling and selected mechanical effects relevant to this work. It also includes mechanical correction and adjustment measures that will be expanded and enhanced throughout the present work.

Chapter 3

Scope and objectives of the present work

High-accuracy weighing devices have been under constant and intense development for decades. Over time, researchers have scrutinized every detail from the mechanical design and its periphery to the opto-electronic components and evaluation strategies for mass comparisons.

Besides rare exceptions, the state of the art identified a clear trend towards compliant mechanism design in precision instrumentation. The comparison to knife-edge bearings highlighted the advantages of compliant mechanisms for a mass comparator application with the obligatory mass exchange during the measurement. Furthermore, the best possible mechanical behavior is achieved with monolithic mechanism designs, for it does exclude mechanical interfaces and the related complex mechanical disturbance.

Extremely thin flexure hinges provide the required elastic stiffness values of current weighing mechanism between 50 N m^{-1} and 200 N m^{-1} . A further decrease of the elastic stiffness of the weighing cell mechanism enhances the resolution. Reducing the flexure hinge thickness beyond the present limit at about $50 \mu\text{m}$ is problematic from a manufacturing perspective, increases the mechanical stress, and decreases the safety margin for fatigue. Hence, other measures are required to reduce the elastic stiffness.

A gravitational stiffness component is added by vertical trim masses. As the literature review in Ch. 2 reveals, the trim masses also affect the tilt sensitivity. The required independent adjustment of stiffness and tilt sensitivity to zero is thus impossible without further measures. Further developed mechanical concepts and simple to implement adjustment solutions are required to adjust the mechanical properties independently.

The field of gravimetry is a complementary field to mass metrology since both measurands are part of the same physical law (cf. (1.2)). Being linked by the same fundamental physical principle, the parallels in instrumentation are numerous: weighing cells and gravimeters require high force sensitivity in measurement direction. To enhance further the sensitivity of the measurement instruments, astatization was introduced by LACOSTE in 1934 [LaC34]. The geometric design of the mechanism destabilizes the mechanical system. Gravimeters are astatized mechanical systems meaning that the mechanical stiffness is adjusted close to zero. The successful implementation of astatization in a monolithic weighing cell is the critical measure in achieving the objective of this work.

The objective of the present work is to find ways to further increase the performance of mass comparators based on EMFC weighing cells. Without neglecting the impact on other subsystems, the clear focus is on the mechanical part of the weighing system, namely its highly specialized compliant mechanism. The critical properties of this mechanism are stiffness at load carrier C , tilt sensitivity at load carrier D , and off-center load sensitivity E_L . These mechanical sensitivities are a current limitation to the achievable measurement uncertainty. Adjusting the mentioned mechanical properties to small residuals thus enhances the mass comparator system.

An overarching treatment of the complex overall system of the mass comparator is beyond the scope of the present work. The considerations are focused on the mechanical system of the EMFC weighing cell with the following preconditions:

- sample mass restricted to 1.000 ± 0.002 kg,
- no consideration of inertia effects,
- material for mechanism fixed to high-strength aluminum alloys,
- no consideration of thermal effects,
- validity of HOOKE's law,
- other components of the EMFC system, like position sensor, actuator and control, are treated in a simplified manner,
- design for measurements under high-vacuum conditions.

Definition 3.1 (Objective of this work). Realize an astatic monolithic weighing cell based on the principle of electromagnetic force compensation with fine adjustable mechanical properties:

- stiffness C ,
- tilt sensitivity D ,
- off-center load sensitivity E_L ,

and by that allow for mass comparisons between 1 kg reference masses with a measurement uncertainty of <5 ng.

The fulfillment of the following criteria are required to achieve the goal:

- increase of the mass/force sensitivity of the weighing system,
- reduction of the sensitivity to external disturbances,
- extension of the mechanical models,
- conceptualization and implementation of a method for the independent adjustment of stiffness and tilt sensitivity,
- realization of in-vacuo adjustment to achieve the required adjustment resolution,
- mitigation of manufacturing influences on the mechanical properties,
- simplification of the manufacturing process.

To achieve the stated objective, the adjustment concept, measurement methods, and prototype weighing cells were designed and tested in the following chapters starting with two modeling chapters in Ch. 4 and 5. Building on these chapters, prototype weighing cells and their experimental investigation are described in Ch. 6. The concept development for the final mass comparator prototype started with a refined and extended metrological model for the weighing system in Ch. 7. The final concept and the solution for the enhanced mass comparator system are described in Ch. 8.

Chapter 4

Flexure hinges

One central aspect of mechanical weighing systems is the design of its bearings. The bearing behavior defines the resolution of the weighing device, affects the repeatability of the indication, and thus enables mass comparisons with small measurement uncertainties.

4.1 Review of bearings for precision instruments

Knife-edge bearings, which belong to the bearings with rolling or sliding friction have been extensively applied in instrument and balance design [Dav72b]. Especially, the rolling type of the knife-edge (cylinder - plane contact) has close to ideal properties since the rolling friction is two orders of magnitude smaller than the sliding friction [Kra04b]. The shift of the instantaneous center of rotation can be effectively minimized using a small radius. Load capacity and the right choice of the material combination is critical for knife-edges, see [Ash11],[Nea13].

The rolling type knife-edge bearing, used at the time CONRADY examined his balances, also denoted as fulcrum or stirrup, constituted knife-edges with preferably small radii. The use of this type of pivot in balances has required great care by the operator [Con22]. Common known errors for balances stemming from rolling-type knife-edge pivots have been identified in [BA63]:

- finite positioning accuracy in releasing the knife-edge couplings (nonplanarity of flats/anvils)
- relative positioning error between pointer and scale of the position sensor
- unpredictable large jumps in the indication ($\Delta m = 150 \mu\text{g}$) due to external vibrations

- faulty parallelism adjustment of multiple knife-edge couplings
- load variations on the knife-edge
- eccentric load application in the direction of the rotational axis

Mitigation of the listed errors has been achieved by retaining the knife-edge always in contact [Gou49]. In addition, the performance has been improved by additionally maintaining a near-constant load on all knife-edge bearings during operation [BA63].

The effects at the frictional interface of the knife-edge bearing are difficult to describe and predict. Many of those can be attributed to the mass exchange procedure in balances. In applications where the mass exchange is not required, the knife-edge bearing has persisted for most demanding applications. In a recent application of a tungsten carbide knife-edge in a tiltmeter, the tiny relative motion between knife and anvil is seen as the deformation of contacting grains rather than an actual rolling behavior [Der+14]. The authors claim to have realized an ultra-thin bearing which is said to be comparable to a metallic flexure hinge - only producing less hysteresis [Der+14]. In the bespoke tiltmeter application, one central pivot has to be realized. In equal beam balances, at least three pivots have to be realized. The relative positions and the orientations of the contact lines can be realized only with finite accuracy, and a change in relative positions during the operation of the balance (especially mass exchange and arrestment) cannot be excluded. A small radius of the knife-edge is favorable for the kinematic properties of the pivot but reduces the load-bearing capacity. It is evident that functionally optimized balances require shielding against shock loads to prevent damage to the sensitive knife-edge bearings [Dav72a], especially when thinking about the shipment of the balance or a faulty behavior of the load exchange mechanism. Even though the knife-edge bearing has been applied successfully in the past, it comes with a number of disadvantages for the mass comparator application.

In 1935, EASTMAN published a paper [Eas35] with the title *Flexure pivots to replace knife edges and ball bearings, an adaptation of beam-column analysis* that proved to be programmatic for further developing precision weighing systems up to now. The change from a knife-edge to compliant pivots represents nothing less than the change from solid body contact to inner-material interfaces. It has helped overcome common problems with frictional contacts, like hysteresis, wear, and unpredictable stochastic effects. The first balances were realized with torsion strips or wires [Eas35]. Furthermore, it needs to be mentioned that the first known wooden

balances were suspended by strings [Koc89]. A recent example of the use of wire suspensions in a mass comparator is presented in [Bee+02].

The use of elastic elements as pivots mitigates many effects of the frictional contact but cannot entirely remove friction from precise weighing processes. Measurable effects arise from the real behavior of the material of the flexure hinges, which deviates from HOOKE'S law. The real behavior comprises the elastic after-effect, time-dependent creep, and hysteresis [Now14]. These effects lead to time-dependent changes of the balance indication and result in an erroneous reading. In precision weighing technology, adapted evaluation strategies are applied to compensate the effect of time-dependent indication changes [SS10; SC94; Glä00]. Anelasticity of the mechanical system can also be considered during the control design [Kuh03].

Monolithic flexure hinges show the highest technical merit for the mass comparator application. One of the reasons is the more robust and repeatable behavior during the weighing process considering the mechanical disturbance related to the obligatory mass changes. In weighing technology, semi-circular flexure hinges are frequently used due to the well-defined kinematic behavior. Kinematic behavior comprises a preferably small shift of the rotational axis over deflection and a high stiffness for loads deviating from the principal motion of the flexure hinge. In addition, semi-circular flexure hinges are comparably simple to manufacture. The thickness of the flexure hinge is preferably small due to the instruments' sensitivity demands, cf. Fig. 4.2. The minimal notch height h lies in the range of 50 to 100 μm , with even thinner flexure hinges ($h = 30 \mu\text{m}$) reported in [Eme01].

4.2 Classification of monolithic flexure hinges

The choice of a flexure hinge geometry for a weighing device is a trade-off between a well-defined kinematic behavior and minimal restoring forces for the intended degree of freedom. A classification of flexure hinge geometries was sketched, based on the two contrary properties. A qualitative overview under consideration of the demand on the manufacturing process is presented in Fig. 4.1. The semi-circular contour leads to a comparably strong concentration of compliance in the central region of the flexure. Flexure hinges only exceed this with a V-shaped contour (V-shaped flexure hinges (VFH)) [LZF16]. In addition, the strong concentration of compliance makes these contours stiffer than other contours ensuring minimal shifts of the rotational axis.

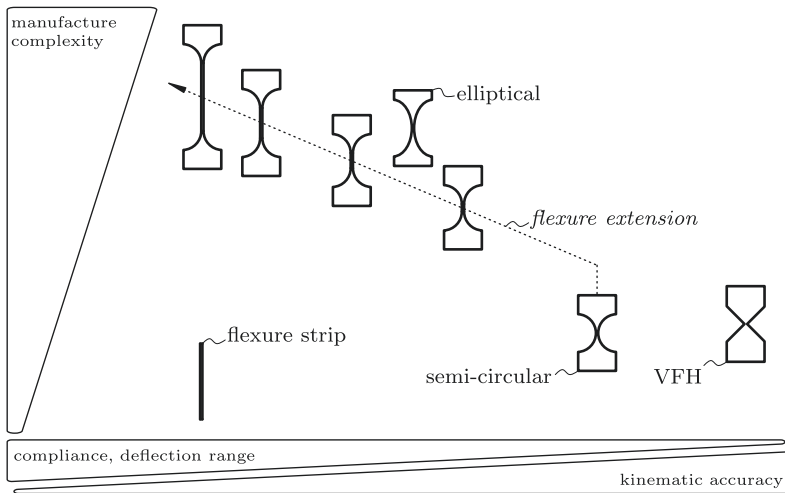


Figure 4.1 – Classification of flexure hinge contours with respect to compliance, kinematic accuracy and manufacturing complexity.

The properties of a flexure hinge can be gradually changed from low compliance to high compliance, here denoted as *flexure extension*. The transition is achieved by conceptually inserting a flexure strip in-between the halves of a semi-circular flexure hinge and changing its length. Despite the increase in compliance, the demands for manufacture are instantly increasing since rotary tools in plunge mode are no longer applicable. Precisely this strategy has been used to design the pivots for the equal arm beam balances in [QSD86; Qui92]. Using the equations in [Eas37], QUINN et al. have found that the effect reaches saturation in compliance gain after a few millimeters depending on the material [QSD86]. Without sacrificing much kinematic accuracy, the compliance in the principal direction of motion can thus be enhanced up to a certain limit. The relation was double-checked using a geometrically nonlinear finite element model; for a detailed explanation, see [Tor18].

Many authors are proposing novel geometric shapes to optimize towards a specific mechanical property [Li+19; Lin+20; Lin15; LSZ17]. Either, the focus is on kinematic accuracy [LZF16; Pin+16], or the thin region of the flexure hinge is extended to reduce stiffness, enlarge the working range, and to extend service life [Qui92; LEZ11].

The necessity in this work to externally compensate the stiffness of the weighing mechanisms renders a compliance increase of the single flexure, e.g., by extension insignificant. Especially, when considering the increased demand on the manufacturing process. Compared to the extended versions, for example, the motion range of the semi-circular flexure hinge is more restricted. However, this is not a relevant aspect in the design of a comparator weighing cell. In conclusion, this work exclusively relies on using the semi-circular flexure hinge geometry for all weighing mechanisms.

4.3 Mechanical modeling of monolithic flexure hinges

The rotational stiffness C_f about the z axis of the flexure hinge in Fig. 4.2 is a function of the geometric dimensions and its engineering material's mechanical properties. Figure 4.2 introduces the geometry parameters of the semi-circular flexure hinges used throughout the present work. The parameters and their associated uncertainty are listed in Tab. B.2.

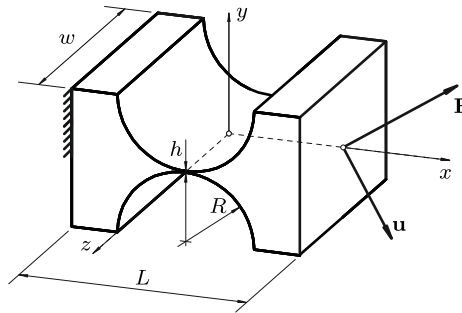


Figure 4.2 – Single semi-circular flexure hinge with geometric parameters.

4.3.1 Analytical models

Mechanical models in the literature are based on ideal geometries and homogeneous material properties [Fri16]. A stiffness matrix \mathbf{C} relates the load vector \mathbf{F} to the displacement vector \mathbf{u} , see Fig. 4.2¹.

$$\mathbf{F} = \mathbf{C}\mathbf{u}$$

The allocations in \mathbf{C} of the semi-circular flexure hinge are presented in (4.1), with its entries derived from the compliance terms given in [Kos+00], which are partly modified equations from [PW65]. The stiffness of the weighing cell mechanism in motion direction is defined by the last matrix row of this exemplary flexure hinge.

$$\begin{pmatrix} F_x \\ F_y \\ F_z \\ M_x \\ M_y \\ M_z \end{pmatrix} = \begin{bmatrix} C_1 & 0 & 0 & 0 & 0 & 0 \\ 0 & C_2 & 0 & 0 & 0 & C_7 \\ 0 & 0 & C_3 & 0 & -C_8 & 0 \\ 0 & 0 & 0 & C_4 & 0 & 0 \\ 0 & 0 & -C_8 & 0 & C_5 & 0 \\ 0 & C_7 & 0 & 0 & 0 & C_6 \end{bmatrix} \begin{pmatrix} u_x \\ u_y \\ u_z \\ \varphi_x \\ \varphi_y \\ \varphi_z \end{pmatrix} \quad (4.1)$$

The stiffness entries of the matrix in (4.1) are listed in (B.1). The rotational stiffness about the z axis is presented due to its relevance for the present work [PW65]:

$$C_f := C_6 = \frac{2 E w h^{5/2}}{9 \pi R^{1/2}} \quad (4.2)$$

The model equations (4.2) are based on the EULER-BERNOULLI beam theory, which presupposes several modeling assumptions. These are [Mah15]:

- plane within the structure without strain: neutral plane
- beam cross sections remain planar
- beam cross sections are perpendicular to the beam axis
- deformations due to transversal contraction are neglected
- homogeneous linear-elastic solid following HOOKE'S law
- slender structures - dimensions of cross-section smaller compared to the length

The last condition is not fulfilled by the geometrical shape of the semi-circular flexure hinges treated in this work. Verification of the provided equations in literature via

¹Note that in literature, \mathbf{C} is often the compliance matrix, whereas, in this work, the letter C is exclusively used for stiffness.

the FE method was required. For the flexure hinge geometry of interest, this has been thoroughly carried out by TORRES MELGAREJO in his master thesis [Tor18]. His results and recommendations enter the content of the following section for the development of a reliable FE model.

The engineering material used throughout the studies of single flexure hinges and weighing cell mechanisms are high-strength aluminum alloys, see Tab. B.1. The availability, costs, and machinability speak for the choice of aluminum alloys, at least throughout the development phase, while being aware of the favorable mechanical properties of special materials used in scientific instruments.

4.3.2 Finite element analysis

The FE method's fundamental concept is the discretization of a domain into smaller, simple to calculate subdomains. For example, the flexure hinge geometry with high aspect ratios is subdivided into smaller units, the finite elements. Several discretization approaches for flexure hinges have been proposed to approximate the mechanical behavior, see Fig. 4.3. The method of equivalent beams in Fig. 4.3

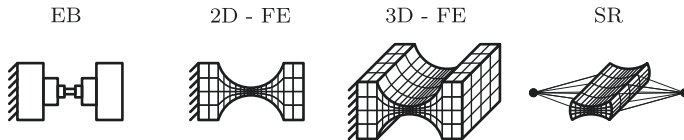


Figure 4.3 – Different approaches for the discretization of the flexure hinge geometry. EB - equivalent beams [ZSZ05a; FLR14], 2D - two-dimensional FE model, 3D - three-dimensional FE model and SR-3D(2D) - significant region [RLF15].

approximates the shape of the semi-circular flexure hinges with a finite number of beam elements with constant cross sections over their finite length [ZSZ05a]. The cross sectional height varies between the beam elements to replicate the circular notch. While having a high saving potential with a 1/1000 reduction in element number [FLR14], the solution can only be as accurate as the underlying beam theory. The use of finite beam elements with variable cross section, further reduces the required element number for the reproduction of the circular shape of the flexure hinge [FLR14].

Modeling the flexure hinge with two-dimensional (2D) elements saves a considerable amount of elements in the thickness direction, but it does not consider the transversal

contraction accurately. The most accurate solution - involving most computational effort - is a mesh independent (converged) three-dimensional (3D) model of the flexure hinge.

A promising addition to the 3D modeling approach is the significant region (SR) model. Due to the pronounced notch geometry, most of the stress concentrates within the central region of the flexure hinge. Only this *significant* volume is modeled with 3D elements, whereas the remaining geometry is treated rigid [RLF15].

For the modeling of a single flexure hinge, the high element number of the 3D model is not yet a limiting factor. Hence, this method was preferred for the creation of a reference model in ANSYS®. The reference model was then compared to the significant region model and a length d_{SR} was determined for which the agreement between the models was sufficient to about 1 %.

Meshing and setup of reference model

A structured mesh with hexahedral elements is preferred over a tetrahedral mesh to achieve an accurate model with minimal computational effort. The flexure hinge geometry can be created through extrusion of the shape along the z axis, compare Fig. 4.2. This allows a sweeping operation on the structured surface mesh. Meshing of the side areas is hampered by the pronounced height transition from several mm to $50\mu\text{m}$ at the center of the notch. A model with a homogeneous element size quickly runs into hardware issues in terms of model size with a minimum possible element size of about $60\mu\text{m}$ for elements with quadratic shape functions. The size of the elements in the central zone should thus differ from those in the stiff peripheral volumes. To avoid excessive distortion of the elements due to the harsh transition, the volume can be divided into several volumes which are meshed independently. Non-matching meshes at the interface are coupled via contact elements. The contact formulation in ANSYS® that combines minimal computational effort with the ability to consider large deflections is the multi point constraint (MPC) technique. It creates rigid links between the nodes of adjacent surfaces and can also be used to couple remote nodes to the surface of a solid. This was used for the application of boundary conditions and loads. Further, it facilitates the evaluation of reaction forces.

A reference model for a thin semi-circular flexure hinge is proposed in [Tor+18; Tor18]. The volume of a single flexure hinge is divided into three domains to be

able to adapt the local mesh to the specific demands. The size of the central zone is defined to have a bending stress value of 10% of the maximum stress at its boundary. The second zone is limited by the end of the circular contour. In a detailed mesh sensitivity analysis, the influence of mesh refinement in the distinct volumes was checked in [Tor18]. Especially, the size of the elements in x direction in the central zone was found to be highly relevant. This is followed by the elements size transition to larger element sizes towards the boundary of the central zone. The element size in the intermediate zone has a minor but not negligible influence on the result. Other changes to the element size, especially in the outer zone are insignificant, cf. [Tor18].

Following the findings in [Tor18], the model is simplified by enlarging the central zone and in turn omitting the intermediate zone, see Fig. 4.4. The boundary of the central zone was calculated according to

$$d_{\text{SR}}(p) = \frac{1}{2} \sqrt{-\frac{h \left(h - 2 h^2 \sqrt{\frac{p}{h^2}} + 4 R p + h p - 4 R h \sqrt{\frac{p}{h^2}} \right)}{p}}$$

and is located at the $p = 1\%$ bending stress level, which amounts to a radius of $d_{\text{SR}}(1\%) = 1.14 \text{ mm}$.

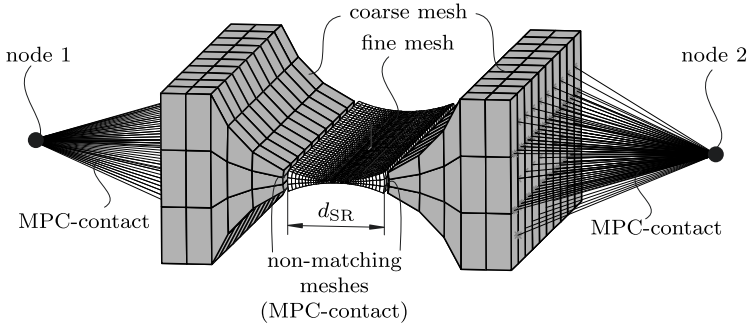


Figure 4.4 – Meshing strategy with refined central zone and coarse mesh on the peripheral volumes.

The pronounced notch and the corresponding stress concentration at the center of the flexure hinge indicates that refinement may be limited to the central region only. It even raises the question which portion of the total length is required to fully represent the mechanical behavior of the flexure hinge.

Significant region

The sole consideration of an elastic central region with a certain length has been discussed in [RLF15]. This region has been designated as significant region by RÖSNER et al., see Fig. 4.5 for a definition. The significant region is a volume of the flexure hinge enclosed by a cylinder with the main axis along z and a diameter of d_{SR} . This region is modeled elastic while the remainder of the volume is treated as rigid. The authors in [RLF15] define the d_{SR} such that the MISES equivalent

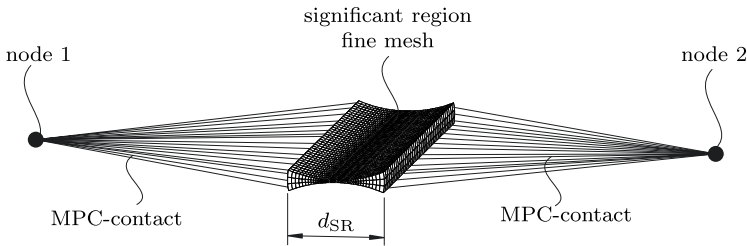


Figure 4.5 – Single flexure with separated significant region as a cylindrical cut-out region with a diameter of d_{SR} . In the mechanical model only this central region is modeled with solid elements, see Fig. 4.3 (SR).

stress from the maximum value to a specified minimum is included in the cylindrical volume enclosing the significant region. If the tolerance value, a relative value of the maximum stress, is decreased d_{SR} increases and vice versa. In this notation, the determination of d_{SR} has been conducted for the load case of a transversal force in y direction.

An application of the approach in a more general sense requires the consideration of other load cases, to check their agreement with the reference model for increasing d_{SR} . An investigation on the significant region model (cf. Fig. 4.5) for the load cases corresponding to the main diagonal of the stiffness matrix (4.1) has been conducted in the master thesis [Xu21]. The evaluation was complemented by the two off-diagonal entries in the stiffness matrix and the results are presented in Fig. 4.6 as relative values to the reference model (cf. Fig. 4.4). One of the findings is a far slower convergence for load cases other than bending about the principal z axis (C_2 , C_6). This is especially relevant for the loading with F_x , F_z and M_y . Here, the adjacent parts to the notch contour contribute relevantly to the overall compliance. For these load cases, convergence is achieved once d_{SR} equals the total length of the reference model. For the weighing cell application, the mentioned load cases are not of high

relevance. Also, the torsion load case can be neglected. It can be concluded that the significant region model yet allows an accurate representation of the principal mechanical properties of a semi-circular flexure hinge². These findings have relevant

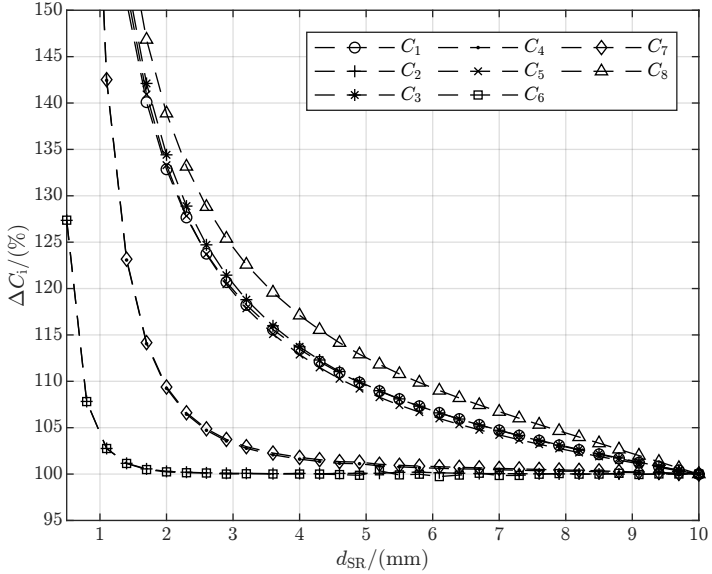


Figure 4.6 – Convergence of the stiffness matrix entries as a function of the size of the significant region d_{SR} .

implications for tolerancing, manufacturing and the geometrical measurement of the flexure hinge, since it can be sufficient to limit the efforts to the significant region. For the rotational stiffness of the flexure hinge C_6 , an effective length of the flexure d_{SR} of 2 mm is yet sufficient to predict the stiffness with an error of 0.01 %. In case of verifying a manufactured flexure geometry by dimensional measurements, accurate results can yet be expected for scanning the surfaces belonging to the volume $d_{SR} = 2$ mm. This equally holds for the manufacture of flexure hinges where the expensive and time consuming finishing processes can be limited to the significant region.

²Other hinge contours, e.g. for a corner-filleted flexure hinge [Har+22], d_{SR} is not significantly smaller than the length of the thin central part.

4.3.3 Transversal contraction

Having an aspect ratio w/h of 200, the typical flexure hinge geometry in this work cannot be regarded as a slender beam as presupposed in beam theory. The condition for *plane stress*, as assumed in many mechanical models of flexure hinges, would require the aspect ratio to be close to zero. In turn, for the *plane strain* condition the aspect ratio needs to be close to ∞ . Strictly, both conditions will never be met by real structural element [ZSZ05b]. This reveals the approximate character of the two model assumptions. The true behavior lies in between the two limiting cases. For a semi-circular flexure hinge undergoing small deflections ($\varphi_z \leq 1^\circ$), the transition has been approximated based on 3D FE calculations in [Tor+18]. Two characteristic ratios are defining the geometry and the correction factors: h/R and w/h . Accordingly, the transition from plane stress to plane strain is described by

$$K_z = 1 + \left(\arctan \left(0.653 \left(\frac{h}{R} \right)^{0.424} \frac{w}{h} \right) - 0.103 \frac{h}{R} - 0.557 \right) \left(\frac{\nu^2}{1 - \nu^2} \right). \quad (4.3)$$

However, the geometric shape of the semi-circular flexure hinge requires another term

$$K_x = 1 - 0.387 \frac{h}{R}. \quad (4.4)$$

The stiffening factor for the rotational stiffness is then written as

$$K_{xz} = K_x K_z. \quad (4.5)$$

Being derived from a three-dimensional FE model, the combination of (4.3) and (4.4) is covering a number of nonlinear effects present in a semi-circular flexure hinge. The support points for the fitting of the correction factors have been calculated in range of h/R from 0.015 to 15 and w/h from 10 to 100. The ratios for the standard flexure hinge geometry in this work is $h/R = 0.016$ and $w/h = 200$ where the latter is off the range displayed in [Tor+18]. However, the support points in [Tor+18] have been calculated up to a ratio of $w/h = 200$ and thus correction factors are still applicable.

4.4 Imperfections of thin flexures

Flexure hinges and compliant mechanisms are foremost manufactured from common engineering materials. Predominantly metal alloys are used. Specialized manufac-

turing processes are required to shape the final thin geometry of the flexure hinge. Process forces and heat input need to be minimized to introduce the least possible changes to the bulk material microstructure, to reduce the introduction of residual stresses, and to maintain the surface integrity to the extent possible. The manufacturing process of wire electrical discharge machining (WEDM) is well suited for precision parts with small wall thicknesses due to the absence of mechanical contact to the tool and the virtual absence of process forces [Koh01]. Machining capabilities allow high accuracy and low surface roughness. To further improve the surface finish, an electro-chemical polishing process can follow as proposed in [Xia+97]. A combined milling and grinding process for CuBe-flexure hinges with hardening prior to the grinding operation has been used in [Qui92]. Each manufacturing process leaves a characteristic surface topography on the notch surfaces which defines the effective minimum notch height of the flexure hinge.

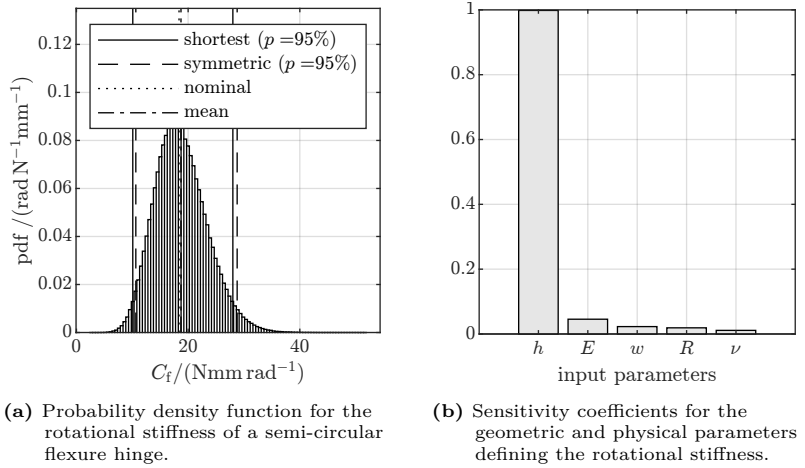


Figure 4.7 – Determination of the rotational stiffness of a semi-circular flexure hinge based on the simplified model equation in [PW65] and corrected to the *plane strain* state by the factor $1/(1-\nu^2)$. The input parameters are listed in Tab. B.2.

The rotational stiffness of the semi-circular flexure hinge is proportional to h with the exponent 2.5. Thus, manufacturing deviations influencing the value of h have a large effect on C_f . In contrast, the influence of surface roughness and waviness lacks a profound scientific investigation. Except for [Mer+07], no publication is known, that addresses the phenomena. In case of flexure hinges with a h between

50 to 150 μm , the effects due to surface topography can result in a decrease in stiffness by up to 40 %. The uncertainty domain of the rotational stiffness over the parameters h is presented in Fig. 4.8.

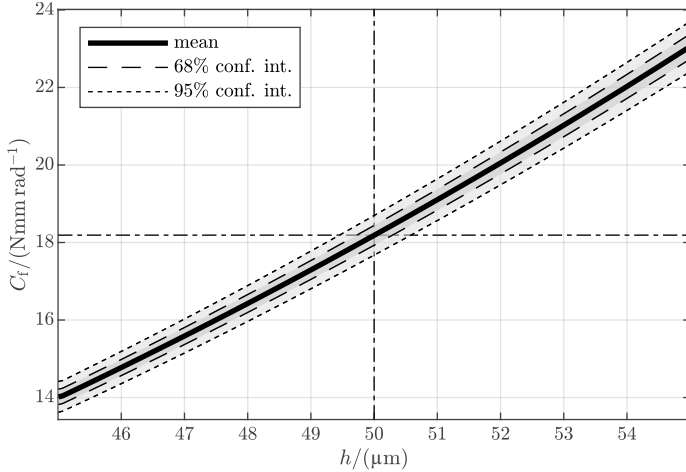


Figure 4.8 – Uncertainty of the flexure hinge rotational stiffness over minimal notch height evaluated using the MONTE CARLO method. The input quantities are assigned with uniform probability density function (PDF) as listed in Tab. B.2.

Surface effects as well as the state of the grain structure within the flexure hinge gain importance with decreasing h . Figure 4.9 provides a schematic sectional view of the central section of a thin flexure hinge with possible influence quantities on the mechanical properties of the flexure hinge. The importance of the surface as a special zone enclosing the bulk material and being affected by the shaping manufacturing process led to the development of the term: surface integrity. Surface integrity is a comprehensive description of all properties of the boundary layers from its topography to the physical changes regarding the bulk material [Dav10]. Certainly, surface integrity and the corresponding health of the surface is affecting the fatigue strength of a flexure hinge [Hen17]. Especially, the large opposing surfaces enclosing the thinnest section of the flexure hinge are relevant. Here, at the outer layer, the maximum of the normal stress builds up as bending occurs.

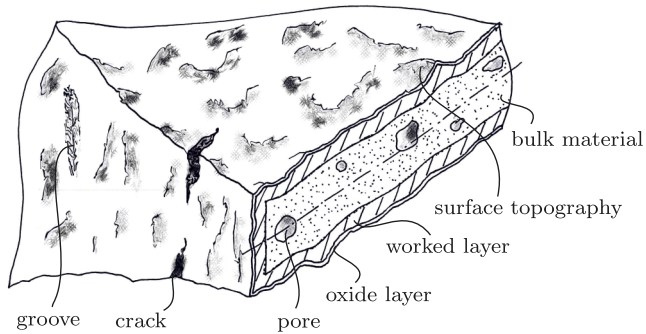


Figure 4.9 – Sectional view of a real flexure hinge with a minimal notch height in the range of $50\ \mu\text{m}$.

Geometrical deviations of the flexure geometry down to surface roughness affect the mechanical properties of the flexure hinge. Neglecting these effects in mechanical models frequently leads to large deviations between the model prediction and the measurement result. Due to the relevance of the flexure hinge stiffness to the application in a weighing cell mechanism, detailed investigation was performed, e.g. in [Cas+20].

It is quite clear that in the near future mechanical models will not be able to cover the rich spectrum of possible defects of a flexure hinge in Fig. 4.9 and it is questionable whether it is necessary. The inclusion of all defects in a model would also require their precise measurement to verify the models in experiments. This is presently impossible even though relevant progress is achieved e.g. in computer tomographic imaging with voxel sizes down to $3\ \mu\text{m}$ for small objects³.

4.5 Approaches for the determination of the rotational stiffness

Viable measurement methods for the elastic stiffness of single flexure specimens have been reported in the literature [DYD16; YL09]. The described setups are rather designed for flexure hinge specimen with a larger h and a considerably larger

³Zeiss METROTOM 6 scout (achievable resolution 2 parts in 100)

C_f . Considering the ultra-thin flexure hinges in this work, the proposed methods cannot be adapted directly. For a detailed characterization of the flexure hinges used, methods for stiffness determination have been developed and used throughout this work. The measurement results were presented as C_f and additionally using h_S as the substitute of h as defined in Def. 4.1:

Definition 4.1. The parameter h_S is introduced as the substitute minimal notch height of a flexure hinge. Measured values for the elastic stiffness $C_{f,\text{meas}}$ can be represented using h_S which provides an intuitive measure for the manufacturing deviations of a flexure hinge. The most basic way to calculate h_S based on [PW65] is

$$h_S = \left(\frac{9 \pi \sqrt{R}}{2 E w} C_{f,\text{meas}} \right)^{2/5}.$$

Solving other rotational stiffness models for h_S provides more accurate results, e.g., [Tor+18].

With the aim of a pure moment application on the flexure hinge, a test bench specifically for thin flexure hinges was designed in [Gar+18], further developed, and applied to flexure hinge specimen. The setup is referred to as flexure test bench and represents a quasi-static approach for the determination of the elastic stiffness.

4.5.1 Quasi-static stiffness measurement

The concept for the quasi-static stiffness measurement is inspired by a compensation mechanism for x-ray interferometry found in [Har68] which is later described in more detail in [SC92]. The concept involves a rotary drive with a pulley and a limp element suspended from the pulley and the body, the moment is applied to. HART has been using fine chain for this purpose. In the present work, an attempt is undertaken to eliminate the frictional contact between the chain elements using a tape - an ultra-thin precision metal foil. The objective is a high-resolution pure moment application in combination with a precise measurement of the resulting angular deflection of the specimen. Figure 4.10 shows the final configuration of the setup. The mechanical working principle with the relevant parameters and a front view of the measurement setup are presented in Fig. 4.11.

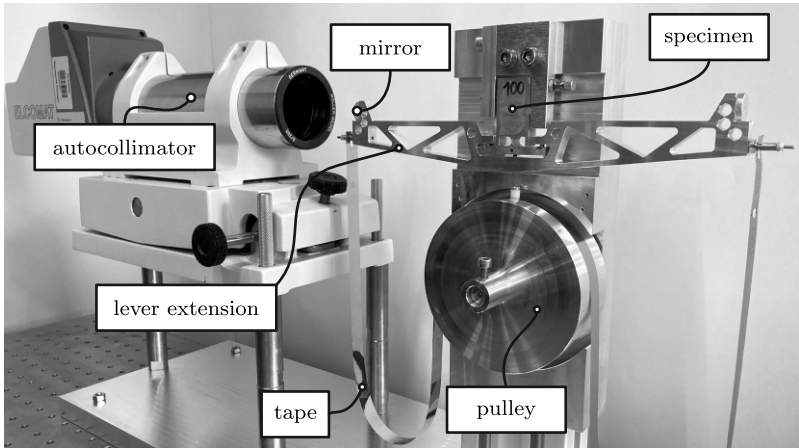


Figure 4.10 – The flexure test bench setup on an air-cushioned table in the laboratory surrounded by an enclosure to shield against air motions.

Measurement concept

The experimental setup in Fig. 4.10 has been developed throughout the master thesis [Gar+18]. The setup was designed to test semi-circular flexure hinges of aluminum alloy (cf. Tab. B.1) with a minimal notch height h ranging from $50\ \mu\text{m}$ to $100\ \mu\text{m}$, $w = 10\ \text{mm}$ and $R = 3\ \text{mm}$. The deflection of the lever extension with mounted plane mirrors is measured with a horizontally mounted electronic autocollimator (ELCOMAT 3000). The rotation of the pulley was realized by a servo motor with a high resolution encoder⁴ in combination with a harmonic drive gear box⁵ with a transmission ratio of $i_{\text{HD}} = 100$. The performance of the setup has been satisfactory [Gar+18]. However, the wide brass tape (2.0321 , $h_{\text{T}} = 20\ \mu\text{m}$, $w_{\text{T}} = 40\ \text{mm}$), used in the setup, had several disadvantages. First, its large width makes the setup very susceptible to air motions. Second, the presence of small irregularities like kinks thin foil could not be avoided. This led to unpredictable clicker effects resulting in instantaneous changes of the deflection angle. These spurious effects were mitigated by replacing the wide brass tape with a narrow stainless steel tape (1.4310 , $h_{\text{T}} = 10\ \mu\text{m}$, $w_{\text{T}} = 12.7\ \text{mm}$). This brought along an increase in moment resolution but a decreased maximal moment.

⁴Faulhaber 3242G024BX4 3692 IER3-10000

⁵HarmonicDrive CSF-11-100-2XH-J

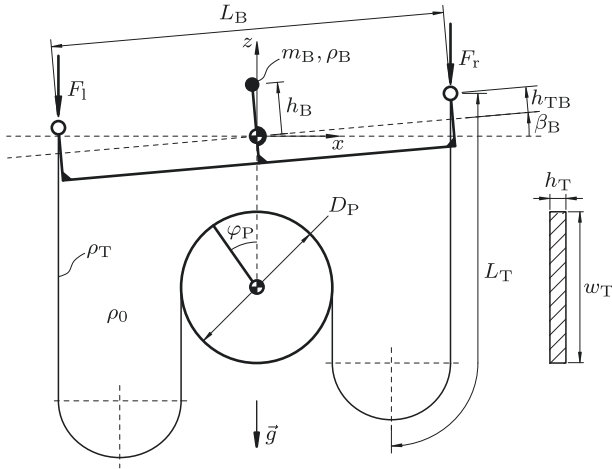


Figure 4.11 – Mechanical principle of the setup with most important parameters.

The moment is generated by a rotation of the central pulley (φ_P), see Fig. 4.10. The rotation shifts parts of the metal foil e.g. from the left to the right side, which increases the force on the right (F_r) and decreases the force on the left (F_l):

$$M(\varphi_P) = M_l(\varphi_P) - M_r(\varphi_P) = \frac{1}{2} L_B (F_l - \Delta F(\varphi_P)) - \frac{1}{2} L_B (F_r + \Delta F(\varphi_P)) \quad (4.6)$$

In the initial state, $F_l = F_r$ holds. Thus, (4.6) simplifies to:

$$M(\varphi_P) = -L_B \Delta F(\varphi_P)$$

The applied moment to the specimen is thus a function of the pulley rotation (φ_P) and the moment is generated without changing the tensile load on the flexure hinge. The absolute moment value additionally depends on the geometric and physical parameters of the setup, which are: the gravitational acceleration (\vec{g}), the dimensions of the tape (h_T , w_T , ρ_T), the diameter of the pulley (D_P) and the lever arm in-between the attachment points of the tape (L_B). A major advantage of the setup is its symmetry in horizontal direction which makes it largely insensitive towards environmental disturbance like temperature fluctuations and air pressure variations.

The ideal moment generation is affected by systematic effects:

- **Tape backward motion:** the deflection of the specimen and the beam extension counteracts the causal tape shift of the pulley and reduces the effective moment on the specimen. The effect is dependent on the measurand - the rotational stiffness of the flexure hinge under test.
- **Linearity:** thickness and width variations of the tape and imperfections within the pulley drive are possible causes for deviations from linearity of the generated moment. It can be approximated by deflecting a flexure specimen with known rotational stiffness and evaluate the linearity of the measured deflection angle.
- **Vertical position of CoG:** like a trim mass, the vertically eccentric CoG of rotating parts alter the measured stiffness.
- **Tape coupling position:** the stiffness is changed by a vertical distance between CoR and the support of the tape at the ends of the beam extension. The effect is proportional to the weight force of the tape acting on the support.
- **Cosine error:** as a result of the deflection of the specimen or the beam extension respectively, the effective lever arm is reduced by the factor $\cos(\beta_B)$. Due to the small angular deflections and the accurate definition of the operating point by the autocollimator, this effect was considered negligible.

Metrological model

The purely mechanical principle of the measurement setup is based on symmetry and its intended dissolution to generate a moment on the flexure hinge under test, see Fig. 4.10. The dimensions are chosen with the objective to deflect the flexure hinge in the measurement range of the autocollimator (1000'') with a pulley rotation limited to 10°. Especially, the moment generation with the tape is subject to uncertainties. The stiffness was evaluated based on a deflection of the specimen in positive and negative direction. Using this approach for calibration and stiffness measurement, unequal lever arms on both sides of the specimen have no effect on the measurement result.

$$C_f(\varphi_P = 0) = \frac{(M(\varphi_P) - M(-\varphi_P))}{(\beta_B(\varphi_P) - \beta_B(-\varphi_P))}$$

The measured deflection angles β_B were directly evaluated from the autocollimator measurement using the mean value of 100 subsequent recordings. To ensure that the

oscillation of the specimen has decayed before the measurement starts, a function checks the standard deviation of the autocollimator measurement and idles until it falls short the threshold value of 0.5". Due to the time required for the decay of the oscillation, the stiffness determined can be denoted as relaxed stiffness [Sau90] meaning that anelastic material effects decayed prior to the measurement. The moment values are calculated based on (4.7).

$$\begin{aligned}
 M(\varphi_P, \beta_B) = & g \left(1 - \frac{\rho_0}{\rho_{cal}} \right) m_{cal} L_B \frac{\varphi_P}{\varphi_{P,cal}} \\
 & \underbrace{-g \beta_B \frac{\pi}{648000} (\rho_T - \rho_0) h_T w_T \left(\frac{L_B}{2} \right)^2}_{\text{tape backward motion by defl.}} \\
 & \underbrace{+ C_f^* \beta_B^*}_{\text{nonlinearity of moment}} \\
 & \underbrace{-h_B m_B \left(1 - \frac{\rho_0}{\rho_B} \right) g}_{\text{center of mass position of lever}} \\
 & \underbrace{-2 h_{TB} (\rho_T - \rho_0) h_T w_T L_T g}_{\text{error by tape coupling point position}} \tag{4.7}
 \end{aligned}$$

It becomes evident, that the generated moment is dependent on the deflection angle of the specimen (β_B) which presupposes an a priori knowledge of the stiffness of the specimen respectively. This is due to a backward motion of the tape which is approximately proportional to the deflection angle of the specimen. It slightly decreases the moment exerted on the specimen, since an increasing amount of the deflected tape is suspended by the pulley. In measurement practice, the measured deflection of the specimen was used to compensate for this systematic deviation and to calculate the corrected moment value. Due to the nature of the setup, the measured C_f is a combination of the elastic stiffness of the flexure hinge and a gravitational stiffness components, e.g resulting from the CoG of the lever. The gravitational component is designed to zero and thus the elastic stiffness was approximated with C_f .

The main parameters of the setup are summarized in Tab. C.1. Since the measurement of every single input parameter of the setup is out of scope, a dead weight calibration was selected to reduce the instrumental measurement uncertainty. A hole in the tape on each side close to its suspension point enabled the attachment of a 10 mg E2 mass standard (wire). Mass standard and tape are sharing the exact same force application point on each side of the lever extension. The calibration

procedure was designed as follows: the calibration mass is attached to one side of the lever arm and the resulting deflection of the lever is compensated by the rotation of the pulley. The nominal moment exerted by the mass standard was 13.24 mN mm. When the lever was brought back in its horizontal deflection state, the pulley rotation was recorded and equated with the moment exerted by the calibration mass. This was repeated for the opposite side. It is essential for the calibration result to determine the lever length with a small measurement uncertainty. Using a coordinate measuring machine (CMM) on the assembled lever, the distance between the tape suspension grooves was measured. The calibration factor was increased by 0.2387 % as a result of the lever length measurement. For previous calibrations with the assumed ideal lever length of 270 mm, the correction factor 1.002 387 was applied. The consideration of the uncertainty budget based on (4.7) was carried out using a MONTE CARLO approach outlined in [JCGM 101:2008]. The nominal values and uncertainties of the parameters are presented in Tab. C.1.

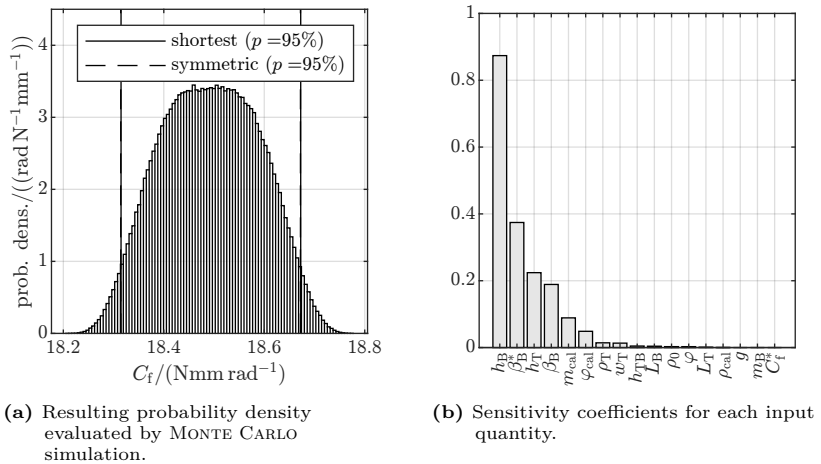


Figure 4.12 – Instrumental measurement uncertainty for a stiffness measurement of a $h = 50 \mu\text{m}$ flexure hinge evaluated based on a MONTE CARLO simulation ($n = 1 \times 10^9$) for the dead weight calibration of the flexure test bench setup.

The total uncertainty budget and the sensitivity coefficients of each parameter were summed up in Fig. 4.12. The instrumental measurement uncertainty estimation for the absolute rotational stiffness of the flexure hinge amounts to $\pm 0.19 \text{ N mm rad}^{-1}$ ($k=2$) which is a relative uncertainty of about $\pm 1\%$. The probability distribution

functions of all input parameters are conservatively estimated. Taking advantage of the dead weight calibration, the geometrical parameters of the setup and their uncertainties were shortcut to a large extent. As a consequence, the height of the CoG of the lever contributes most to the uncertainty budget for the stiffness measurement.

Measuring the extremely low stiffness of the thin flexure hinges using a quasi-static approach proved to be a demanding task, given the disturbances in the environment and the measurement of small deflection angles. The developed measurement setup worked well, but the measurement was time consuming, especially due to the low damping and the slow decay of the oscillations. Air film damping between the tape and parallel plates was found to highly decrease the measurement time. However, its effective realization required a tiny clearance between tape and plate which proved to be unreliable because of the occasional mechanical contact during operation. A further option for the future optimization is the automation of the dead weight calibration procedure, which would omit the critical opening and closing of the setup enclosure. The quest for an alternative and more simple measurement method lead to the development of a second setup for the stiffness determination which is introduced in the following section.

4.5.2 Stiffness determination based on natural frequency

Dynamic approaches for the determination of mechanical properties have been frequently applied. The adjustment state of equal arm beam balances, for example, has been expressed in period of free oscillation, see e.g. [Qui92]. For this type of instruments, the oscillation period of several seconds is comparably easy to measure. Both, the spatial distribution of mass on the moving part(s) and the stiffness of the flexure hinge(s) determine the period. An approach for a determination of the stiffness of a flexure hinge in such way has been reported in [QSD86]. The flexure hinge has been in a vertical orientation in the test setup and the minimal notch height h has been determined with an uncertainty of $\pm 5 \mu\text{m}$.

Measurement concept

The realization of a test bench for the determination of the natural frequency or first eigenfrequency of the flexure hinge specimen requires the measurement of the oscillation in terms of linear or angular deflection. The time-displacement signal can then be analyzed using e.g. the fast FOURIER transform (FFT) to extract the

frequency spectrum of the signal and determine the frequency value at its first peak. The orientation of the flexure hinge specimen was intentionally chosen to be such that the nominal rotational axis (z) coincides with the direction of \vec{g} . In this orientation, the stiffness effect of the CoG of the moving part vanishes and can be neglected. Thus, the measurement gives the pure elastic stiffness of the flexure hinge. Since strains within the flexure hinge are constantly changing during the oscillation allowing no decay of anelastic effects, one can speak of the unrelaxed stiffness [Sau90].

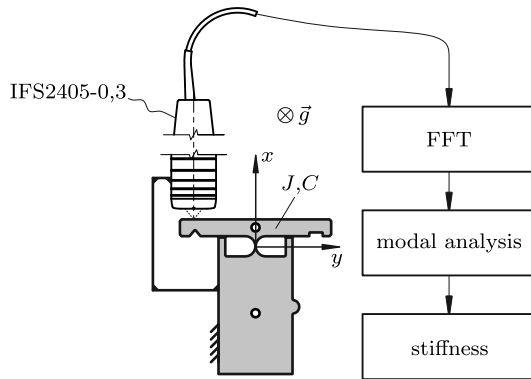


Figure 4.13 – Basic principle and setup for the stiffness determination based on natural frequency measurement of the flexure hinge specimen.

The basic principle of the measurement setup is presented in Fig. 4.13. The chromatic-confocal displacement sensor⁶ is used to record the oscillation signal over time. It samples with 10 kHz, has a sufficiently high dynamic resolution of 20 nm and allows the direct measurement against a machined metal surface. In most occasions, there was no need to trigger the oscillation of the specimen, since the mounting action already served as a trigger. The signal was recorded for a time window of 100 s which results in a frequency resolution of 0.01 Hz. Based on the results from a parametric modal analysis, this corresponds to a stiffness resolution of $\approx 0.01 \text{ N mm rad}^{-1}$ and a resolution for the determination of the minimal notch height of $\approx 0.02 \mu\text{m}$.

A systematic measurement deviation could occur due to the fact of measuring the damped eigenfrequency of the flexure hinges specimen. The eigenfrequency of a

⁶MICRO-EPSILON IFS2405-0,3

damped system is always smaller compared to the undamped counterpart [KR19]. Especially the vicious damping in the surrounding air, results in energy dissipation and a slow decrease in amplitude. From the envelope function of the decaying oscillation, the decay coefficient δ was determined to 0.0231 s^{-1} which corresponds to a damping ratio of $\vartheta = 1.1 \times 10^{-3}$ [Dar+21a]. With

$$\omega_0 = \sqrt{\omega_d^2 - \delta^2}$$

[KR19], the difference between undamped and damped eigenfrequencies amounts to $13.2 \times 10^{-6} \text{ Hz}$ which is falling short the resolution $10 \times 10^{-3} \text{ Hz}$ of this measurement method - it is negligible.

Metrological model

The natural frequency of rotary oscillators with one DOF is given by (4.8). Here, C_f is the measurand which is to be determined. The rotational inertia J is the major source of uncertainty since its value cannot be measured within the scope of this work.

$$f_0 = \frac{1}{2\pi} \sqrt{\frac{C_f}{J}} \tag{4.8}$$

For the estimation of the instrumental measurement uncertainty, the moving body

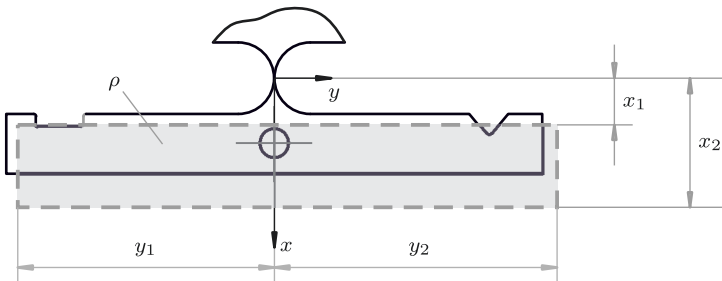


Figure 4.14 – Sketch for the indication of the model parameters for estimating the uncertainty of the dynamic stiffness measurement on a single flexure hinge.

is modeled as a cuboid eccentric to the rotational axis, see Fig. 4.14. The rotational inertia is then calculated according to (4.9).

$$J = \frac{1}{12} m \left((x_2 - x_1)^2 + (y_2 - y_1)^2 \right) + m \left(\frac{x_1 + x_2}{2} \right)^2 \quad (4.9)$$

The measured frequency f is an uncertain input parameter in the measurement equation (4.10):

$$C_f = 4 \pi^2 J f^2 \quad (4.10)$$

The MONTE CARLO computation yields the probability density function shown in Fig. 4.15a. The value for the uncertainty is especially driven by the imprecise

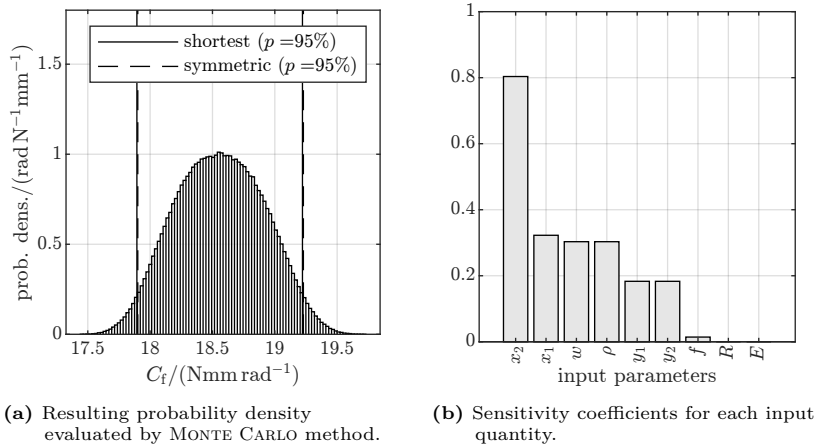


Figure 4.15 – Dynamic stiffness measurement with its corresponding PDF and sensitivity coefficients. C_f can be determined with $\pm 0.71 \text{ N mm rad}^{-1}$ ($k=2$) which is a relative uncertainty of about $\pm 3.8\%$. h_S is estimated with $\pm 0.83 \mu\text{m}$ which amounts to a relative uncertainty of 1.6% .

knowledge about the mass and its distribution. Here, the general tolerances from ISO 2768-1 (fine) and a density tolerance of 1% were presumed. The input values for the calculation of the uncertainty are summarized in Tab. C.2. The instrumental measurement uncertainty for a stiffness measurement yields $\pm 0.71 \text{ N mm rad}^{-1}$ ($k = 2$) which is a relative uncertainty of about $\pm 3.8\%$. If the geometrical tolerances was tighter, the contour of the moving part was entirely machined by WEDM and the tabular value of the density was corrected for by measurement, the uncertainty can still be reduced. To complement the function related measurements with a

method that can be used prior to the operating state, C_f was calculated on the basis of dimensional measurement data from a CMM.

4.5.3 Dimensional measurement

Manufacture of the adjacent surfaces of thin flexure hinges is crucial to keep the rotational stiffness of the flexure C_f within its specified tolerances. Among all geometric and material parameters, the minimal notch height h has the most dominant influence on C_f , see Fig. 4.7b. Therefore, the manufactured minimum notch height h needs to be measured accurately to enable a model-based estimation of C_f and to enable adjustments to the manufacturing process. The technical surfaces defining h exhibit a number of deviations in the micrometer-scale, namely form deviation, waviness and roughness, see [DIN 4760:1982-06]. The detailed and quantitative determination of these deviations is difficult. Measurement methods for surface metrology are: white-light interferometry, laser scanning microscopy, electron microscopy, scanning probe microscopy, near field microscopy, scanning electron microscopy, atomic force microscopy, . . . [Lea11]. Generally, these measurement devices require good accessibility to the surface in normal direction. In case of flexure hinges within a compliant mechanism, this is rarely possible. No thickness information can be obtained directly.

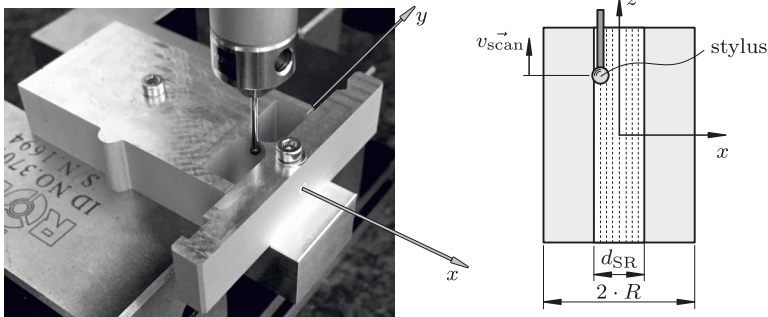


Figure 4.16 – Stylus of the CMM in contact with a flexure hinge specimen manufactured by WEDM.

The use of a CMM with a preferably small probe sphere was the most convenient solution to measure flexure hinges within a planar compliant mechanism. Accessibility was not a major issue and thickness measurement was possible by subtraction

of two distinct measurements on each side. The measurement of the thin flexure hinges was tested on a CMM from Carl Zeiss Industrial Metrology GmbH with the designation UMM550 and a specified resolution of $0.1\ \mu\text{m}$. Figure 4.16 shows the stylus of the CMM in scanning mode along the z axis of the flexure. The specifications of the CMM are summarized in Tab. C.3.

The probing strategy is summarized in Tab. C.3. By scanning profiles according to Fig. 4.16, a point cloud of measurement values is obtained for each side of the flexure hinge. Using two-dimensional interpolation with the measurement values on each side, values for common x - z location in a fine grid can be calculated. The aligned values were used to calculate a grid of thickness values. These are then numerically integrated to calculate a stiffness value. For more detailed information on the algorithm for the stiffness evaluation from tactile measurements see Subsec. C.3.1.

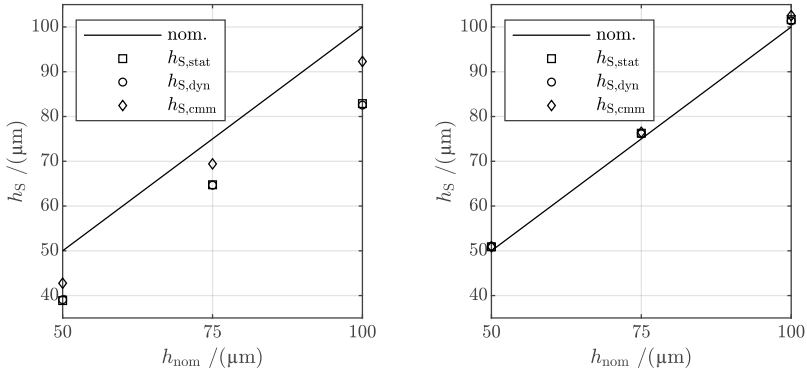
4.5.4 Comparison of qualification methods

Each of the proposed methods for determining the rotational stiffness C_f of thin flexure hinges, the quasi-static measurement (Subsec. 4.5.1), the dynamic measurement (Subsec. 4.5.2), and the dimensional measurement (Subsec. 4.5.3), provided meaningful measurement results. Each of these methods has its own strengths and weaknesses. The selection of the most suitable method depends on the application. Table 4.1 summarizes the measurement duration and the measurement uncertainty of an exemplary stiffness measurement on a $50\ \mu\text{m}$ semi-circular flexure hinge. The uncertainty of the dimensional stiffness determination method was estimated in Subsec. C.3.3. The methods have been applied to an exemplary set of

Table 4.1 – Specifications of the stiffness measurement methods.

method	meas. unc. ($k = 2$)	t_{meas}
quasi-static stiffness meas.	$\pm 0.19\ \text{N mm rad}^{-1}$	$\approx 2\ \text{h}$
dynamic stiffness meas.	$\pm 0.71\ \text{N mm rad}^{-1}$	$\approx 10\ \text{min}$
dimensional stiffness meas. (CMM)	$\pm 1\ \text{N mm rad}^{-1}$	$\approx 1.5\ \text{h}$

semi-circular flexure hinges manufactured from EN AW-7075 T651 (see Tab.B.1) with h ranging from 50 to $100\ \mu\text{m}$. Using the analytic equation for C_f , the measured stiffness values were used to evaluate h_s . The results are presented in Fig. 4.17.



(a) Results of the three methods on flexure hinge specimen set 1.

(b) Results of the three methods on flexure hinge specimen set 2.

Figure 4.17 – Application of the stiffness determination methods on two flexure hinge sets from distinct WEDM manufacturing partners.

The comparison of the proposed methods in Fig. 4.17 shows a very good accordance of the functional characterization methods, namely the static and dynamic measurement approaches. The deviations between the results in Subfigs. 4.17a and 4.17b are within $\pm 0.5\%$ relative deviations. In terms of deviation from the nominal, *set 2* is far more accurate than *set 1*.

For the high quality flexure hinges in *set 2* the CMM measurements agree with the other measurement methods. The results of *set 1* indicates that the CMM measurement method provides a value that is overestimating h_S . A connection to the nature of the manufacturing process and the achieved surface roughness was suspected. The surface roughness partly justifies the pronounced deviation from the nominal value of *set 1* and additionally provides an explanation for the deviation of the tactile measurement. Here, the overestimation of the evaluated thickness occurs due to the size of the probing sphere ($d_{\text{CMM}} = 1.5 \text{ mm}$). The overestimation is dependent on the surface roughness and its spatial frequency.

A first test of this hypothesis was performed by the numerical simulation of the probing on a white light interferometry measurement of the machined surface. The direct measurement on the flexure hinge surfaces was not possible with the white light interferometry due to the geometry of the specimen (cf. Fig. 4.13). A side surface, also machined in the same setting on the WEDM machine was considered instead. Figures 4.18 and 4.19 reveal the larger peak-to-valley roughness of the

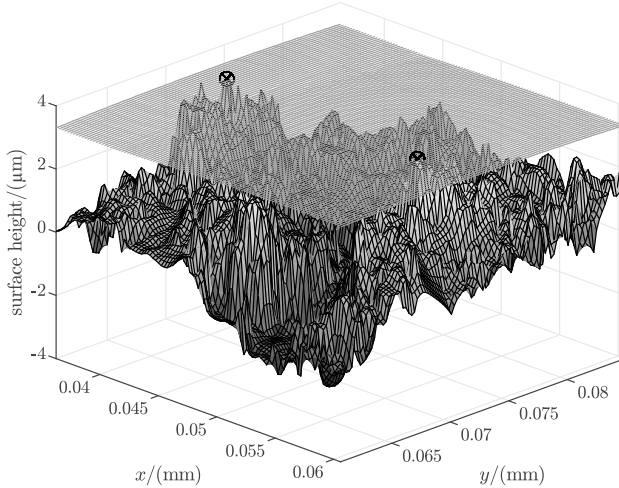


Figure 4.18 – Probing simulation of surface on *set 1*.

surface of *set 1*. The high spatial frequency of both surfaces lead to few contact points between probing sphere and surface peaks, which in turn results in the bespoke overestimation of the thickness measurement. While the overestimation in Fig. 4.19 is smaller than $2\ \mu\text{m}$, the overestimation in Fig. 4.18 amounts to almost $4\ \mu\text{m}$. For the thickness evaluation, the effect contributes twice.

Since elastic deformations of the structure and the roughness peaks due to the probing force are not yet considered, the results have to be viewed with caution. Nevertheless, it was proven that the large deviation of the CMM measurement on *set 1* largely stems from the mechanical filter of the probing sphere on the CMM and the corresponding overestimation of h_S . For more detailed information about the algorithm for the contact simulation see Subsec. C.3.2.

4.6 Chapter summary

Semi-circular flexure hinges are, despite being fairly simple in their structure, a scientific branch with an arbitrary level of complexity ranging from mechanical modeling over manufacturing and testing. This is especially true for a minimal notch height in the range of $50\ \mu\text{m}$. High aspect ratios and a strong notch effect

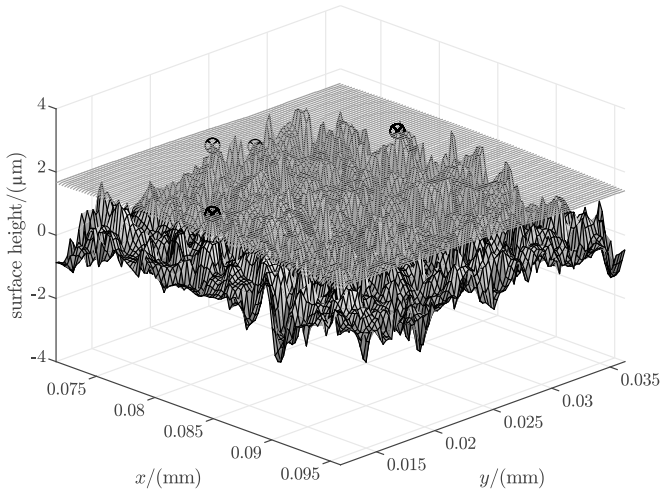


Figure 4.19 – Probing simulation of surface on *set 2*.

increase the complexity for accurate mechanical models and lead to a considerable effort in computation. Readily neglected effects of the engineering materials become increasingly important as the minimal notch height is in the range of the average grain size of aluminum alloys [Hen17; TBP19]. Analogously, all effects connected to surface integrity are of high relevance. It was shown, that the impact of roughness and waviness cannot be neglected for tight tolerances on the rotational stiffness.

Three developed and rigorously verified testing methods enable an accurate determination of the rotational stiffness and can thus be used to fine adjust a specific manufacturing process. This tuned process can then be used to manufacture complete compliant mechanisms including multiple flexure hinges. Flexure hinges in a weighing cell mechanism are treated in the following chapter.

Chapter 5

Mechanical modeling and adjustment strategies

The centerpiece of an EMFC weighing cell is its mechanical system - the focus of this modeling chapter. The mechanism structure and its most important geometric dimensions are presented in Fig. 5.1.

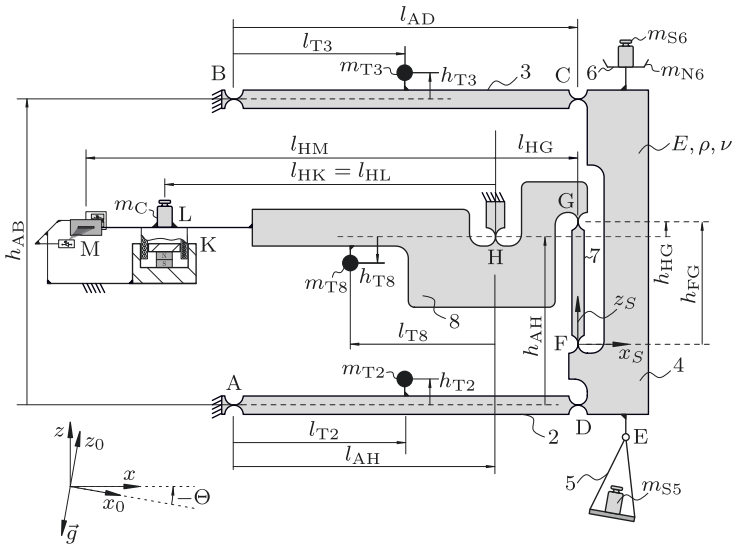


Figure 5.1 – EMFC weighing cell with its most important components and the indication of its parameters. The displayed geometry belongs to the first prototype with the designation standard kinematic prototype (PROT-S).

The standard mechanism of an EMFC weighing cell is composed of two functional units: the parallelogram guide (2, 3, 4) as the quasi-linear guide for the weighing pan, and the transmission lever (8) to counterbalance the mass on the weighing pan. A coupling element (7) mechanically connects the two sub-mechanisms to strongly reduce over-constraining. The purely mechanical behavior of the system, with a clear focus on adjusting the weighing system, is calculated in this chapter. The following mechanical parameters are adjusted:

- stiffness C ,
- tilt sensitivity D_{Θ} ,
- off-center load sensitivity E_L .

The adjustment of the stiffness and tilt sensitivity with trim masses and the compensation of the initial elastic stiffness via astatization are discussed and combined to a sound adjustment concept. As indicated in Fig. 5.1, the adjustment concept considers several trim masses on different levers of the weighing cell mechanism. The trim mass on the transmission lever (8) m_{T8} is common in EMFC weighing cells. The masses on the levers of the parallelogram guide m_{T2} and m_{T3} are new and key to the adjustment concept. The combination of the trim masses enables the quasi-independent adjustment of stiffness and tilt sensitivity.

The stiffness of the weighing cell is a combination of the elastic stiffness of the compliant mechanism and the gravitational stiffness components from net- and trim masses. The principal objective of this work is the minimization of the stiffness and a concurrent reduction of the tilt sensitivity.

The off-center load sensitivity is independent from the adjustment of stiffness and tilt sensitivity and thus treated separately. The complex interaction with the components of the EMFC system are touched upon towards the end of the chapter. The chapter begins with an introduction to the mechanical models, followed by the derivation of the analytical rigid body model.

5.1 Overview mechanical models

Table 5.1 lists the mechanical models developed and used throughout the present work. Calculations with higher-order mechanical models were conducted in the software ANSYS®.

Table 5.1 – Mechanical models.

model	description
rigid body models	
analytic rigid body model (ARB)	LAGRANGE equation of second kind, quasi static, small angle approximation
numeric rigid body model (NRB)	rigid body model in ANSYS [®] , 2D, quasi static, nonlinear
finite element models	
finite element model (FE)	ANSYS [®] , 3D, quasi static, nonlinear
significant region model (SR)	combined rigid elements and 3D finite element model at the flexure hinges in ANSYS [®]

5.1.1 Rigid body models

The rigid body model idealizes the stiffness of structural components and treats flexure hinges as kinematically ideal pivots. In its analytical form, the rigid body model provides equations which are easy to interpret and give a good overview of the mechanical behavior. The validity of the derived equations was checked with the numerical rigid body model. For general modeling assumptions of the rigid body model see Tab. 2.1. In the numeric rigid body model in ANSYS[®], the mechanical structure of the weighing cell is composed of rigid links (MPC184-rigid link) between the idealized pivots (MPC184-revolute joint). The rotational stiffness of the semi-circular flexure used for the MPC184-revolute joint in ANSYS[®]. The stiffness was calculated with the analytic equation in [Tor+18] using (4.2) multiplied with (4.5). The rigid body models allow for nonlinear calculations but neglect deformations of structural parts and flexure hinges. Out-of-plane effects like an off-center load in y direction of a tilt about the x axis cannot be calculated.

5.1.2 Finite element models

A three-dimensional FE model was used for detailed calculations on specific weighing cell mechanisms. It is the highest-order mechanical model in use. The FE model resolves the mechanical effects that cannot be mapped with the analytical- and numerical rigid body model. These effects result from the deformation of structural parts and parasitic deflections of the thin flexure hinges, which are especially important for the final design studies of new weighing cells. The FE model of the weighing mechanism can have different dimensionality. One can distinguish between a 2D and a 3D analysis. The computationally more expensive 3D analysis needed to

be chosen to include out-of-plane force components and thus enables the complete evaluation of tilt sensitivity and off-center load sensitivity.

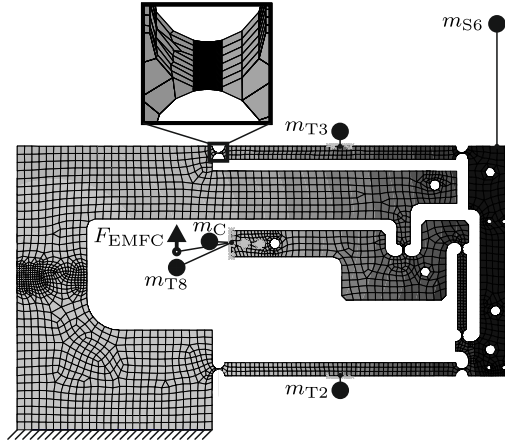


Figure 5.2 – Finite element model of PROT-S.

The meshing strategy for the flexure hinges is adopted from the single flexure hinges in Ch. 4. The stiff structural elements are meshed using a coarse mesh - where possible, with hexahedral elements. Only the significant region of the thin flexure hinges was finely meshed. The non-matching meshes were linked with multi-point constraint contacts. Mounted components to the weighing cell as the weighing pan, counter mass, and trim masses were modeled as point masses. These were attached to the structure by multi-point constraint contacts, see Fig. 5.2. The boundary conditions were created similarly using remote nodes attached by multi-point constraint contacts. The settings used throughout the models are listed in Tab. B.3. Using the geometry import and meshing capabilities in ANSYS® workbench, the model could be quickly adapted to new weighing cell geometries and was thus well suited for the development of new concepts. For further technical details on the FE model see Subsec. B.6.

To reduce the computational effort, a sub-type of the FE model was established: the SR model, see Fig. 5.3. The underlying idea of the significant region model is based on the pronounced concentration of mechanical stress within the mechanism in the central region of the flexure hinges. As described in Subsec. 4.3.2, a cylindrical region of 2 mm diameter around the z axis is sufficient to describe the rotational

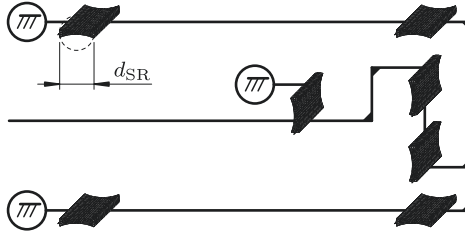


Figure 5.3 – Schematic depiction of the significant region model. The detailed meshing is restricted to a cylindrical region central to the flexure hinges.

stiffness entries in the stiffness matrix accurately. Thus, a model can be set up with finely meshed significant regions connected by rigid beam elements. The total number of elements was significantly decreased compared to the full three-dimensional model. The behavior of a weighing cell mechanism was modeled efficiently.

5.2 Analytical rigid body model

The analytical model of a standard EMFC weighing cell geometry is derived in the following section. First, the model parameters are defined. Their definition entails the specification of the coordinate system for the weighing cell mechanism in Fig. 5.1, which applies generally throughout this work.

5.2.1 Coordinate system and definition of parameters

Two coordinate systems were defined to cover the tilt deflection of the weighing cell's base relative to the vector of gravitational acceleration \vec{g} . One is the fixed reference coordinate system (x_0, y_0, z_0) , whose z_0 axis coincides with the negative direction of \vec{g} . The second coordinate system (x, y, z) is the weighing cell's local coordinate system which moves with its base. The x axis is defined to be parallel to the axis of the transmission lever with a positive direction towards the weighing pan. The z axis is the vertical axis, perpendicular to the weighing pan surface pointing upwards. The y axis is parallel to the rotation axis of the flexure hinges.

Definition 5.1 (vertical / horizontal). The terms *vertical* and *horizontal* are frequently used. They are defined for zero deflection and zero tilt ($q_8 = 0, \Theta = 0$):
vertical: parallel to the z axis.
horizontal: parallel to the x axis.

As indicated in Fig. 5.1, all considered adjustment parameters were included in the model. These are: the nonlinear coupling described by the geometric parameter h_{HG} , and the trim masses with their vertical position referenced by h_{T2} , h_{T3} , and h_{T8} .

Definition 5.2 (Lengths and distances). All lengths in x and z direction for $q_8 = 0$ are labeled systematically:
 x direction: l_{ij} , with the starting point i and the end point $j \rightarrow l_{ij} = x_j - x_i$;
 z direction: h_{ij} , with the starting point i and the end point $j \rightarrow h_{ij} = z_j - z_i$.
 The sign is unambiguously defined.

Definition 5.3. Adjustment is an intentional change to a functional element within a technical system to achieve the required characteristic values, [Han64].

Two fundamental methods are distinguished for the setup of the analytical model: the NEWTON-EULER approach and the EULER-LAGRANGE equation. The advantage of the first is the ability to extract the forces at the joints between the bodies at the expense of a more laborious setup of the model, see [Mar+17]. Instead, the weighing cell properties were evaluated based on the EULER-LAGRANGE equation. The model was exclusively derived for the quasi-static load case.

5.2.2 Trim mass

The quasi-static mechanical effect of a trim mass can be derived using the EULER-LAGRANGE equation:

$$\frac{d}{dt} \left(\frac{\partial L}{\partial \dot{q}_j} \right) - \frac{\partial L}{\partial q_j} = Q_j \quad j = 1, 2, \dots, m_f. \quad (5.1)$$

For a depiction of the mechanical system with its parameters, see Fig. 2.9. In (5.1), j represents the number of independent system variables, Q_j the generalized forces

and m_f the mobility of the mechanical system. The trim mass on the transmission lever (8) has mobility of $m_f = 1$ and (5.1) yields:

$$\frac{d}{dt} \left(\frac{\partial L}{\partial \dot{q}_8} \right) - \frac{\partial L}{\partial q_8} = Q_{\text{EMFC}} \quad \text{with} \quad L = T_{\text{kin}} - U.$$

The kinetic energy T_{kin} and the time derivatives are zero to present a quasi-static state. The relation simplifies to:

$$\frac{\partial U}{\partial q_8} = Q_{\text{EMFC}} \quad (5.2)$$

The focus is on the gravitational stiffness, and any elasticity in the system is neglected. Thus, the potential energy U_{grav} of the trim mass m_{T8} is formulated as:

$$U_{\text{grav}} = (-1) m_{\text{T8}} \vec{g} \cdot \vec{r}_{\text{T8}} \quad (5.3)$$

The position vector of the point mass in the x_0 - z_0 plane reads:

$$\vec{r}_{\text{T8}} = \begin{pmatrix} -l_{\text{T8}} \cos(q_8 + \Theta) - h_{\text{T8}} \sin(q_8 + \Theta) \\ -l_{\text{T8}} \sin(q_8 + \Theta) + h_{\text{T8}} \cos(q_8 + \Theta) \end{pmatrix}$$

Partial differentiation according to (5.2) with $\vec{g} = (0; -g)$ yields:

$$\frac{\partial^2 U_{\text{grav}}}{\partial q_8^2} = m_{\text{T8}} g h_{\text{T8}} \cos(q_8 + \Theta)$$

Stiffness and tilt sensitivity are evaluated by setting $\Theta = 0$ or $q_8 = 0$ respectively. Based on the small-angle approximation, the sine function is replaced by the first term of the MACLAURIN series. Finally, the resulting term is differentiated once to yield the stiffness or tilt sensitivity:

$$\frac{\partial^2 U_{\text{grav}}}{\partial q_8^2} (\Theta = 0) = C = -m_{\text{T8}} g h_{\text{T8}} \quad (5.4)$$

$$-\frac{\partial^2 U_{\text{grav}}}{\partial q_8^2} (q_8 = 0) = D_{\Theta} = m_{\text{T8}} g h_{\text{T8}} \quad (5.5)$$

Equations (5.4) and (5.5) hold for a trim mass on the transmission lever of a weighing cell. Equation (5.4) provides a moment over deflection angle in N m rad^{-1} and (5.5) a moment over tilt angle in N m rad^{-1} . The sign of the latter is defined by Def. 5.4.

Definition 5.4 (Tilt sensitivity). An labile mathematical pendulum $C < 0$ is tilt sensitive $D > 0$. Therefore, $\partial^2 U_{\text{grav}} / \partial q_s^2 (q_s = 0, \Theta)$ is multiplied by (-1) . Then for $D > 0$, a positive angle Θ corresponds to a tilt-induced virtual mass increase on the weighing pan $\Delta m > 0$.

5.2.3 Weighing cell mechanism

Figure 5.4 presents the weighing cell mechanism reduced to a rigid body model. The angular deflection $q_7(q_8)$ of the coupling element between the subsystems transmission lever and parallelogram guide is of particular interest for the mechanical model of the weighing cell. The system of equations for the quasi-static mechanical properties was derived using the EULER-LAGRANGE formalism in the preceding Subsec. 5.2.2. The potential energy $U = U_{\text{grav}} + U_{\text{el}}$ of the weighing cell, including

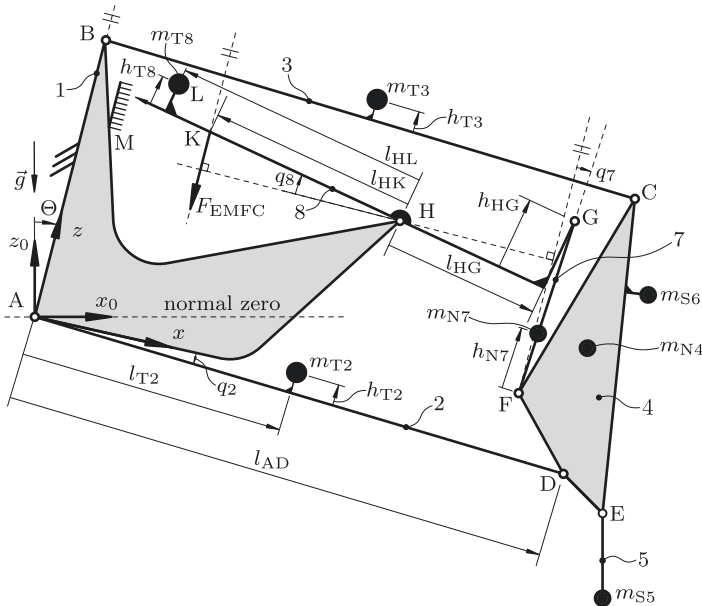


Figure 5.4 – Rigid body model of an EMFC weighing cell in a deflected state for both the mechanism deflection angle q_8 and the tilt angle Θ .

elastic- and gravitational potential energy, is formulated as:

$$U_{\text{grav}} = (-1) (m_{S5} \vec{g} \cdot r_{S5} + m_{S6} \vec{g} \cdot r_{S6} + \dots) \quad (5.6)$$

$$U_{\text{el}} = \underbrace{\frac{1}{2} C_H q_8^2}_{\text{pivot H}} + \underbrace{\frac{1}{2} (C_A + C_B + C_C + C_D) q_2^2}_{\text{pivot A to D}} + \underbrace{\frac{1}{2} C_G (q_8 + q_7)^2}_{\text{pivot G}} + \underbrace{\frac{1}{2} C_F q_7^2}_{\text{pivot F}} \quad (5.7)$$

With the definition of the gravity vector

$$\vec{g} = \begin{pmatrix} 0 \\ -g \end{pmatrix}$$

and the definition of the position vectors, the system was described based on the independent variables q_2 , q_7 and q_8 . The weighing cell mechanism has mobility equal to one and is thus fully described by one independent variable q_8 . The derivation of the transmission ratio and its verification is described in Subsec. B.5. The linearized transmission ratio between q_2 and q_8 yields:

$$q_2 = \left(l_{HG} - h_{HG} \frac{q_8}{2} \right) \frac{q_8}{l_{AD}} + \frac{h_{FG} q_7^2}{2 l_{AD}} \quad (5.8)$$

$$q_7 = \frac{\left(q_8^2 \tau + h_{HG} q_8 \right)}{h_{FG}} \quad (5.9)$$

$$\tau = \frac{\left(l_{AD} l_{HG} - l_{HG}^2 \right)}{2 l_{AD}} \quad (5.10)$$

The resulting equation from (5.6) and (5.7) is written with q_8 as independent system variable using (5.8), (5.9) and (5.10). Differentiated twice by ∂q_8 yields:

$$\frac{\partial^2 U}{\partial q_8^2} := 0 = f(q_8, \Theta, \dots) \quad (5.11)$$

Since the mechanical system of the weighing cell is deflected only by fractions of 1° , the small angle approximation was used to improve the readability of the resulting equation.

$$m_G = (m_{N2} l_{N2} + m_{T2} l_{T2} + m_{N3} l_{N3} + m_{T3} l_{T3}) l_{AD}^{-1} + m_{N4} + m_{N5} + m_{N6} + m_{N7} + m_{S5} + m_{S6} \quad (5.12)$$

Together with $\xi = l_{HG}/l_{AD}$, (5.11) and (5.12), the linearized system equations sorted by the respective mechanical properties reads:

$$\begin{aligned}
 C = \frac{\partial^2 U}{\partial q_8^2}(\Theta = 0) = & \\
 & \underbrace{\left(\frac{h_{HG}^2}{h_{FG}} - h_{HG} \right) m_G g}_{\text{astatization}} \\
 & \underbrace{-h_{T8} m_{T8} g - h_{T2} m_{T2} g \xi^2}_{\text{gravitational stiffness}} \\
 & \underbrace{+ (C_A + C_B + C_C + C_D) \xi^2 + C_F \left(\frac{h_{HG}}{h_{FG}} \right)^2 + C_G \left(1 - \frac{h_{HG}}{h_{FG}} \right)^2}_{\text{elastic stiffness}} + \mathbb{G}_{H3}
 \end{aligned}$$

$$\begin{aligned}
 D_{\Theta} = - \frac{\partial^2 U}{\partial q_8^2}(q_8 = 0) = & \\
 & g \left(h_{N2} m_{N2} \xi + h_{N3} m_{N3} \xi + h_{T2} m_{T2} \xi + h_{T3} m_{T3} \xi \right. \\
 & \left. + h_{N8} m_{N8} + h_{T8} m_{T8} + h_{HL} m_C + \frac{h_{HG} h_{N7}}{h_{FG}} m_{N7} \right)
 \end{aligned} \tag{5.14}$$

$$\begin{aligned}
 M_B = \frac{\partial^2 U}{\partial q_8^2}(q_8 = 0, \Theta = 0) = & \\
 & F_{EMFC} l_{HK} \\
 & + l_{HL} m_{T8} g - l_{HG} m_G g
 \end{aligned} \tag{5.15}$$

Equation (5.13) describes the stiffness C in N m rad^{-1} , (5.14) the tilt sensitivity D_{Θ} in N m rad^{-1} and (5.15) the static balance M_B in N m . All parameters are listed with reference to the rotational DOF of the transmission lever q_8 . The parameters were converted to the translational DOF at the weighing pan to adapt to the values determined in the experiments: the rotational stiffness (5.13) was multiplied by l_{HG}^{-2} and the tilt sensitivity by l_{HG}^{-1} .

The analytical model for the stiffness (5.13) closely replicates the nonlinear numerical rigid body model in ANSYS® and enhances the general understanding of the system: equation (5.13) indicates that the astatization effect is independent of the transmission ratio ξ . This has been checked with the nonlinear numerical rigid body

(NRB) model with the result that any effect that may be present is insignificant. For the considered geometry, the error between analytic and numeric model in ANSYS® amounts to 0.0036%. The analytic model can thus be used with no significant loss in modeling accuracy.

Additional effects occur when loosening the restrictions of the rigid body model - all bodies are deformable and the ideal pivots are replaced by flexure hinges. Especially, the properties tilt sensitivity and off-center load sensitivity are affected by minute deflections within the structure. Their modeling requires a higher-order model.

5.3 Mechanical effects within the monolithic weighing mechanism

Mechanical effects within the weighing cell mechanism are presented in this section. The findings provide a sound foundation for the development of novel mechanism concepts and adjustment strategies. First, trim masses attached to different parts of the weighing cell mechanism are investigated. The change in position of the CoG relative to the CoR changes the rotational inertia according to the HUYGENS–STEINER theorem. Thus, the Eigenfrequencies of the mechanism change. Compared to the overall inertia of the mechanical system with a sample mass of 1 kg, these changes are usually small and have a minor impact. The quasi-static nature of the mass comparison process and the quiet environment emphasizes the quasi-static effects.

5.3.1 Manipulation of the centers of mass

Trim masses are a common adjustment measure in precision weighing systems. They are attached to links in the mechanism and serve to manipulate the vertical position of the CoG thereof. The intended change of the gravitational stiffness occurs on parts undergoing a rotary motion. As indicated in Sec. 5.2.2, the vertical shift of the trim mass affects both the stiffness and the tilt sensitivity. Thus, no independent adjustment is possible. A way forward has been discovered by combining at least two trim masses within the mechanism [Mar+17]: the effect of a trim mass (m_{T8}) on the transmission lever (8) is described with (5.4) and (5.5). As long as the deflection angle of the transmission lever is well below 1° , the underlying small-angle approximation is valid. The novelty is an additional trim

mass (e.g. m_{T2}) on the lower lever (2) of the parallelogram guide. The effects on stiffness and tilt sensitivity are both influenced by the transmission ratio within the mechanism ξ :

$$C_{T2} = -m_{T2} g h_{T2} \xi^2 \quad (5.16)$$

$$D_{\Theta, T2} = m_{T2} g h_{T2} \xi \quad (5.17)$$

Interestingly, the stiffness effect in (5.16) is proportional to ξ^2 , whereas the tilt sensitivity in (5.17) scales with ξ . The different dependency on the transmission ratio enables a quasi-independent adjustment of tilt sensitivity and stiffness. For the sake of symmetry, it is recommended to attach a trim mass to the upper lever as well (m_{T3}). The mechanical effect of m_{T3} is equal to the one of m_{T2} on the lower lever.

The linear system of equations for both properties with $h_{T23} = h_{T2} = h_{T3}$ is written as follows:

$$0 = C_0 l_{HG}^2 - (m_{T2} + m_{T3}) g h_{T23} \xi^2 - m_{T8} g h_{T8}$$

$$0 = D_0 l_{HG} + (m_{T2} + m_{T3}) g h_{T23} \xi + m_{T8} g h_{T8}.$$

If C_0 and D_0 of the weighing cell are measured and all other parameters are known with sufficient accuracy, h_{T23} and h_{T8} can be determined for the adjustment. The system of equations was solved for h_{T23}^* and h_{T8}^* resulting in:

$$h_{T8}^* = -\frac{l_{HG} (C_0 l_{HG} + D_0 \xi)}{(\xi - 1) g m_{T8}} \quad (5.18)$$

$$h_{T23}^* = \frac{l_{HG} (C_0 l_{HG} + D_0)}{g (m_{T2} + m_{T3}) \xi (\xi - 1)} \quad (5.19)$$

A necessary condition for the adjustment concept becomes evident from the term $\xi - 1$ in the denominator of both terms. The transmission ratio between the subsystems ξ must not equal 1.

In practice, the adjustment concept has some limitations, especially with regard to the compensation of manufacturing deviations. Compared to the initial elastic stiffness of a weighing cell mechanism which can be in the range of 50 to 200 N m⁻¹, the stiffness compensation effect of a trim mass is comparably small: on transmission lever, a mass with 50 g and a positive vertical shift of 10 mm compensates ≈ 6.7 N m⁻¹ or 15 to 3% of the elastic stiffness. A larger mass and/or a larger vertical distance is required to compensate for the elastic stiffness. The required mass for the

compensation of manufacturing deviations creates a pronounced tilt sensitivity which needs to be compensated by the trim masses on the levers of the parallel guide. Here, the gravitational force of the trim masses results in a lateral force to the horizontally oriented flexure hinges. Ultimately, the elastic limit of the mechanism material restricts the use of large trim masses.

Adjusting the weighing cell to a state with $C = D_{\Theta} = 0$ using trim masses is theoretically feasible but hindered by practical considerations. Among those are the minimization of the overall building space, the handling of the device and the elastic limit of the flexure hinges. Therefore, the adjustment method is rather suited for a fine adjustment of stiffness and tilt sensitivity after the initial elastic stiffness of the mechanism has been strongly reduced.

5.3.2 Astatization

Astatization bridges the gap between the initial elastic stiffness of the mechanism and a maximum stiffness that can be reasonably fine-adjusted by trim masses. Astatization in general comprises means to bring a mechanically stable system close to an indifferent state as introduced in Ch. 2. Within the weighing cell mechanism, a nonlinearity can be introduced such that the mass on the weighing pan results in a pronounced negative gravitational stiffness. The astatizing structure was realized by introducing a vertical distance between the pivots H and G - the parameter h_{HG} . The large effect on the stiffness and a practically unaffected tilt sensitivity represents a favorable option to improve the system. A 1 kg-mass comparator with an approximately constant load represents the perfect use case. Astatization via h_{HG} was thus chosen to compensate for the initial elastic stiffness. Two superimposed nonlinearities occur that can be distinguished for different load cases of the mechanism:

Load independent stiffness change The introduction of the parameter $h_{HG} \geq 0$ in the weighing cell mechanism provides a small stiffness reduction, as shown in Fig. 5.5. The stiffness reduction is independent of the gravitational load on the mechanism. The stiffness change results from a change of the deflection angles of the pivots F and G. The weighing cell's elastic stiffness equation includes this effect by h_{HG} -dependent pre-factors for each flexure hinge stiffness in the mechanism.

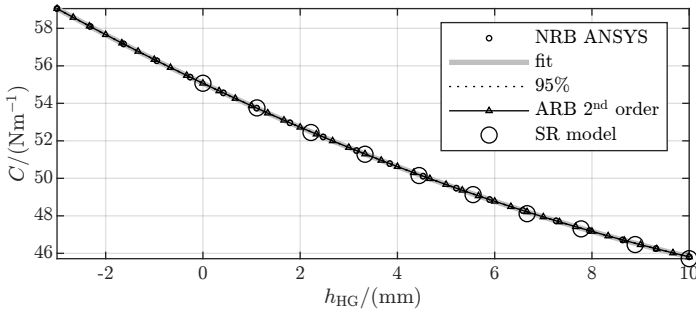


Figure 5.5 – Elastic stiffness of the weighing cell mechanism without gravitational stiffness. NRB - numerical rigid body model in ANSYS®, ARB - analytic rigid body model, SR - significant region finite element model.

Load induced stiffness compensation The parameter h_{HG} in combination with a large mass on the weighing pan is a strong measure for stiffness manipulation. In terms of stiffness, all masses suspended at pivot G act as trim mass - without significantly affecting the tilt sensitivity. In Fig. 5.6 an overlain quadratic effect is evident. In the useful operating range ($h_{HG} > 0$), the quadratic effect reduces the stiffness compensation compared to the linear model. This nonlinearity is not covered by the 1st-order analytical rigid body (ARB) model, which considers the astatization as

$$C_{HG} = -h_{HG} m_G g.$$

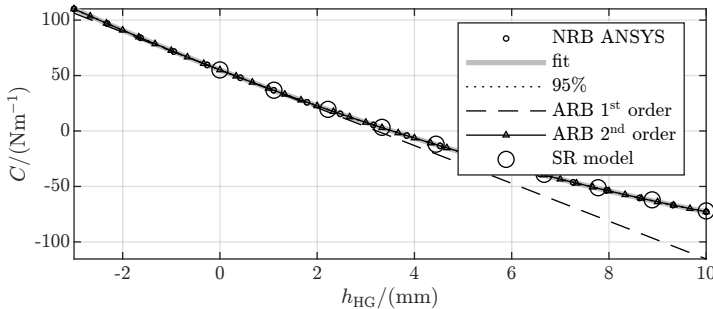


Figure 5.6 – Rigid body model of PROT-S geometry with $m_S = 1175.5$ g. Elastic and gravitational stiffness effects are superimposed. NRB - numerical rigid body model in ANSYS®, ARB - analytic rigid body model, SR - significant region finite element model.

With the angle of the coupling element q_7 considered, the term changes to

$$C_{\text{HG}} = \left(\frac{h_{\text{HG}}^2}{h_{\text{FG}}} - h_{\text{HG}} \right) m_{\text{G}} g.$$

The results in Fig. 5.6 were calculated for a coupling element length of $h_{\text{FG}} = 40$ mm. Parametric studies in [Dar+18c] revealed that the length of the coupling element is strongly affects the gravitational stiffness component.

Coupling element length variation In [Dar+18c], it was concluded that the use of a short coupling element reduces the stiffness compensation effect. The results for a varying h_{FG} with a fixed $h_{\text{HG}} = 5$ mm are presented in Fig. 5.7. With a growing

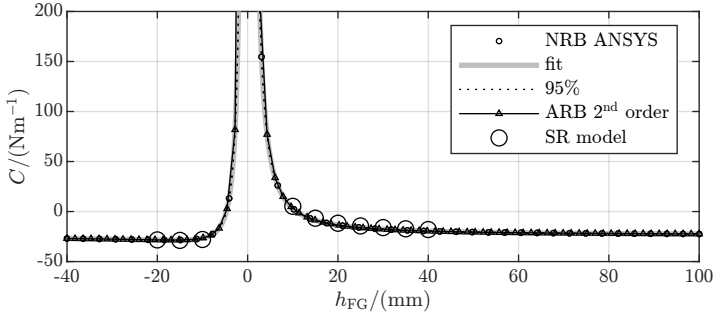


Figure 5.7 – Variation of h_{FG} in the model with h_{HG} fixed to 5 mm. NRB - numerical rigid body model in ANSYS®, ARB - analytic rigid body model, SR - significant region finite element model.

length of the coupling element, the gravitational stiffness converges to $-m_{\text{G}} g h_{\text{HG}}$. For a coupling element shorter than $h_{\text{FG}} < 10 h_{\text{HG}}$, a relevant increase of the absolute stiffness was observed. The stiffness compensation effect is decreasing. The pole at $h_{\text{FG}} = 0$ shows that the absolute stiffness tends to ∞ for a decreasing distance between F and G. In case F is designed to be above G, a compression force acts on the coupling element, the stiffness compensation effect reaches its maximum at $h_{\text{FG}} = -h_{\text{HG}}$ with $-2 h_{\text{HG}} m_{\text{G}} g$. However, it is counteracted by an increase of the elastic stiffness term for pivot G to four times its rotational stiffness $4 C_{\text{G}}$. For a growing negative distance between F and G, the absolute stiffness increases slightly. The astatization effect is most effective for a preferably long coupling element under tensile force or a short coupling element under compression load. The latter is an interesting discovery for minimizing the building space. Within the present work,

all coupling elements were designed for a tensile load. Mostly, the ratio h_{FG}/h_{HG} exceeded 10.

5.3.3 Combination of adjustment measures

Astatization (Subsec. 5.3.2) and the manipulation of trim masses (Subsec. 5.3.1) were combined. The combined adjustment measures enable a compensation of the initial elastic stiffness of the weighing cell and a following fine-adjustment of the properties stiffness and tilt sensitivity.

The system of equations for the weighing cell with the combined adjustment concept is presented in (5.13) for stiffness and in (5.14) for tilt sensitivity. With a fixed values for h_{HG} , solving the system of equations gives the trim mass adjustment parameters:

$$h_{T8}^* = \frac{(-C_{el} l_{HG}^2 - D_{\Theta} l_{HG} \xi + g h_{HG} m_G) h_{FG} - g h_{HG}^2 m_G}{h_{FG} g m_{T8} (\xi - 1)}$$

$$h_{T23}^* = \frac{C_{el} h_{FG} l_{HG}^2 - g h_{FG} h_{HG} m_G + g h_{HG}^2 m_G + D_{\Theta} h_{FG} l_{HG}}{g h_{FG} (m_{T2} + m_{T3}) \xi (\xi - 1)}$$

If stiffness and tilt sensitivity are measured with the nominal mass on the weighing pan and $m_G g$ already acting on the pivot G, the equations (5.18) and in (5.19) need to be applied as the measured values already include the astatization effect.

5.3.4 Off-center load sensitivity adjustment

The cause of the off-center loading error is the parallel offset between the two major forces acting vertically on the load carrier [Met96]. The forces are the weight force of the sample mass F_{S6} and the counter-force at pivot F (F_F). The reference for the lateral offset is the center of the coupling element or the force application point of F_F . The lateral offset perpendicular to the centerline of the weighing pan can either be in x direction (ϵ_{Sx}) or in y direction (ϵ_{Sy}). Figure 5.8 shows the offset in x direction. These are the weight force F_{S6} of the mass on the weighing pan and the counter force F_F in the opposing direction with its force application point at pivot F. The force couple creates a moment about y on the load carrier. The levers of the parallelogram guide constrain the rotation of the load carrier and thus take the moment load. In case of parallel levers, the force is guided to the

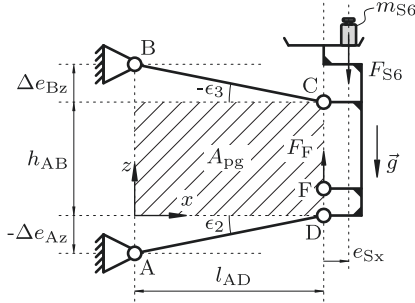


Figure 5.8 – Depiction of the mechanical system for the calculation of the off-center load sensitivity in x direction.

base without influencing the force balance in z direction. The slightest deviation from parallelism, results in a vertical force components which is changing the force balance of the weighing cell. Therefore, off-center load sensitivity adjustment of a weighing cell is a manipulation of the parallelogram guide sub-mechanism. More specifically, it aims at restoring the parallelism between upper and lower lever in the loaded (deformed) condition of the weighing cell.

$$E_{Lx} \approx \frac{\epsilon_3 - \epsilon_2}{h_{AB}} \approx \frac{(\Delta e_{Az} - \Delta e_{Bz})}{h_{AB} l_{AD}} \quad (5.20)$$

To express E_{Lx} in $\text{N kg}^{-1} \text{mm}^{-1}$, (5.20) needs to be multiplied with $9.81 \times 10^{-3} \text{N m kg}^{-1} \text{mm}^{-1}$. The magnitude of the off-center load sensitivity E_{Lx} is inversely proportional to the area enclosed by the parallelogram guide A_{pg} , given a position error of the flexure hinges in z direction (e.g. Δe_{Az}). Thus, the lever length and the lever distance should be preferably large. As correctly pointed out in [Kec+21], a square provides a slight advantage over a rectangular area.

Mass comparators for highest demands employ a gimbal-mounted hanging weighing pan. The pendulum type hanging weighing pan has a natural self-centering property. For a gimbal in form of flexure hinges a certain elastic stiffness is present. Thus, the moment introduced by a mass offset is reduced but not fully eliminated. Assuming a large gravitational torque and small elastic reaction forces of the gimbal, the reduction factor is calculated according to

$$K_{hwp} \approx \frac{C_E}{m_{S5} g h_{S5E}}.$$

With an exemplary mass of $m_{S5} = 1.2\text{ kg}$, a length of the pendulum of $h_{S5E} = 400\text{ mm}$ and a stiffness of the gimbal of $C_E = 14.6\text{ N mm rad}^{-1}$, the reduction factor for the torque on the load carrier amounts to $K_{\text{hwp}} = 3.1 \times 10^{-3}$. The benefit of using a hanging weighing pan can thus be considered by multiplying K_{hwp} with the off-center load sensitivity of a top-loaded weighing cell.

The FE model of a weighing cell structure was used to investigate all three components of the off-center load sensitivity. Due to the comparably simple geometry, the planar weighing cell PROT-S is considered. Results of parametric models have been presented in [Dar+20]. One result is presented in Fig. 5.9 which is showing the purely mechanical change of the force balance within the mechanism as mass change on the weighing pan. The local coordinate system for the displacements ϵ_{Sx} , ϵ_{Sy} , ϵ_{Sz} is defined in Fig. 5.1 with its origin in F.

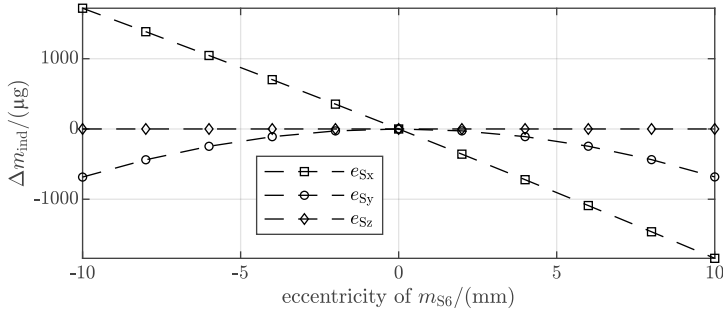


Figure 5.9 – Effect of off-center load on the indication of the FE model of the PROT-S weighing cell structure.

It is obvious that eccentricities in x direction show the largest effect. In y direction a symmetric quadratic mass change is present. Position changes of the mass in z direction were comparably insignificant. The z offset ϵ_{Sz} is typically not considered in literature. Numerical calculations in [Dar+20] using a three-dimensional FE model prove the insignificance of the off-center load sensitivity in z direction for large eccentricities ϵ_{Sz} .

The analytic model equations for the off-center load sensitivity (5.20) suggest a linear increase of the Δm_{ind} for growing eccentricities. In x direction, this is supported by the FE model, see the pronounced linear effect in Fig. 5.9. However, in [Dar+20] an offset quadratic effect was identified. For a pronounced x displacement of the weighing pan the off-center load sensitivity was reduced to

zero. It was found that this behavior results from a moment-induced deformation of the load carrier. The behavior was experimentally verified as documented in Section C.5.

5.4 Electro-magnetic force compensation

For a complete picture of the mechanical effects within the weighing system, the interdependence of mechanism and attached EMFC subsystem needs to be taken into account. Figure 5.10 shows the tilt-induced lateral deformations (y direction). Those have been measured on the tilted PROT-S weighing cell at the position of the actuator (K). These error motions, which are not corresponding to the mechanism's intended DOF (in measurement direction) are directly influencing functional components of the weighing cell, the position sensor and the voice coil actuator. This interdependence with the EMFC system is a tilt-induced source of uncertainty.

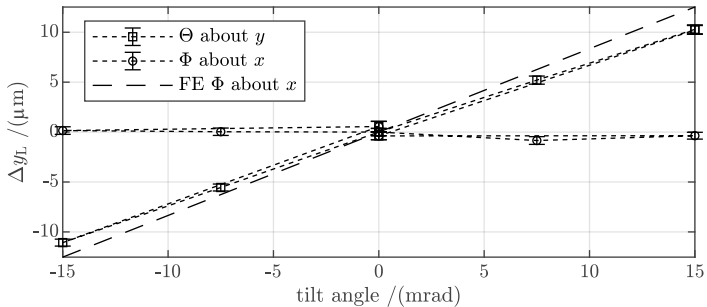


Figure 5.10 – Lateral deflection of the PROT-S transmission lever as a result of tilts. The deflection was measured using the chromatic-confocal displacement sensor (MICRO-EPSILON IFS2405-0,3).

5.4.1 Zero-indicator

Ideally, the position sensor only responds to displacements in z direction. However, the real system is influenced by cross-talk in other directions. These effects have been measured and discussed in [Mar19], especially concerning changes in sensitivity. A complex analytical model for the position sensor taking into account the elliptical

light distribution of the LED is presented in [Pfe96]. A perfect alignment of the

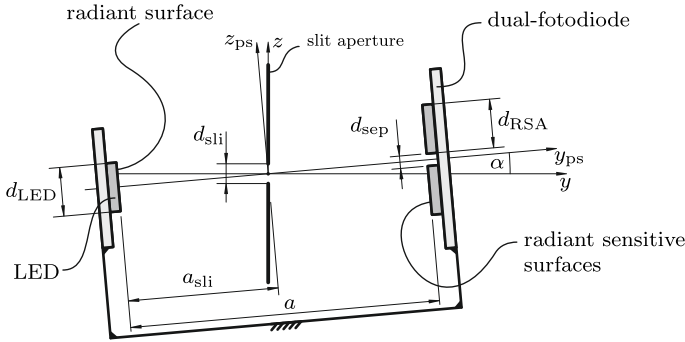


Figure 5.11 – Depiction of the position sensor assembly.

sensor to the weighing cell coordinate system cannot be guaranteed. Consequently, a certain angular misalignment angular misalignment of position sensor housing about x axis α in Fig. 5.11 is always present. The inclination of the optical axis relative to the mechanism y axis creates the sensitivity to y deflections of the aperture slit. Any lateral deflection of the aperture slit results in a position error for the mechanism. Since the control loop compensates the position error by a deflection of the mechanism, a weighing cell mechanism with finite stiffness shows an erroneous indication.

5.4.2 Actuator

Relative position changes of the coil in the annular air gap of the cylindrical magnet system lead to changes of the actuator constant Bl . Due the rotational symmetry of the actuator, one can distinguish between an axial (z_C) and radial (x_C, y_C) offset of the coil resulting both in a change of the effective Bl of the actuator.

A simplified but complete analytic model for the computation of force and torque values on the coil is provided in [Pfe96]. Here, all DOF are considered as well as all force and torque components. A schematic section view of the actuator is presented in Fig. 5.12.

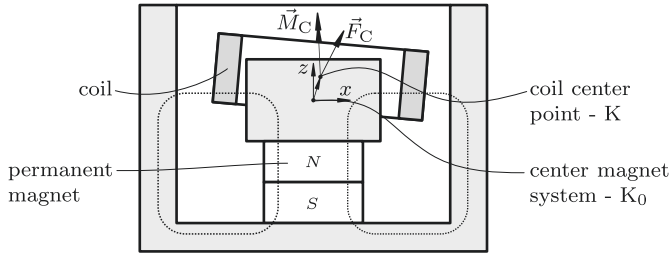


Figure 5.12 – Section view of the electro-magnetic actuator.

For a z displacement, the change of Bl has been approximated in [Pfe96] as:

$$Bl(z_C) = Bl_0 + Bl_1 \Delta z_C + Bl_2 \Delta z_C^2$$

5.4.3 Modeling of electromechanical components

An important detail within the numeric models was the implementation of the EMFC system. The modeling of both position sensor and voice coil actuator is demanding. With the clear focus on the mechanical properties of the weighing cell, two simplified modeling approaches were used. The approach in Subfig. 5.13a was the most basic implementation. A z displacement constraint was imposed on a remote node in the FE model, representing the actuator and the positions sensor. Hereby, distinct locations of position sensor and actuator with slightly different deflections were neglected.

The second version in Subfig. 5.13b is accounting for the different locations of actuator and positions sensor and can be described as quasi-static position control. The level of detail is increased at the cost of a higher level of computational effort.

The third version of EMFC modeling in Subfig. 5.13c imitates the principle of the position controller and was thus capable of capturing errors resulting from the nonlinearities within the position sensor and the voice coil actuator. An external node on the aperture slit of the position sensor (M) was used as position reference during the solution process whereas another external node at the coil position (K) was used to represent the actuator. In a loop, the deflection of point M is measured and compared to a predefined set point. The control difference was amplified and inserted as a displacement at node K. For the sake of robustness

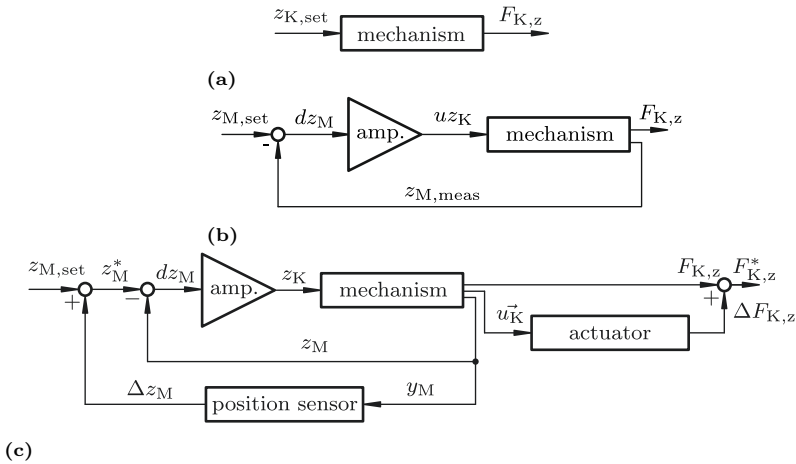


Figure 5.13 – Modeling approaches for the EMFC system comprising position sensor and actuator. (a) displacement constraint with evaluation of corresponding reaction force (b) quasi-static position control (c) quasi-static position control under consideration of nonlinearities of EMFC components. K - actuator force application point, L - CoG counter mass, M - position measurement.

concerning the nonlinear solution of the model, the introduction of a displacement was preferred over the exertion of the actuator force directly. The actuator force was evaluated at the displacement constraint on node (K). The process was repeated until the control difference was falling short a predefined error bound of 1×10^{-9} m.

5.5 Chapter summary

The modeling chapter introduced several mechanical models to estimate the mechanical system parameters and their adjustment. Together with the preceding chapter on flexure hinges, the chapter's content represents an important foundation for the following contents of the work. The analytical rigid body model provides a good overview of the important mechanical properties. Its verification was proven by the numerical rigid body model in ANSYS®, since both model are based on equal modeling assumptions. The three-dimensional finite element models were set up to overcome the limitations of the rigid body model by including the de-

formation of the flexure hinges and other structural parts. The three-dimensional finite element model additionally allowed to compute the out-of-plane behavior in terms of tilt sensitivity and off-center load sensitivity, which have relevant implications when the interplay between mechanism and the EMFC system is considered. Relative changes within the models, e.g., adjustments, were mapped with high-precision. The following general statements can be derived from the finding in this chapter:

- The astatization parameter h_{HG} introduces a load dependency of the stiffness (cf. Fig. 6.6). A weighing cell used as an analytical balance with $h_{\text{HG}} \neq 0$ would be subject to different mass sensitivities over its weighing range.
- The mechanical modeling of the gravitational stiffness components requires a nonlinear structural analysis (cf. Fig. 5.6). Analytically and excluding parasitic deformations, the stiffness variation is well described with

$$C_{\text{grav}} = \left(\frac{h_{\text{HG}}^2}{h_{\text{FG}}} - h_{\text{HG}} \right) m_{\text{G}} g,$$

where m_{G} comprises all masses suspended at flexure hinge G.

- When defining the parameter h_{HG} by machining the flexure hinges, the exact knowledge of the elastic stiffness is missing. The uncertainty concerning the elastic stiffness is largely influenced by manufacturing deviations at the flexure hinges. The manufacturing process requires repeatability of better than a micrometer to realize a reliable starting point for the fine-adjustment with trim masses.
- A short coupling element smaller than $0.1 \cdot h_{\text{HG}}$ severely reduces the gravitational stiffness component of the astatization. For a small length, even a high stiffness increase is to be expected (cf. Fig. 5.7). A possibility for a short coupling element and an optimization of the building space is placing flexure hinge F above G and thus create a negative value for h_{FG} . For $h_{\text{FG}} < 0$, the coupling element is under compression load. By rotating each flexure hinge by 180° about their rotational axis while maintaining their connection point, the flexure can still be loaded with a tensile load, which is generally considered advantageous.

The cross-talk between mechanism and position sensor is a very complex multi-physical problem which was treated in a highly simplified fashion. The most problematic effect for the weighing cell prototypes proved to be the lateral deflection of aperture slit as a result of Φ -tilt and ϵ_{Sy} off-center load. If the optical axis of the

position sensor (connecting line between LED and dual-fotodiode) is not parallel to the mechanism's y axis, any lateral deflection of the lever results in an offset of the measured zero-position. Thus, the angular position of the transmission lever is dependent on the lateral deformation thereof. With the stiffness of the mechanism, this results in direct errors of the indicated mass. The error can be mitigated by aligning the optical axis with the mechanism y axis. A better solution is the reduction of any lateral deformations of the lever in the first place.

The actuator, a coil in the annular air gap of a permanent magnet system, is affected by linear and angular offsets of the coil from its nominal position. These are affecting the required coil current to uphold the force balance within the weighing cell. Since the indicated mass is calculated based on the coil current, the deviations lead to direct measurement errors. Mitigation of any lateral offsets of the coil within the magnet system is key to reduce measurement error stemming from the actuator.

This interplay between model and experiment is the core of the following chapter on the experimental investigation of weighing cell prototypes.

Chapter 6

Weighing cell prototypes

The previous chapter on mechanical modeling of monolithic weighing cell mechanisms theoretically verified the proposed adjustment concept. Experimental verification requires weighing cells with built-in trim masses according to the proposed adjustment concept using m_{T2} , m_{T3} , and m_{T8} . The astatization parameter h_{HG} was implemented in the weighing cell mechanism. Two mass comparator prototypes were designed to verify the mechanical models, test the adjustment concept, and implement alternative mechanical concepts.

After the brief introduction to the prototype weighing cells and their most important design features, the methods for determining the mechanical system properties (C , D) are described. The off-center load sensitivity measurements (E_L) were excluded from this chapter to focus on stiffness and tilt sensitivity measurements. More specific measurements on the stiffness follow: all stiffness measurement methods were tested on an exemplary weighing cell prototype. Subsequently, the stiffness values of all built prototypes were compared to the model-based predictions. Tilt measurements in two axes follow this comparison. Finally, the steps of the adjustment concept are experimentally verified, including the rough adjustment by astatization followed by fine adjustment with trim masses.

6.1 Prototype weighing cells

The prototype weighing cells are the PROT-S weighing cell with a standard mechanism design and the equal-arm prototype (PROT-EA). Both prototypes have a planar mechanism and use the complete implementation of the adjustment concept, comprising the adjustment parameters (h_{HG} , h_{T2} , h_{T3} , h_{T8}). All prototype mass comparators were designed for a nominal mass of $m_{S6} = 1$ kg.

6.1.1 Standard kinematic mechanism: PROT-S

The PROT-S weighing cell is the most extensively investigated prototype weighing cell in this work. The fundamental idea behind this EMFC weighing cell design was the use of a well-known and preferably simple mechanical structure to verify the application of the complete adjustment concept experimentally. In addition, emphasis was placed on robustness, good accessibility, and a simple geometry for manufacture in a single setting on the machine. The planar and monolithic weighing cell mechanism PROT-S fulfills these criteria. The final design of the PROT-S prototype is presented in Fig. 6.1. It employs the standard kinematic system with a parallelogram linkage as a linear guide for the weighing pan and a transmission lever in the center, connected by a coupling element. The flexure hinges correspond to the geometry treated in Ch. 4 with a nominal minimal notch height of $50\ \mu\text{m}$ and a width of $10\ \text{mm}$ resulting in an aspect ratio of 200. The adjustment concept

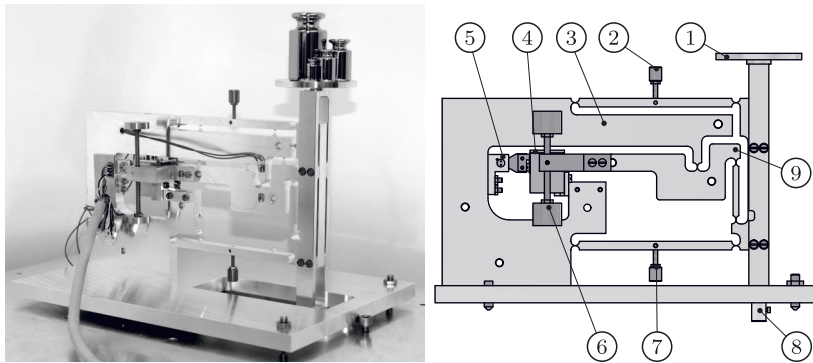


Figure 6.1 – PROT-S weighing cell prototype with its most relevant components indicated: ① substitution weighing pan ② m_{T3} ③ base structure ④ actuator ⑤ position sensor ⑥ m_{T8} ⑦ m_{T2} ⑧ gimbal mount for hanging weighing pan ⑨ h_{HG} .

was implemented utilizing brass trim masses. The vertical position is adjusted via threads. The trim mass on the transmission lever m_{T8} is designed with a relatively large mass and a large adjustment range compared to the trim masses on the levers. The extensive adjustment range was intended to compensate for possible manufacturing and mounting deviations concerning the parts attached to the transmission lever. The long threaded rods allow the attachment of smaller masses for fine adjustment.

The EMFC components, actuator and position sensor, are commercial of the shelf parts. Characteristic for each weighing cell mechanism is the astatization parameter h_{HG} . Thus, this parameter in millimeters, multiplied by 100, enters the designation of the respective weighing cell. For example, a PROT-S mechanism with $h_{HG} = 3.15$ mm has the following designation: PROT-S-HG315-x, where x is a consecutive number.

6.1.2 Equal-arm weighing cell: PROT-EA

The equal-arm prototype weighing cell in Fig. 6.2 was designed as the consequential continuation of the equal-arm beam balance concepts for the most accurate mass comparators. The concept unites the advantage of complete symmetry with the

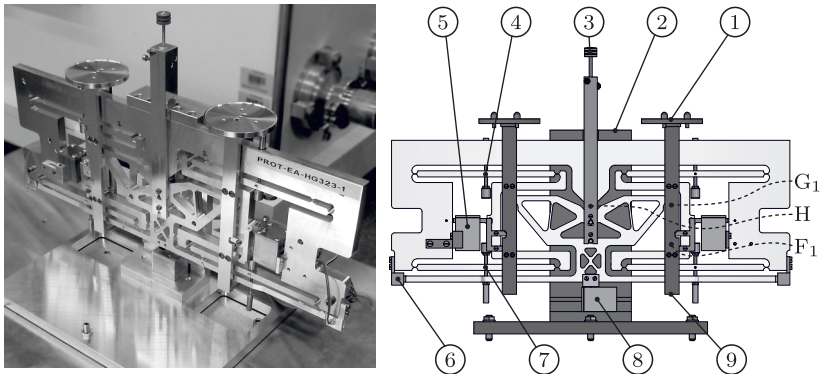


Figure 6.2 – PROT-EA weighing cell prototype with its most relevant components indicated: ① substitution weighing pan ② base connection ③ m_{T8} ④ m_{T3} ⑤ actuator ⑥ position sensor ⑦ m_{T2} ⑧ horizontal actuator ⑨ attachment point hanging weighing pan. The central flexure hinge H and the coupling elements with flexure hinges F and G are hidden by mounted components.

mechanical concept of the EMFC weighing cells. The symmetric setup mitigates several spurious influences arising from temperature fluctuations, changes in air density and vertical ground motion components. Further, the equal-arm balance concepts allow the application of both the substitution- and transposition weighing method. The developed prototype provides further advantages: the planar mechanism was realized as a monolithic compliant mechanism which enables the

machining in one setting on the machine, tight tolerances, and minimum mounting effort. The following design details were implemented:

- base connection directly above the central flexure hinge of the transmission lever (H) allows for the rigid support of the main force flow,
- CoG of transmission lever close to CoR at flexure hinge H and fine adjustable with m_{TS} ,
- multiple operation modes were enabled with one vertical actuator on each load carrier and one horizontal actuator on the transmission lever below H,
- full implementation of the adjustment concept with astatization and fine adjustment of C and D_{\ominus} using trim masses,
- two symmetric position sensors can be used to eliminate non-rotational motions of the transmission lever,
- topology optimized transmission lever for high stiffness and low net mass.

To reduce costs and manufacturing effort, the parts attached to PROT-EA were largely adopted from the PROT-S prototype. The characteristic variable h_{HG} entered the designation of the prototype weighing cells as PROT-EA-HG323-1, indicating a $h_{HG} = 3.23$ mm on both sides of the transmission lever. The particularities of this mechanism are described in [EP 000004119908 A1]. The numerous opportunities for the operation of this concept have been described in the patent [DE 102016106695 B4]. Measurement results for this prototype are not discussed within this document.

6.2 Measurement methods and results

Measurement of the mechanical properties is essential to monitor the adjustment process. In addition, the measurements were used to verify the mechanical models in Ch. 5 and to check the feasibility of the adjustment concept. Measurements were conducted especially for stiffness and tilt sensitivity¹.

6.2.1 Stiffness measurement

The determination of the stiffness was performed in different configurations, essentially distinguished by the weighing cell's assembly state and its orientation relative

¹The practical realization of the measurements with operational weighing cell prototypes was carried out by M.Sc. Markus Pabst.

to the vector of gravitational acceleration (\vec{g}). The methods listed in Tab. 6.1 have been applied to PROT-S weighing cells.

Table 6.1 – Stiffness evaluation methods for the weighing cell PROT-S.

abbreviation	description	orientation
CMM-1	measurement of h_S with a CMM and model based calculation of the stiffness (mechanism with manufacturing fixation)	no relevance
CMM-2	measurement of flexure geometry with a CMM and model based calculation of the stiffness (manufacturing fixation removed, Zeiss UMM550)	no relevance
OLHD	open-loop operation of weighing cell with actuator in otherwise disassembled state and horizontal orientation	$\vec{g} \parallel y$ axis
NF	completely disassembled mechanism in horizontal orientation	$\vec{g} \parallel y$ axis
CLVA	closed-loop operation mode of the weighing cell in fully assembled condition	$\vec{g} \parallel z$ axis

Figure 6.3 compares the results of all stiffness measurement methods applied to the PROT-S-HG415-2 weighing cell. The measurements were sorted in chronological order. Repeated measurements especially for closed-loop-vertical-assembled (CLVA) have been performed to find the root-cause for the comparably large discrepancy between the CLVA values and the results from other measurement methods.

The measurement CMM-1 was provided by the manufacturer of the weighing cell mechanism in form of a dimensional measurement protocol meaning that the details concerning the CMM measurement procedure are unknown. The CMM-1 stiffness result is closest to the nominal stiffness value (dotted line). For CLVA-1 and CLVA-2 in Fig. 6.4, stiffness and a tilt sensitivity values were measured. A correction was performed on the measured stiffness value C_{meas} according to (6.1)

$$C_{\text{corr}} = C_{\text{meas}} + D_{\Theta, \text{meas}} l_{\text{HG}}^{-1}, \quad (6.1)$$

compensating the residual tilt sensitivity to zero, $D_{\Theta} = 0$. Using the correction, vertically misaligned CoGs are not falsifying the stiffness result.

The first CLVA measurements 1-2 show a pronounced negative stiffness value, suggesting that the elastic stiffness is close to zero. The flexure hinges would require a very small minimal notch height of approximately 25 to 35 μm . The CMM-1 measurement however provides values for the minimal notch height between 46 to 48 μm and the CMM-2 in the range of 43 to 49 μm . This comparison provides evidence that the CLVA measurements seem to be unreliable. Misalignment between EMFC components and the weighing cell mechanism are a potential root cause.

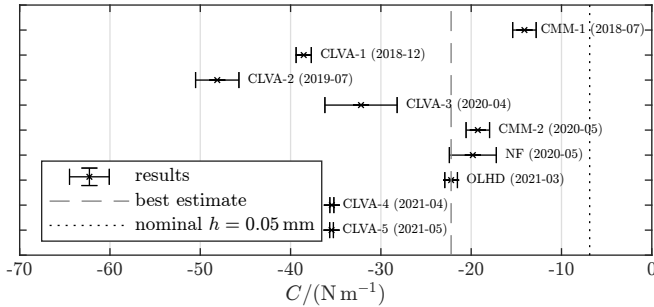


Figure 6.3 – Comparison of different stiffness determination methods applied to PROT-S-HG415-2. CMM-1 - coordinate measuring machine at manufacturer, CMM-2 - coordinate measuring machine using Zeiss UMM550, CLVA - closed-loop vertical assembled, NF - natural frequency measurement, OLHD - open-loop horizontal disassembled.

Accurate and repeatable alignment was not ensured in the design of the PROT-S weighing cell.

The results from CMM-2, NF, and OLHD are in good agreement. To enable a direct comparison with the CLVA measurements, each determined stiffness value was corrected with the theoretical gravitational stiffness component of -58.84 N m^{-1} ($m_S = 1 \text{ kg}$). This correction was also applied to CMM-1.

The repeated CLVA measurements 3-5 show a higher stiffness value. These have been performed after disassembly of the weighing cell and a following reassembly which again suggest that misalignments are responsible for the change in measured stiffness. Additionally, a pronounced effect was determined for stiffness measurements for different z positions of the weighing pan as Fig. 6.4 shows. The EMFC components are expected to contribute significantly to the behavior shown in Fig. 6.4. One contribution may result from a quadratic sensitivity change of the position sensor, see Subsec. 2.4.5.

Despite the uncertainty associated to the results of the CLVA measurement results, the shortfall of the determined stiffness values compared to the nominal value is a striking observation for the majority of the measured weighing cells. The overview of the predicted stiffness values vs. measured stiffness in Fig. 6.5 supports the observation. The CLVA stiffness measurements results for all manufactured PROT-S weighing cells with different h_{HG} values are displayed. The measure-

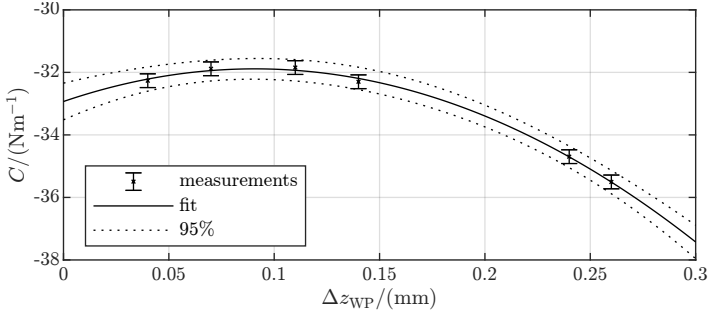


Figure 6.4 – Measured stiffness of PROT-S-HG415-2 for different z positions of the weighing pan z_{WP} .

ments were conducted with the nominal sample mass of 1 kg on the weighing pan.

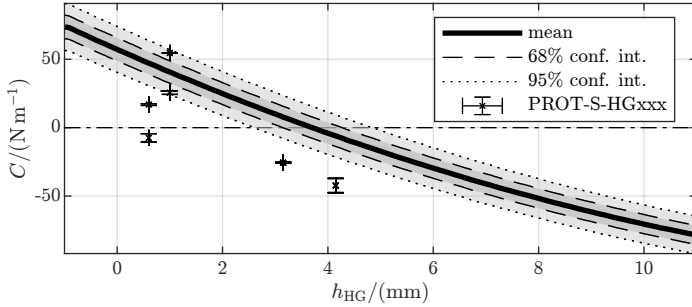


Figure 6.5 – Analytical rigid body model stiffness estimation for a variation of the parameter h_{HG} including MONTE CARLO simulation and uncertain input parameters. The model input for $m_G = 1.1755$ kg corresponds to a sample mass of 1 kg in the experiment. A nominal minimum notch height at the flexure hinges of $h = 50 \pm 5$ μm was assumed and thus presents the nominal stiffness values. The measurement method used is CLVA according to Tab. 6.1.

A MONTE CARLO based computation displays the nominal behavior according to the analytic rigid body model with the expected manufacturing deviations, especially concerning the minimal notch height of the flexure hinges of 50 ± 5 μm . Every error bar stands for multiple measurements on a single manufactured and assembled PROT-S, which was loaded with the nominal load of 1 kg.

Figures 6.5 clearly shows a tendency of the realized prototype weighing cells to deviate from the model prediction, presumably caused by mentioned manufacturing deviations at the flexure hinges. The dilemma behind the observation is that the astatization in the mechanism (h_{HG}) cannot account for a deviation from the nominal elastic stiffness after manufacturing. Manufacturing multiple PROT-S weighing cells with different h_{HG} values ranging from 0.6 to 4.15 mm was intended to cover the uncertainty of the elastic stiffness. However, this approach presumes an excellent repeatability of the manufacturing process. Neither of the realized weighing cells was close to the nominal values. The weighing cells with a h_{HG} of 0.6 mm show the smallest deviation to the aspired value $C = 0$.

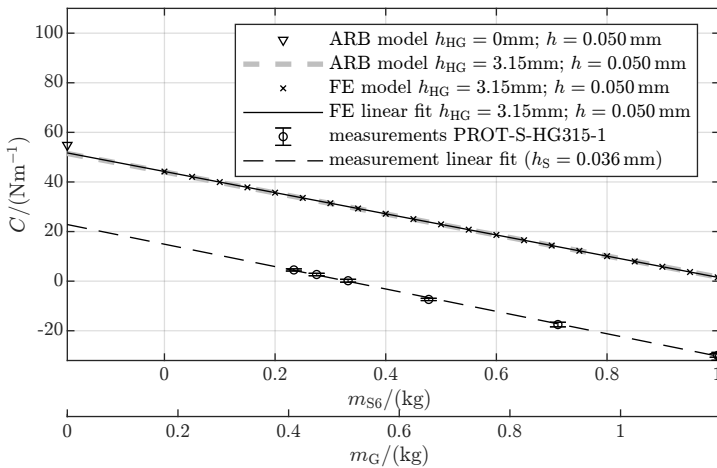


Figure 6.6 – Comparison of model and experiment for PROT-S-HG315-1 and a variation of the mass on the weighing pan. The different models are in good agreement and the measured stiffness values for the prototype show a pronounced offset to the nominal curve. A reduction of the model input h to about 36 μm leads to a parallel shift and brings model and experiment in agreement. (ARB - analytical rigid body model, FE - finite element analysis model)

For the specific prototype PROT-S-HG315-1 with a fixed h_{HG} , the stiffness is linearly dependent on the total mass suspended at G (m_G). This was proven in the numeric models and the experiment for PROT-S-HG315-1. The results are presented in Fig. 6.6. The pronounced negative stiffness offset between the measurements and the models agrees with the observations in Fig. 6.5.

The linear relationship between stiffness and sample mass on the weighing pan in Fig. 6.6 can be exploited by a method known as substitution. Initially, it refers to the addition or the removal of masses to/from the (substitution) weighing pan to maintain roughly constant loading of the balance in case another sample mass is supposed to be measured. Similarly, the substitution had been used to bring PROT-S-HG315-1 close to zero stiffness by reducing the sample mass (m_{SG}) on the weighing pan from 1 kg to 0.335 kg. The reduction of the sample mass deviates from the goal of building a 1 kg mass comparator. However, it allows proceeding with the test of the complete adjustment concept and the fine adjustment of stiffness and tilt sensitivity using the foreseen trim masses.

In conclusion, it can be stated that the applied manufacturing process was not repeatable enough to work with fixed h_{HG} values prior to the manufacturing of the mechanism. Therefore, either the manufacturing process must be tuned to give more reliable results or measures for an a-posteriori adjustment of h_{HG} need to be implemented. The alignment features for the mounted components on the PROT-S weighing cell were not sufficient to allow for reliable and repeatable absolute stiffness measurements.

6.2.2 Tilt sensitivity measurements

The tilt sensitivities Θ and Φ were measured on a high-resolution tilt table designed for delicate instruments and rather heavy payloads up to 35 kg. The tilt platform has an angular motion range of $\pm 17.6 \mu\text{rad}$ or $\pm 1^\circ$ in both axes with a resolution, backlash, repeatability, and cross-sensitivity better than $1''$ [RKF14]. The full angular range of the tilt table represents a very pronounced tilt for a mass comparator which will not occur in this scale during operation. Nevertheless, it was advantageous to have these rather large tilt angles to resolve small tilt sensitivities under atmospheric conditions. The setup in Fig. 6.7 was used for all tilt measurements presented throughout the document.

The tilt reaction of a weighing cell can be modeled by introducing an angle in-between the reference coordinate system (x_0, y_0, z_0) and the weighing cell coordinate system (x, y, z) . The weighing cell is rotated relative to the quasi-stationary gravitational acceleration vector in a tilt sensitivity measurement on the tilt table. Within the

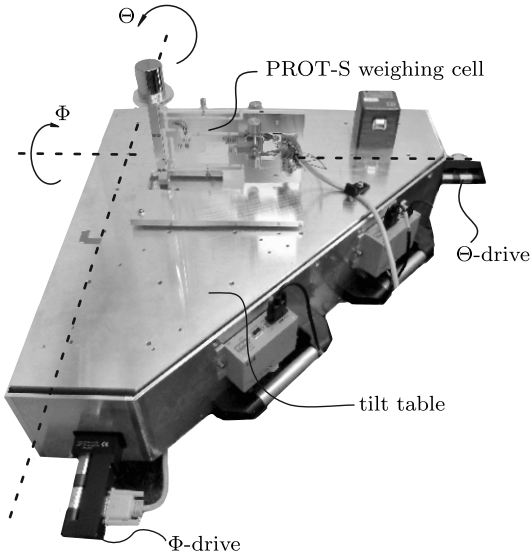


Figure 6.7 – Tilt-table measurement setup with a PROT-S prototype weighing cell [RKF14].

numerical models, the gravitational acceleration vector \vec{g} was rotated according to:

$$\vec{g}(\Theta, \Phi) = g \begin{pmatrix} \sin(\Theta) \cos(\Phi) \\ \sin(\Phi) \cos(\Theta) \\ \cos(\Theta) \cos(\Phi) \end{pmatrix}$$

For both cases, the sign of the tilt sensitivity is defined according to Def. 5.4. For each relative orientation between weighing cell and \vec{g} , the tilt reaction as $\Delta m_{\text{ind}}(\Theta, \Phi)$ was evaluated. Parametric studies with numerical models and measurements on the tilt table revealed the following characteristic behavior, observed in Fig. 6.8. The tilt reaction over both angles has a linear and a quadratic component. For Θ , the linear component stems from vertically eccentric CoGs. For the tilt about Φ of a planar weighing cell mechanism, the linear component is proportional to the off-center load of m_{S6} in the y direction ($m_{S6} \cdot \epsilon_{Sy}$). It was shown that both quadratic terms are equal and proportional to the force exerted by the actuator according to:

$$\left(1 - \cos\left(\sqrt{\Theta^2 + \Phi^2}\right)\right) F_{\text{EMFC}}. \quad (6.2)$$

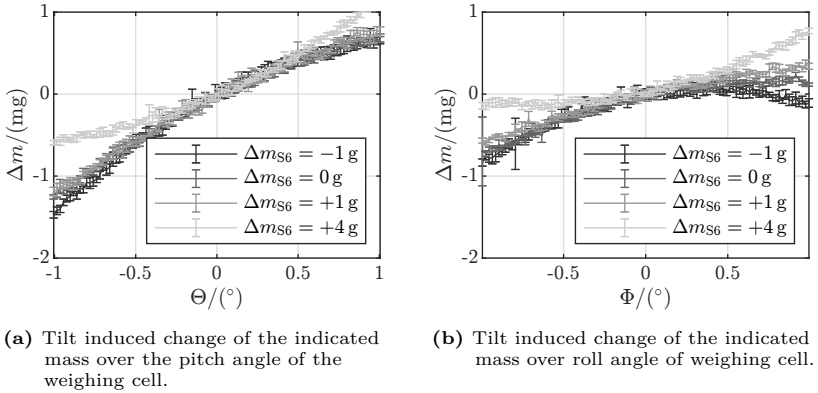


Figure 6.8 – Adjusted commercially available weighing cell tilted about two perpendicular axes. The mass on the weighing pan was slightly varied to show a second order effect which is proportional to the force exerted by the actuator (F_{EMFC}). The mass on the weighing pan for $F_{EMFC} \approx 0$ amounts to $m_S = 281$ g.

The described characteristic was only evident for a well-adjusted weighing cell. Otherwise, with vertically eccentric CoGs, a pronounced linear component is superimposed, see [DFT19].

An exemplary tilt measurement in two axes is presented in Fig. 6.8. The weighing cell under investigation is a commercially available weighing cell which was not in its original but a well-adjusted state. In Subfig. 6.8a, the pitch motion of the weighing cell from -1 to 1° was investigated. The tilt reaction was evaluated as a change in indicated mass. It shows a linear behavior that is superimposed by a second-order effect. The latter is proportional to the mass imbalance or the actuator force (F_{EMFC}) within the weighing system, see (6.2). The quadratic effect vanishes for a mass on the weighing pan close to the electrical zero of the balance ($F_{EMFC} = 0$).

6.3 Experimental verification of the adjustment concept

The described tilt sensitivity measurement combined with the stiffness measurement enables the fine adjustment of the prototype weighing cell. The fine adjustment process was conducted on the precision tilt table to monitor C and D_Θ after each

adjustment step. The process of the manual adjustment is displayed in Fig. 6.9 and follows the adjustment plan in Def. 6.1:

Definition 6.1 (adjustment plan).

1. measure C and D_Θ ,
2. calculate the theoretically required adjustment steps: Δh_{T8} , Δh_{T2} , Δh_{T3} according to (5.18) and (5.19),
3. perform the manual adjustment calculated in the previous step and set the new values for h_{T8} , h_{T2} , h_{T3} ,
4. compare to the adjustment objective C^* and D_Θ^* ,
5. repeat step 1-3 until adjustment objective is fulfilled: $|C| \leq C^* \wedge |D_\Theta| \leq D_\Theta^*$.

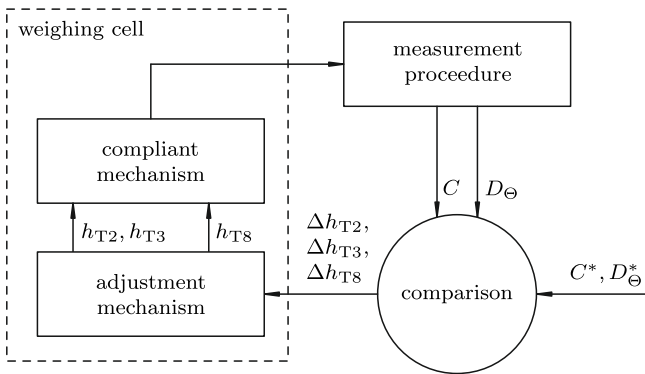


Figure 6.9 – Schematic drawing of the manual adjustment process inspired by [Kra00].

The experimental proof of the adjustment concept was performed on the weighing cell prototype PROT-S-HG315-1. The fine adjustment with the trim masses m_{T2} , m_{T3} , and m_{T8} was applied. The load dependency of the astaticized weighing mechanism was exploited to achieve a viable starting point with C and D_Θ close to zero. Figure 6.6 shows that the mass m_{S6} needs to be reduced to about 335 g to minimize the residual stiffness [Dar+19]. This accounts for the missing 15 μm of effective minimal notch height between h_S and h_{nom} of the prototype under consideration. From this state, with a stiffness of $C = -0.0335 \text{ N m}^{-1}$ and a tilt sensitivity of $D_\Theta = 0.00551 \text{ N rad}^{-1}$, the required adjustment parameters were

estimated with (5.19) and (5.18) to: $h_{T2} = -6.075$ mm and $h_{T8} = 0.019$ mm. The results can be retraced in Fig. 6.10.

Figure 6.10 proofs the existence of a common zero for stiffness and tilt sensitivity experimentally [Dar+19]. The achievable values are restricted by the precision of the measurement of stiffness and tilt sensitivity under atmospheric conditions. A further reduction of the absolute values for stiffness and tilt sensitivity will be enabled by in-vacuo adjustment.

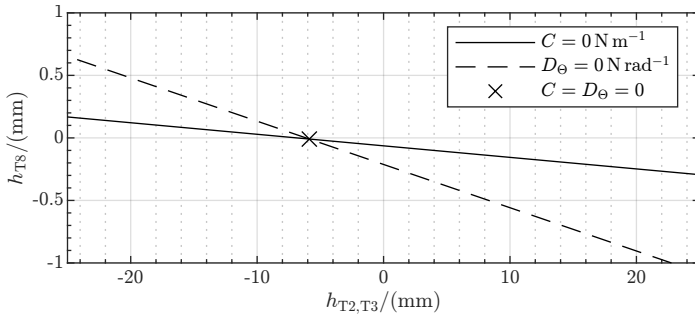


Figure 6.10 – Fine adjustment of the properties C and D_{Θ} for PROT-S-HG315-1. The graph shows the linear function where each property equals zero. The experiment is in good agreement with the model prediction and the existence of the $C = D_{\Theta} = 0$ was experimentally verified.

6.4 Chapter summary

Monolithic weighing cell prototypes were investigated based on mechanical models and experiments with weighing cell prototypes. Both the numerical models and the measurement methods were suited to reproduce the adjustment concept, including astatization (h_{HG} , m_{S6}) and fine-adjustment with trim masses (h_{T8} , h_{T2} , h_{T3}). The qualitative agreement between model and experiment was generally excellent. In contrast, the exact quantitative agreement in terms of absolute values was prone to manufacturing deviations and required the adjustment of model input parameters, especially concerning the minimal notch height of the flexure hinges h . For aligning the model with the measurement, the parameter h_S was introduced. It can be interpreted as the effective average minimal notch height of the flexure hinges in the mechanism. It is recalculated based on the measured elastic stiffness of the complete

mechanism. The measurements on weighing cell prototypes in this chapter showed a strong tendency for a shortfall of the substitute minimal notch heights of the flexure hinges relative to the nominal value of $50\ \mu\text{m}$: $h_S < h_{\text{nom}}$.

The tilt sensitivity measurement using a high-precision tilt platform with tilt angles between -1 to 1° was a well-working and indispensable element for adjusting the weighing cell prototypes. The useful resolution was limited by the experimental standard deviation slightly above the objective value $2.5 \times 10^{-6}\ \text{N rad}^{-1}$ when being measured under atmospheric conditions. A possibility to evaluate the tilt sensitivity under a vacuum atmosphere will be required to reliably adjust the tilt sensitivity to a value within the threshold.

Measures for off-center load sensitivity adjustment were not implemented in the prototype weighing cells. It was shown though that E_{Lx} can be manipulated by deformations of the load carrier affecting the parallelism between the upper and lower lever. The quantitative agreement was between experiment and model good, see Subsec. C.5. Given the required positioning accuracy in the sub-micrometer range, the experimental data was likely influenced by position errors of the flexure hinges caused by the manufacturing process. In the model the imperfections of the mechanism were neglected and explain the present deviations.

The proposed adjustment concept with coarse and fine adjustment of the mechanical weighing cell properties C and D_\ominus has been proven to remove the first-order error components. This enhances the mass comparator metrologically. The main findings are summarized:

The implemented astatization concept compensates comparably large amounts of elastic stiffness without significantly affecting the tilt sensitivity. The effective stiffness compensation comes at the cost of an introduced load sensitivity - the adjustment state is dependent on the mass on the weighing pan. The load sensitivity is not a limiting factor for a 1 kg mass comparator due to its sufficiently constant loading condition. The astatization parameter h_{HG} variation affects the elastic stiffness and has a more pronounced linear and quadratic gravitational stiffness component. The numeric models are in excellent agreement with the derived analytical model. The experimental verification was tedious since every value for h_{HG} required the build of a complete weighing cell. Small manufacturing deviations at the flexure hinges proved a large impact on the elastic stiffness. The elastic stiffness could not be predicted with sufficient accuracy to set the correct value of h_{HG} prior to manufacturing. Consequently, additional solutions need to be implemented to adjust the astatization after manufacturing.

The fine adjustment of C and D_{Θ} to a common zero has been successfully conducted experimentally. A systematic adjustment was implemented by combining trim masses on the transmission lever and the levers of the parallelogram guide. The required adjustment parameters were calculated based on the measurement of stiffness and tilt sensitivity and known geometric relations within the mechanism. A prediction of the required adjustment is possible which reduces the adjustment effort.

PROT-S

The PROT-S prototype has been designed as a preferably simple weighing system including the fine-adjustment capability with trim masses. The planar design has many advantages for the machining, however, it required compromises. Some were identified to have negative implications on the investigated mechanical properties:

- The mechanical sub-systems of the PROT-S mechanism are coupled with a wide coupling element including flexure hinges with equal width. Consequently, the mechanical coupling in y direction is strong. Lateral loads on the load carrier thus lead to rather large lateral deflection of the transmission lever where the EMFC system is located, resulting in measurement errors and a larger measurement uncertainty.
- The zero position of the monolithic mechanism is lost after the weighing cell is set up and put into operation. At least for the scientific investigations in this work, a reliable setting of the zero position proved to be very important. Consequently, a reference element needs to be incorporated in the mechanism design to allow for a repeatable setting of the zero position in the sub-micron range (applies equally for PROT-EA).
- The repeatable and accurate alignment of EMFC components to the weighing cell mechanism is important for reliable stiffness measurements in the operational state (CLVA).
- In operation, the position sensor is the datum for the mechanism. The adjustment and the long-term stability of this datum influences the metrological performance of the mass comparator. Therefore, a highly stable fixation of the position sensor is important.
- The PROT-S mechanism was designed with a C-bracket structure from the base connection to the fixation of flexure hinge H. Under nominal load, the deformation of this structure also affects the parallelism of the parallelogram levers. A systematic off-center load sensitivity is introduced which can be

mitigated by fixing of the mechanism close to the flexure hinge H instead of its original base connection.

- The counter mass assembly accommodates the two large trim mass on transmission lever m_{T8} trim masses and has a significant overall mass. Its z position therefore has a large influence on the stiffness and the tilt sensitivity. Especially, the relative z position to pivot H needs to be set with a higher accuracy, to allow for precise stiffness comparisons between different weighing cells.

A re-design under consideration of the listed aspects is expected to be beneficial for the weighing performance, the repeatability of the assembly process, and the measured stiffness values.

PROT-EA

- The investigation of the PROT-EA weighing mechanism was limited to the measurement of stiffness and tilt sensitivity. However, the weighing system allows for multiple operational modes which require further experimental investigation.
- The symmetric design of PROT-EA with its two weighing pans allows for the transposition weighing method. The simultaneous exchange of both sample masses under comparison call for a suitable mass exchanger which needs to be realized to enable reliable measurements on the performance of this operational mode of PROT-EA.
- The bounding box of the PROT-EA assembly is comparably large and impractical to fit into commonly sized vacuum chambers. Hence, decreasing the overall size of the design is possible and advantageous.

Chapter 7

Metrological model

Improving the mechanical properties of the mass comparators is key to reduce the uncertainty of mass comparisons under vacuum condition to ± 5 ng. The required tolerance limits for adjusting the mechanism were estimated for a single weighing with the EMFC weighing cell. However, the complete mass comparison process within the mass comparator needs to be considered. It consists of multiple and subsequent weighings with the EMFC weighing cell.

A single and simplified weighing process is depicted in Fig. 7.1. All previously evaluated mechanical properties of the weighing cell and experimentally verified relations were considered.

The input at the bottom left-hand-side ① is the coupling point to the mass exchanger. Here, the respective sample mass m_S is placed on the weighing pan of the mass comparator. Buoyancy forces add to its gravitational force. The buoyancy forces vanish in a high-vacuum atmosphere ($\rho_0 \approx 0$). The resulting force F_S is then transferred to the transmission lever and converted according to the transmission ratio to F_L . The counter-mass compensates for the largest part of F_L and reduces the force F_K to a force within the weighing window. The actuator requires a particular coil current I_C , which is also influenced by temperature fluctuations ΔT and the temperature coefficient of the actuator. The coil current I_C is the output ② of the weighing cell subsystem, from which the mass value can be calculated.

Additional external error sources were evaluated as a force at the weighing pan F_{par} , which was added to the gravitational force F_S . It consists of components resulting from the residual stiffness C_{EMFC} combined with the position sensor's error Δz_M , tilt sensitivities D_Θ , D_Φ with ground tilt and the off-center load sensitivities E_{Lx} , E_{Ly} with off-center loads. Several cross-sensitivities have been discovered: both

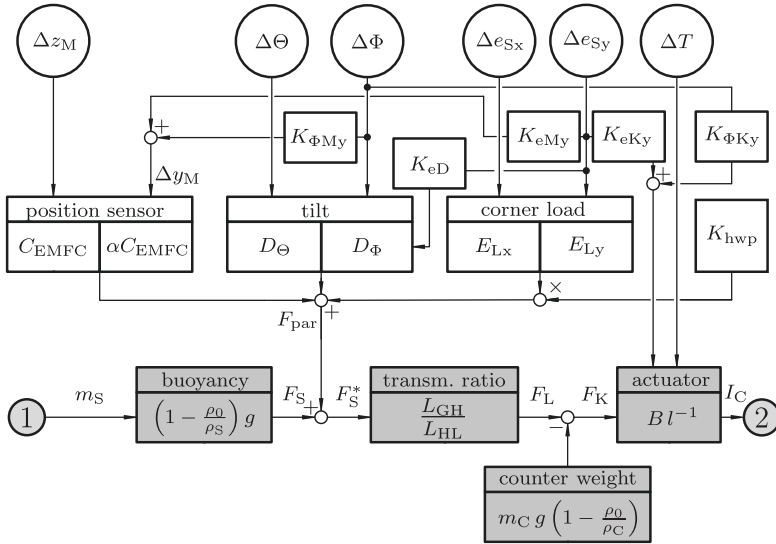


Figure 7.1 – Schematic of the weighing process with an EMFC weighing cell. The graphic is divided into the main functional flow of the weighing cell (bottom, gray) and parasitic force components (top, white).

a tilt $\Delta \Phi$ and an off-center load in the y direction (ϵ_{Sy}) can trigger a y deflection of the transmission lever (Δy_K) affecting the y position of the aperture slit. This cross-talk of the position sensor is described by the constants $K_{\Phi My}$ and K_{eMy} . If the optical axis of the positions sensor is inclined to the y axis (α), the zero point of the sensor in z changes leading to a deflection of the mechanism Δz . An off-center load in y direction adds a first-order component to the tilt sensitivity D_Φ via the constant K_{eD} .

7.1 Uncertainty consideration for weighing cell

The functional properties of the weighing cell are highly dependent on many parameters. Among those are geometrical properties, material properties, and environmental influences. A comprehensive analytical model is developed based on the gathered experience with models and experiments. The uncertainty of the system properties can thus be evaluated based on the uncertainty distributions

of the model input parameters. The consideration was based on the PROT-S weighing cell. The objective for the instrumental measurement uncertainty of a single weighing with the mass comparator weighing cell was about 5 ng. Thus, each of the five error components C_{EMFC} , D_{Θ} , D_{Φ} , E_{Lx} , and E_{Ly} should be smaller than <1 ng:

The maximum permissible value for the stiffness was calculated based on the error of the position sensor of $z_M = 1 \text{ nm}$ to $10 \times 10^{-3} \text{ N m}^{-1}$, according to:

$$C_{\text{EMFC}} \leq \Delta m_{\text{max}} g z_K^{-1}.$$

The result corresponds to a stiffness at the weighing pan of $C \approx 40 \times 10^{-3} \text{ N m}^{-1}$.

The tilt sensitivities D_{Θ} and D_{Φ} were calculated based on the assumption that ground tilts are limited to $\pm 4 \mu\text{rad}$. Then, the tilt sensitivities need to be adjusted to $< 2.5 \times 10^{-6} \text{ N rad}^{-1}$.

The hanging weighing pan reduces the off-center loads with $K_{\text{hwp}} = 3.1 \times 10^{-3}$. A lateral positioning accuracy on the hanging weighing pan of $\pm 10 \mu\text{m}$ was presupposed, leading to a maximum off-center load of $3.1 \times 10^{-5} \text{ kg mm}$. The off-center load sensitivities E_{Lx} and E_{Ly} are thus assigned with tolerance limit of $30 \times 10^{-8} \text{ N kg}^{-1} \text{ mm}^{-1}$.

7.2 Metrological model for a mass comparator application

The consideration was extended from the single weighing process to the sequential structure of multiple weighings within the mass comparator. The arrestment of the balance, the mass exchange, and the integration time for the measurement add up to the cycle time t_{cycle} . As several measurement cycles are executed, a considerable amount of time passes. Within this time, the environmental conditions and physical parameters are subject to slight variations. The developed model accounts for these effects.

The following modeling assumptions were presupposed for the setup of the model:

- the temperature is either controlled or sufficiently stable $\Delta T \leq \pm 10 \text{ mK}$; compensation measures are reducing the temperature coefficient by a factor of 100,
- vacuum pressure fluctuations are neglected,
- ground tilt is within $\Delta\Theta = \Delta\Phi \leq \pm 4 \mu\text{rad}$,

- the mass exchange process has a positioning accuracy of $\Delta\epsilon_{Sx} = \Delta\epsilon_{Sy} \leq \pm 100 \mu\text{m}$,
- desorption processes on the surfaces are neglected; it is assumed these processes have decayed in the high-vacuum environment prior to measurements with the weighing cell,
- all peripheral devices have arrived at stable operation conditions; effect on the measurement process are neglected,
- the influence of calibration is neglected.

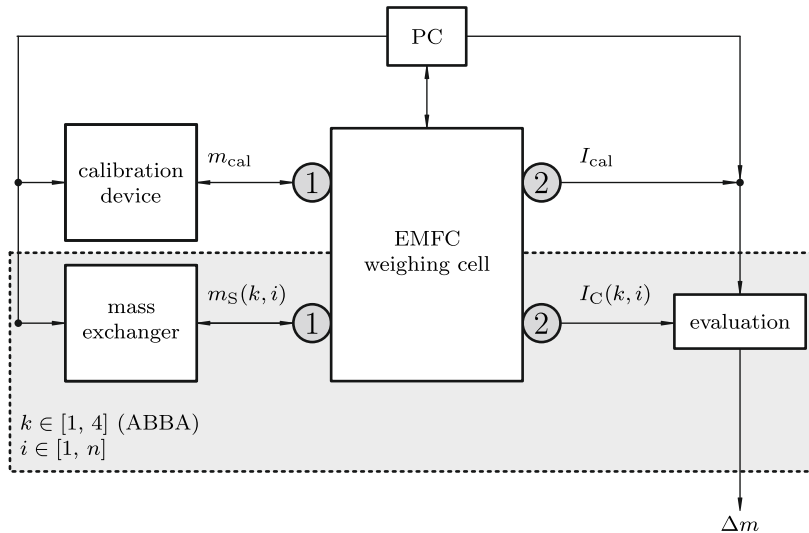


Figure 7.2 – A weighing cell integrated in the mass comparator. The weighing process is a sequence of n ABBA-cycles where A and B are the masses to be compared. The total number of measurements is $(4n)$. An in-situ calibration with calibration masses within the electrical weighing window of the mass comparator is a vital part of the process.

The sequential process within a mass comparator (see Ch. 2) with a slow periodic change of the environmental conditions were evaluated numerically based on the MONTE CARLO method. The process is visualized in Fig. 7.3 with the subsequent placings of the masses A and B on the weighing pan. The integration time is shorter than the time required for the mass exchange. At the beginning of each integration

interval, the temperature has changed slightly according to the following functions of time:

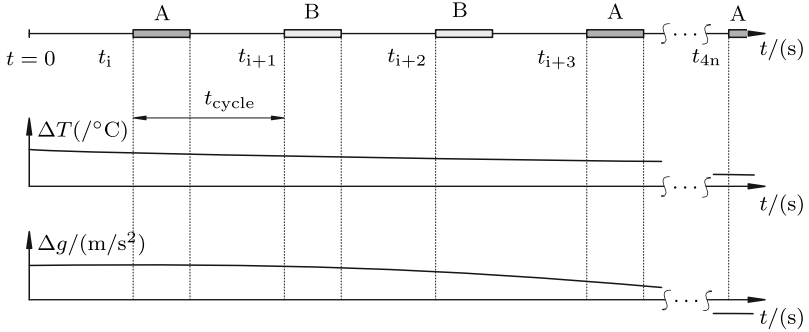


Figure 7.3 – Time scheme for the repeated mass comparison process according to a repeated ABBA_n-cycle.

$$\Delta T(t) = \hat{T} \cos \left(\left((t + t_{\text{ran}} + t_{\text{ps}}) \frac{2\pi}{t_{\text{pT}}} \right) \right).$$

Where \hat{T} is the amplitude of temperature fluctuation, t_{ran} is a random time offset, t_{ps} is the phase shift relative to noon (12 am), and t_{pT} is the period for the temperature fluctuation of 24 h. A similar function was created for time-dependent changes to the gravitational acceleration which, has an amplitude of $\hat{g} = 1.5 \times 10^{-7}$ according to [RS17]. The tides introduce the periodic behavior of the gravitational acceleration with a period t_{pg} of 12 h 25 min:

$$\Delta g(t) = \hat{g} \cos \left(\left((t + t_{\text{ran}} + t_{\text{ps}}) \frac{2\pi}{t_{\text{pg}}} \right) \right).$$

Other non-stationary parameters are the ground tilt angles and the eccentricity of the masses on the weighing pan. These are considered with their respective probability distribution function for each weighing within the sequence. While the model input guarantees a mechanically well-adjusted weighing cell where the mechanical error contributions are limited to 5 ng, the time-dependent changes of the temperature and the gravitational acceleration are further limiting factors for the uncertainty of the mass comparison. The mass difference from the sequential

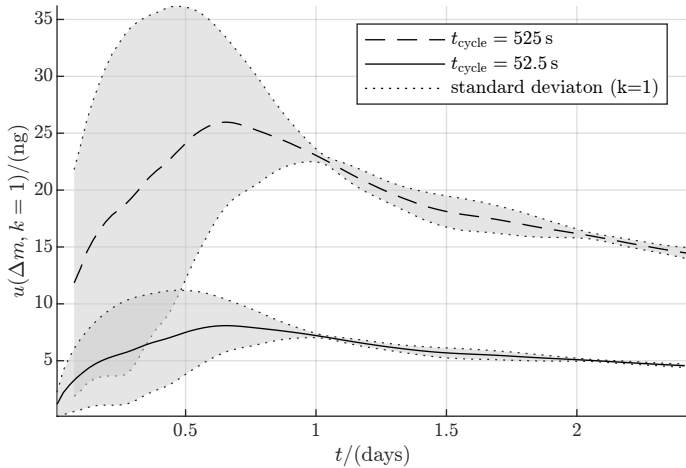


Figure 7.4 – Uncertainty consideration for a EMFC-weighing cell in a mass comparison sequence with $(4 \cdot n)$ repeated measurements.

mass measurements of the two sample masses were evaluated following the equations in [Bor+12]: the mean mass difference was evaluated using:

$$\Delta m_i = \frac{1}{2} (m_{B2}(i) - m_{A1}(i) + m_{B3}(i) - m_{A4}(i))$$

$$\overline{\Delta m} = \frac{1}{n} \sum_{i=1}^n \Delta m_i.$$

The expanded uncertainty ($k = 1$) is evaluated using:

$$\sigma^2 = \frac{1}{n-1} \sum_{i=1}^n (\Delta m_i - \overline{\Delta m})^2$$

$$u = \frac{s}{\sqrt{n}}$$

Figure 7.4 shows the uncertainty over the total elapsed time starting at $n = 3$ which is the minimum number of ABBA cycles for class E₁-weights according to [OIML R 111-1:2004]. Repetitions $n \geq 6$ are demanded in [GB09]. The curves show the calculated uncertainty ($k = 1$) of the mean mass difference for different cycle times t_{cycle} . The upper dashed curve was calculated for a relatively long cycle time of

$t_{\text{cycle}} = 525 \text{ s}$ and the lower solid curve with one-tenth of this cycle time. With the chosen cycle times, the calculation covers a technically feasible range. The time-dependent variations of ΔT and Δg define the characteristic depending on the start time ($t_{\text{ps}} + t_{\text{ran}}$). The effect of the start time variation as the standard deviation of the uncertainty is displayed by gray areas bound with dotted lines. Its width decreases for a larger number of ABBA cycles n .

7.3 Chapter summary

The tolerance limits for the mechanical properties have been estimated to achieve an uncertainty of 5 ng in a single weighing with the EMFC weighing cell. See Tab. 7.1 for the results. Obtaining these mechanical prerequisites is the primary objective of this work and is vital for the design specifications of the mass comparator weighing cell in the upcoming last chapter.

Table 7.1 – Adjustment thresholds for the mechanical properties of the weighing cell.

parameter	adjustment tolerance
C_{EMFC}	$\pm 10 \times 10^{-3} \text{ N m}^{-1}$
C	$\pm 40 \times 10^{-3} \text{ N m}^{-1}$
D_{\ominus}	$\pm 2.5 \times 10^{-6} \text{ N rad}^{-1}$
D_{Φ}	$\pm 2.5 \times 10^{-6} \text{ N rad}^{-1}$
E_{Lx}^a	$\pm 30 \times 10^{-8} \text{ N kg}^{-1} \text{ mm}^{-1}$
E_{Ly}^a	$\pm 30 \times 10^{-8} \text{ N kg}^{-1} \text{ mm}^{-1}$

^a presuming: $K_{\text{hwp}} = 3.1 \times 10^{-3}$

Additional error components influence the measurement result when the adjusted weighing cell is used in a mass comparator application. Some have been numerically simulated in a simplified manner:

A weighing cell adjusted to Tab. 7.1 was considered within a mass comparison sequence. The process was modeled numerically using the MONTE CARLO method. The sequential nature of the mass comparison, using the substitution method, was considered, and corresponding time-dependent effects were included. The consideration provides a first approximation of uncertainty contributions which seem to be further limiting factors for achieving the objective of 5 ng in high-vacuum.

The temperature coefficient of the system can be significantly reduced by temperature compensation within the magnetic system using a magnetic shunt or by temperature compensation as part of the evaluation. These measures are estimated to reduce the effective temperature variation by a factor of 100. A general limiting factor for mass comparisons is the relative variation of \vec{g} over time. The effect could be reduced with concurrent measurements of the gravitational acceleration using a relative gravimeter and a model-based compensation of the effect on the mass comparison. A more convenient measure is minimizing the actuator force or the imbalance within the weighing cell. In the model, the weighing cell was adjusted to have its electrical zero at $(m_A + m_B)/2$. The nominal mass difference amounts to 1 mg, which is twice the maximum uncertainty of E1 weight specified in [OIML R 111-1:2004].

Model simplifications and corresponding unconsidered effects can further increase the estimation for the type A uncertainty. For sufficiently small mass differences and faster cycle time, achieving an uncertainty in the single nanogram range seems viable using a weighing cell with the mechanical properties in Tab. 7.1. The required fine-adjustable weighing cell is developed throughout the following chapter.

Chapter 8

Prototype mass comparator weighing cell

The chapter provides an overview of the development and design of the advanced stiffness compensation prototype (PROT-ASC) weighing cell. The weighing cell system with its auxiliary adjustment drives is presented in Fig. 8.1. The present chapter describes the development of the weighing device from concept to the first experimental tests and measurements.

The motivation for the design of the weighing cell prototype stems from the insights gained from the previous investigations on PROT-S and PROT-EA. The metrological model in the preceding chapter refined the adjustment objectives for the mass comparator weighing cell. Mechanical first-order error components need to be reduced down to small residual values summarized in Tab. 7.1. The theoretical and experimental investigation with PROT-S weighing cells revealed two main challenges for canceling out mechanical first-order error components from a weighing cell: cross-sensitivities between the mechanical parameters and the compensation of manufacturing deviations.

Cross-sensitivities especially off-center loads and tilt angles are mutually affecting the adjustment state in terms of tilt sensitivity and off-center load sensitivity, see Fig. 7.1. The weighing cell design needs to be optimized to reduced the mentioned cross-sensitivities.

Manufacturing deviations at the flexure hinges and the correlated scattering of the elastic stiffness are the second major challenge. To achieve the tolerance limits for the stiffness of the weighing cell based on manufacturing accuracy only, the flexure hinges would have to be manufactured with a minimal notch height deviations in the single nanometer range. With reasonable effort, some micrometers deviation are technically feasible which exceeds the requirement by a factor of 1000. Fine adjustment of the stiffness is thus indispensable. A fine adjustment method based

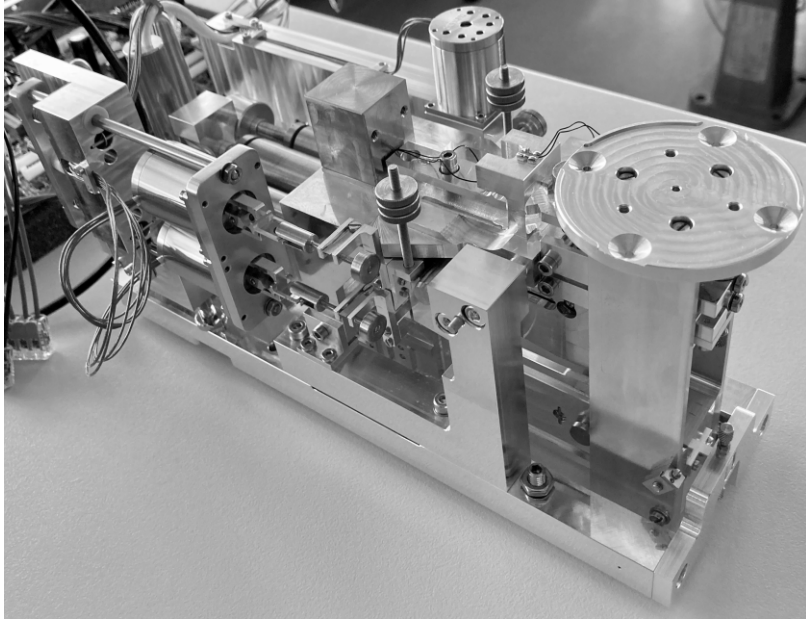


Figure 8.1 – Complete system of the PROT-ASC weighing cell with adjustment devices.

on a combination of trim masses has been elaborated in Ch. 5 and experimentally verified in Ch. 6. However, a reliable starting point for the fine adjustment, a stiffness sufficiently close to zero, was not achieved (cf. Fig. 6.5). Thus, astatization itself requires adjustment to account for manufacturing deviations.

8.1 Concept development

The linearized equation for the gravitational stiffness effect of the astatization reads: $-h_{HG} m_G g$. Either the vertical distance h_{HG} or the gravitational force of m_G can be varied to manipulate the astatization effect. The first option requires the manipulation of the flexure hinge G's vertical position within the monolithic mechanism (cf. Fig. 5.1). Despite the practicability of this adjustment, laid out in the master thesis [Pom19], the implementation was not pursued. The proposed

solution requires mechanical interfaces within the measurement loop which may lead to unpredictable effects.

The second option, the variation of the gravitational force, is known as substitution. Substitution on the weighing pan strongly affects the electrical zero of the weighing cell. Branching the force flow through two independent lever systems enables the introduction of two or more h_{HG} -values. The stiffness can thus be adjusted maintaining a constant electrical zero by altering the force balance between the load paths. The key aspect of the novel adjustment concept is the branching of the force flow through multiple lever systems. The manufacturing of various PROT-S weighing cells with different h_{HG} values during the first prototype phase enabled a preliminary test of the novel concept.

8.1.1 Proof of concept for stiffness adjustment

Two weighing cells were mechanically coupled with a limp element at their load carriers. Figure 8.2 presents the realized setup with PROT-S-HG100-1 (left) and PROT-S-HG315-1 (right). A thin tungsten wire of 100 μm diameter couples the

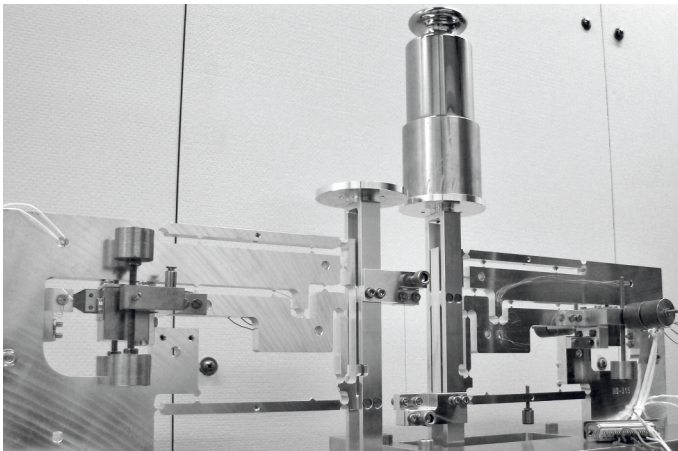


Figure 8.2 – Setup for preliminary testing of the stiffness adjustment concept.

weighing cells mechanically. A tensile force in the wire was ensured by placing the 2 kg sample mass on the weighing cell carrying the lower connection to the tungsten

wire. Despite a careful alignment of the two weighing cells a residual misalignment cannot be excluded. Resulting lateral force components on the load carriers of both weighing cells were minimized by the high compliance of the wire connection. The force flow balance between the two weighing cells was changed by removing parts from the counter mass of one weighing cell and adding the removed mass to the counter mass of the other weighing cell.

The stiffness values of the monolithic weighing cells were measured before they were mechanically coupled at the load carriers. The results are presented in Tab. C.4 and the measurement configurations (① - ⑤) are summarized in Fig. C.8.

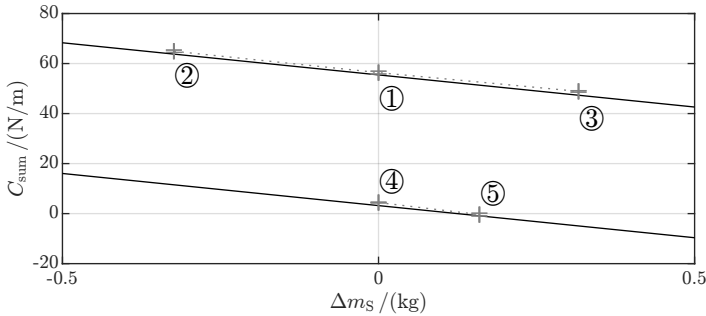


Figure 8.3 – Measurement results for the stiffness of the combined PROT-S weighing cells from setup ① - ⑤. The prediction of the rigid body model is displayed with solid lines.

Parts of the counter-mass were shifted from the weighing cell with the smaller h_{HG} value to the one with the larger h_{HG} . Care was taken to avoid any changes to the vertical position of the counter mass CoG positions. The results are summarized in Fig. 8.3 and show an excellent agreement with the model prediction. The remaining parallel offset between the measurement and model can be justified either by a stiffening resulting from the connection of the weighing cells or by uncertain vertical positions of the CoGs in the experiment. Given the preliminary nature of the measurement setup, the agreement was very satisfactory and verified the predicted mechanical behavior.

8.1.2 Detailed solution concept

The concept for the weighing cell design was fundamentally based on the *separation of functions* principle, ensuring that each functional unit can be optimized for its specific function. In precision measurement devices the separation into a force- and a metrology loop is highly beneficial (e.g. [SC92]). The force loop takes the load and may deform while the measurement loop is isolated from the major force components. It thus represents a highly stable reference frame, e.g. for dimensional measurements. In a mass comparator, the force- and the metrology loop are inherently coupled

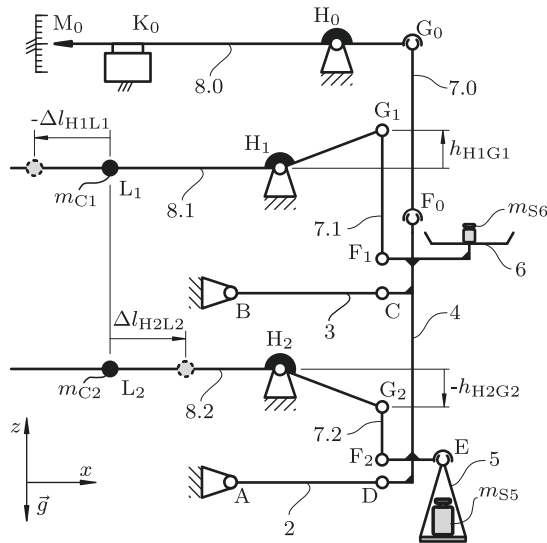


Figure 8.4 – Concept of the novel weighing system with model parameters and an exemplary setting of h_{H1G1} and h_{H2G2} . The joints at G_0 , F_0 , and E represent two-axis flexure hinges with $m_f = 2$.

and cannot be fully separated. However, it was found that the main force flow can be divided into a high- and low-force subsystem, of which the latter is the measurement system (metrology loop). This concept takes advantage of the small electrical weighing window of a 1 kg-mass comparator: ± 2 g. It was realized by a third lever (8.0) in Fig. 8.4. The small force differences within the weighing window equivalent to ± 2 g were guided through the third lever (8.0), which holds the EMFC

system. The so called *measurement lever* is characterized by $h_{H0G0} = 0$ mm and its CoG is located at the CoR of its main flexure H_0 .

As indicated in Fig. 8.4, the flexure hinges F_0 and G_0 are two-axis flexure hinges to weaken the y constraint between the high- and low-force system. As a result, unavoidable deformations of the force transmission system in y direction show only minor effects on the measurement lever. The reduced lateral deflections withing the EMFC components mitigate the cross-sensitivities of the mechanical properties (constants: $K_{\Phi K_Y}, K_{\Phi M_Y}, K_{eK_Y}, K_{eM_Y}$).

The kinematic structure is depicted in Fig. 8.4. The levers 8.1 and 8.2 provide the stiffness adjustment capability whereas the measurement lever 8.0 mitigates the cross-sensitivities of the weighing cell. Horizontally relocatable counter masses on levers 8.1 and 8.2 enable the manipulation of the force balance between the levers without changing the static equilibrium of the overall system. The mechanical stiffness of the mechanism is adjustable - without changing the static equilibrium of the weighing system. Assuming equal masses and displacements, this was achieved by shifting both counter masses alongside the levers - in opposing direction.

As discussed in Ch. 5, the destabilizing mechanical effect of the parameter h_{HG} is affected by higher-order nonlinear effects. The second-order analytical model from Ch. 5 was used to derive the astatization effect within the novel mechanism concept. The rotational stiffness variation of the two-lever mechanism is described as:

$$\Delta C_{\text{rot,grav}} = \left(\frac{h_{H1G1}^2}{h_{F1G1}} - h_{H1G1} \right) \Delta F_{G1} + \left(\frac{h_{H2G2}^2}{h_{F2G2}} - h_{H2G2} \right) \Delta F_{G2} \quad (8.1)$$

The stiffness variation is defined for each lever by the force at G_i , and the parameters h_{HG} and h_{FG} . The change of the forces through G_1 and G_2 is key to the function principle and is described as a horizontal displacement of the counter mass on the respective lever:

$$\Delta F_{G_i} = -m_{C_i} g \Delta l_{H_i L_i} \frac{1}{l_{HG}} \quad (8.2)$$

Combining Eqs. (8.1) and (8.2) yields:

$$\Delta C_{\text{rot,grav}} = \frac{g}{l_{HG}} \left(- \left(\frac{h_{H1G1}^2}{h_{F1G1}} - h_{H1G1} \right) m_{C1} \Delta l_{H1L1} \right)$$

$$- \left(\frac{h_{\text{H2G2}}^2}{h_{\text{F2G2}}} - h_{\text{H2G2}} \right) m_{\text{C2}} \Delta l_{\text{H2L2}} \Bigg)$$

Assuming equal masses and contrary displacements on levers 8.1 and 8.2 ($\Delta l_{\text{HL}} = \Delta l_{\text{H1L1}} = -\Delta l_{\text{H2L2}}$), the equation for the stiffness change with ($m_{\text{C}} = m_{\text{C1}} + m_{\text{C2}}$, $h_{\text{H1G1}} > h_{\text{H2G2}}$, $h_{\text{F1G1}} > 0$, $h_{\text{F2G2}} > 0$) reads:

$$\Delta C_{\text{rot,grav}} = \frac{1}{2} m_{\text{C}} \Delta l_{\text{HL}} \frac{g}{l_{\text{HG}}} \left(- \left(\frac{h_{\text{H1G1}}^2}{h_{\text{F1G1}}} - h_{\text{H1G1}} \right) + \left(\frac{h_{\text{H2G2}}^2}{h_{\text{F2G2}}} - h_{\text{H2G2}} \right) \right)$$

The stiffness variation at the weighing pan is described as:

$$\Delta C_{\text{grav}} = \frac{1}{2} m_{\text{C}} \Gamma \Delta l_{\text{HL}} \frac{g}{l_{\text{HG}}^3} \quad (8.3)$$

$$\text{with } \Gamma = (h_{\text{H1G1}} - h_{\text{H2G2}}) + \frac{h_{\text{H2G2}}^2 h_{\text{F1G1}} - h_{\text{H1G1}}^2 h_{\text{F2G2}}}{h_{\text{F1G1}} h_{\text{F2G2}}}.$$

The stiffness of the weighing system can thus be adjusted before and even during operation according to (8.3).

8.2 Monolithic weighing cell design

The realization of the mechanical concept as a prototype weighing cell demanded several design decisions. The new stiffness adjustment functionality added more complexity to the system (see Fig. 8.4) and introduced new effects. Some of those have been estimated during the early design phase to select a suitable principle solution for the design of the mechanism.

8.2.1 Arrangement of subsystems and mitigation of cross-sensitivities

The novel weighing cell structure has three main functional subsystems. These are:

- quasi-linear guide (2, 3, 4)
- force transmission system (7.1, 7.2, 8.1, 8.2)

- measurement system (7.0, 8.0)

Their arrangement within the monolithic weighing cell is critical to performance, machinability, and mountability. Many designs for EMFC weighing cells feature the force transmission within the parallelogram linkage of the linear guide (see, e.g., PROT-S). This arrangement generally leads to a larger parallelogram linkage which decreases both stiffness and off-center load sensitivity in the x direction. For the current weighing cell design, manufacturing and mounting accessibility demanded the lever systems (force transmission system, measurement lever) outside of the parallelogram guide. The levers were stacked on top of the parallelogram guide.

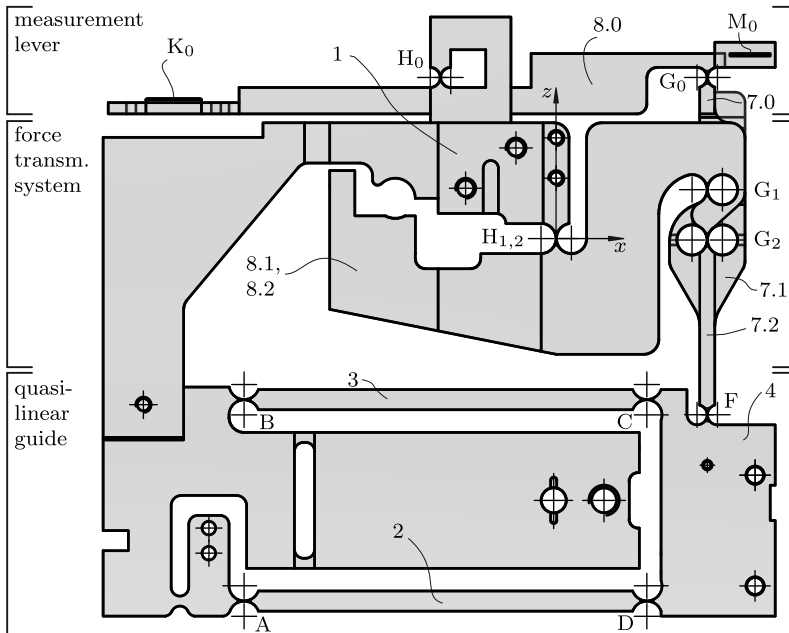


Figure 8.5 – Depiction of the realized monolithic setup of the weighing cell prototype separated into three functional groups: linear guide (2, 3, 4), force transmission (7.1, 7.2, 8.1, 8.2), measurement lever (7.0, 8.0, K_0 , M_0).

The force transmission system, see central area in Fig. 8.5, was designed as a two-lever system. It was required to realize the two-lever system without negatively

affecting other properties of the weighing cell mechanism. To this end, especially the arrangement of the levers and their respective coupling elements was crucial. The intended change in force distribution from one lever (8.1) to the other (8.2) introduces a systematic off-center load on the load carrier (4) if the coupling elements were attached at different lateral positions. The choice fell on a design with nested levers and symmetry in the y direction to circumvent the mentioned introduction of off-center loads and to achieve a compact design. The arrangement is optimized in terms of function at cost of a more complex manufacturing process.

An overview of the nested lever system excluding the parallelogram guide and base is provided in Fig. 8.6. The main difference between the central lever (1) and the outer lever (2) is the different value for h_{HG} which can be visually identified in Fig. 8.6. The central lever (1) is equipped with the larger positive $h_{H_1G_1}$ value whereas the outer lever (2) even has a slightly negative $h_{H_2G_2}$ value. Increasing the force flow through the central lever (1) and reducing the force flow through the outer lever (2) thus leads to a decrease in stiffness and vice versa.

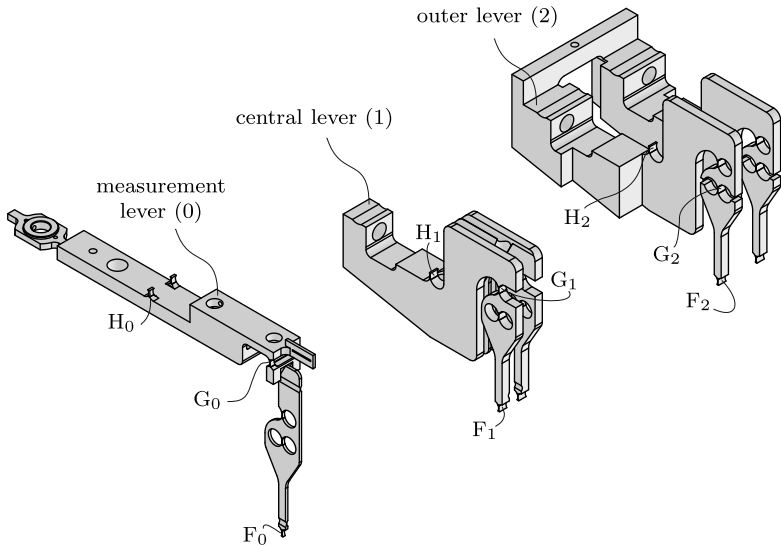


Figure 8.6 – Exploded view of the nested lever system of PROT-ASC.

The measurement lever was located on top of the weighing cell. It implements a stable metrology loop within the mass comparator weighing cell. The lever directly

interfaces with the EMFC components. Its lateral error motions should therefore be minimized. The maximum force flow through the lever was limited to an equivalent of $\pm 2\text{g}$ - the electrical weighing range of the prototype mass comparator. A direct consequence is the absence of a rather heavy counter-mass that tends to deflect the lever laterally for $\Phi \neq 0$. Contrarily, by design and adjustment, its center of mass can be directly positioned to the CoR, which minimizes any tilt-induced deformations.

The aperture slit was located directly above the coupling element. The lever is suspended by two flexure hinges in the middle, in proximity to the base connection of the weighing cell. The coil and the magnet system were mounted on the opposite side of the equal-arm measurement lever. Care was taken to position the CoG close to H_0 to minimize the tilt sensitivity D_Φ .

The measurement lever's coupling element was placed inside the nested coupling elements of the force transmission system with additional compliance in the y direction. The length of the coupling element was maximized to minimize the undesired mechanical coupling between the force transmission- and the measurement system in the x and y direction. The pivots F_0 and G_0 were designed as two-axis flexure hinges. For manufacturing reasons, their perpendicular axes have an offset in the z direction. The laterally compliant mechanical coupling of the subsystems minimizes the transfer of lateral deflections to the measurement lever. These lateral deflections of the force transmission system result from ground tilt or off-center loads on the weighing pan. All sources of heat dissipation within the EMFC system, the coil, and the position sensor's optoelectronic components, were placed on top of the mechanism to minimize thermal influences.

8.2.2 Stiffness adjustment and compensation of manufacturing deviations

The weighing system was designed to allow both stiffness and tilt sensitivity to be adjusted independently through the displacement of trim masses. The adjustment concept involves coarse- and fine-adjustment subsystems. The tolerance limits define the required adjustment resolution, while the expected offsets from the objective values define the required adjustment ranges. Accordingly, the achievable resolution of the coarse adjustment sets the range for the fine adjustment. However, coarse adjustment is limited to atmospheric measurements resulting in higher disturbance of the measurement signal, thus limiting the useful resolution for the stiffness adjustment to about 0.05 N m^{-1} .

The elastic stiffness of the mechanism in Fig. 8.4 is described with (8.4):

$$\begin{aligned}
 C_{\text{el}} = & (C_A + C_B + C_C + C_D) \cdot l_{\text{AD}}^{-2} \\
 & + \left(C_{\text{F0}} \left(\frac{h_{\text{H0G0}}}{h_{\text{F0G0}}} \right)^2 + C_{\text{G0}} \left(1 - \frac{h_{\text{H0G0}}}{h_{\text{F0G0}}} \right)^2 + C_{\text{H0}} \right) l_{\text{H0G0}}^{-2} \\
 & + \left(C_{\text{F1}} \left(\frac{h_{\text{H1G1}}}{h_{\text{F1G1}}} \right)^2 + C_{\text{G1}} \left(1 - \frac{h_{\text{H1G1}}}{h_{\text{F1G1}}} \right)^2 + C_{\text{H1}} \right) l_{\text{H1G1}}^{-2} \\
 & + \left(C_{\text{F2}} \left(\frac{h_{\text{H2G2}}}{h_{\text{F2G2}}} \right)^2 + C_{\text{G2}} \left(1 - \frac{h_{\text{H2G2}}}{h_{\text{F2G2}}} \right)^2 + C_{\text{H2}} \right) l_{\text{H2G2}}^{-2} \quad (8.4)
 \end{aligned}$$

The required adjustment range for the coarse adjustment has been designed based on the uncertain input parameters defined by the manufacturing tolerances for the monolithic mechanism. The most decisive parameter, the minimal notch height of the flexure hinges h , was assigned with the tolerance $\pm 5 \mu\text{m}$. The results of the MONTE CARLO method for the adjustment parameters l_{H1L1} and l_{H2L2} are presented as probability density function in Fig. 8.7. Due to retrospective design changes to the mechanism, the calculated mean position for each counter-weight is slightly eccentric to the adjustment range. All considered input parameter deviations can

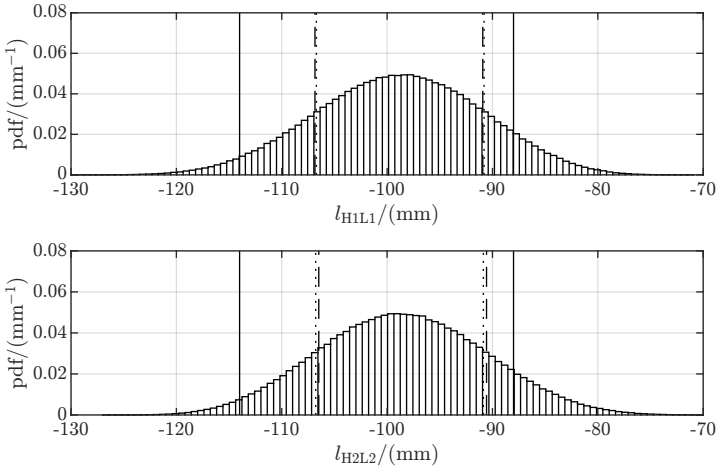


Figure 8.7 – Probability distribution of the calculated positions for the counter weights on lever 8.1 and 8.2 to achieve a static equilibrium and zero stiffness. The solid vertical lines restrict the actual adjustment range of the realized prototype.

be compensated with a probability larger than 68 %.

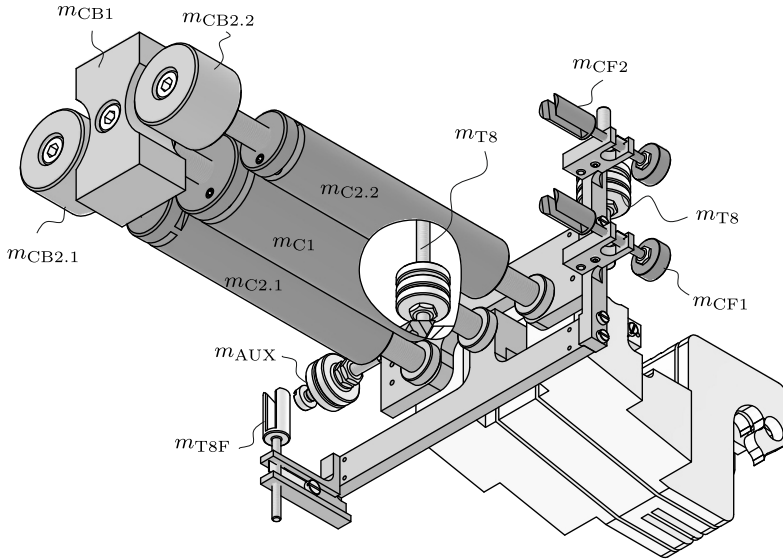


Figure 8.8 – Designation of the masses attached to the free end of the main lever system.

The trim masses on the force transmission system are depicted in Fig. 8.8. The levers 8.1 and 8.2 were equipped with horizontally relocatable counter-masses ($m_{C1}, m_{C2.1}, m_{C2.2}$). The cylindrical counter-masses were mounted to threaded rods clamped to the monolithic weighing cell structure. Smaller horizontal trim masses realized the fine-adjustment (m_{CF1}, m_{CF2}). The fine adjustment is carried out with actuators under high vacuum conditions using a special interface. Despite of imperfections in the adjustment device, the achievable minimal stiffness is fundamentally limited by two temperature-induced effects:

- The temperature coefficient of the YOUNGS modulus of aluminum alloy is in the range of $1 \times 10^{-4} \text{ K}^{-1}$. Assuming a temperature fluctuation during and after the adjustment of the weighing cell mechanism of 0.1 K, the stiffness variation amounts to $\approx 5.5 \times 10^{-4} \text{ N m}^{-1}$, which fundamentally limits the achievable absolute value of the stiffness.

- The in-situ measurement of the stiffness involving the EMFC components is another temperature induced variation source. Here, the relative temperature coefficient of the permanent magnet is dominant, which is in the range of $0.4 \times 10^{-3} \text{ K}^{-1}$. Temperature compensation measures are capable of further reducing the temperature effect.

The stiffness adjustment capability of the prototype weighing cell was modeled using a FE model. In the model, all attached components and their respective net mass have been considered with point masses, see Fig. 8.9. The relocatable counter masses were modeled as point masses connected to the levers. Their x position was changed according to the adjustment parameter Δl_{HL} ($l_{H1L1} = +\Delta l_{HL}$, $l_{H2L2} = -\Delta l_{HL}$). The z position was corrected according to the estimated bending deformation of the threaded rods, which was calculated analytically.

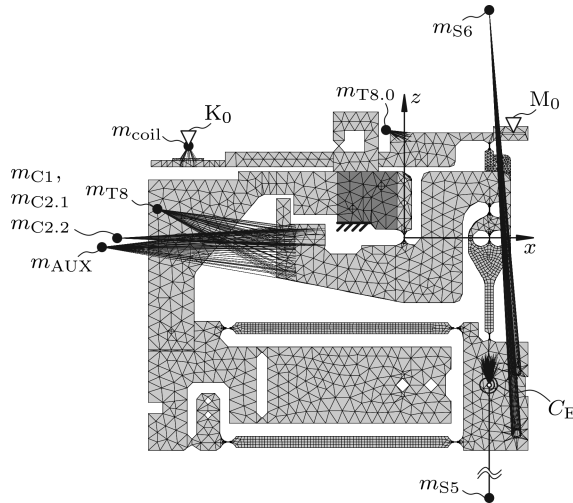


Figure 8.9 – FE model of the PROT-ASC weighing cell in ANSYS®.

8.2.3 Experimental verification

The manufacturing of the weighing cell involved unexpected complexity due to residual stress within the material. The second attempt with an optimized manufacturing strategy lead to the successful realization of the monolithic compliant

mechanism. The PROT-ASC weighing cell was set up for experimental testing. The monolithic weighing cell of the PROT-ASC prototype is presented in the photograph in Fig. 8.10. The first tests after the assembly of the weighing cell were proof-of-concept measurements with a constant load of 1 kg and manual adjustments. These measurements aim at a verification of the adjustment concept and the developed mechanical models. The prototype was placed in the vacuum chamber to provide a largely undisturbed environment. The measurements were conducted under atmospheric conditions with the hanging weighing pan attached.

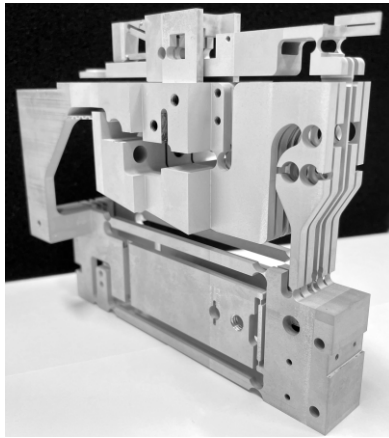


Figure 8.10 – Novel weighing cell mechanism with manufacturing fixtures. The geometry is optimized for electrical discharge machining.

The effect of a contrary horizontal displacement of the counter masses within the finite element model is shown in Fig. 8.11. The gradient predicted by the analytic rigid-body model (8.3) is slightly larger. The difference in gradient between finite element model and measurement may result from the preliminary nature of the measurements or from effects which are not covered by the finite element model.

It is important to mention that the absolute values for the measured stiffness for $\Delta l_{HL} = 0$ is much higher than predicted. The ideal mechanism is designed for $C = 0 \text{ N m}^{-1}$. The measured mechanism yielded a mean of $C = 223.43 \text{ N m}^{-1}$. To confirm the measured value and the large discrepancy of the absolute stiffness, a

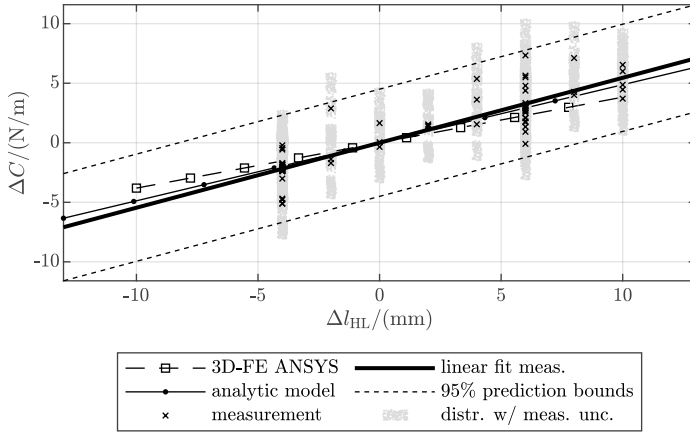


Figure 8.11 – Modeling the stiffness coarse adjustment based on the two nested levers of the PROT-ASC weighing cell shown in Fig. 8.5. The counter masses have a mass of $m_C = 2 \cdot 170$ g and the geometric parameters are $h_{H1G1} = 9.715$ mm and $h_{H2G2} = -0.285$ mm.

second measurement in disassembled condition based on the natural frequency of the monolithic mechanism was conducted (cf. natural frequency measurement (NF)). The results of both measurements and the corresponding substitute minimum notch height is summarized in Tab. 8.1. A third measurement with a CMM was performed on a single accessible flexure hinge to confirm the results obtained from the other non-tactile measurement methods.

Table 8.1 – Absolute stiffness measurements for PROT-ASC.

description	measurement result	$h_S/(\mu\text{m})$
measurement during operation (CLVA)	$C = 223.43 \text{ N m}^{-1}$	93.6 μm
disassembled horizontal orientation (NF)	$f_0 = 6.5897 \text{ Hz}$	91.9 μm
tactile measurement of flexure hinge A (CMM)	$h_{\text{meas}} = 96.6 \mu\text{m}$	96.6 μm

The excellent agreement between the resulting h_S values in Tab. 8.1 allows two conclusions: first, the design improvements concerning the alignment of the components relative to the monolithic mechanism have drastically improved the reliability of the CLVA stiffness measurement results compared to the measurements on PROT-S. Second, the large substitute minimum notch height h_S values suggest that either

all flexure hinges exceed the nominal minimal notch height by $42.7\ \mu\text{m}$, or single flexure hinges have an even higher positive offset from the nominal. The tolerance for the minimal notch height of $\pm 5\ \mu\text{m}$, specified on the manufacturing drawing, was based on the robust design optimization. The first prototype exceeds the tolerance more than eightfold. An adjustment to $C = 0\ \text{N m}^{-1}$ is not feasible. A new mechanism within the specified tolerances needs to be manufactured. This additional effort was out of scope for the present project both concerning lead time and cost.

8.2.4 In-vacuo adjustment capability

The tolerance limits for the adjustments of the mechanical parameters of the weighing cell put high demands on measuring the mechanical properties of the EMFC weighing cell. To reliably reach an adjustment state within the tolerances, the weighing cell needed to be placed in a highly stable environment. In-situ adjustment under vacuum conditions was required.

The in-vacuo adjustment requires automation. Four drives were required for the adjustment of C and D_{Θ} . The choice concerning the fine adjustment of C and D_{Θ} fell on vacuum compatible stepper motors. After each adjustment step, the adjustment drives have to be fully mechanically decoupled to measure the adjustment state regarding stiffness and tilt sensitivity. A slot-screw-driver-type coupling with sufficient backlash and with compensation of lateral misalignment was designed based on the work in [Hoh19]. To measure the tilt sensitivity after each adjustment steps in the closed vacuum chamber, the base of the weighing cell needed to be tilted. The tilt angle was introduced by a vacuum-compatible linear drive which was vertically mounted to the weighing cell's base structure at the back of the assembly. After the final adjustment step, the adjustment unit can be fully removed from the vacuum chamber to avoid any disturbance during final operation.

8.3 Chapter summary

The main accomplishment within the novel concept is the fine adjustment of the stiffness, which is now independent of the tilt sensitivity. Most importantly it provides the capability to compensate manufacturing deviations in the monolithic mechanism. The potential of reducing the elastic stiffness under vacuum to about

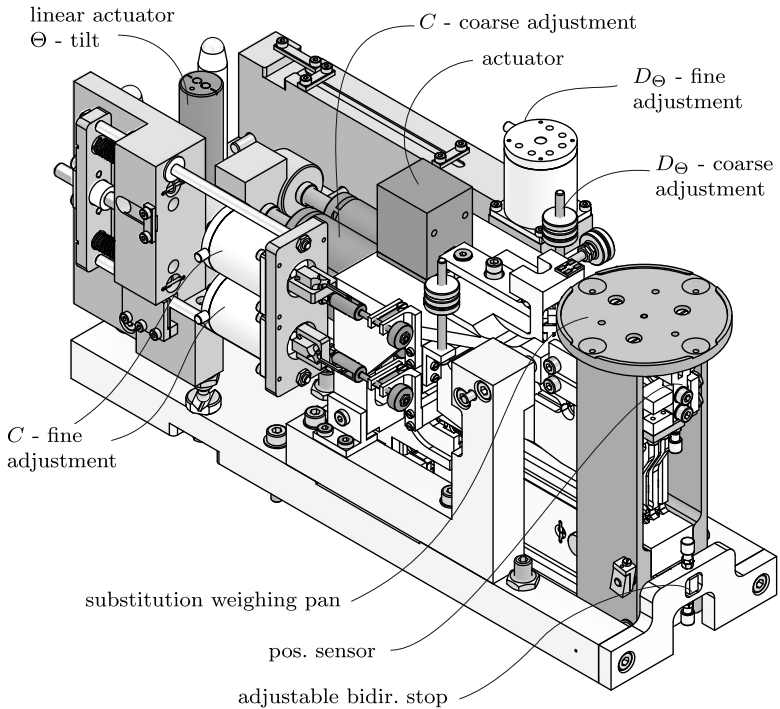


Figure 8.12 – Complete EMFC weighing cell subsystem of the vacuum mass comparator with adjustment unit for stiffness and tilt sensitivity.

16.4 ppm of the initial elastic stiffness constitutes a significant improvement to the state of the art, reduces the demands on the position sensor and decrease its uncertainty contribution.

The second important detail of the novel design is establishing a force- and a metrology loop within the monolithic weighing cell. This concept takes advantage of the limited weighing range of a 1 kg mass comparator and can effectively shield the measurement lever from parasitic deflections in lateral deflection. In standard designs (e.g. PROT-S) these deformations affect the EMFC components and thus contribute to the overall uncertainty. The implementation of the measurement lever mitigates these effects significantly.

The tilt sensitivity D_{Θ} can be adjusted using a single trim mass on the transmission lever, split into m_{T8} for coarse- and m_{T8F} for in-vacuo fine adjustment. The adjustment of the tilt sensitivity should be scheduled prior to the adjustment of the stiffness. The reason is the D_{Θ} adjustment slightly affects C , whereas the C adjustment will not affect D_{Θ} significantly.

The weighing system is designed to be buoyancy independent, meaning that the indicated weighing value is invariant for changes of the air pressure. The buoyancy independence mitigates larger changes to the electrical zero when the weighing system is transferred from atmospheric to vacuum conditions.

The off-center load sensitivity needs to be adjusted manually with the vacuum chamber opened. The vertical positions of the two flexure hinges A can be manipulated with a resolution of at least $0.5\ \mu\text{m}$. Following the successful adjustment, the position can be rigidly clamped. The coupling elements and weighing pans are aligned in the x - y plane to minimize the off-center load in the first place. Additionally, the coincident rotational axes of the monolithic gimbal were located in z direction in the center of the parallelogram linkage. The main force flow is routed directly from H1/H2 to the rigid base structure to minimize the influence of deformations like present in the PROT-S weighing cell.

The developed EMFC weighing cell mechanism approaches the mechanically ideal mass comparator in the considered aspects: stiffness, tilt sensitivity and off-center load sensitivity. It was ensured that these properties are adjustable to within their respective tolerance limit in order to achieve 5 ng uncertainty in a single weighing. Furthermore, the concept and design particularities minimized the cross-sensitivities between the parameters.

Chapter 9

Conclusion and outlook

Vacuum mass comparators are highly specialized mechanical systems. Their heart-piece was the focus of the present work: a monolithic weighing cell based on electromagnetic force compensation. To further reduce the uncertainty for comparisons of 1 kg reference masses, EMFC weighing cells were investigated concerning their design and adjustment. Detailed mechanical models were set up and verified by experiments on prototype weighing cells.

9.1 Summary

Three well-known mechanical properties were selected for an in-depth study. These are stiffness C , tilt sensitivity D , and off-center load sensitivity E_L . The stiffness generally limits the mass sensitivity of the weighing cell and contributes to the measurement uncertainty via errors of the position sensor. Ground tilt in a laboratory environment easily reaches amplitudes of several microradians. In a tilt-sensitive weighing cell, the ground tilt results in an indication change, leading to a measurement error. Since ground tilt has no specific direction, the tilt sensitivity of the weighing cell needed to be investigated in every possible direction. The tilt angles Θ (pitch) and Φ (roll) were considered.

Chapter 4 was dedicated to an in-depth study on very thin flexure hinges enabling precision and accuracy of monolithic weighing cells. A brief justification for choosing the semi-circular notch contour out of many geometry types is followed by aspects concerning the mechanical modeling. It ranges from analytic models in the literature to three-dimensional finite element models. The large aspect ratios of the thin flexure hinge geometry proved to be a challenge for the setup of the finite element model. Additionally, the pronounced aspect ratios have consequences for the modeling of the flexure hinges: many references in the literature propose analytical models based on

the EULER-BERNOULLI beam theory. While the corresponding modeling assumptions may be acceptable in most applications, ignoring the transversal contraction leads to an underestimation of the rotational stiffness of up to 12%.

Reducing the model size was considered necessary for mechanical models of weighing cell mechanisms with multiple flexure hinges. The model size was reduced by establishing distinct meshing zones. Large stress gradients in the central region of the notch require a fine mesh, whereas a coarse mesh is sufficient for the stiff outer parts of the flexure hinge. These non-congruent meshes were linked via contact elements. An even larger saving potential provides the significant region model, where only the thin central part was modeled with a fine mesh of solid elements. The outer zones were either modeled by rigid or stiff beam elements. The significant region's diameter was chosen such that the rotational stiffness still replicated the one of the full model with a small error of $<0.1\%$. The common flexure hinge geometry in this work required only one-third of the notch contour to be finely meshed ($d_{SR} = 2\text{ mm}$). The geometry in this significant region of the flexure hinges almost exclusively defines the rotational stiffness. Manufacturing and dimensional measurements efforts can thus be limited to this region which offers a high saving potential.

The pronounced influence of the minimal notch height h on the rotational stiffness raised the question whether the surface topography of the opposing surfaces contributes significantly to the deviations of the rotational stiffness. The surface topography has found no consideration in the revised literature. In a more general sense, the question is how the surface integrity of the adjacent surfaces affects the rotational stiffness. In a simplified mechanical model, roughness and waviness parameters were superimposed on the ideal surface and enabled a theoretical estimation of their impact on the rotational stiffness.

Three measurement methods were implemented to determine the rotational stiffness of a single flexure hinge specimen. The first was based on a quasi-static measurement approach, the second on the measurement of the natural frequency, and the last on a dimensional measurement using a coordinate measuring machine. The measurement methods have been used to characterize manufacturing deviations on flexure hinge specimen and to qualify manufacturing processes. A comparison of the three methods for a set of flexure hinges with different nominal notch heights showed a correspondence of the results to within 1% or $\approx 0.25\text{ }\mu\text{m}$ projected to a substitute value of the minimal notch height.

The gathered experience with single flexure hinges was required to develop a weighing mechanism holding a minimum number of seven flexure hinges. A limiting factor for the adjustments of precision weighing mechanisms is described in the state of the art in Chapter 2: using trim masses, the adjustment of the stiffness C and the tilt sensitivity D_{Θ} is interdependent. Thus, the optimal adjustment can only be found for either one of the mentioned properties. This limitation was documented in the literature for equal-arm balances but equally holds for EMFC weighing cells.

A quasi-independent adjustment of the C and D was achieved using a systematic adjustment with a combination of trim masses on different levers (m_{T8}, m_{T2}, m_{T2}). The concept was simulated in mechanical models both analytically and numerically. The prototype weighing cells PROT-S and PROT-EA were equipped with this set of trim masses to investigate the adjustment concept experimentally. The realization of the prototype weighing cells, including conceptualization, design, manufacturing, assembly, and operation, was the prerequisite for the experimental test of the adjustment concept. All steps were accomplished. A good agreement between model and experimental results was achieved. The experiment proved the applicability of the adjustment concept and the opportunity to systematically adjust C and D to values very close to zero. The adjustment sensitivity and the measurement of the adjustable mechanical properties C and D were limiting the overall adjustment resolution.

The concept of astatization was implemented for the initial compensation of the elastic stiffness of the mechanism. The astatization parameter h_{HG} has to be set prior to machining without knowledge about the manufacturing deviation that is introduced. Manufacturing deviations in the micrometer range have a pronounced effect on the elastic stiffness. Methods for the stiffness determination of monolithic weighing cell structures were developed and tested to investigate the large variance of the elastic stiffness.

Despite the manufacturing of six prototype weighing cells, a reliable starting point for the fine-adjustment with trim masses was not achieved. Most of the manufactured PROT-S weighing cells showed a shortfall of the elastic stiffness compared to the nominal value (cf. Fig. 6.5). The only outlier in that respect was the weighing cell PROT-S-HG100-1, which was measured with a positive deviation from the nominal stiffness. The significant scattering of the elastic stiffness of the weighing cells was the major difficulty to overcome to reliably realize weighing systems with $C = D = 0$.

The fine-adjustment concept was verified using the PROT-S-HG315-1 weighing cell which was falling short the nominal stiffness value (cf. Fig. 6.5). The sample mass was reduced from 1 kg to 0.335 kg to compensate for the manufacturing deviation at the flexure hinges and reach a stiffness value sufficiently close to $C = 0$. The experiment proved the viability of the fine-adjustment concept.

The problem concerning the pronounced scattering of the elastic stiffness values of the monolithic weighing cells rendered the choice of a reliable h_{HG} value impossible. Therefore, either the manufacturing deviations needed to be reduced, or a post-machining adjustability for the astatization needed to be implemented. Through a systematic consideration of the possible technical solution principles, a way forward was discovered that maintained the monolithic setup of the weighing cell. It enabled the adjustment of the stiffness even during operation. Moreover, the novel concept was not limited to the compensation of manufacturing deviations. It also enables the fine adjustment of the stiffness without affecting the tilt sensitivity and the fine adjustment of the electrical zero of the weighing cell. Its realization in the final prototype setup enabled the fine adjustment of the stiffness under vacuum conditions. With this additional measure of stiffness adjustment, the initial adjustment strategy using additional masses on the levers of the parallelogram linkage became obsolete. Instead, the new concept used a single trim mass on the transmission lever (m_{T8}) for the tilt sensitivity adjustment.

The measurement on the first working weighing cell PROT-ASC showed a good agreement between the predicted and measured gradients for the astatization adjustment. However, the absolute values of the stiffness suggests that the mean manufacturing deviation across all flexure hinges amounts to $\approx 42.7 \mu\text{m}$. This pronounced deviation is exceeding the presumed manufacturing deviation of $\pm 5 \mu\text{m}$. Consequently, the mechanism cannot be adjusted to $C = 0 \text{ N m}^{-1}$ within the available adjustment range. However, if the complex manufacturing process is further improved, the robust design of the weighing cell including the adjustment measures is expected to comply with the aspired tolerance limits of the parameters C , D_{\ominus} , and E_{L} . The novel weighing cell design thus constitutes a significant further development to the state of the art.

9.2 Conclusion

A weighing cell for a mass comparator application was developed to cancel out first-order mechanical error components by combining rough- and fine adjustments.

As a result, the residual error is solely limited by the realized adjustment resolution, the ability to observe the adjustment result by measurement, and the stability of the adjustment state. The fine adjustment needs to be performed under vacuum conditions to enhance the precision of the measurements.

Achieving these demanding mechanical requirements within tight tolerance limits paves the way for mass comparisons of 1 kg-standards with uncertainties in the single nanogram-range. Astatization within a monolithic weighing cell in a mass comparator application is a highly beneficial measure to compensate the elastic stiffness of the mechanism.

If astatization succeeds in achieving a sufficiently small stiffness while keeping tilt sensitivity small, $C = D_{\Theta} = 0$ can be achieved using a systematic adjustment and a combination of trim masses. The minimum requirement is a transmission ratio $\xi \neq 1$ and at least one trim mass on the transmission lever and one on the levers of the parallelogram guide. The concept has been experimentally verified using the PROT-S weighing cell and its built-in trim masses.

The implementation of the astatization measures was complicated by a large sensitivity of the elastic stiffness to small manufacturing deviations. A solution was found by combining PROT-S weighing cells with different h_{HG} values linked by a thin tungsten wire. The concept, based on a variation of the force flow through each coupling element, has been implemented in the weighing cell PROT-ASC.

The PROT-ASC weighing cell enables the compensation of at least 68% of the expected uncertainties of all considered model parameters. The most influential parameter, the minimal notch height of the flexure hinges h , has been considered as a uniform probability density function with bounds of $\pm 5 \mu\text{m}$. The weighing cell is thus capable of compensating manufacturing deviations. Mechanical first-order error components related to stiffness, tilt sensitivity, and off-center load sensitivity can be removed by fine adjustment.

9.3 Outlook

The vacuum mass comparator represents a system of arbitrary complexity when aiming for mass comparisons with uncertainties in the single nanogram range. Starting points for future studies to further reduce the measurement uncertainty were identified. These effects are external to the mechanical weighing system and

represent limiting factors for mass comparisons as the simplified consideration of $T(t)$ and $g(t)$ in Ch. 7 suggested. Due to limited time and resources, the current set of available prototype weighing cells has not been fully investigated experimentally. Especially, PROT-ASC needs to be investigated further in terms of metrological performance, in-vacuo adjustment, and adjustability of all first-order error sources, see Fig. 7.1. Expanding on the results of the present work, the adjustment of the dynamic response of the mass comparator system to external or internal excitation is an optimization approach in addition or as replacement of the quasi-static approach in this work. A change in material for the entire mechanism or solely for the flexure hinges can improve the anelastic material behavior. A crucial prerequisite for stability of the weighing cell's indication is establishing a temperature invariant electromagnetic force compensation system. Testing for fatigue on the ultra-thin flexure hinges should be analyzed to gain confidence that manufacturing deviations and surface defects have no significant impact on the lifetime of the weighing cells. Fluctuations of the local gravitational acceleration are fundamentally limiting the achievable measurement uncertainty. The effect is proportional to the mass imbalance in the weighing cell. If the weighing window of ± 2 g is maintained, a simultaneous measurement with e.g. a relative gravimeter may allow for correction of the measurement result.

A Publications

Table A.1 – Supervised student theses. BA - bachelor thesis; MA - master thesis.

name	year	type	title
Markus Pabst	2017	MA	Konzeption und Realisierung einer vakuumtauglichen Schwerpunktjustierung für höchste Ansprüche in der Präzisionswägetechnik
Mario André Torres Melgarejo ^a	2018	MA	Modeling of the elastic mechanical behavior of thin compliant joints under load for highest-precision applications
Braulio Jesús Gracia Ayala	2018	MA	Experimental setup for measuring the mechanical behavior of loaded thin compliant joints with highest precision
Victor Arturo Pomiano Picon	2019	MA	Adjustment of the relative position of compliant joints within a monolithic mechanism
Dominik Hohmann	2019	BA	Justierung von Präzisionswägezellen in Massekomparatoren
Matthias Wolf ^b	2020	BA	Drehmomentkompensierende Antriebslösung für die Einleitung von Drehbewegungen an mechanisch empfindlichen Geräten im Vakuum
Maria Paula Castillo Zevillanos ^c	2020	BA	Modellierung von Festkörpergelenken unter Berücksichtigung der Oberflächentopografie
Yang Xu ^c	2021	MA	Finite Elemente Modell zur Simulation des statischen und dynamischen mechanischen Verhaltens von Präzisionswägezellen

^a co-supervision by Dr. Sebastian Linß.

^b co-supervision by Florian Weigert.

^c co-supervision by Mario Torres.

Table A.2 – Publications.

short	title
authorship	
[Dar17]	<i>Optimierung monolithischer Mechanismen in der Kraftmess- und Wägetechnik</i>
[Dar+17b]	“Design of high-precision weighing cells based on static analysis”
[Dar+17a]	“Contribution to the mechanical enhancement of load cells in precision weighing technology by means of advanced adjustment strategies”
[Dar+18a]	“Modellierung der Drehsteifigkeit dünner Festkörpergelenke in der Präzisionsgerätetechnik”
[Dar+18c]	“Static behavior of weighing cells”
[Dar+18b]	“On precise modelling of very thin flexure hinges”
[DFT19]	“Tilt sensitivity modeling of a monolithic weighing cell structure”
[Dar+19]	“Mechanical properties of an adjustable weighing cell prototype”
[Dar+20]	“Corner loading and its influence on the tilt sensitivity of precision weighing cells”
[Dar+21a]	“Characterization of Thin Flexure Hinges for Precision Applications Based on First Eigenfrequency”
[Dar+21b]	<i>Justierung nachgiebiger Mechanismen für Vakuummassekomparatoren – Herausforderungen und Ziele</i>
[DE 102021132093 E3]	“Wägevorrichtung und Verfahren zu deren Betrieb”
[DE 102021118060 A1]	“Elektromagnetisch kompensierende Balkenwaage”
[EP 000004119908 A1]	“Electromagnetic Compensating Beam Scale”
co-authorship	
[Tor+18]	“On Modeling the Bending Stiffness of Thin Semi-Circular Flexure Hinges for Precision Applications”
[The+18]	“State of the art precision motion systems based on compliant mechanisms”
[Pab+19]	“Measuring and adjusting the stiffness and tilt sensitivity of a novel 2D monolithic high precision electromagnetic force compensated weighing cell: NCSL International Workshop & Symposium Metrology in Motion August 24-29, 2019 Cleveland, Ohio”
[Sas+19]	“Generation of a static torque in the range of 1 mNm to 1 Nm according to the Jokey-weight principle”
[Wed+21]	“Conceptual Design of a Microscale Balance Based on Force Compensation”
[Pab+21]	“A3.1 Adjustment Concept for Compensating Stiffness and Tilt Sensitivity of a Novel Monolithic EMFC Weighing Cell”
[Pab+22]	“Adjustment concept for compensating for stiffness and tilt sensitivity of a novel monolithic electromagnetic force compensation (EMFC) weighing cell”
[Wit+22]	“Investigations on a torque-compensating adjustment drive for mechanically sensitive devices”

B Definitions and Modeling

This chapter provides additional information about the mechanical models used in this work.

B.1 Performance measures for mass comparators

The ideal mass comparator compares the weight forces of two physical objects without being sensitive to internal or external influence factors. Like every technical system, the actual EMFC weighing cell-based mass comparator deviates from the ideal mass comparator in many aspects. Therefore, the measurement system is characterized by standardized performance measures. Unless in brackets, these are following the *International vocabulary of metrology* [JCGM 100:2008]:

- **sensitivity:**

ideal: arbitrarily small mass differences can be discriminated - the sensitivity is infinite.

real: the sensitivity describes the change in indication divided by the causal mass change on the weighing pan [OIML R 76-1:2006]. It is limited by the mechanical stiffness at the weighing pan, the resolution of the position sensor, and the transmission ratio between the position sensor and the weighing pan. It is assumed that the smallest increment of the current supply is not a limiting factor for the mass resolution. The sensitivity can be dependent on the measurand [JCGM 100:2008]. In [CW80], the terms *sensitivity* and *sensibility* are distinguished. *Sensitivity* describes the pure mechanical property of the balance mechanism - the reciprocal of the stiffness. Its magnitude describes the deflection relative to the applied load. In turn, the term *sensibility* considers the complete measurement system including the mechanism and the EMFC subsystem. Modern mass comparators are equipped with a digital readout. The term *digit* has become established to describe the smallest increment of the digital indication [Pro95]. A mass comparator with a weighing range of 2 g and the smallest increment of 0.1 μg requires 20×10^6 digits.

perf. measure: (mass) resolution, discrimination threshold, sensitivity (this work: C^{-1}), (sensibility (this work: C_{EMFC}^{-1}))

- **capacity:**

ideal: no limit for the maximum mass on the weighing pan

real: the mechanical system of the mass comparator is subject to the limits of the engineering materials in its force flow. Their ability to sustain stress is limited, and thus the maximum load of mass comparators needs to be restricted. For mass comparators, the limit for loading of the weighing pan is rather restricted by the small weighing range around the nominal than by stress limits.

perf. measure: limiting operating condition, (capacity)

- **linearity:**

ideal: linear relationship between the input quantity and its indication

real: the weighing range of a high-resolution mass comparator is defined to 0.1 to 1% of the maximum load [GB09]. A mass increment leads to a proportional change of the indication. The proportionality factor is the *sensibility* of the instrument. Deviations from this ideal sensor characteristic are combinations of offset, inclination error and linearity error.

perf. measure: (linearity) [TO98]

- **temperature fluctuation, pressure variation:**

ideal: homogeneous or inhomogeneous changes in ambient temperature and pressure variations do not affect the indicated mass.

real: the subsystems of a mass comparator are affected by fluctuations of the ambient conditions, e.g., the permanent magnet system and the coil of the actuator, position sensor components, and the mechanical system (lever lengths).

perf. measure: stability of the measuring instrument, instrument drift, (temperature coefficient), (zero point stability)

- **precision:**

ideal: the subsequent weighing of the same mass gives the same weighing value.

real: the indication of the weighing instrument shows scattering indications in a series of measurements using the same mass under specified conditions. This behavior is quantified, e.g. by the standard deviation σ . The specified conditions define which subcategory of measurement precision is defined according to [JCGM 100:2008]. The measured standard deviation tends to increase from repeatability- over intermediate precision- to reproducible conditions.

perf. measure: measurement precision

- **hysteresis:**

ideal: no energy dissipation occurs not in the flexure hinges nor within the actuator.

real: *hysteresis* of the weighing system can be observed if the mass range is measured from the most minor to the highest value and vice versa. The hysteresis is the deviation of the indications for both loading directions, e.g., at 50 % of the load range [Nor08].

perf. measure: (hysteresis)

Even for the ideal mass comparator system, the measured mass differences are subject to minor variations due to the imperfection of the mass standards, which are not part of the mass comparator system. There are several effects which are influencing the measured mass difference. For example, the adsorption of molecular surface layers on the surface of the masses which are outgassing when the ambient pressure is reduced in the vacuum chamber. This outgassing of the surface layer results in a mass change of 7 to 8 μg for cleaned 1 kg standards [GB09]. The cleaning process of the mass standards is another particular issue described in [CM01; MFR12]. Other investigations suggest that surface area- and pressure-dependent mass changes can be expected in a vacuum [BD08]. Thus, the sample mass contributes to the experimentally determined repeatability of a mass comparator. It is larger than the actual repeatability of the mass comparator itself, assuming a perfect mass standard on the weighing pan.

The described issue affects another core function of the mass comparator: Traceability to an international standard requires calibration of the mass comparator. The standard method for calibration is done with reference masses which can be internal or external to the mass comparator system [Pro95]. Since the reference masses themselves have associated uncertainties concerning their mass, the calibration of the mass comparator represents a limiting factor for the uncertainty of the mass comparison.

An additional limitation of the ideal mass comparator system is that it still measures weight (force) instead of mass. Hence, it is sensitive to any fluctuations concerning the gravitational acceleration \vec{g} [JDS84]. These are dependent on the location on the earth's surface and the height above sea level. Small, time-dependent fluctuations of $\vec{g}(t)$ occur if the location is kept constant.

B.2 Further disturbances

The section lists further sources of disturbance with a high relevance for the weighing process but not in the focus of the present work.

B.2.1 Gravitational acceleration

GALILEO GALILEI concluded in 1604 that the gravitational acceleration is constant and independent of the mass of, e.g., a falling object [Mar12]. Since then, a large number of different measurement principles have been implemented to determine \vec{g} with advances in resolution and accuracy. Recently, the most sophisticated gravimeters (superconducting gravimeters) can resolve time-dependent variations of \vec{g} with relative uncertainties down to 5×10^{-12} [Mar12] and for absolute gravimeters 2×10^{-9} [Jia+11]. Especially relative gravimeters resolve time-dependent variations of the gravitational acceleration which is a source of uncertainty for the mass comparison process. The relative change of \vec{g} due to tides, for instance, has an amplitude of 1.5×10^{-7} [RS17].

B.2.2 Buoyancy

Every body under atmospheric conditions is floating in air. Assuming quasi-static conditions, at least two forces act on the CoG of a body, exactly opposing each other. One force is the weight force due to the earth's gravitational field, and the other is the buoyancy force of the displaced volume of air [RJK14]. In precision weighing, the latter cannot be neglected. For comparisons of a platinum-iridium (Pt-Ir) prototype kilogram (density $21\,500 \text{ kg m}^{-3}$) with a frequently used austenitic stainless steel weight (density 8000 kg m^{-3}), a buoyancy correction of about 95 mg has to be considered [KG00]. Over 450 mg of buoyancy correction is required to compare a Pt-Ir-standard against a silicon sphere [Abd+05]. Given the uncertainties of mass comparators in the microgram range, the buoyancy correction dominates the overall measurement uncertainty [KG00]. To this end, the local density of the moist air has to be calculated with high accuracy, which can be accomplished using the CIPM-2007 equation for the density of moist air [Pic+08]. The air density is directly proportional to the constantly varying atmospheric air pressure. Concurrent measurement of environmental parameters yields an uncertainty for the calculated air density of $1.7 \times 10^{-4} \text{ mg cm}^{-3}$ has been reported in [JY01] and $2.4 \times 10^{-4} \text{ mg cm}^{-3}$ in [Hil+16]. Air density can also be determined directly

using a vacuum mass comparator and buoyancy artifacts. Using this method, an uncertainty of $6 \times 10^{-5} \text{ mg cm}^{-3}$ in [GSM91] and $2 \times 10^{-5} \text{ mg cm}^{-3}$ [MUF04] have been achieved.

To circumvent the necessity of a buoyancy correction, the new definition of the kilogram is founded on measurements under vacuum conditions [BS16]. However, at some point in the dissemination chain of the mass scale, a transition from vacuum to atmospheric conditions is necessary. For the measurements within the scope of this work, these effects are largely neglected, assuming only vacuum measurements for the final application of the mass comparator.

B.2.3 Sorption, contaminations, and cleaning

The precise understanding of the physical processes connected to surface effects on mass standards is of high importance for the stability of mass standards over decades or even centuries. Hence, considerable effort has been devoted to investigating this mass metrology subtopic. Especially, mass standards undergoing transitions from atmospheric to vacuum conditions are subject to sorption and desorption [GSM91]. The corresponding and reversible mass difference for a 1 kg Pt-Ir mass standard is in the range of $6 \mu\text{g}$ [PF04]. In [GSM91], a surface dependent coefficient of $0.2 \mu\text{g cm}^{-2}$ is reported. Together with the surface area of the Pt-Ir standard of 71.5 cm^2 [BD08], the total mass difference yields $14.3 \mu\text{g}$ which is more than twice the value in [PF04]. A possible reason for the difference of about $8 \mu\text{g}$ may be the omission of a cleaning process in [GSM91]. In [PF04], the authors report a dependency of the desorption on the state of contamination of the mass standard. Further studies determined a correlation to cleaning, surface polishing, and the relative humidity under normal pressure [Bee+02; Sch94], stressing the need for well-defined and repeatable cleaning procedures of the mass standards.

MASSEN et al. report that up to a relative humidity of 0.8, only a monomolecular layer of water would be adsorbed with a mass gain of $0.01 \mu\text{g cm}^{-2}$ [Mas+86]. Compared to a comparison of 1 kg mass standards in air, the measurement in a vacuum would reduce the measurement uncertainty by a factor of two [DBB04]. However, many effects related to the surface of the weights have to be taken into account. BERRY et al. show that depositions on the mass standards surface can occur even under stable vacuum conditions. The source of particles is an inverted magnetron gauge used to determine the chamber pressure between 1 to $1 \times 10^{-7} \text{ Pa}$. At a vacuum pressure higher than 0.024 Pa , a mass gain of $0.021 \mu\text{g d}^{-1} \text{ cm}^{-2}$ could be observed

[BD08]. The mentioned surface effects may also affect the mechanical system and the components of the mass comparator itself [Mas+86].

B.2.4 Electrostatic and electromagnetic fields

A model-based approach for determining effects on the indication stemming from electrostatic- and electromagnetic fields is a highly complicated task.

Electromagnetic The magnetic susceptibility of the weighing cells engineering material is influenced by the purity of the used alloys, e.g., residual iron content. For balances within external magnetic fields, time-dependent influences on the indication occur. The authors in [Sun+08] found that the cutting manufacturing process contaminates the material with iron particles. The authors say machining with high-speed steels should be preferred over high-carbon steels to reduce contamination. Acid washing of the metal parts in a solution of 3% concentrated hydrochloric acid for 10 min is reported to remove the gained contamination by the tooling.

Interesting results from a measurement of the magnetic field distributions above the weighing pan of exemplary precision weighing systems and its influence on the apparent mass of masses have been reported in [Glä01]. An analytic equation for the resulting force in a vacuum is given in [GB09].

The volumetric magnetic susceptibility of common engineering material has been documented in [KJ89]. Aluminum alloys have been measured with 24 times lower volumetric magnetic susceptibility than a copper-beryllium alloy (CuBe alloy). For mass standards, maximum values for volume susceptibility of weights and accuracy classes are defined [KG00].

Electrostatic Based on COULOMB's law for the attraction of point charges, the corresponding mass change can be expressed as [Mas+86]:

$$\Delta m \approx 1 \times 10^{-2} U^2 \quad ([\Delta m] = \mu\text{g})$$

Electrical conductivity throughout the structural parts of the balance and their interfaces, especially concerning the sample mass, is thus vital to eliminate effects on the weighing process [CW80].

B.2.5 Temperature fluctuations

Temperature fluctuations and the corresponding physical changes to precision instruments are a significant source of uncertainty, which is often mitigated by corrective measures. These are based on temperature measurements and model based corrections [WA08]. The theoretical background and implementation of temperature corrections for precision instruments are covered in [Frö98; FJH06]. The prominent heat sources in an EMFC weighing cell are the actuator and the position sensor. In the voice coil actuator, the heat power is generated according to the JOULE law. The heat power is proportional to the electrical resistance and the square of the coil current [LBL18]. The position sensor's heat generation is by loss mechanisms within the LED. Its heat dissipation power can be conservatively estimated by multiplying the driving current and the voltage drop across the LED to approximately 10 mW. The generated heat dissipation from the source is limited to conduction and radiation in a vacuum. Especially for components within the force flow, inhomogeneous temperature fields eventually leads to asymmetric length changes of the levers within the weighing mechanism, changing the static equilibrium and the indication.

Another prominent source of temperature-induced errors is the electromagnetic actuator. The field strength or the magnetic flux density of the permanent magnet system has a temperature coefficient, as does the length of the coil wire. Temperature coefficients in permanent magnet systems can be reduced [LRM90] and adjusted by using a magnetic shunt out of a material with a high temperature coefficient of the magnetic reluctance [Bau+13]. A temperature coefficient of the magnetic flux as low as 5 ppm/K has been obtained using an adjusted shunt within the magnetic circuit, [Eic+12]. A viable alloy for the magnetic shunt that has been applied to analog instruments [SB70] is THERMOFLUX (NiFe with 30 % Fe) [Vac02].

KNUDSEN forces resulting from thermal gas flow around the balance's parts are estimated to impact the indication. The resulting updraft in a 1 kg mass comparator has been investigated in [Sch+15]. A geometry-dependency has been discovered. A temperature difference between a 1 kg sample mass and the surrounding air of 1 mK yet results in an equivalent mass change of 1 μg [GB09]. In [Sch+15], a decrease of the effect with decreasing ambient pressure. Thus, under high-vacuum conditions, this effect vanishes and can thus be neglected.

B.2.6 Noise

Noise is present in every unit of the measurement system, starting from the mechanical system to the opto-electronic and electronic components used for control and evaluation. Usually, the effects of noise are minor compared to the magnitude of the signal - the signal-to-noise-ratio (S/N) is large. However, in delicate mechanical instruments - as the vacuum mass comparator - the noise can make up a significant portion of the signal, which ultimately limits the performance.

Following the fluctuation-dissipation theorem, a proportionality between energy dissipation and thermal noise exists [Sau90]. Within the weighing cell in a vacuum environment, energy dissipation occurs within the material of the flexure hinges, within the voice coil actuator, the opto-electronic and electronic components of the position sensor, and to a very small amount due to the surrounding residual gas molecules. A detailed investigation of thermal effects in very sensitive, pure mechanical instruments with low damping can be found in [Sau90].

In case additional damping measures for pan swing are installed, a new thermal noise source is introduced. In [Qui92], it is concluded that pan swing damping and the corresponding thermal noise has a negligible effect on the measured mass difference of about ≈ 0.1 ng for single weighing. The low impact on the indication is due to the restricted mechanical coupling between the swinging weighing pan and a sufficiently leveled balance beam. In an EMFC weighing cell, the coupling is limited by the parallelogram guide.

In [RJK14], the influence of BROWNIAN motion is estimated to be 6 ng. An equation for estimating the influence on a compensation balance under atmospheric conditions is presented. The consideration is based on the random impact of the gas molecules hitting the moving parts of the balance.

In [CW80], the spurious effect of BROWNIAN motion is estimated for three cases: the undamped balance without feedback, the critically damped balance without feedback and an automated balance with feedback, where the influence decreases in the said order from 6 ng to 0.4 ng. However, these calculated values do not apply for measurements in a high-vacuum atmosphere.

Considering the position sensor noise involves all the complexity of effects within the opto-electronic components and the electrical circuit for the amplification of the signal. The detailed discussion of these effects is clearly out of scope for this work, nevertheless it remains a fundamental limit.

B.3 Material properties

The flexure hinges and compliant mechanisms in this work have been manufactured from three different high-strength aluminum alloys. The aluminum alloys receive their superior mechanical properties from precipitation hardening. Their most important input parameters for the mechanical models are listed in Tab. B.1: The single flexure hinges that were investigated in Sec. 4.5 - Fig. 4.17 were man-

Table B.1 – Physical properties of high-strength aluminum alloys.

designation	E	ν	$R_{p0.2}$	ρ
EN AW-2024 T351 ^a	73.1 GPa	0.33	324 MPa	2780 kg m ⁻³
EN AW-7021 T62 ^b	72.0 GPa	0.33	380 MPa	2780 kg m ⁻³
EN AW-7075 T651 ^c	71.7 GPa	0.33	503 MPa	2810 kg m ⁻³

^a <http://asm.matweb.com>, access: 2022-02-26.

^b <http://matweb.com>, access: 2022-02-26.

^c <http://asm.matweb.com>, access: 2022-02-26.

ufactured from EN AW-7075 T651. PROT-S and PROT-EA were manufactured from EN AW-7075 T651. The PROT-ASC weighing cell was manufactured from EN AW-2024 T351.

B.4 Semi-circular flexure hinge

Table B.2 – Parameters of the semi-circular flexure hinge geometry.

param.	description	value	uncertainty	unit	distribution
geometric parameters					
h	minimal notch height	50	± 5	μm	normal
w	width	10	± 0.1	mm	uniform
R	radius of the notch	3	± 0.05	mm	uniform
physical parameters^a					
E	YOUNG's modulus	71.7	± 1.434	GPa	uniform
ν	POISSON's ratio	0.33	± 0.007	-	uniform

^a EN AW-7075 T651

The flexure hinges geometry in this work was fixed to a semi-circular geometry. The flexure hinge specimen investigated in Ch. 4 and the prototype weighing cells PROT-S and PROT-EA in Ch. 5 are entirely based on the geometry specified in Tab. B.2.

The matrix entries of the stiffness matrix (4.1) for the semi-circular flexure hinge according to [Kos+00] are listed in (B.1):

$$\begin{aligned}
 C_1 &= \frac{E w}{\pi \left((R/h)^{1/2} - 0.5 \right)}, \\
 C_2 &= \frac{2 E w h^{5/2}}{3 \pi R^{3/2} (3 R + h)}, \\
 C_3 &= \frac{E w^3}{12 \pi R^2 \left((R/h)^{1/2} - 1/4 \right)}, \\
 C_4 &= \frac{4 G w h^{5/2}}{9 \pi R^{1/2}}, \\
 C_5 &= \frac{E w^3}{12 \left(\pi (R/h)^{1/2} + (2 + \pi) / 2 \right)}, \\
 C_6 &= \frac{2 E w h^{5/2}}{9 \pi R^{1/2}}, \\
 C_7 &= \frac{2 E w h^{5/2}}{3 \pi R^{3/2}}, \\
 C_8 &= \frac{E w^3}{12 R \left(\pi (R/h)^{1/2} + (2 + \pi) / 2 \right)}. \tag{B.1}
 \end{aligned}$$

B.5 Nonlinear coupling within the weighing cell mechanism

The kinematic coupling between the two subsystem transmission lever (8) and parallelogram guide (2, 3, 4) is realized by the coupling element (7), see Fig. 5.1. It introduces a nonlinearity in the system which is responsible for the astatization effect.

Either the coupling element consists of a limp element (distributed compliance) or stiff element connected via two flexure hinges F and G. The latter is used for its well-defined CoRs. The introduction of a coupling element is necessary since the coupling points F and G experience different deflections in x direction for

$l_{\text{HG}} \neq l_{\text{AD}}$, see Figure 5.4. A transmission ratio $\xi \neq 1$ is the common case in EMFC weighing cells.

Modeling of the weighing cell mechanism with numerical models revealed a nonlinear decrease of the stiffness over h_{HG} , see Fig. 7 in [Dar+18c]. A model with a constant transmission ratio $\xi = l_{\text{HG}}/l_{\text{AD}} = \text{const.}$ between q_2 and q_8 does not show the astatization effect for $h_{\text{HG}} \neq 0$.

The differing x displacements of pivot F and pivot G and the corresponding angular deflection of the coupling rod $q_7 \neq 0$ are strongly magnified by the introduction of $h_{\text{HG}} \neq 0$ with the following effects on the mechanical system:

- nonlinear change of transmission ratio
- load dependency of the stiffness
- lateral force components on the flexure hinges

With the assumption of a rigid body model, $l_{\text{AD}} = l_{\text{BC}}$ and $h_{\text{AB}} = h_{\text{DC}}$, the structure of the weighing cell was simplified without changing the kinematic behavior. This holds because the load carrier approximately performs a translational motion with $q_4 \equiv 0$, resulting in parallel motion paths for the points C, D, E and F. For simplification, part 7 can thus be directly coupled to part 2 via joint D, see Fig. B.1.

EMFC weighing cells are practically not deflected during operation. Mechanical stops restrict the angular deflection to a maximum of $q_8 \approx \pm 0.1^\circ$ - a pre-condition for the following simplification. See Fig. B.1a for the definition of the parameters.

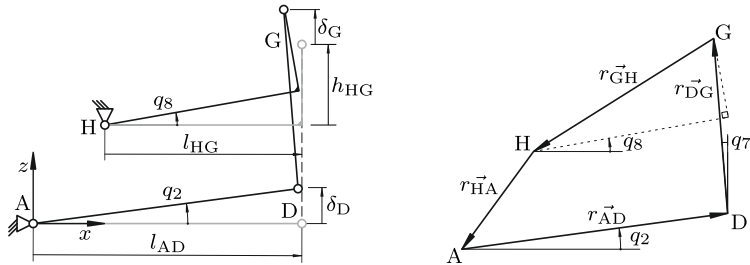
$$\delta_{\text{F}} \approx \delta_{\text{G}} \tag{B.2}$$

Expressed with the independent variables of the subsystems, (B.2) yields:

$$l_{\text{AD}} \sin(q_2) = l_{\text{HG}} \sin(q_8) - h_{\text{HG}} (1 - \cos(q_8)).$$

The trigonometric functions were approximated by their respective MACLAURIN-series truncated after the second term ($\sin(x) \approx x$, $\cos(x) \approx 1 - \frac{1}{2}x^2$).

$$\begin{aligned} l_{\text{AD}} q_2 &= l_{\text{HG}} q_8 - \frac{1}{2} h_{\text{HG}} q_8^2 \\ \iota(q_8) &= \frac{q_2}{q_8} = \frac{l_{\text{HG}} - \frac{1}{2} h_{\text{HG}} q_8}{l_{\text{AD}}} \end{aligned} \tag{B.3}$$



(a) Kinematically identical mechanism. (b) Closed vector loop.

Figure B.1 – Kinematically equivalent system of the EMFC weighing cell with closed vector loop for the kinematic analysis.

The approximated transmission ratio is shown in (B.3).

$$q_2 = \frac{l_{HG} - \frac{h_{HG}}{2} q_8}{l_{AD}} q_8$$

The angular deflection of the coupling rod q_7 is defined by:

$$q_7 = \arctan \left(\frac{(\delta_G - \delta_F)}{h_{FG}} \right) \approx \frac{(\delta_G - \delta_F)}{h_{FG}}$$

The x displacements of the coupling points F and G are written as follows. For the determination of δ_F a constant transmission ratio ($\xi = l_{HG}/l_{AD}$) was assumed.

$$\begin{aligned} \delta_F &\approx l_{AD} (1 - \cos(\xi q_8)) \\ \delta_G &\approx l_{HG} (1 - \cos(q_8)) - h_{HG} \sin(q_8) \end{aligned}$$

The small angle approximation with $\cos(x) \approx 1 - x^2/2$ and $\sin(x) \approx x$ yields:

$$\begin{aligned} \delta_F &\approx \xi^2 \frac{q_8^2}{2} \\ \delta_G &\approx l_{HG} \frac{q_8^2}{2} - h_{HG} q_8 \end{aligned}$$

The difference between the displacements is expressed by the approximated relationship:

$$(\delta_G - \delta_F) = l_{HG} \frac{q_8^2}{2} - h_{HG} q_8 - \frac{l_{HG}^2}{l_{AD}^2} \frac{q_8^2}{2}$$

$$\text{with: } \tau := \frac{(-l_{\text{HG}}^2 + l_{\text{HG}} l_{\text{AD}})}{2l_{\text{AD}}}$$

Finally q_7 is written as:

$$q_7 \approx \frac{(h_{\text{HG}} q_8 + \tau q_8^2)}{h_{\text{FG}}}$$

The effect of the coupling rod angle can be directly observed. For small angles the h_{HG} represents the major contribution to the angle. The change in transmission ratio by the reduction of the vertical distance between F and G by q_7 was now added to the equation:

$$\begin{aligned} \Delta q_2 &= \frac{h_{\text{FG}} q_7^2}{2l_{\text{AD}}} \\ q_2 = \iota(q_8) q_8 + \Delta q_2 &= \iota(q_8) q_8 + \frac{h_{\text{FG}} q_7^2}{2l_{\text{AD}}} \end{aligned} \quad (\text{B.4})$$

Equation (B.4) is the approximated nonlinear transmission ratio that is used to derive the quasi-static analytical rigid body model in Subsec. 5.2.3.

To check the accuracy of the analytic representation of the transmission ratio ι , a numeric model was set up in MATLAB to evaluate the nonlinear transmission ratio. The kinematic behavior of the simplified mechanism in Fig. B.1 is described by the closed vector loop:

$$r_{\vec{\text{AD}}} + r_{\vec{\text{FG}}} + r_{\vec{\text{GH}}} + r_{\vec{\text{GH}}} + r_{\vec{\text{HA}}} = \vec{0}. \quad (\text{B.5})$$

Equation (B.5) yields the following nonlinear system of equations for the kinematic system:

$$\begin{pmatrix} -l_{\text{AH}} + l_{\text{AD}} \cos(q_2) - l_{\text{HG}} \cos(q_8) - h_{\text{FG}} \sin(q_7) + h_{\text{HG}} \sin(q_8) \\ +h_{\text{AH}} - h_{\text{FG}} \cos(q_7) + h_{\text{HG}} \cos(q_8) - l_{\text{AD}} \sin(q_2) + l_{\text{HG}} \sin(q_8) \end{pmatrix} = \begin{pmatrix} 0 \\ 0 \end{pmatrix}$$

The comparison of the analytically derived nonlinear transmission ratio (B.4) with the numerical solution from the closed vector loop in Fig. B.1b is presented in Fig. B.3 and reveals only minor deviations. The agreement between the models in the range of interest ($h_{\text{HG}} \in [0 \text{ } 10] \text{ mm}$) is excellent. Equation (B.4) was thus considered suitable for the description of the weighing cell's transmission ratio.

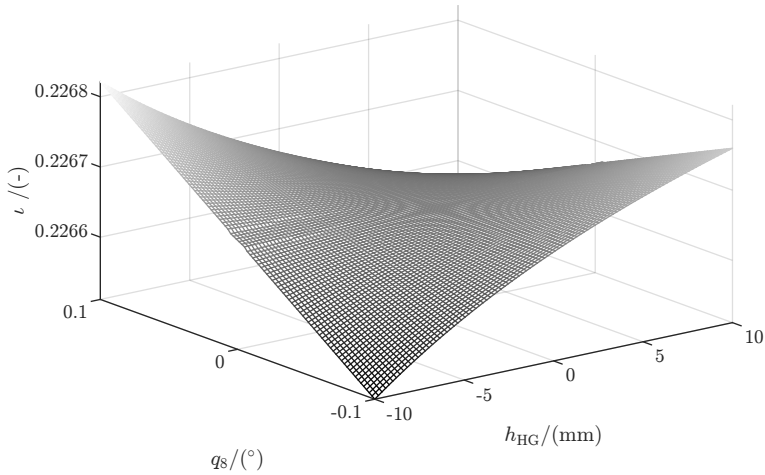


Figure B.2 – Transmission ratio $\iota = q_2/q_8 = f(h_{HG}, q_8)$ determined numerically from the nonlinear equation system in B.5.

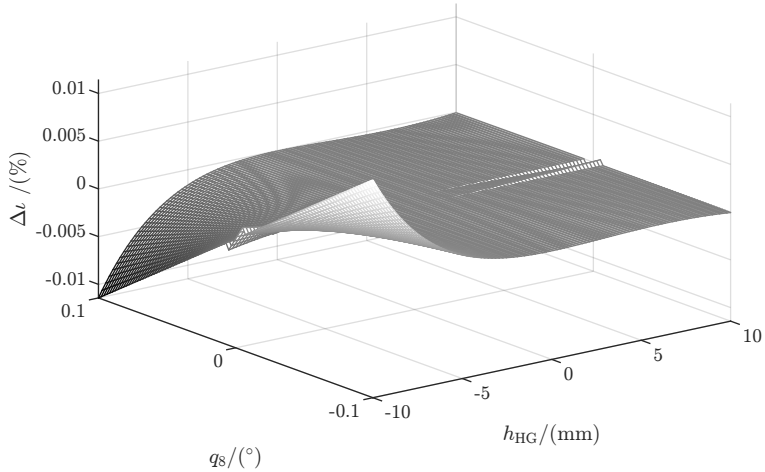


Figure B.3 – Percentage deviation of the approximated and the numerically determined transmission ratio.

B.6 Finite element models

The model definition in the FE software ANSYS[®] is largely based on the ANSYS Parametric Design Language (APDL). However, the meshing of complex geometry was done in ANSYS[®] workbench. The thin flexure hinges require a completely different mesh density than the remaining structures within the compliant mechanism. Following the strategy based on different non congruent meshing zones enables a highly refined mesh in the central zone of the flexure hinge. The mesh in the central region of the flexure hinges was set using the following options:

- defeaturing: off
- wall thickness: on
- curvature: on
- number of elements over gap: 3

To connect the non matching meshes and to attach point masses to the structure, MPC contacts were used. The settings documented in Tab. B.3 were used throughout all FE models. For more details on the meshing strategies for thin flexure hinges

Table B.3 – Settings of the multi point constraint contacts in ANSYS[®].

APDL	description
point mass to structure	
ET,x,TARGE170	target element (pilot node)
KEYOPT,x,2,1	user-defined selection of constraints
KEYOPT,x,4,111111	activate all DOF (rx,ry,rz,ux,uy,uz)
ET,y,CONTA174	contact element
KEYOPT,y,2,2	contact algorithm: Multipoint constraint (MPC)
KEYOPT,y,4,1	contact surface: force-distributed constraint
KEYOPT,y,12,5	bonded (always), changes settings of the local coordinate system
mesh-to-mesh surface contact	
ET,x,TARGE170	target element
KEYOPT,x,2,1	user-defined selection of constraints
KEYOPT,x,4,111111	activate all DOF (rx,ry,rz,ux,uy,uz)
ET,y,CONTA174	contact element
KEYOPT,y,2,2	contact algorithm: Multipoint constraint (MPC)
KEYOPT,y,4,1	contact surface: force-distributed constraint
KEYOPT,y,12,5	bonded (always)

and other FE modeling topics, see [Tor18] and [Xu21].

C Measurements and Experiments

This chapter further describes measurement methods and provides additional data in support of the measurements mentioned in the main text predominantly in Ch. 4 and Ch. 6.

C.1 Quasi-static flexure hinge stiffness measurement

The parameters and associated uncertainty contributions for the flexure test bench setup are summarized in Tab. C.1. This data was used as input for the metrological model in Subsec. 4.5.1 to estimate the measurement uncertainty of the quasi-static measurement of the stiffness.

Table C.1 – Parameters of the quasi-static stiffness measurement setup ((u) - uniform PDF); (n) - normal PDF).

param.	description	value	uncertainty	unit
geometric parameters				
h_T	tape thickness ^a	0.01	± 0.002 (u)	mm
w_T	tape width	12.7	± 0.100 (u)	mm
h_B	z-pos. COM-beam	0.000	± 0.15 (u)	mm
D	pulley diameter	110.0	± 0.300 (u)	mm
φ	angle pulley	182.5×10^{-3}	$\pm 4.8 \times 10^{-6}$ (u)	rad
φ_{cal}	angle pulley cal.	182.5×10^{-3}	$\pm 8 \times 10^{-5}$ (u)	rad
α	defl. angle flexure ^b	7.105×10^{-4}	$\pm 1.21 \times 10^{-6}$ (u)	rad
α^*	nonlinearity	0.0	$\pm 2.42 \times 10^{-6}$ (u)	rad
L_B	length lever	270.6445	± 0.00465 (u)	mm
L_T	length susp. tape	257.85	± 5 (u)	mm
h_{TB}	coupling tape-beam	1.65	± 0.15 (u)	mm
mass values				
m_B	mass beam ass.	100.0	± 5 (u)	g
m_{cal}	cal. mass (E2)	10×10^{-3}	$\pm 8 \times 10^{-6}$ (u)	g
physical parameters				
g	gravitational accel. ^c	9.810 157 72	$\pm 0.16 \times 10^{-6}$ (n)	m s^{-2}
ρ_T	density tape mat.	7900.0	± 100 (u)	kg m^{-3}
ρ_{cal}	density cal. mass	8000.0	± 100 (u)	kg m^{-3}
ρ_0	density air	1.225	± 0.2 (u)	kg m^{-3}
C^*_{rot}	rotational stiffness	18.5	± 1.0 (u)	N mm rad^{-1}

^a H+S Präzisionsfolien data sheet

^b data sheet ELCOMAT 3000: accuracy $\pm 0.25''$

^c measurement by: Bundesamt für Kartographie und Geodäsie

C.2 Dynamic stiffness measurement

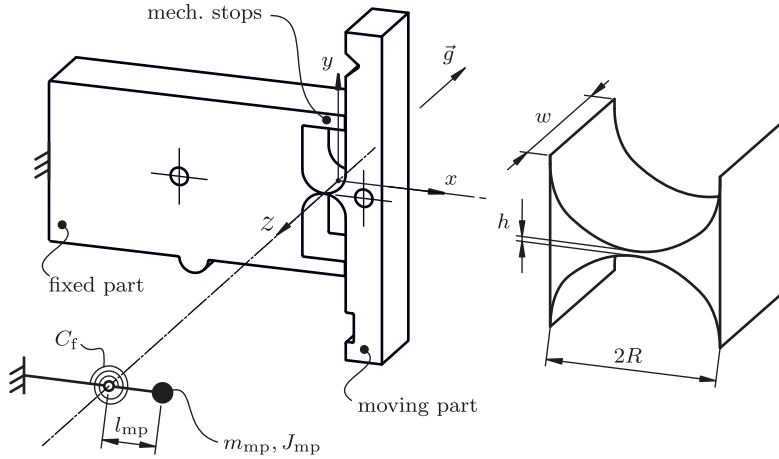


Figure C.1 – Sketch and indication of the model parameters for the single flexure hinge specimen with its rigid body model in the foreground.

The extremely low stiffness of precision weighing devices complicates the external measurement of the mechanical properties. A common way to circumvent this problem is the measurement of the period of oscillation or the natural frequency of the setup respectively [Spe87; Qui92; Sho+97; Pic04; Pin+07]. Besides providing a measure for the actual stiffness of the compliant mechanism, the measured period is highly dependent on the inertia within the system, e.g., the large mass on the weighing pan. For the flexure hinge specimen in Fig. C.1 the inertia of the moving part is relevant for the determination of the stiffness. With the aim of an accurate determination of the mechanical stiffness, a limitation of the mass induced influences can be achieved by precise manufacture and a well-known density. In case of a weighing cell, disassembly and horizontal orientation of the mechanism reduces the uncertainty contribution by inertia. The plane of motion of the mechanism is thus perpendicular to the direction of gravitational acceleration (\vec{g}). This omits any gravitational stiffness components, both concerning the trim masses and the astatization for a weighing cell mechanism. Merely, the net masses of the bodies within the mechanism cannot be removed which also holds for the single flexure hinge specimen. Their rotational inertia represent a major source of uncertainty for this type of measurement. The measurement principle based on the chromatic confocal

displacement sensor is presented in Fig. 4.13. The slightest external mechanical disturbance triggers an oscillation of the specimen in its natural frequency. The oscillation easily lasts several minutes due to the low damping. The frequency of the disassembled PROT-S mechanism lies in the range of $f_0 = 3$ Hz which enables a visual observation. The natural frequency of the flexure hinge specimen is around $f_0 = 20$ Hz. The $f_s = 10$ kHz sample rate of the sensor is sufficiently high ($f_s \gg f_0 \cdot 10$ [Hof15]) and the signal was recorded for 100 s. The FFT analysis of the recorded displacement over time yield a resolution for the natural frequency of 0.01 Hz [Hof15].

The stiffness evaluation requires an intermediate modeling step which is linking the f_0 with C . This can either be a modal analysis or an analytical model based on a substitute rotational inertia [DH16]. A sensitivity analysis in this respect with an expected $\pm 2\%$ density uncertainty of the material of yields an uncertainty $\pm 0.71 \text{ N m}^{-1}$.

$$C = f(f_0, J(\rho_{Al}))$$

Table C.2 – Parameters of the dynamic stiffness measurement setup ((u) - uniform PDF); (n) - normal PDF). The dimensions have a general tolerance according to ISO 2768-1: f (fine).

param.	description	value	uncertainty	unit
geometric parameters				
x_1	cuboid x-dir 1 st value	3	± 0.05 (u)	mm
x_2	cuboid x-dir 2 nd value	7.25	± 0.1 (u)	mm
y_1	cuboid y-dir left value	-22.5	± 0.1 (u)	mm
y_2	cuboid y-dir right value	22.5	± 0.1 (u)	mm
w	depth of the structure	10	± 0.1 (u)	mm
R	radius of flexure hinge contour	3	± 0.05 (u)	mm
physical parameters				
ρ	density	2810	± 28.1 (u)	kg m^{-3}
E	YOUNG's modulus	71.7	± 0.717 (u)	GPa
f_0	measured natural freq.	21.250	± 0.005 (u)	Hz

C.3 Tactile measurements on flexure hinges and related computational methods

The method for tactile measurements on flexure hinges in compliant mechanisms was detailed in Fig. 4.16. The accuracy of the presented CMM method is highly dependent on a number of effects which require careful consideration or correction. The most relevant are:

Table C.3 – Measurement strategy for the CMM measurement including key parameters of the Zeiss UMM550 according to www.hggmbh.de, access: 2020-03-22.

parameter	value	unit
measurement strategy		
\vec{e}_z measurement length	9.0	mm
\vec{e}_x measurement length	2.0	mm
\vec{e}_z spatial resolution	10.0	μm
\vec{e}_x spatial resolution	20.0	μm
scanning speed	1.0	mm s^{-1}
measurement force	50.0	mN
key parameters		
max. spatial resolution	0.1 to 0.2	μm
speed	0.5 to 65 000	mm s^{-1}
measurement force	0.1 to 2	N
measurement range X	500	mm
measurement range Y	500	mm
measurement range Z	400	mm
measurement uncertainty	$2.3 + L/200$	μm

- deformation due to the probing force (compliance of structure, clamping),
- mechanical filter due to finite size of probing sphere,
- simplified consideration of edge region on both sides.

The listed aspects are covered in the following section.

Typical surface topography of the flexure hinges has peak-to-peak heights between $1 \mu\text{m}$ and $10 \mu\text{m}$. The high-resolution of $0.1 \mu\text{m}$ is sufficient to measure these small features. Since the overall dimensions of the measurement region are within a few millimeters, it is expected to undercut the specified measurement uncertainty given by: $2.3 \mu\text{m} + L/(\text{mm})/200$.

The experimental determination of the measurement uncertainty of a CMM in scanning mode is not yet covered by the relevant standards [DIN EN ISO 10360-1:2003-07], VDI/VDE 2617 and [DKD-R 4-3 Blatt 18.1], see [Wei19] for more information. All reference scans in [Wei19] have been conducted with a scanning speed of 1 mm s^{-1} . The scanning speed for the high-accuracy measurements in this work were set to this value. The measurement length or scanning range is defined to be 1 mm shorter than the width (w) of the flexure hinge to be measured.

During the measurement, the stylus axis on the CMM is parallel the z axis of the flexure hinge see Fig. 4.16. This way, both surfaces of the flexure can be measured by lateral probing. The scanning motion direction is parallel to the stylus axis. As discussed in Sec. 4.3.2, the measured region can be restricted to the significant region without accuracy losses in terms of rotational stiffness. Following the results

in Fig. 4.6, this zone is defined by $d_{\text{SR}} = 2 \text{ mm}$ corresponding to an opening angle of $\pm 19.1^\circ$ on the two cylinders with 3 mm radius. Allowance was added to the width of the probing region due to position deviations of the flexure hinge center in x direction.

For n repeated measurements of a profile on a rigid gauge block, a deviation of $\pm 0.32 \mu\text{m}$ ($n = 5, k = 2$) has been determined. The value slightly increases to about $\pm 0.69 \mu\text{m}$ ($n = 11, k = 2$) for the profile scan on a flexure hinge which is more compliant and has a more rough surface than the gauge block. The repetition of the scan on a complete flexure hinge with subsequent stiffness evaluation gave a stiffness uncertainty that is falling short $\pm 0.3 \text{ N mm rad}^{-1}$ ($n = 2, k = 1$) within a compliant mechanism and for a single flexure hinge even $\pm 0.044 \text{ N mm rad}^{-1}$ ($n = 3, k = 1$) has been obtained.

Deformations of the measurement object itself due to the probing force of 50 mN may significantly influence the measurement result. The probing force of 50 mN cannot be further reduced in the present machine configuration. A special probing strategy with linear extrapolation to zero probing force is available, but not applicable for profile scanning. A way forward would be the application of this probing mode for two exemplary points for a reference thickness determination and the subsequent deformation correction of the scanned profiles. Another is a correction by FE calculations.

The form measurement deviation arising from elastic deformation of the flexure hinge was estimated in a FE. A probe sphere with diameter 1.5 mm was brought into contact with the ideal geometry at the center of the flexure hinge. Both sides of the flexure hinge were fixed by displacement constraints. The compliance of the contact and the structure was determined to $\approx 12 \mu\text{m N}^{-1}$. The probing force of 50 mN thus may lead to an underestimation of the flexure thickness by $< 1 \mu\text{m}$ due to the probing on both sides.

Further considerations in Subsec. C.3.2 on the probing sphere acting as a morphological filter suggest an effect of similar absolute value with contrary sign. Both effects would approximately cancel out.

C.3.1 Stiffness evaluation from dimensional data

Scanning of the flexure hinge on both sides provides two point clouds of measurement points. The lateral x - z position of each actual point is slightly influenced by deviations of the surface. Therefore, it is meaningful to create a grid independent

function by interpolation of the measurement points. The point cloud on each side was interpolated to determine an actual thickness value for a specific x - z position by subtraction. The implementation of the interpolation function is based on the `scatteredInterpolant()` class in MATLAB which allows the creation of an interpolation function from the point cloud that can be queried effectively in subsequent calculations [Mat20]. An algorithm was designed to calculate C_f of the flexure hinge by integration. Prior to the stiffness calculation, it is crucial to perform a precise centering of the data to ensure, that the thinnest section of the flexure hinge is at $x = 0$ mm. This was achieved numerically with a spatial resolution of $\Delta x = 10 \mu\text{m}$.

The underlying equations for the stiffness evaluation adapted from [PW65] with the correction proposed in [Tor+18]:

$$E I_z(x) \frac{d^2 y}{dx^2} = M_z$$

$$C = \frac{M_z}{\alpha_z} = \left(\int_x \frac{dx}{E I_z(x)} \right)^{-1} = \left(\int_x \frac{12 dx}{E h(x) w} \right)^{-1} \quad (\text{C.1})$$

Equation (C.1) was discretized in z direction (cf. C.2) since the determined flexure hinge thickness varies in x and in z direction: $h(x, z)$:

$$C_i = \frac{M_z}{\alpha_z} = \left(\int_z \int_x \frac{dx dz}{E I_z(x, z)} \right)^{-1} = \left(\int_z \int_x \frac{12 dx dz}{E h(x, z)^3 w} \right)^{-1}$$

For each z value a shallow flexure element is integrated over the x axis. The results of the shallow flexure hinge slices are added up to the total stiffness. In z direction, 9 mm of the total length of 10 mm is measured. From this value $w_{\text{eval}} = 8.9$ mm were evaluated. Accordingly, the resulting integrated stiffness has to be corrected by the factor:

$$K_{\text{ml}} = \frac{w}{(w_{\text{eval}} + \delta w)} \quad (\text{C.2})$$

By using (C.2) the measured mean deviations over the measurement length of 8.9 mm are projected on the outer region of the flexure hinge (0.5 mm on each side). This simplification bases on the assumption that the deviations on the outside of the flexure hinge do not significantly differ from the measured values within the

measurement length of 8.9 mm. The final equation for the determination of the stiffness is:

$$C_f = \left(\sum_{i=1}^{n_w} \left(\left(\int_x \frac{12}{E h(x, z_i)^3} dx \right)^{-1} \delta w \right) \right) \cdot K_{ml} \quad (C.3)$$

The integral within the inner brackets of (C.3) was approximated with the MATLAB function `trapz` based on the trapezoid rule [CK08; Mat20]. This was done at one specific z position (z_i) of the n_w subdivisions. This way, C_f of a thin flexure hinge with the width δw was calculated. Figure C.2 visualizes the principle of the stiffness calculation with the integration of small flexure slices in x direction and the subsequent summation of the slice stiffness to the total stiffness. The sum of the stiffness was corrected in (C.2) with K_{ml} due to the fact that the outer parts of the flexure hinge have not been covered by the CMM measurement.

The integrand is presented in Fig. C.3 for measured values of the flexure hinge in Fig. 4.16. The surface plot emphasizes the relevance of the thickness values close to the center of the flexure hinge to achieve exact rotational stiffness values.

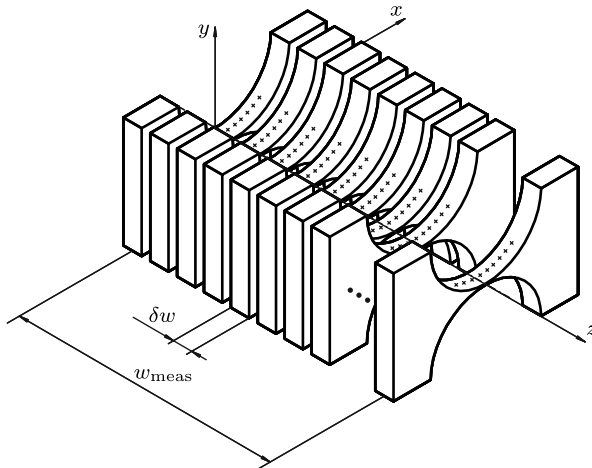


Figure C.2 – Calculation strategy to evaluate the rotational stiffness from the cloud of measurement points. The small marks on the curved surface depict interpolated measurement points at a specific z position.

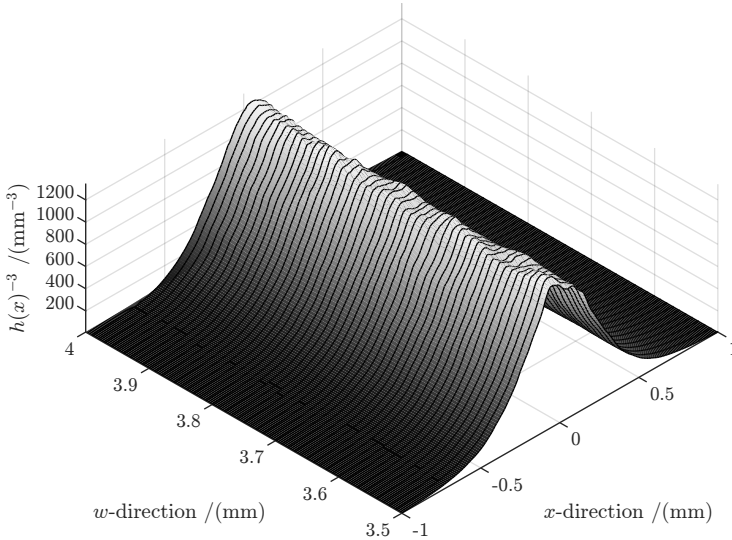


Figure C.3 – Section of the function to be integrated ($1/h^3(x)$) in x direction with interpolated measurement points.

C.3.2 Tactile probing simulation

The probing sphere acts as a mechanical filter which is suppressing small or shallow concave geometrical features. Mathematically, the filter is described as morphological dilatation which is undesired and needs to be minimized by selecting the smallest probe sphere diameter possible. The required measurement length of >10 mm and an uncritical HERTZIAN stress in the contact zone needed to be ensured. The selected probing sphere material silicon nitride is well suited for scanning (sliding) over the aluminum surface of the flexure hinge [Bos13]. The smallest available probe sphere diameter with a measurement length of >10 mm was 1.5 mm. To prove the feasibility, the probing sphere was compared to a roughness profile in Fig. C.4. The profile was extracted from the measurement data of a white light interferometry image on the outside surface of an exemplary flexure hinge. The scaled data in Fig. C.4 shows that the sphere diameter of 1.5 mm is sufficient to discriminate form deviation and waviness of the profile. However, the roughness of the surface is filtered mechanically. By applying the morphological operation, corresponding to the scanning operation with the 1.5 mm sphere, the effect can be estimated and

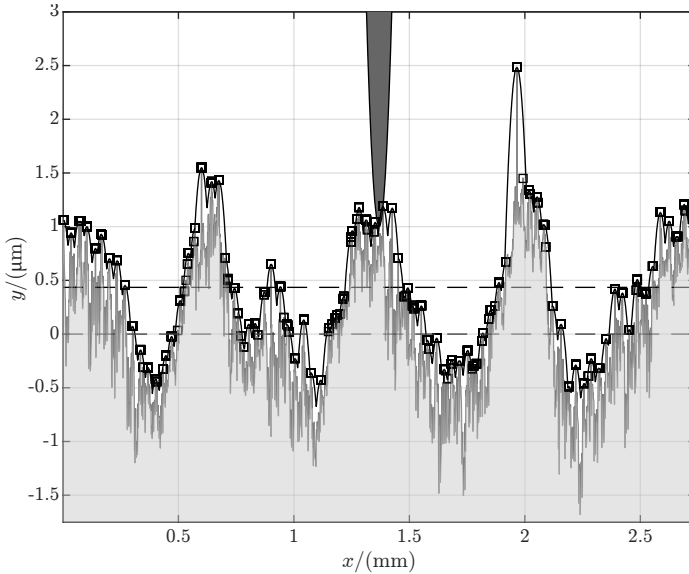


Figure C.4 – Profile scanning simulation with a 1.5 mm diameter probing sphere. The original profile was extracted from a white light interferometry measurement on a milled surface. The locations at which contact occurs are indicated by black squares. The mean of the probed profile deviates by approx. $0.5\ \mu\text{m}$ from the mean of the original profile.

the shift of the profile mean value of by approx. $0.5\ \mu\text{m}$ can be observed, which represents a systematic measurement deviation.

The algorithm for the probing simulation is based on the DELAUNAY triangulation. The grid of measurement data is meshed with a triangular mesh using the `delaunayTriangulation` function in MATLAB. The function `dsearchn` determines the closest node in the created triangular mesh relative to the coordinates of a random point (x_P, y_P, z_P) . The output is the minimum distance and the point number. The idea is to gradually move closer to the surface using the center of an ideal probing sphere as the input for the `dsearchn`-function. The output of the function is compared to the radius of the probing sphere. For each position in a fine x - y grid this procedure is repeated until the evaluated distance is smaller than the radius of the probing sphere. The last z position $z_C(x, y)$ and the contact node before the virtual interference is recorded and visualized. The probed profile is

calculated from the motion path of the probe sphere center shifted by the radius of the probe sphere towards the surface.

C.3.3 Uncertainty estimation for tactile probing

The estimation of the uncertainty of the determined rotational stiffness of a flexure hinge by tactile probing is based on repeated measurements with the CMM. Figure C.5 presents a repeated profile-scan on a flexure hinge surface of PROT-S-HG415-2.

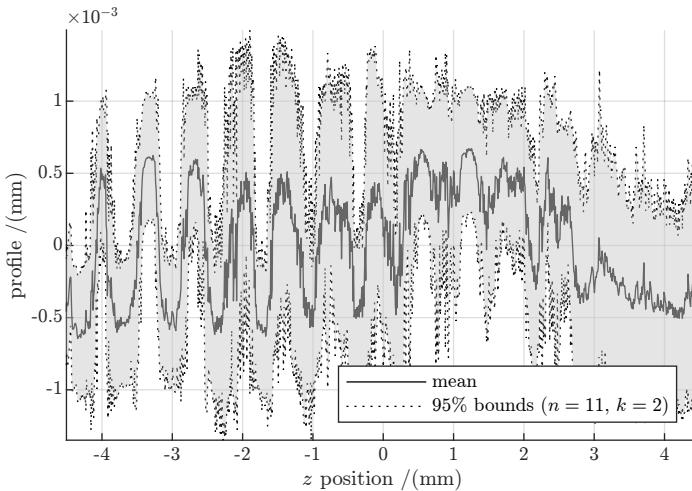


Figure C.5 – Repeated scan of a line on one the surface of flexure hinge D of PROT-S-HG415-2 in y direction in the weighing cell coordinate system and in z direction in the flexure hinge coordinate system.

The mean value for $2 \cdot \sigma$ amounts to $0.69 \mu\text{m}$ which translates into a standard deviation of the rotational stiffness of the flexure hinge of $1.26 \text{ N mm rad}^{-1}$. The value was double checked by a complete repetition of the stiffness evaluation process on flexure hinges A. The difference in stiffness between two subsequent evaluations amounts to $0.47 \text{ N mm rad}^{-1}$. Adding the uncertainty contribution of the other parameters from Fig. 4.8, excluding h , a value of 1 N mm rad^{-1} is conservatively estimated.

C.4 Weighing cell operation

All prototypes were operated using a digital control with a control frequency of ≤ 20 Hz. The photocurrent of the aperture slit position sensor was amplified and output as voltage signal by a transimpedance amplifier. The voltage was measured by an $8\frac{1}{2}$ -digit digital multimeter (DMM) (HP 3458 A) and served as process variable of the digital PID-controller implemented in a personal computer (PC). The calculated output current was sourced by the high-accuracy source HP 3245 A and fed into the windings of the voice coil actuator. Using the described digital control, the manipulation of the controller set-point was possible which was a requirement for the measurement of the stiffness C during operation.

C.5 Influence of deformations on the off-center load sensitivity

The off-center load sensitivity was measured by laterally displacing masses on the weighing pan while the sum of masses on the weighing pan was kept constant. The different positions for the masses on the weighing pan are defined according to Fig. C.6a.

The PROT-S weighing cell prototype was the perfect object of investigation for off-center load sensitivity variation in x direction due to deformations of the structural components of the weighing cell [Dar+20]. The mechanical effect can be explained based on particularities of the weighing cell design: the monolithic mechanism of the PROT-S mechanism demanded that all components were linked in a planar design. The chosen solution was a rigid connection between A, B and H, with a mechanical structure in the form of a C-shape, see Fig. 5.1. This C-shape structure is loaded at H by a vertical force of at least $(1 + \xi) m_G g$. The force flow goes through the structure to the base on the opposite site of the C-structure. The result is a significant bending deformation which is affecting the position of B and the parallelism between upper and lower lever. The upper lever tends to a negative deflection angle resulting in a positive E_{Lx} ($h_{AB} < h_{DC}$).

Interestingly, the apparently linear behavior in x direction (see Fig. 5.9) is actually quadratic with a pronounced origin shift. A position of the mass exists where $E_{Lx} = 0$ holds. It was found that the position is closely related to the distortion of the parallelogram guide and the deviation of the levers from parallelism. The causes for the distortion are not limited to manufacturing deviations but are affected by

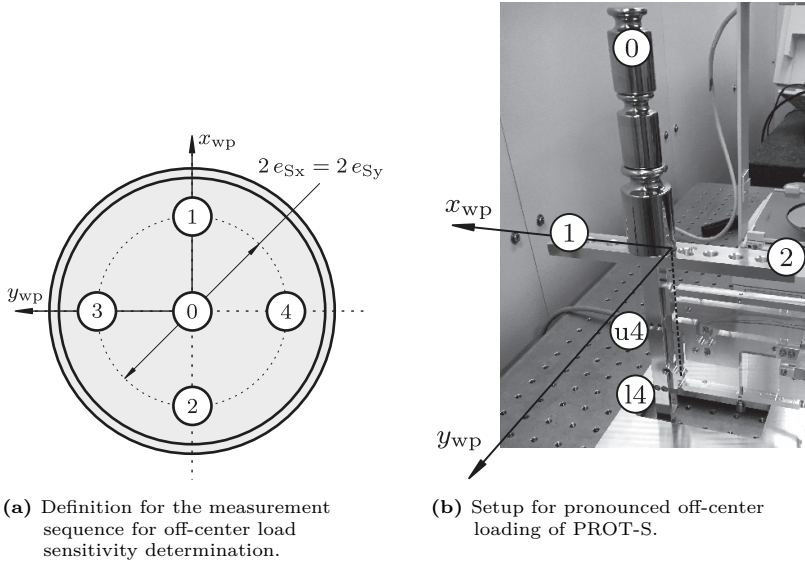


Figure C.6 – Experimental setup for the indication change due to pronounced off-center loads in x direction. The 200 g mass on top of the stack was taking positions $\textcircled{0}$ - $\textcircled{2}$ and each time the indicated mass was recorded. $\textcircled{0}$ - $\epsilon_{Sx} = 16$ mm, $\textcircled{1}$ - $\epsilon_{Sx} = 86$ mm, and $\textcircled{2}$ - $\epsilon_{Sx} = -86$ mm. The measurement procedure was repeated for three mounting conditions between load carrier and weighing pan: $\textcircled{u4}$ - upper four screws mounted, $\textcircled{l4}$ - lower four screws mounted, $\textcircled{a4}$ - all eight screws mounted.

the deformations of the structure belonging to the base and the load carrier. The way, the weighing pan is attached to the load carrier is affecting the characteristic of its deformation and shows an effect in model and experiment.

To restore parallelism between the levers, h_{DC} needs to be reduced. Within the FE model it was discovered that minute bending deformations evoked by the off-center load itself change the off-center load sensitivity in x direction. The replication of these results in an experiment are presented in Fig. C.7. Despite numerous uncertainties, manual positioning of the 200 g mass on the weighing pan and unknown manufacturing deviations, a qualitative agreement was achieved. The x position where $E_{Lx} = 0$ holds exist and can be experimentally determined. Furthermore, qualitative agreement with the FE model was proven: for the dis-

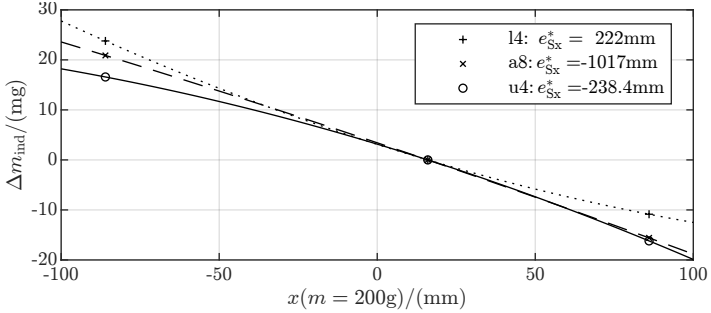


Figure C.7 – The total mass on the weighing pan of the PROT-S-HG315-1 prototype is $m_{S6} = 700$ g. A part of m_{S6} , a 200 g-mass is displaced on the modified weighing pan and the indicated mass value is evaluated for each position. The measurement was repeated for different mounting configurations between weighing pan and load carrier: (u4) - only 4 upper screws fixed, (a4) - all 8 screws fixed, (l4) - only 4 lower screws fixed.

placement of a 200 g mass, the model predicts (u4) = -503 mm, (a8) = -2046 mm, and (l4) = 1326 mm.

The experiment in Fig. C.7 additionally proves the relevance of the force/torque application point to the load carrier. Depending on the clamping position, the bending deformation of the load carrier changes its characteristic. As indicated, this is affecting the location of the mass position e_{Sx}^* for $E_{Lx} = 0$. If all eight screws are tightened, the load carrier is stiffened and large eccentricity of ≈ -1 m is required. In contrast, the unstiffened load carrier undergoes a larger bending deformation which reduces the required eccentricity by the factor of four. The change between upper and lower screw connection changes the sign of the bending deformation and thus also the sign of the eccentricity required (e_{Sx}^*).

C.6 Preliminary test of stiffness adjustment concept

In Ch. 8.1, the concept for the new stiffness adjustment is introduced. Two PROT-S weighing cells with different h_{HG} values were used for a proof of the adjustment concept. The weighing cells need to be mechanically connected in the z direction. Prerequisite for the comparison between measurement and model is the determination of the weighing cells' stiffness. First, the stiffness of each weighing cell was determined, see Tab. C.4. The measurement sequence for the connected

Table C.4 – Measured stiffness values prior to the combination of the weighing cells.

prototype	meas. descr.	value	unit
①-③:			
PROT-S-315-1 ^a	$m_{S6} = 1.000 \text{ kg}$	1.46	N m^{-1}
PROT-S-100-1	$m_{S6} = 1.000 \text{ kg}$	54.00	N m^{-1}
④-⑤:			
PROT-S-315-1	$m_{S6} = 1.010 \text{ kg}$	-30.09	N m^{-1}
PROT-S-100-1	$m_{S6} = 0.986 \text{ kg}$	52.98	N m^{-1}

^a h_{T8} was negative to increase the stiffness

weighing cells is documented in Fig. C.8. Parts of the counter mass were transferred from on weighing cell to the other resulting in a changing force flow through each weighing cell and thus a varying astatization effect on the stiffness of the combined system.

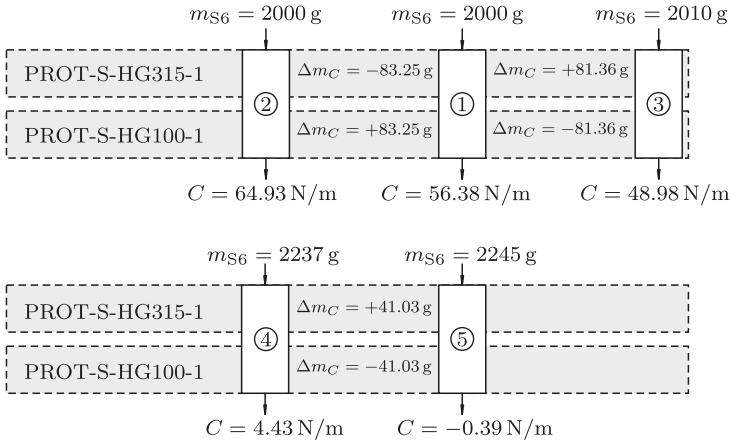


Figure C.8 – Description of the setups for the preliminary testing of the novel adjustment concept for the prototype mass comparator weighing cell.

Bibliography

- [Abd+05] ABDEL KAREEM, A. M. et al. Improvement of Mass Determination Using AT-1006 Comparator in NIS – Egypt: IMEKO-TC3-2005. 2005.
- [Ash11] ASHBY, M. F. *Materials selection in mechanical design, fourth edition*. 4th ed. Amsterdam et al.: Elsevier et al., 2011. ISBN 9781856176637. Available from DOI: 10.1016/C2009-0-25539-5.
- [Bau+13] BAUMANN, H. et al. Design of the new METAS watt balance experiment Mark II. *Metrologia*. 2013, vol. 50, (3), pp. 235–242. Available from DOI: 10.1088/0026-1394/50/3/235.
- [Bau15] BAUMGARTL, H. S. *Optimierung dynamischer Waagen nach dem Prinzip der elektromagnetischen Kraftkompensation mittels numerischer Modelle zur Systemsimulation*. Ilmenau, 2015. PhD thesis. Technische Universität Ilmenau. Supervised by G. JÄGER.
- [Bee+02] BEER, W. et al. The METAS 1 kg vacuum mass comparator - adsorption layer measurements on gold-coated copper buoyancy artefacts. *Metrologia*. 2002, vol. 39, (3), pp. 263–268. ISSN 0026-1394. Available from DOI: 10.1088/0026-1394/39/3/3.
- [Bee83] BEETZ, B. Analyse und Modellbildung von Checkweiger-Wägesystemen / Analysis and modelling of checkweigher weighing systems. *tm - Technisches Messen*. 1983, vol. 50, (JG). ISSN 0171-8096. Available from DOI: 10.1524/teme.1983.50.jg.337.
- [BG70] BENNETT, S. J.; GATES, J. W. C. The design of detector arrays for laser alignment systems. *Journal of Physics E: Scientific Instruments*. 1970, vol. 3, (1), pp. 65–68. ISSN 0022-3735. Available from DOI: 10.1088/0022-3735/3/1/315.
- [BD08] BERRY, J.; DAVIDSON, S. Contamination deposited on mass standards in vacuum from an inverted magnetron gauge. *Measurement Science and Technology*. 2008, vol. 19, (11), p. 115102.

- [Bes+99] BESSASON, B. et al. Vibration criteria for metrology laboratories. *Measurement Science and Technology*. 1999, vol. 10, (11), pp. 1009–1014. ISSN 0957-0233. Available from DOI: 10.1088/0957-0233/10/11/306.
- [BS16] BETTIN, H.; SCHLAMMINGER, S. Realization, maintenance and dissemination of the kilogram in the revised SI. *Metrologia*. 2016, vol. 53, (5), A1–A5. Available from DOI: 10.1088/0026-1394/53/5/A1.
- [BCH94] BICH, W.; COX, M. G.; HARRIS, P. M. Uncertainty Modelling in Mass Comparisons. *Metrologia*. 1994, vol. 30, (5), p. 495.
- [Bip19] BIPM. *The International System of Units (SI): 9th edition*. 2019.
- [Bor+12] BORYS, M. et al. *Fundamentals of Mass Determination*. Berlin, Heidelberg: Springer Berlin Heidelberg, 2012. ISBN 978-3-642-11936-1. Available from DOI: 10.1007/978-3-642-11937-8.
- [Bos13] BOS, E. *Best Practice Guide on tactile metrology*. 2013.
- [BA63] BOWMAN, H. A.; ALMER, H. E. Minimization of the arrestment error in one-pan, two-knife balance systems. *Journal of Research of the National Bureau of Standards, Section C: Engineering and Instrumentation*. 1963, vol. 67C, (3), p. 227. ISSN 0022-4316. Available from DOI: 10.6028/jres.067C.020.
- [BM59] BOWMAN, H. A.; MACURDY, L. B. A photoelectric followup and recording system, and its application to remote observations of the beam in high-precision balances. *Journal of Research of the National Bureau of Standards, Section C: Engineering and Instrumentation*. 1959, vol. 63C, (2), p. 91. ISSN 0022-4316. Available from DOI: 10.6028/jres.063C.013.
- [BM60] BOWMAN, H. A.; MACURDY, L. B. Gimbal device to minimize the effects of off-center loading on balance pans. *Journal of research of the National Bureau of Standards*. 1960, vol. 64C, (4).
- [CD82] CAGE, M. E.; DAVIS, R. S. An Analysis of Read-Out Perturbations Seen on an Analytical Balance with a Swinging Pan. *Journal of Research of the National Bureau of Standards*. 1982, vol. 87, (1), p. 23. ISSN 0160-1741. Available from DOI: 10.6028/jres.087.004.
- [Cas+20] CASTILLO ZEVILLANOS, M. P. et al. *Modellierung von Festkörpergelenken unter Berücksichtigung der Oberflächentopografie*. Ilme-

- nau, 2020. BA thesis. Technische Universität Ilmenau, Precision Engineering Group. Supervised by R. THESKA.
- [CK08] CHENEY, W.; KINCAID, D. *Numerical mathematics and computing*. 6th ed. Belmont, Calif.: Brooks/Cole, 2008. ISBN 978-0-495-11475-8.
- [Che+02] CHENG, Y. et al. Tilt sensor and servo control system for gravitational wave detection. *Classical and Quantum Gravity*. 2002, vol. 19, (7), pp. 1723–1729. ISSN 0264-9381. Available from DOI: 10.1088/0264-9381/19/7/367.
- [Cho+04] CHOI, I. M. et al. Parallelism error analysis and compensation for micro-force measurement. *Measurement Science and Technology*. 2004, vol. 15, (1), p. 237.
- [CM01] CLARKSON, M. T.; MAY, B. J. An investigation of methods for cleaning stainless-steel weights. *Metrologia*. 2001, vol. 38, (2), pp. 161–171. Available from DOI: 10.1088/0026-1394/38/2/8.
- [Con22] CONRADY, A. E. A Study of the Balance. *Proceedings of the Royal Society of London. Series A, Containing Papers of a Mathematical and Physical Character*. 1922, vol. 101, (710), pp. 211–224. ISSN 09501207.
- [CH06] COX, M. G.; HARRIS, P. M. Measurement uncertainty and traceability. *Measurement Science and Technology*. 2006, vol. 17, (3), pp. 533–540. Available from DOI: 10.1088/0957-0233/17/3/S13.
- [CW80] CZANDERNA, A. W.; WOLSKY, S. P. *Microweighing in vacuum and controlled environments*. Amsterdam et al.: Elsevier Scientific Pub. Co. et al., 1980. Methods and phenomena, their applications in science and technology. ISBN 0-444-41868-7.
- [Dar17] DARNIEDER, M. *Optimierung monolithischer Mechanismen in der Kraftmess- und Wägetechnik*. Dresden, 2017. 11. Tagung Feinwerktechnische Konstruktion.
- [DFT19] DARNIEDER, M.; FRÖHLICH, T.; THESKA, R. Tilt sensitivity modeling of a monolithic weighing cell structure. In: KECSKEMÉTHY, A. et al. (eds.). *Interdisciplinary Applications of Kinematics*. Cham: Springer International Publishing, 2019. ISBN 978-3-030-16422-5.
- [Dar+17a] DARNIEDER, M. et al. Contribution to the mechanical enhancement of load cells in precision weighing technology by means of advanced

- adjustment strategies. In: BILLINGTON, D.; PHILLIPS, D. (eds.). *Proceedings of the 17th international conference of the european society for precision engineering and nanotechnology*. 2017, pp. 411–412. ISBN 978-0-9957751-0-7.
- [Dar+17b] DARNIEDER, M. et al. Design of high-precision weighing cells based on static analysis. *Engineering for a changing world : 59th IWK, Ilmenau Scientific Colloquium, Technische Universität Ilmenau, 11th-15th September 2017 : proceedings*. 2017.
- [Dar+18a] DARNIEDER, M. et al. Modellierung der Drehsteifigkeit dünner Festkörpergelenke in der Präzisionsgerätetechnik. In: PRENZEL, W.-D. (ed.). *Jahrbuch Optik und Feinmechanik 2018*. Görlitz: OPTIK-Verlag, 2018, pp. 139–165. ISBN 978-3-00-061720-1.
- [Dar+18b] DARNIEDER, M. et al. On precise modelling of very thin flexure hinges. In: BILLINGTON, D. (ed.). *Proceedings of the 18th International Conference of the European Society for Precision Engineering and Nanotechnology : June 4th-8th June 2018, Venice, IT*. Bedford, 2018, pp. 87–88. ISBN 9780995775121.
- [Dar+18c] DARNIEDER, M. et al. Static behavior of weighing cells. *Journal of Sensors and Sensor Systems*. 2018, vol. 7, (2), pp. 587–600. ISSN 2194-878X. Available from DOI: 10.5194/jsss-7-587-2018.
- [Dar+19] DARNIEDER, M. et al. Mechanical properties of an adjustable weighing cell prototype. In: LEACH, R. K. (ed.). *Proceedings of the 19th International Conference of the European Society for Precision Engineering and Nanotechnology*. Bedford: euspen, 2019, pp. 86–89. ISBN 978-0-9957751-4-5.
- [Dar+20] DARNIEDER, M. et al. Corner loading and its influence on the tilt sensitivity of precision weighing cells. In: LEACH, R. K. (ed.). *Proceedings of the 20th International Conference of the European Society for Precision Engineering and Nanotechnology*. Bedford: euspen, 2020, pp. 95–98. ISBN 9780995775176.
- [Dar+21a] DARNIEDER, M. et al. Characterization of Thin Flexure Hinges for Precision Applications Based on First Eigenfrequency. In: ZENTNER, L.; STREHLE, S. (eds.). *Microactuators, Microsensors and Micromechanisms*. Cham: Springer International Publishing, 2021,

- vol. 96, pp. 15–24. Mechanisms and Machine Science. ISBN 978-3-030-61651-9. Available from DOI: 10.1007/978-3-030-61652-6_2.
- [Dar+21b] DARNIEDER, M. et al. *Justierung nachgiebiger Mechanismen für Vakuummassekomparatoren – Herausforderungen und Ziele*. Dresden, 2021. 14. Tagung Feinwerktechnische Konstruktion.
- [Dat+03] DATTA, T. et al. Tidal effects on gravity experiments with a balance. *Physical Review Letters*. 2003, vol. 91, (10), 109001, author reply 109002. ISSN 0031-9007. Available from DOI: 10.1103/PhysRevLett.91.109001.
- [Dav72a] DAVIDSON, A. *Handbook of Precision Engineering: Mechanical Design Applications*. London: Macmillan Education UK, 1972. ISBN 978-1-349-01025-7. Available from DOI: 10.1007/978-1-349-01023-3.
- [Dav72b] DAVIDSON, A. (ed.). *Handbook of Precision Engineering: Volume 5 Joining Techniques*. London et al.: Macmillan Education UK, 1972. Philips Technical Library. ISBN 978-1-349-01022-6. Available from DOI: 10.1007/978-1-349-01020-2.
- [DPB04] DAVIDSON, S.; PERKIN, M.; BUCKLEY, M. *The Measurement of Mass and Weight: Measurement Good Practice Guide No. 71*. 2004.
- [DBB04] DAVIDSON, S.; BROWN, S.; BERRY, J. *A report on the potential reduction in uncertainty from traceable comparisons of platinum-iridium and stainless steel kilogram mass standards in vacuum*. 2004.
- [Dav10] DAVIM, P. J. (ed.). *Surface integrity in machining*. London: Springer, 2010. ISBN 978-1-84882-873-5.
- [Der+14] DERGACHEV, V. et al. A high precision, compact electromechanical ground rotation sensor. *The Review of scientific instruments*. 2014, vol. 85, (5), p. 054502. ISSN 0034-6748. Available from DOI: 10.1063/1.4875375.
- [Die17] DIETHOLD, C. *Lorentzkraft-Anemometrie von elektrisch schwach leitfähigen Fluiden*. Ilmenau, 2017. PhD thesis. Technische Universität Ilmenau. Supervised by G. JÄGER.
- [Die+10] DIETHOLD, C. et al. *High precision optical position sensor for electromagnetic force compensated balances*. 2010.

- [Die+14] DIETHOLD, C. et al. Determination of force to displacement curves using a nanopositioning system based on electromagnetic force compensated balances. *Measurement*. 2014, vol. 51, pp. 343–348. ISSN 02632241. Available from DOI: 10.1016/j.measurement.2014.02.034.
- [DH16] DRESIG, H.; HOLZWEISSIG, F. *Maschinendynamik*. 12. aktualisierte Auflage. Berlin: Springer, 2016. ISBN 978-3-642-29570-6.
- [DYD16] DU, Z.; YANG, M.; DONG, W. Multi-objective optimization of a type of ellipse-parabola shaped superelastic flexure hinge. *Mechanical Sciences*. 2016, vol. 7, (1), pp. 127–134. ISSN 2191-916X. Available from DOI: 10.5194/ms-7-127-2016.
- [Eas35] EASTMAN, F. S. *Flexure pivots to replace knife edges and ball bearings, an adaptation of beam-column analysis*. Seattle: University of Washington, 1935.
- [Eas37] EASTMAN, F. S. The Design of Flexure Pivots. *Journal of the Aeronautical Sciences*. 1937, vol. 5, (1), pp. 16–21. ISSN 1936-9956. Available from DOI: 10.2514/8.499.
- [Eic+12] EICHENBERGER, A. et al. The METAS watt balance Mark II experiment. In: *2012 Conference on Precision Electromagnetic Measurements (CPEM 2012)*. Piscataway, NJ: IEEE, 2012, pp. 426–427. ISBN 978-1-4673-0442-9. Available from DOI: 10.1109/CPEM.2012.6250985.
- [Eme01] EMERY, J.-C. A sub-ppm precision monolithic force sensor based on articulated structures with flexible bearings: Sensors Expo & Conference 2001. 2001.
- [Erd82] ERDEM, U. Force and weight measurement. *Journal of Physics E: Scientific Instruments*. 1982, vol. 15, (9), pp. 857–872. ISSN 0022-3735. Available from DOI: 10.1088/0022-3735/15/9/002.
- [Esw+07] ESWARD, T. J. et al. A Monte Carlo method for uncertainty evaluation implemented on a distributed computing system. *Metrologia*. 2007, vol. 44, (5), pp. 319–326. Available from DOI: 10.1088/0026-1394/44/5/008.
- [FR80] FALLER, J. E.; RINKER, R. L. Super spring. *The Journal of the Acoustical Society of America*. 1980, vol. 68, (6), p. 1900. ISSN 0001-4966. Available from DOI: 10.1121/1.385186.

- [FFH05] FEHLING, T.; FRÖHLICH, T.; HEYDENBLUTH, D. The new Sartorius 1Kg-Prototype Balance for High Precision Mass Determination and Research Applications. In: SCHARFF, P. (ed.). *Mechanical engineering from macro to nano*. Ilmenau: Verl. ISLE, 2005. ISBN 3-932633-98-9.
- [Feh+13] FEHLING, T. et al. *Vacuum transfer system for loading the Sartorius prototype mass comparator CCL1007*. Ilmenau: Univ.-Bibliothek et al., 2013.
- [Fer+11] FERRO, A. et al. High precision tilt observation at Mt. Etna Volcano, Italy. *Acta Geophysica*. 2011, vol. 59, (3), pp. 618–632. ISSN 1895-6572. Available from DOI: 10.2478/s11600-011-0003-7.
- [Fra93] FRANZ, E. *Dynamik von elektromechanischen Präzisionswaagen: Zugl.: München, Univ., Diss. Als Ms. gedr.* Düsseldorf: VDI-Verl., 1993. Fortschritt-Berichte VDI Reihe 18, Mechanik, Bruchmechanik. ISBN 3-18-142418-8.
- [FLR14] FRIEDRICH, R.; LAMMERING, R.; RÖSNER, M. On the modeling of flexure hinge mechanisms with finite beam elements of variable cross section. *Precision Engineering*. 2014, vol. 38, (4), pp. 915–920. ISSN 01416359. Available from DOI: 10.1016/j.precisioneng.2014.06.001.
- [Fri16] FRIEDRICH, R. *Modellierung und Optimierung nachgiebiger Mechanismen auf Basis elastischer Festkörpergelenke mit Hilfe von nichtlinearen Finiten Balkenelementen*. Hamburg, 2016. PhD thesis. Helmut-Schmidt-Universität. Supervised by R. LAMMERING.
- [Frö98] FRÖHLICH, T. *Dynamische Temperaturkompensation von Präzisionsmeßgeräten*. Ilmenau, 1998. PhD thesis. Technische Universität Ilmenau. Supervised by G. JÄGER.
- [FJH06] FRÖHLICH, T.; JÄGER, G.; HASCHKE, K. *Temperaturkompensation von Präzisionsmeßgeräten*. Ilmenau, 2006. Habilitation. Technische Universität Ilmenau. Supervised by G. JÄGER.
- [Gar+18] GARCÍA AYALA, B. J. et al. *Experimental setup for measuring the mechanical behavior of loaded thin compliant joints with highest precision*. Ilmenau, 2018. MA thesis. Technische Universität Ilmenau, Precision Engineering Group. Supervised by R. THESKA.

- [GJJ07] GEBAUER, A.; JAHR, T.; JENTZSCH, G. Recording and interpretation/analysis of tilt signals with five ASKANIA borehole tiltmeters at the KTB. *Review of Scientific Instruments*. 2007, vol. 78, (5), p. 054501. ISSN 00346748. Available from DOI: 10.1063/1.2736506..
- [GB09] GLÄSER, M.; BORYS, M. Precision mass measurements. *Reports on Progress in Physics*. 2009, vol. 72, (12), p. 126101. ISSN 0034-4885. Available from DOI: 10.1088/0034-4885/72/12/126101.
- [GSM91] GLÄSER, M.; SCHWARTZ, R.; MECKE, M. Experimental Determination of Air Density Using a 1 kg Mass Comparator in Vacuum. *Metrologia*. 1991, vol. 28, (1), pp. 45–50. Available from DOI: 10.1088/0026-1394/28/1/007.
- [Glä00] GLÄSER, M. Cycles of comparison measurements, uncertainties and efficiencies. *Measurement Science and Technology*. 2000, vol. 11, (1), pp. 20–24. ISSN 0957-0233. Available from DOI: 10.1088/0957-0233/11/1/303.
- [Glä01] GLÄSER, M. Magnetic interactions between weights and weighing instruments. *Measurement Science and Technology*. 2001, vol. 12, (6), pp. 709–715. ISSN 0957-0233. Available from DOI: 10.1088/0957-0233/12/6/309.
- [Goo99] GOODKIND, J. M. The superconducting gravimeter. *Review of Scientific Instruments*. 1999, vol. 70, (11), p. 4131. ISSN 00346748. Available from DOI: 10.1063/1.1150092.
- [Gou49] GOULD, F. A. A Knife-Edge Balance for Weighings of the Highest Accuracy. *Proceedings of the Physical Society. Section B*. 1949, vol. 62, (12), p. 817. ISSN 0370-1301. Available from DOI: 10.1088/0370-1301/62/12/308.
- [Gra14] GRABE, M. *Measurement uncertainties in science and technology*. Second edition. Cham et al.: Springer, 2014. ISBN 9783319048888. Available from DOI: 10.1007/978-3-319-04888-8.
- [GF11] GROTE, K.-H.; FELDHUSEN, J. *Dubbel*. Berlin, Heidelberg: Springer Berlin Heidelberg, 2011. ISBN 978-3-642-17305-9. Available from DOI: 10.1007/978-3-642-17306-6.

- [Gup12] GUPTA, S. V. *Mass Metrology*. Berlin, Heidelberg: Springer Berlin Heidelberg, 2012. ISBN 978-3-642-23411-8. Available from DOI: 10.1007/978-3-642-23412-5.
- [Han95] HANADA, H. Ground Vibrations and Tilts. *eConf*. 1995, vol. C951114, p. 034.
- [Han64] HANSEN, F. *Justierung: eine Einführung in das Wesen der Justierung von technischen Gebilden*. VEB Verlag Technik, 1964.
- [Har+22] HARFENSTELLER, F. et al. Modeling of corner-filletted flexure hinges under various loads. *Mechanism and Machine Theory*. 2022, vol. 175, p. 104937. ISSN 0094114X. Available from DOI: 10.1016/j.mechmachtheory.2022.104937.
- [HC14] HARRIS, P. M.; COX, M. G. On a Monte Carlo method for measurement uncertainty evaluation and its implementation. *Metrologia*. 2014, vol. 51, (4), S176–S182. Available from DOI: 10.1088/0026-1394/51/4/S176.
- [Har68] HART, M. An angström ruler. *Journal of Physics D: Applied Physics*. 1968, vol. 1, (11), pp. 1405–1408. ISSN 00223727. Available from DOI: 10.1088/0022-3727/1/11/303.
- [HKL20] HÄRTIG, F.; KNOPF, D.; LEHRMANN, K. Das Kilogramm im neuen SI. *tm - Technisches Messen*. 2020, vol. 87, (4), pp. 237–247. ISSN 0171-8096. Available from DOI: 10.1515/teme-2019-0154.
- [Hen17] HENSGEN, L. *Auswirkung der Drahtfunkenerosion auf die mechanischen Eigenschaften von Festkörpergelenken*. Aachen, 2017. PhD thesis. Rheinisch-Westfälischen Technischen Hochschule Aachen. Supervised by F. KLOCKE.
- [HRF17] HILBRUNNER, F.; RAHNEBERG, I.; FRÖHLICH, T. Watt balance with lever transmission based on commercial EMFC load cell. *tm - Technisches Messen*. 2017, vol. 85, (11), pp. 658–679. ISSN 0171-8096. Available from DOI: 10.1515/teme-2017-0065.
- [Hil+10] HILBRUNNER, F. et al. Comparison of different load changers for EMFC-balances. *IMEKO TC3 & TC5 & TC22 International Conference : [IMEKO 2010 ... held in Pattaya, Thailand from 21st to 25th November 2010 ; Metrology in modern context]*. 2010, pp. 65–68.

- [Hil+16] HILBRUNNER, F. et al. *Traceable Mass Determination and Uncertainty Calculation: CENAM Simposio de Metrologia, 10 – 23 Septiembre 2016*. 2016.
- [HC52] HODSMAN, G. F.; CHAPPELL, F. A. The effective radius of curvature of knife edges. *Journal of Scientific Instruments*. 1952, vol. 29, (10), pp. 330–332. ISSN 0950-7671. Available from DOI: 10.1088/0950-7671/29/10/308.
- [Hof15] HOFFMANN, J. *Taschenbuch der Messtechnik*. München: Carl Hanser Verlag GmbH & Co. KG, 2015. ISBN 978-3-446-44271-9. Available from DOI: 10.3139/9783446445116.
- [Hoh19] HOHMANN, D. *Justierung von Präzisionswägezellen in Massekomparatoren*. Ilmenau: Feinwerktechnik, 2019. Bachelorthesis. Technische Universität Ilmenau.
- [HMO13] HOWELL, L. L.; MAGLEBY, S. P.; OLSEN, B. M. (eds.). *Handbook of compliant mechanisms*. Chichester: Wiley, 2013. ISBN 978-1-119-95345-6. Available from DOI: 10.1002/9781118516485.
- [JY01] JABBOUR, Z. J.; YANIV, S. L. The Kilogram and Measurements of Mass and Force. 2001.
- [JDS84] JAEGER, K. B.; DAVIS, R. S.; STANDARDS, U. S. N. B. o. *A Primer for Mass Metrology*. U.S. Department of Commerce, National Bureau of Standards, 1984. Industrial measurement series.
- [Jia+11] JIANG, Z. et al. Final report on the Seventh International Comparison of Absolute Gravimeters (ICAG 2005). *Metrologia*. 2011, vol. 48, (5), pp. 246–260. ISSN 0026-1394. Available from DOI: 10.1088/0026-1394/48/5/003.
- [Jon79] JONES, B. E. Feedback in instruments and its applications. *Journal of Physics E: Scientific Instruments*. 1979, vol. 12, (3), pp. 145–158. ISSN 0022-3735. Available from DOI: 10.1088/0022-3735/12/3/001.
- [Kec+21] KECK, L. et al. Design of an Electrostatic Balance Mechanism to Measure Optical Power of 100 kW. *IEEE Transactions on Instrumentation and Measurement*. 2021, vol. 70, pp. 1–9. ISSN 1557-9662. Available from DOI: 10.1109/TIM.2021.3060575.

-
- [KJ89] KEYSER, P. T.; JEFFERTS, S. R. Magnetic susceptibility of some materials used for apparatus construction (at 295 K). *Review of Scientific Instruments*. 1989, vol. 60, (8), pp. 2711–2714. ISSN 00346748. Available from DOI: 10.1063/1.1140646.
- [KAH16] KHELIFA, N.-E.; AVERLANT, P.; HIMBERT, M. Traceability of small force measurements and the future international system of units (SI). *International Journal of Metrology and Quality Engineering*. 2016, vol. 7, (3), p. 306. ISSN 2107-6847. Available from DOI: 10.1051/ijmqe/2016022.
- [Kib75] KIBBLE, B. P. A Modification to a Precision Balance Incorporating Substitution Weighing and Feedback Control which gives Improved Accuracy and Convenience. *Metrologia*. 1975, vol. 11, (1), pp. 1–5. ISSN 0026-1394. Available from DOI: 10.1088/0026-1394/11/1/002.
- [Kno+19] KNOPF, D. et al. A quantum of action on a scale? Dissemination of the quantum based kilogram. *Metrologia*. 2019, vol. 56, (2), p. 024003. Available from DOI: 10.1088/1681-7575/ab0851.
- [Koc89] KOCHSIEK, M. *Handbuch des Wägens*. 2., bearbeitete und erweiterte Auflage. Wiesbaden et al.: Vieweg+Teubner Verlag, 1989. ISBN 978-3-322-90574-1. Available from DOI: 10.1007/978-3-322-90573-4.
- [KG00] KOCHSIEK, M.; GLÄSER, M. *Comprehensive mass metrology*. Weinheim et al.: Wiley-VCH, 2000. ISBN 3-527-29614-X. Available from DOI: 10.1002/3527602992.
- [KM87] KOCHSIEK, M.; MEISSNER, B. *Load cells: Principles, accuracy, application for approved weighing machines*. Bremerhaven: NW-Verl., Verl. für Neue Wiss, 1987. ISBN 3883146633.
- [Koh01] KOHKONEN, K. E. Manufacturing precision and delicate parts. In: *Proceedings: Electrical Insulation Conference and Electrical Manufacturing and Coil Winding Conference (Cat. No.01CH37264)*. IEEE, 2001, pp. 115–118. ISBN 0-7803-7180-1. Available from DOI: 10.1109/EEIC.2001.965597.
- [KL93] KOHL, M. L.; LEVINE, J. Measuring Low Frequency Tilts. *Journal of research of the National Institute of Standards and Technology*. 1993, vol. 98, (2), pp. 191–202. ISSN 1044-677X. Available from DOI: 10.6028/jres.098.014.
-

- [Kos+00] KOSEKI, Y. et al. Kinematic analysis of translational 3-DOF micro parallel mechanism using matrix method. In: *Proceedings / 2000 IEEE/RSJ International Conference on Intelligent Robots and Systems (IROS 2000)*. Piscataway, NJ: IEEE Operations Center, 2000, pp. 786–792. ISBN 0-7803-6348-5. Available from DOI: 10.1109/IR0S.2000.894700.
- [Kra04a] KRAUSE, L. Vergleich von Kompensations- und Ausschlagprinzip am Beispiel der Wägetechnik (Comparison between the Principles of Compensation and Deflection Demonstrated by the Example of Weight Measurements). *tm - Technisches Messen*. 2004, vol. 71, (12-2004), pp. 643–650. ISSN 0171-8096. Available from DOI: 10.1524/teme.71.12.643.54697.
- [Kra04b] KRAUSE, W. *Konstruktionselemente der Feinmechanik*. 3., stark bearb. Aufl. München: Hanser, 2004. ISBN 3-446-22336-3.
- [Kra00] KRAUSE, W. *Gerätekonstruktion in Feinwerktechnik und Elektronik*. 3., stark bearbeitete Aufl. München et al.: Hanser, 2000. ISBN 978-3446196087.
- [Küh13] KÜHNEL, M. *Rückführbare Messung der mechanischen Eigenschaften von Federkörpern für die Kraftmesstechnik*. Ilmenau, 2013. PhD thesis. Technische Universität Ilmenau. Supervised by G. JÄGER.
- [KFF18] KÜHNEL, M.; FERN, F.; FRÖHLICH, T. Novel monolithic pendulum tiltmeter with Nanorad resolution. *tm - Technisches Messen*. 2018, vol. 85, (4), pp. 244–251. ISSN 0171-8096. Available from DOI: 10.1515/teme-2017-0097.
- [Küh+14a] KÜHNEL, M. et al. Dual axis tiltmeter with nanorad resolution based on commercial force compensation weigh cells. *Shaping the future by engineering : 58th IWK, Ilmenau Scientific Colloquium, Technische Universität Ilmenau, 8 - 12 September 2014 ; proceedings*. 2014.
- [Küh+14b] KÜHNEL, M. et al. Precise tiltmeter and inclinometer based on commercial force compensation weigh cells. *22nd IMEKO TC3 International Conference on Measurement of Force, Mass and Torque 2014*. 2014, pp. 48–51.
- [Kuh03] KUHNNEN, K. Modeling, Identification and Compensation of Complex Hysteretic Nonlinearities: A Modified Prandtl-Ishlinskii Approach.

- European Journal of Control*. 2003, vol. 9, (4), pp. 407–418. ISSN 09473580. Available from DOI: 10.3166/ejc.9.407-418.
- [KR19] KUTTNER, T.; ROHNEN, A. *Praxis der Schwingungsmessung*. Wiesbaden: Springer Fachmedien Wiesbaden, 2019. ISBN 978-3-658-25047-8. Available from DOI: 10.1007/978-3-658-25048-5.
- [Lac13] LACARBONARA, W. *Nonlinear Structural Mechanics: Theory, Dynamical Phenomena and Modeling*. Boston, MA: Springer, 2013. ISBN 978-1-4419-1275-6. Available from DOI: 10.1007/978-1-4419-1276-3.
- [LaC34] LACOSTE, L. J. B. A New Type Long Period Vertical Seismograph. *Physics*. 1934, vol. 5, (7), pp. 178–180. ISSN 0148-6349. Available from DOI: 10.1063/1.1745248.
- [LM99] LAUBSTEIN; MICHAEL. *Monolithische Wägesysteme - eine Innovation in der Wägetechnik*. 1999.
- [Lea11] LEACH, R. *Optical Measurement of Surface Topography*. Berlin, Heidelberg: Springer Berlin Heidelberg, 2011. ISBN 978-3-642-12011-4. Available from DOI: 10.1007/978-3-642-12012-1.
- [LS18] LEACH, R.; SMITH, S. T. *Basics of Precision Engineering*. Milton: Taylor and Francis, 2018. ISBN 978-1-4987-6085-0.
- [Li+19] LI, L. et al. Design, modeling, and analysis of hybrid flexure hinges. *Mechanism and Machine Theory*. 2019, vol. 131, pp. 300–316. ISSN 0094114X. Available from DOI: 10.1016/j.mechmachtheory.2018.10.005.
- [LBL18] LINDNER, H.; BRAUER, H.; LEHMANN, C. *Taschenbuch der Elektrotechnik und Elektronik: Mit 631 Bildern und 99 Tabellen*. 10., aktualisierte Auflage. München: Fachbuchverlag Leipzig im Carl Hanser Verlag, 2018. ISBN 978-3-446-44497-3.
- [Lin+20] LING, M. et al. Kinetostatic and Dynamic Modeling of Flexure-Based Compliant Mechanisms: A Survey. *Applied Mechanics Reviews*. 2020, vol. 72, (3), p. 1. ISSN 0003-6900. Available from DOI: 10.1115/1.4045679.
- [Lin15] LINSS, S. *Ein Beitrag zur geometrischen Gestaltung und Optimierung prismatischer Festkörpergelenke in nachgiebigen Koppelmechanismen*. Ilmenau, 2015. ISBN 978-3-86360-122-5. PhD thesis. Technische Universität Ilmenau.

- [LEZ11] LINSS, S.; ERBE, T.; ZENTNER, L. *Design and simplified manufacturing of large-deflective flexure hinges based on polynomial contours*. Ilmenau: Universitätsbibliothek Ilmenau, 2011. International scientific colloquium / Ilmenau University of Technology.
- [LSZ17] LINSS, S.; SCHORR, P.; ZENTNER, L. General design equations for the rotational stiffness, maximal angular deflection and rotational precision of various notch flexure hinges. *Mechanical Sciences*. 2017, vol. 8, (1), pp. 29–49. ISSN 2191-916X. Available from DOI: 10.5194/ms-8-29-2017.
- [LZF16] LIU, M.; ZHANG, X.; FATIKOW, S. Design and analysis of a high-accuracy flexure hinge. *The Review of scientific instruments*. 2016, vol. 87, (5), p. 055106. ISSN 0034-6748. Available from DOI: 10.1063/1.4948924.
- [LRM90] LIU, S.; RAY, A. E.; MILDRUM, H. F. Temperature-compensated 2:17-type permanent magnets with improved magnetic properties. *Journal of Applied Physics*. 1990, vol. 67, (9), pp. 4975–4977. ISSN 0021-8979. Available from DOI: 10.1063/1.344721.
- [MPS16] MAGNUS, K.; POPP, K.; SEXTRO, W. *Schwingungen: Grundlagen - Modelle - Beispiele*. 10., überarbeitete Auflage. Wiesbaden: Springer Vieweg, 2016. ISBN 9783658138219. Available from DOI: 10.1007/978-3-658-13821-9.
- [Mah15] MAHNKEN, R. *Lehrbuch der Technischen Mechanik - Elastostatik*. Berlin, Heidelberg: Springer Berlin Heidelberg, 2015. ISBN 978-3-662-44797-0. Available from DOI: 10.1007/978-3-662-44798-7.
- [Mar19] MARANGONI, R. R. *Traceable multicomponent force and torque measurement*. Ilmenau, 2019. PhD thesis. Technische Universität Ilmenau. Supervised by G. JÄGER.
- [Mar+17] MARANGONI, R. R. et al. Analysis of weighing cells based on the principle of electromagnetic force compensation. *Measurement Science and Technology*. 2017, vol. 28, (7), p. 075101. ISSN 0957-0233. Available from DOI: 10.1088/1361-6501/aa6bcd.
- [Mar+18] MARANGONI, R. R. et al. A self-calibrating multicomponent force / torque measuring system. *Measurement Science and Technology*. 2018, vol. 29, (7), p. 074002. Available from DOI: 10.1088/1361-6501/aac00f.

- [Mar12] MARSON, I. A Short Walk along the Gravimeters Path. *International Journal of Geophysics*. 2012, vol. 2012, (1), pp. 1–9. Available from DOI: 10.1155/2012/687813.
- [MFR12] MARTI, K.; FUCHS, P.; RUSSI, S. Cleaning of mass standards: a comparison of new and old techniques. *Metrologia*. 2012, vol. 49, (6), pp. 628–634. ISSN 0026-1394. Available from DOI: 10.1088/0026-1394/49/6/628.
- [Mas+86] MASSEN, C. H. et al. Disturbances in weighing - part II. *Thermochimica Acta*. 1986, vol. 103, (1), pp. 39–44. ISSN 00406031. Available from DOI: 10.1016/0040-6031(86)80009-0.
- [Mat20] MATLAB. *PDF Documentation revised for Version 9.8 (R2020a)*. Ed. by THE MATHWORKS INC. Natick, Massachusetts: The MathWorks Inc, 2020.
- [Mer+07] MERKEN, P. et al. *Mechanical based circular notch hinge design*. 2007.
- [Met18] METTLER TOLEDO. *Comparator Balances*. 2018.
- [Met96] METZING, U. *Elektronische Ecklastfehler-Kompensation*. 1. Aufl. Göttingen: Cuvillier, 1996. ISBN 3895884413.
- [MUF04] MIZUSHIMA, S.; UEKI, M.; FUJII, K. Mass measurement of 1 kg silicon spheres to establish a density standard. *Metrologia*. 2004, vol. 41, (2), S68–S74. Available from DOI: 10.1088/0026-1394/41/2/S07.
- [MH10] MORSCH, F. M.; HERDER, J. L. Design of a Generic Zero Stiffness Compliant Joint. In: *ASME 2010 International Design Engineering Technical Conferences and Computers and Information in Engineering Conference*. 2010, pp. 427–435. Available from DOI: 10.1115/DETC2010-28351.
- [MWR08] MÜLLER, M.; WOLF, M.; RÖSSLEIN, M. MUSE: Computational aspects of a GUM supplement 1 implementation. *Metrologia*. 2008, vol. 45, (5), pp. 586–594. Available from DOI: 10.1088/0026-1394/45/5/013.
- [Nat+08] NATER, R. et al. *Wägellexikon: Leitfaden wägetechnischer Begriffe*. Berlin, Heidelberg: Springer-Verlag, 2008. ISBN 978-3-54-075908-9. Available from DOI: 10.1007/978-3-540-75908-9.

- [Nea13] NEALE, M. J. *Bearings: A Tribology Handbook*. Burlington: Elsevier Science, 2013. ISBN 9781560913931.
- [Nes+09] NESTEROV, V. et al. A new facility to realize a nanonewton force standard based on electrostatic methods. *Metrologia*. 2009, vol. 46, (3), pp. 277–282. ISSN 0026-1394. Available from DOI: 10.1088/0026-1394/46/3/016.
- [Nor08] NORDEN, K. E. *Handbook of Electronic Weighing*. Hoboken: Wiley-VCH, 2008. ISBN 9783527295685.
- [Now14] NOWICK, A. *Anelastic Relaxation In Crystalline Solids*. Saint Louis: Elsevier Science, 2014. ISBN 9780323143318.
- [Pab+21] PABST, M. et al. A3.1 Adjustment Concept for Compensating Stiffness and Tilt Sensitivity of a Novel Monolithic EMFC Weighing Cell. In: *SMSI 2021 - Sensors and Instrumentation*. AMA Service GmbH, Von-Münchhausen-Str. 49, 31515 Wunstorf, Germany, 2021, pp. 53–54. Available from DOI: 10.5162/SMSI2021/A3.1.
- [Pab+19] PABST, M. et al. Measuring and adjusting the stiffness and tilt sensitivity of a novel 2D monolithic high precision electromagnetic force compensated weighing cell: NCSL International Workshop & Symposium | Metrology in Motion August 24-29, 2019 | Cleveland, Ohio. In: 2019.
- [Pab+22] PABST, M. et al. Adjustment concept for compensating for stiffness and tilt sensitivity of a novel monolithic electromagnetic force compensation (EMFC) weighing cell. *Journal of Sensors and Sensor Systems*. 2022, vol. 11, (1), pp. 109–116. ISSN 2194-878X. Available from DOI: 10.5194/jsss-11-109-2022.
- [PW65] PAROS, J. M.; WEISBORD, L. How to design flexure hinges. *Machine design*. 1965, pp. 151–156.
- [PD98] PEATTIE, G.; DAVIDSON, S. *Design and Assessment of an Automatic 50 kg Weight Exchanger: NPL Report CMAM 23*. 1998.
- [Pet90] PETERS, R. D. Mechanically adjustable balance and sensitive tilt meter. *Measurement Science and Technology*. 1990, vol. 1, (11), pp. 1131–1135. Available from DOI: 10.1088/0957-0233/1/11/001.

- [Pfe96] PFEIFFER, A. *Integrierter Kappa -Regler-Filterentwurf für elektromechanische Präzisionswaagen: Zugl.: München, Techn. Univ., Diss., 1996.* Als Ms. gedr. Düsseldorf: VDI-Verl., 1996. Fortschritt-Berichte VDI Reihe 8, Meß-, Steuerungs- und Regelungstechnik. ISBN 3183573083.
- [Pic04] PICARD, A. The BIPM flexure-strip balance FB-2. *Metrologia*. 2004, vol. 41, (4), p. 319.
- [PF04] PICARD, A.; FANG, H. Methods to determine water vapour sorption on mass standards. *Metrologia*. 2004, vol. 41, (4), pp. 333–339. ISSN 0026-1394. Available from DOI: 10.1088/0026-1394/41/4/016.
- [Pic+08] PICARD, A. et al. Revised formula for the density of moist air (CIPM-2007). *Metrologia*. 2008, vol. 45, (2), pp. 149–155. ISSN 0026-1394. Available from DOI: 10.1088/0026-1394/45/2/004.
- [Pin+16] PINOT, P. et al. Static phase improvements in the LNE watt balance. *The Review of scientific instruments*. 2016, vol. 87, (10), p. 105113. ISSN 0034-6748. Available from DOI: 10.1063/1.4964293.
- [Pin+07] PINOT, P. et al. Theoretical analysis for the design of the French watt balance experiment force comparator. *Review of Scientific Instruments*. 2007, vol. 78, (9), p. 095108. ISSN 00346748.
- [Pom19] POMIANO PICON, V. A. *Adjustment of the relative position of compliant joints within a monolithic mechanism*. Ilmenau, 2019. MA thesis. Technische Universität Ilmenau, Precision Engineering Group. Supervised by R. THESKA.
- [Pro95] PROWSE, D. B. *The calibration of balances*. Melbourne: CSIRO, 1995. ISBN 0643038299.
- [Puf+13] PUFKE, M. et al. *Precision and low cost position detection using capacitive sensor technology*. Ilmenau: Univ.-Bibliothek et al., 2013.
- [Qui92] QUINN, T. J. The beam balance as an instrument for very precise weighing. *Measurement Science and Technology*. 1992, vol. 3, (2), pp. 141–159. Available from DOI: 10.1088/0957-0233/3/2/001.
- [QSD86] QUINN, T. J.; SPEAKE, C. C.; DAVIS, R. S. A 1 kg Mass Comparator Using Flexure-Strip Suspensions: Preliminary Results. *Metrologia*. 1986, vol. 23, (2), p. 87. Available from DOI: 10.1088/0026-1394/23/2/002.

- [RFD16] RICHARD, P.; FANG, H.; DAVIS, R. S. Foundation for the redefinition of the kilogram. *Metrologia*. 2016, vol. 53, (5), A6–A11. Available from DOI: 10.1088/0026-1394/53/5/A6.
- [RKF14] RIVERO, M.; KÜHNEL, M.; FRÖHLICH, T. High precision dual axis tilt stage. *Shaping the future by engineering : 58th IWK, Ilmenau Scientific Colloquium, Technische Universität Ilmenau, 8 - 12 September 2014 ; proceedings*. 2014.
- [RJK14] ROBENS, E.; JAYAWEERA, S. A. A.; KIEFER, S. *Balances*. Berlin, Heidelberg: Springer Berlin Heidelberg, 2014. ISBN 978-3-642-36446-4. Available from DOI: 10.1007/978-3-642-36447-1.
- [RLF15] RÖSNER, M.; LAMMERING, R.; FRIEDRICH, R. Dynamic modeling and model order reduction of compliant mechanisms. *Precision Engineering*. 2015, vol. 42, pp. 85–92. ISSN 01416359. Available from DOI: 10.1016/j.precisioneng.2015.04.003.
- [Rot+18] ROTHLEITNER, C. et al. The Planck-Balance—using a fixed value of the Planck constant to calibrate E1/E2-weights. *Measurement Science and Technology*. 2018, vol. 29, (7), p. 074003. ISSN 0957-0233. Available from DOI: 10.1088/1361-6501/aabc9e.
- [RS17] ROTHLEITNER, C.; SCHLAMMINGER, S. Invited Review Article: Measurements of the Newtonian constant of gravitation, G. *Review of Scientific Instruments*. 2017, vol. 88, (11), p. 111101. ISSN 0034-6748. Available from DOI: 10.1063/1.4994619.
- [Sar14] SARTORIUS. *Mass Metrology - Professional Equipment for Absolute Precision*. 2014.
- [Sas+19] SASIUK, T. et al. Generation of a static torque in the range of 1 mNm to 1 Nm according to the Jokey-weight principle. *Messunsicherheit - Prüfprozesse 2019*. 2019, pp. 111–120.
- [Sau90] SAULSON, P. R. Thermal noise in mechanical experiments. *Physical Review D*. 1990, vol. 42, (8), pp. 2437–2445. ISSN 0556-2821. Available from DOI: 10.1103/PhysRevD.42.2437.
- [Sch12] SCHOONOVER, R. M. A Look at the Electronic Analytical Balance. *Analytical Chemistry*. 2012, vol. 54, (8), 973A–980A. ISSN 0003-2700. Available from DOI: 10.1021/ac00245a785.

-
- [Sch+15] SCHREIBER, M. et al. Quantification of free convection effects on 1 kg mass standards. *Metrologia*. 2015, vol. 52, (6), p. 835.
- [SB70] SCHÜLER, K.; BRINKMANN, K. *Dauermagnete*. Berlin, Heidelberg: Springer Berlin Heidelberg, 1970. ISBN 978-3-642-93003-4. Available from DOI: 10.1007/978-3-642-93002-7.
- [SGR12] SCHULZ, V.; GERLACH, G.; RÖBENACK, K. Compensation method in sensor technology: A system-based description. *Journal of Sensors and Sensor Systems*. 2012, vol. 1, (1), pp. 5–27. ISSN 2194-878X. Available from DOI: 10.5194/jsss-1-5-2012.
- [Sch83] SCHUSTER, A. *Industrielle Wägetechnik : ein Beitrag zum Stand der Technik nach 100 Jahren Waagenbau im Hause Schenck*. Darmstadt: Schenck, 1983.
- [Sch94] SCHWARTZ, R. Precision Determination of Adsorption Layers on Stainless Steel Mass Standards by Mass Comparison and Ellipsometry: Part II: Sorption Phenomena in Vacuum. *Metrologia*. 1994, vol. 31, (2), pp. 129–136. ISSN 0026-1394. Available from DOI: 10.1088/0026-1394/31/2/005.
- [SBS07] SCHWARTZ, R.; BORYS, M.; SCHOLZ, F. *Guide to mass determination with high accuracy*. Bremerhaven: Wirtschaftsverl. NW Verl. für neue Wissenschaft, 2007. PTB-Bericht MA, Mechanik und Akustik, no. PTB-MA-80e. ISBN 9783865096692.
- [Sha18] SHAW, G. A. Current state of the art in small mass and force metrology within the International System of Units. *Measurement Science and Technology*. 2018, vol. 29, (7), p. 072001. ISSN 0957-0233. Available from DOI: 10.1088/1361-6501/aaac51.
- [Sho+97] SHOEMAKER, G. H. N. et al. A 10 kg transportable flexure-strip beam balance. *Review of Scientific Instruments*. 1997, vol. 68, (10), pp. 3777–3784. ISSN 00346748. Available from DOI: 10.1063/1.1148026.
- [SC92] SMITH, S. T.; CHETWYND, D. G. *Foundations of ultraprecision mechanism design*. Yverdon, Switzerland: Gordon and Breach Science Publishers, 1992. Developments in nanotechnology. ISBN 2-88449-001-9.
- [Spe87] SPEAKE, C. C. Fundamental Limits to Mass Comparison by Means of a Beam Balance. *Proceedings of the Royal Society A: Mathematical,*
-

- Physical and Engineering Sciences*. 1987, vol. 414, (1847), pp. 333–358. ISSN 1364-5021. Available from DOI: 10.1098/rspa.1987.0147.
- [Ște11] ȘTEFĂNESCU, D. M. *Handbook of Force Transducers*. Berlin, Heidelberg: Springer Berlin Heidelberg, 2011. ISBN 978-3-642-18295-2. Available from DOI: 10.1007/978-3-642-18296-9.
- [Sun+08] SUNDERLAND, A. et al. Reducing the magnetic susceptibility of parts in a magnetic gradiometer. 2008.
- [SC94] SUTTON, C. M.; CLARKSON, M. T. A General Approach to Comparisons in the Presence of Drift. *Metrologia*. 1994, vol. 30, (5), pp. 487–493. Available from DOI: 10.1088/0026-1394/30/5/004.
- [SS10] SWANSON, H. E.; SCHLAMMINGER, S. Removal of zero-point drift from AB data and the statistical cost. *Measurement Science and Technology*. 2010, vol. 21, (11), p. 115104. ISSN 0957-0233. Available from DOI: 10.1088/0957-0233/21/11/115104.
- [Tak+11] TAKAMORI, A. et al. Novel compact tiltmeter for ocean bottom and other frontier observations. *Measurement Science and Technology*. 2011, vol. 22, (11), p. 115901. ISSN 0957-0233. Available from DOI: 10.1088/0957-0233/22/11/115901.
- [TBP19] THANGAPANDIAN, N.; BALASIVANANDHA PRABU, S.; PADMANABHAN, K. A. Effect of Temperature on Grain Size in AA6063 Aluminum Alloy Subjected to Repetitive Corrugation and Straightening. *Acta Metallurgica Sinica (English Letters)*. 2019, vol. 32, (7), pp. 835–844. ISSN 1006-7191. Available from DOI: 10.1007/s40195-018-0866-6.
- [The+18] THESKA, R. et al. State of the art precision motion systems based on compliant mechanisms. *The 4th International Conference Mechanical Engineering in XXI Century : Niš, April 19-20, 2018 : proceedings*. 2018, pp. 3–8.
- [Tor+18] TORRES MELGAREJO, M. et al. On Modeling the Bending Stiffness of Thin Semi-Circular Flexure Hinges for Precision Applications. *Actuators*. 2018, vol. 7, (4), p. 86. ISSN 2076-0825. Available from DOI: 10.3390/act7040086.
- [Tor18] TORRES MELGAREJO, M. A. *Modeling of the elastic mechanical behavior of thin compliant joints under load for highest-precision ap-*

- plications*. Ilmenau, 2018. MA thesis. Technische Universität Ilmenau, Precision Engineering Group. Supervised by R. THESKA.
- [Trä14] TRÄNKLER, H.-R. (ed.). *Sensortechnik: Handbuch für Praxis und Wissenschaft*. 2., völlig neu bearb. Aufl. Berlin: Springer Vieweg, 2014. Technik. ISBN 978-3-642-29942-1.
- [TO98] TRÄNKLER, H.-R.; OBERMEIER, E. *Sensortechnik*. Berlin, Heidelberg: Springer Berlin Heidelberg, 1998. ISBN 978-3-662-09867-7. Available from DOI: 10.1007/978-3-662-09866-0.
- [Vac02] VACUUMSCHMELZE. Weichmagnetische Werkstoffe und Halbzeuge. 2002.
- [Val17] VALCU, A. Between parallel mirrors — An electronic weighing instrument. In: *2017 - 10th International Symposium on Advanced Topics in Electrical Engineering (ATEE)*. Piscataway, NJ: IEEE, 2017, pp. 136–140. ISBN 978-1-4799-7514-3. Available from DOI: 10.1109/ATEE.2015.7133754.
- [Wal55] WALDERSEE, J. The effect of the finite radii of the knife edges on the performance of an equi-arm balance. *Australian J. App.* 1955, pp. 158–166.
- [Wan+15] WANG, J. et al. Uncertainty Evaluation for a System of Weighing Equations for the Determination of Microgram Weights. *IEEE Transactions on Instrumentation and Measurement*. 2015, vol. 64, (8), pp. 2272–2279. ISSN 0018-9456. Available from DOI: 10.1109/TIM.2015.2393396.
- [Wed+21] WEDRICH, K. et al. Conceptual Design of a Microscale Balance Based on Force Compensation. In: ZENTNER, L.; STREHLE, S. (eds.). *Microactuators, Microsensors and Micromechanisms*. Cham: Springer International Publishing, 2021, vol. 96, pp. 103–114. Mechanisms and Machine Science. ISBN 978-3-030-61651-9. Available from DOI: 10.1007/978-3-030-61652-6_9.
- [WA08] WEIS, H. S.; AUGUSTIN, S. Simulation of Thermal Behavior in High-Precision Measurement Instruments. *International Journal of Thermophysics*. 2008, vol. 29, (3), pp. 1184–1192. Available from DOI: 10.1007/s10765-007-0365-x.
- [Wei19] WEISSGERBER, M. *Bestimmung der spezifischen, oberflächenbedingten Scanning - Antastabweichung für taktile 3D - Koordinatenmess-*

- geräte. Chemnitz, 2019. PhD thesis. Technischen Universität Chemnitz. Supervised by S. GRÖGER.
- [Wen92] WENTE, H. *Ein Beitrag zur intelligenten Dämpfung schwingungsfähiger elastischer Systeme unter besonderer Berücksichtigung elektromechanischer Waagen*. Braunschweig, 1992. PhD thesis. Technischen Universität Carolo-Wilhelmina. Supervised by K. HORN.
- [Wie10] WIELAND, E. *Seismic Sensors and their Calibration*. 2010.
- [Wie75] WIELANDT, E. *Ein astasiertes Vertikalpendel mit tragender Blattfeder*. 1975.
- [Wit+22] WITTKKE, M. et al. Investigations on a torque-compensating adjustment drive for mechanically sensitive devices. *Proceedings of the 22nd International Conference of the European Society for Precision Engineering and Nanotechnology*. 2022, pp. 81–82.
- [Wit48] WITTRICK, W. H. *The theory of symmetrical crossed flexure pivots*. 1948.
- [Xia+97] XIAOWEI, L. et al. A combined electrical machining process for the production of a flexure hinge. *Journal of Materials Processing Technology*. 1997, vol. 71, (3), pp. 373–376. ISSN 09240136. Available from DOI: 10.1016/S0924-0136(97)00100-3.
- [Xu21] XU, Y. Finite Element Modell zur Simulation des statischen und dynamischen mechanischen Verhaltens von Präzisionswägezellen. 2021.
- [YL09] YONG, Y. K.; LU, T.-F. Comparison of circular flexure hinge design equations and the derivation of empirical stiffness formulations. *Advanced Intelligent Mechatronics, 2009. AIM 2009. IEEE/ASME International Conference on*. 2009, pp. 510–515. ISSN 2159-6255. Available from DOI: 10.1109/AIM.2009.5229961.
- [Zen14] ZENTNER, L. *Nachgiebige Mechanismen*. München: De Gruyter, 2014. ISBN 978-3-486-85890-7. Available from DOI: 10.1524/9783486858907.
- [ZSZ05a] ZETTL, B.; SZYSZKOWSKI, W.; ZHANG, W. J. Accurate low DOF modeling of a planar compliant mechanism with flexure hinges: the equivalent beam methodology. *Precision Engineering*. 2005, vol. 29, (2), pp. 237–245. ISSN 01416359. Available from DOI: 10.1016/j.precisioneng.2004.09.001.

- [ZSZ05b] ZETTL, B.; SZYSZKOWSKI, W.; ZHANG, W. J. On Systematic Errors of Two-Dimensional Finite Element Modeling of Right Circular Planar Flexure Hinges. *Journal of Mechanical Design*. 2005, vol. 127, (4), p. 782. ISSN 10500472. Available from DOI: 10.1115/1.1898341.

Patents

- [DE 19741584 C1] BAJOHR, U. *Weighing system with first parallel guide consisting of top and bottom rods*. DE 19741584 C1. 1998.
- [EP 2615433 B1] BEGUIN, C. et al. *Device and method for adjusting the corner load error of a parallel guide*. EP 2615433 B1. 2013.
- [CH 698191 B1] BIERICH, E.; BOETCHER, G.; LAUBSTEIN, M. *Wäge-aufnehmer mit Parallelführung und Ecklaststellhebel*. CH 698191 B1. 2009.
- [EP 1409971 B1] BIERICH, E.; MARTENS, J. P.; MAAZ, G. *Weigh sensor with parallel guide and corner load regulation*. EP 1409971 B1. 2005.
- [WO 2008145427 A1] BURKHARD, H. R. et al. *Adjustable parallel guide for compact gravimetric measuring instruments*. WO 2008145427 A1. 2010.
- [DE 102008062742 B4] COVIC, H.; DOERNER, J.; ERBEN, D. *Oberschalige Waage*. DE 102008062742 B4. 2013.
- [EP 000004119908 A1] DARNIEDER, M.; HILBRUNNER, F. *Electromagnetic Compensating Beam Scale*. EP 000004119908 A1. 2023.
- [DE 102021118060 A1] DARNIEDER, M.; HILBRUNNER, F. *Elektromagnetisch kompensierende Balkenwaage*. DE10 2021 118 060 A1. 2023.
- [DE 102021132093 B3] DARNIEDER, M. et al. *Wägevorrichtung und Verfahren zu deren Betrieb*. DE 102021132093 B3. 2023.
- [DE 102009015029 B4] DOERNER, J.; GROESCHE, D.; SCHRADER, C. *Electronic weighing scales has optical sensors, at the corners, to register if the load is off-center on the weighing tray*. DE 102009015029 B4. 2013.

- [DE 19502694 C1] EGER, M. et al. *Elektronische Waage mit Ecklastsensor*. DE 19502694 C1. 1996.
- [WO 2010054743 A1] EGER, M. et al. *Oberschalige elektronische Waage mit Ecklastsensormesssystem*. WO 2010054743 A1. 2010.
- [DE 102016106695 B4] FRÖHLICH, T. et al. *Elektromagnetisch kompensierende Balkenwaage, Verfahren zu deren Kalibrierung und Verfahren zur Bestimmung eines Testgewichts*. DE 102016106695 B4. 2018.
- [DE 4103619 C1] KUHLMANN, O. *Self-centering weighing pan for overhead pan balance - has flexural springs connecting intermediate element to base and loading part of pan*. DE 4103619 C1. 1992.
- [EP 2041531 B1] MUELLER, M.; SCHULZE, W.; MÜLLER, M. *Top-pan scales with corner load sensor*. EP 2041531 B1. 2015.
- [EP 0393323 A1] NEGRI, E. *Mass transducer with electromagnetic compensation*. EP 0393323 A1. 1990.
- [DE 9010327 U1] SARTORIUS AG. *Oberschalige elektronische Waage*. DE 9010327 U1. 1990.
- [DE 9404206 U1] SARTORIUS AG. *Oberschalige Waage mit Lenkerparallelführung*. DE 9404206 U1. 1994.

Standards / Guidelines

- [DIN 4760:1982-06] Gestaltabweichungen: Begriffe; Ordnungssystem, 1982.
- [DIN 32567-3:2014-10] Fertigungsmittel für Mikrosysteme – Ermittlung von Materialeinflüssen auf die optische und taktile dimensionelle Messtechnik – Teil 3: Ableitung von Korrekturwerten für taktile Messgeräte. Berlin: Beuth, 2014-10.
- [DKD-R 4-3 Blatt 18.1] Kalibrieren von Messmitteln für geometrische Messgrößen, Kalibrieren der messtechnischen Eigenschaften von Koordinatenmessgeräten (KMG) nach

- DIN EN ISO 10360 und VDI/VDE 2617 : Richtlinie DKD-R 4-3 Blatt 18.1: Physikalisch-Technische Bundesanstalt (PTB), 2018.
- [DIN EN ISO 10360-1:2003-07] Annahmeprüfung und Bestätigungsprüfung für Koordinatenmessgeräte (KMG): Teil 1: Begriffe, 2003.
- [JCGM 100:2008] Evaluation of measurement data - Guide to the expression of uncertainty in measurement: JCGM 100:2008: GUM 1995 with minor corrections, 2008.
- [JCG08] Evaluation of measurement data - Supplement 1 to the GUM, 2008.
- [JCGM 101:2008] Evaluation of measurement data - Supplement 1 to the GUM, 2008.
- [OIML R 111-1:2004] Weights of classes E1, E2, F1, F2, M1, M1-2, M2, M2-3 and M3 Part 1: Metrological and technical requirements, 2004.
- [OIML R 76-1:2006] Non-automatic weighing instruments Part 1: Metrological and technical requirements - Tests, 2006.
- [VDI 2221-1:2018-03] Entwicklung technischer Produkte und Systeme Modell der Produktentwicklung, 2018-03.

Liste der bisher erschienenen Bände, Stand 12.03.2024

Berichte aus dem Institut für Maschinenelemente und Konstruktion (IMK), 1990 – 2010

- Band 1 Institut für Maschinenelemente und Konstruktion der TU Ilmenau (Hrsg.):
Forschung und Lehre im Institut für Maschinenelemente und Konstruktion
(Institutsbericht). ISLE, Ilmenau 1999. ISBN 3-932633-37-7.
- Band 2 Spiller, Frank:
Möglichkeiten der rechentechnischen Umsetzung von Erkenntnissen aus der
Konstruktionssystematik unter Nutzung der Featuretechnologie (Dissertation
TU Ilmenau 1998). ISLE, Ilmenau 1998. ISBN 3-932633-20-2.
- Band 3 Leibl, Peter:
Entwicklung eines featureorientierten Hilfsmittels für die Konstruktion
kostengünstiger Produkte (Dissertation TU Ilmenau 1998). ISLE, Ilmenau
1998. ISBN 3-00-003695-4.
- Band 4 Lutz, Steffen:
Kennlinie und Eigenfrequenzen von Schraubenfedern (Dissertation TU
Ilmenau 2000). ISLE, Ilmenau 2000. ISBN 3-932633-47-4.
- Band 5 Kletzin, Ulf
Finite-Elemente-basiertes Entwurfssystem für Federn und
Federanforderungen (Dissertation TU Ilmenau 2000). ISLE, Ilmenau 2000.
ISBN 3-932633-48-2.
- Band 6 Volz, Andreas K.:
Systemorientierter Karosserie-Konzeptentwurf am Beispiel der
Crashsimulation (Dissertation TU Ilmenau 1998). ISLE, Ilmenau 2000.
ISBN 3-932633-52-0.
- Band 7 Brix, Torsten:
Feature- und constraint-basierter Entwurf technischer Prinzipie (Dissertation
TU Ilmenau 2001). ISLE, Ilmenau 2001. ISBN 3-932633-67-9.
- Band 8 Rektor der TU Ilmenau und Institut für Maschinenelemente und Konstruktion
der TU Ilmenau (Hrsg.) in Zusammenarbeit mit Carl Zeiss Jena GmbH: .
Vom Arbeitsblatt zum virtuellen Prototyp – 50 Jahre Konstruktionssystematik
(Institutsbericht). ISLE, Ilmenau 2002. ISBN 3-932633-68-7.
- Band 9 Liebermann, Kersten:
Rechnergestütztes Entwurfs- und Optimierungssystem für
Schraubendruckfedern (Dissertation TU Ilmenau 2003). ISLE, Ilmenau 2003.
ISBN 3-932633-74-1.
- Band 10 Meissner, Manfred; Denecke, Klaus:
Die Geschichte der Maschinenelemente als Fachgebiet und Institut an der
Technischen Universität Ilmenau von 1953 bis 2003 (Institutsbericht). ISLE,
Ilmenau 2003. ISBN 3-932633-82-2.
- Band 11 Geinitz, Veronika:
Genauigkeits- und auslastungsoptimierte Schraubendruckfedern
(Dissertation TU Ilmenau 2006). ISLE, Ilmenau 2006. ISBN 3-938843-11-X.
- Band 12 Institut für Maschinenelemente und Konstruktion (Hrsg.):
Festschrift zum Ehrenkolloquium anlässlich der Emeritierungen von Univ.-
Prof.Dr.-Ing. habil. Dr. h.c. Günter Höhne und Univ.-Prof. Dr.-Ing. habil.
Hans-Jürgen Schorcht (Institutsbericht). ISLE, Ilmenau 2005.
ISBN 3-932633-97-0.

- Band 13 Wittkopp, Tobias:
Mehrkörpersimulation von Schraubendruckfedern (Dissertation TU Ilmenau 2005). ISLE, Ilmenau 2005. ISBN 3-938843-07-1.
- Band 14 Frank, Stefan:
Justierdrehen – eine Technologie für Hochleistungsoptik (Dissertation TU Ilmenau 2007). ISLE, Ilmenau 2008. ISBN 978-3-938843-35-4.
- Band 15 Schilling, Thomas:
Augmented Reality in der Produktentstehung (Dissertation TU Ilmenau 2008). ISLE, Ilmenau 2008. ISBN 978-3-938843-42-0.
- Band 16 Lotz, Markus:
Konstruktion von Messspiegeln hochgenauer Mess- und Positioniermaschinen (Dissertation TU Ilmenau 2009). ISLE, Ilmenau 2009. ISBN 978-3-938843-46-8.
- Band 17 Hackel, Tobias:
Grundlegende Untersuchungen zu vertikalen Positioniersystemen für Nanopräzisionsmaschinen (Dissertation TU Ilmenau 2010). Monsenstein & Vannerdat, Münster 2010. ISBN 978-3-86991-111-3.
- Band 18 Frank, Thomas:
Konzeption und konstruktive Gestaltung der Messkreise von Nanomessmaschinen (Dissertation TU Ilmenau 2010). Monsenstein & Vannerdat, Münster 2010. ISBN 978-3-86991-194-6.

Berichte aus dem Institut für Maschinen- und Gerätekonstruktion (IMGK), 2010 – ...

- Band 19 Sondermann, Mario:
Mechanische Verbindungen zum Aufbau optischer Hochleistungssysteme (Dissertation TU Ilmenau 2010). Universitätsverlag, Ilmenau 2011. ISBN 978-3-939473-94-7. URN urn:nbn:de:gbv:ilm1-2010000489.
- Band 20 Husung, Stephan:
Simulation akustischer Produkteigenschaften unter Nutzung von Virtual Reality während der Produktentwicklung (Dissertation TU Ilmenau 2011). Universitätsverlag, Ilmenau 2012. ISBN 978-3-86360-026-6. URN urn:nbn:de:gbv:ilm1-2011000510.
- Band 21 Dobermann, Dirk:
Stabilisierung der Bildlage abbildender optischer Systeme (Dissertation TU Ilmenau 2012). Universitätsverlag, Ilmenau 2013. ISBN 978-3-86360-056-3. URN urn:nbn:de:gbv:ilm1-2012000409.
- Band 22 Taubmann, Peter:
Analyse der Ventildfederbewegung als Beitrag zur Beeinflussung der Verschleißursachen an den Auflageflächen (Dissertation TU Ilmenau 2013). Universitätsverlag, Ilmenau 2013. ISBN 978-3-86360-059-4. URN urn:nbn:de:gbv:ilm1-2013000043.
- Band 23 Erbe, Torsten:
Beitrag zur systematischen Aktor- und Aktorprinzipauswahl im Entwicklungsprozess (Dissertation TU Ilmenau 2013). Universitätsverlag, Ilmenau 2013. ISBN 978-3-86360-060-0. URN urn:nbn:de:gbv:ilm1-2013000129.

- Band 24 Ginani, Luciano Selva:
Optical Scanning Sensor System with Submicron Resolution (Dissertation TU Ilmenau 2013). Universitätsverlag, Ilmenau 2013. ISBN 978-3-86360-068-6.
URN urn:nbn:de:gbv:ilm1-2013000337.
- Band 25 Heidler, Nils:
Untersuchungen zylindrischer Gasführungselemente für Hochvakuumanwendungen (Dissertation TU Ilmenau 2015).
Universitätsverlag, Ilmenau 2016. ISBN 978-3-86360-130-0.
URN urn:nbn:de:gbv:ilm1-2015000598.
- Band 26 Reich, René:
Möglichkeiten und Grenzen bei der Auslegung von Schraubendruckfedern auf Basis von Umlaufbiegeprüfungen (Dissertation TU Ilmenau 2016).
Universitätsverlag, Ilmenau 2016. ISBN 978-3-86360-139-3.
URN urn:nbn:de:gbv:ilm1-2016000247.
- Band 27 Resch, Jens:
Kontextorientierte Entwicklung und Absicherung von festen Verbindungen im Produktentstehungsprozess der Automobilindustrie (Dissertation TU Ilmenau 2016). Universitätsverlag, Ilmenau 2016. ISBN 978-3-86360-143-0.
URN urn:nbn:de:gbv:ilm1-2016000373.
- Band 28 Scheibe, Hannes:
Aktiv-adaptive Polierwerkzeuge zur Herstellung rotationssymmetrischer Asphären (Dissertation TU Ilmenau 2016). Universitätsverlag, Ilmenau 2017.
ISBN 978-3-86360-147-8. URN urn:nbn:de:gbv:ilm1-2016000551.
- Band 29 Reeßing, Michael:
Softwarewerkzeuge für den phasen- und domänenübergreifenden Entwurf (Dissertation TU Ilmenau 2016). Universitätsverlag, Ilmenau 2017.
ISBN 978-3-86360-169-0. URN urn:nbn:de:gbv:ilm1-2016000892.
- Band 30 Lux, Rüdiger:
Wärmebehandlung von SiCr-legiertem, ölschlussvergütetem Federstahldraht (Dissertation TU Ilmenau 2018). Universitätsverlag, Ilmenau 2018.
ISBN 978-3-86360-185-0. URN urn:nbn:de:gbv:ilm1-2018000210.
- Band 31 Thomisch, Marco:
Methodik zur Bestimmung optimaler Parameter beim Drahtumformen (Dissertation TU Ilmenau 2018). Universitätsverlag, Ilmenau 2018.
ISBN 978-3-86360-187-4. URN urn:nbn:de:gbv:ilm1-2018000300.
- Band 32 Wohlfahrt, Fabian:
Kraftgesteuerte Messzelle für Dilatometeranwendungen (Dissertation TU Ilmenau 2018). Universitätsverlag, Ilmenau 2019. ISBN 978-3-86360-193-5.
URN urn:nbn:de:gbv:ilm1-2018000443.
- Band 33 John, Kerstin:
Untersuchung von Umlenkelementen zur Anwendung in der interferometrischen Längenmesstechnik (Dissertation TU Ilmenau 2018).
Universitätsverlag, Ilmenau 2019. ISBN 978-3-86360-197-3.
URN urn:nbn:de:gbv:ilm1-2018000555.
- Band 34 Mack, Benjamin:
Untersuchungen zum Schadensmechanismus Torsionsschwingbruch durch Kontakttermüdung an Schraubendruckfedern (Dissertation TU Ilmenau 2018).
Universitätsverlag, Ilmenau 2019. ISBN 978-3-86360-198-0.
URN urn:nbn:de:gbv:ilm1-2018000564.

- Band 35 Hesse, Miriam:
Untersuchung der Absicherung von Montageprozessen am Beispiel von Produktionsanläufen in der Automobilindustrie (Dissertation TU Ilmenau 2019). Universitätsverlag, Ilmenau 2020. ISBN 978-3-86360-221-5.
URN urn:nbn:de:gbv:ilm1-2019000681.
- Band 36 Scheler, Marcel:
Auswahl robuster Wirkprinzipien auf Basis einer Erweiterung des CPM/PDDAnsatzes (Dissertation TU Ilmenau 2020). Universitätsverlag, Ilmenau 2020. ISBN 978-3-86360-225-3.
DOI 10.22032/dbt.45602. URN urn:nbn:de:gbv:ilm1-2020000270.
- Band 37 Schienbein, Ralf:
Grundlegende Untersuchungen zum konstruktiven Aufbau von Fünffachs-Nanopositionier- und Nanomessmaschinen (Dissertation TU Ilmenau 2020). Universitätsverlag, Ilmenau 2020. ISBN 978-3-86360-229-1.
URN urn:nbn:de:gbv:ilm1-2020000376.
- Band 38 Mahboob, Atif:
Modelling and Use of SysML Behaviour Models for Achieving Dynamic Use Cases of Technical Products in Different VR-Systems (Dissertation TU Ilmenau 2020). Universitätsverlag, Ilmenau 2021. ISBN 978-3-86360-234-5.
DOI 10.22032/dbt.47179. URN urn:nbn:de:gbv:ilm1-2020000595.
- Band 39 Weber, Christian:
Weimar – a Personal Tribute. Universitätsverlag, Ilmenau 2023.
DOI 10.22032/dbt.58077. URN urn:nbn:de:gbv:ilm1-2023100040.
- Band 40 Hahm, Christoph:
Direkt abgeformte Betonbauteile für Präzisionsanwendungen im Maschinen- und Gerätebau. Universitätsverlag, Ilmenau 2023.
DOI 10.22032/dbt.59146. URN urn:nbn:de:gbv:ilm1-2023000307.
- Band 41 Darnieder, Maximilian:
Design and adjustment of weighing cells for vacuum mass comparators. Universitätsverlag, Ilmenau 2024.
DOI 10.22032/dbt.59666. URN urn:nbn:de:gbv:ilm1-2024000040.
- Band 42 Layher, Michel:
Maschinen- und Verfahrensentwicklung zum laserunterstützten, großvolumigen Schmelzschichten. Universitätsverlag, Ilmenau 2024.
DOI 10.22032/dbt.59543. URN urn:nbn:de:gbv:ilm1-2024000021.

Maximilian Darnieder: Design and adjustment of weighing cells for vacuum mass comparators

Weighing cells based on compliant mechanisms are the backbone of mass metrology. The mechanical properties of the instruments and their adjustment define the metrological performance. The current work focuses on the design and adjustment of weighing cell mechanisms for a 1 kg vacuum mass comparator application. Three mechanical parameters of the compliant mechanisms define the metrological performance: stiffness, tilt sensitivity and off-center load sensitivity. An entire chapter is devoted to the ultra-thin flexure hinges used in the weighing cell mechanism. It covers their modeling, their manufacturing, and measurement. Starting from the concept level, two weighing cell prototypes were developed, assembled, and tested. Mechanical modeling, ranging from analytical models to finite element models, was used throughout the development. A quasi-independent adjustment of stiffness and tilt sensitivity based on the combination of trim masses was modeled and experimentally verified. A metrological model was used to define the requirements for the robust design of the final weighing cell. It allows the compensation of manufacturing deviations. The implemented adjustment methods were designed to eliminate the mechanical first-order error components of the weighing cell and thus enable a further reduction of measurement uncertainties in the mass comparison process.

